

Asp1 kinase modulated mitosis in the fission yeast
Schizosaccharomyces pombe

Inaugural dissertation

for the attainment of the title of doctor
in the Faculty of Mathematics and Natural Sciences
at the Heinrich Heine University Düsseldorf

presented by

Natascha Andrea Künzel

from Kassel

Düsseldorf, July 2017

from the Institute for Functional Genome Research of Microorganisms, Eukaryotic
Microbiology

at the Heinrich Heine University Düsseldorf

Published by permission of the
Faculty of Mathematics and Natural Sciences at
Heinrich Heine University Düsseldorf

Supervisor: Prof. Dr. Ursula Fleig

Co-supervisor: Prof. Dr. Johannes Hegemann

Date of the oral examination: 12.09.2017

Table of contents

Table of contents	1
Abbreviations	5
Zusammenfassung	7
Summary	9
1 Introduction	10
1.1 Chromosome segregation and diseases	10
1.2 <i>Schizosaccharomyces pombe</i> as a model organism	11
1.2.1 Mitotic processes are conserved among eukaryotes.....	11
1.2.2 Mitosis is part of the <i>S. pombe</i> cell cycle.....	12
1.3 Mitosis in <i>S. pombe</i>	13
1.3.1 Mitosis is orchestrated and requires several structures	15
1.3.1.1 The mitotic spindle.....	15
1.3.1.1.1 The mitotic spindle goes through different spindle phases.....	15
1.3.1.1.2 Microtubule-associated proteins are required for spindle dynamics	17
1.3.1.2 The structure of centromere chromatin	20
1.3.1.2.1 Centromere chromatin as the foundation of KT assembly.....	20
1.3.1.2.2 Centromere chromatin in <i>S. pombe</i> is the point of KT assembly.....	22
1.3.1.3 The KT-complex is assembled on centromere chromatin	24
1.3.1.3.1 The Mis16-Mis20-complex interacts with the Sim4-complex to promote KT integrity	25
1.3.1.3.2 The Sim4-complex is a constitutive KT-subcomplex	25
1.3.1.3.2.1 Mal2 and Fta2 are closely related proteins within the Sim4-complex	27
1.3.1.3.2.2 The CCAN-complex in humans.....	28
1.3.1.3.3 The DASH-complex connects the Sim4-complex to spindle MTs	29
1.3.1.3.4 The NMS-complex establishes connections at the KT-MT interface.....	29
1.3.1.3.4.1 The MIND-complex is the foundation of the NMS-complex.....	30
1.3.1.3.4.2 The Spc7-complex attaches to MTs via Mal3	31
1.3.1.3.4.3 The Ndc80-complex contacts MT-associated proteins.....	32
1.3.1.4 The SAC monitors entry into anaphase A.....	33
1.3.2 Mitochondria and mitosis	35
1.4 Inositol-pyrophosphates: production and significance.....	36
1.4.1 Asp1 in <i>S. pombe</i>	39
1.4.1.1 Asp1-generated IP ₈ regulates interphase microtubules and the mitotic spindle	41
1.5 Aim of this work	43
2 Material and Methods.....	44
2.1 Equipment.....	44
2.2 Chemicals	44
2.3 Antibodies	48
2.4 Enzymes and PCR-Kits	49

2.5	Kits	49
2.6	Other materials	50
2.7	Oligonucleotides	50
2.8	Plasmids	53
2.9	Strains.....	55
2.9.1	<i>S. pombe</i> strains	55
2.9.2	<i>S. cerevisiae</i> strains.....	58
2.9.3	<i>E.coli</i> strains.....	58
2.10	Media and cultivation	58
2.10.1	<i>S. pombe</i> media	58
2.10.2	<i>S. cerevisiae</i> media.....	60
2.10.3	<i>E.coli</i> media.....	61
2.11	DNA preparations	61
2.11.1	DNA preparation from <i>S. pombe</i>	61
2.11.2	DNA preparation from <i>S. cerevisiae</i>	62
2.11.3	DNA preparation from <i>E. coli</i>	63
2.11.4	DNA sequencing	64
2.12	Transformation.....	64
2.12.1	Transformation in <i>S. pombe</i>	64
2.12.2	Transformation in <i>S. cerevisiae</i>	65
2.12.3	Transformation in <i>E. coli</i>	66
2.12.3.1	1' Transformation in <i>E. coli</i>	66
2.12.3.2	Electroporation in <i>E. coli</i>	66
2.13	Serial dilution patch test	67
2.14	Survival rate.....	67
2.15	Minichromosome loss assay	67
2.16	PCR.....	68
2.16.1	Colony-PCR	68
2.16.2	Taq-PCR.....	68
2.16.3	Q5-PCR	69
2.16.4	Site-directed mutagenesis	69
2.17	Cloning.....	69
2.18	Strain construction	70
2.19	Mating	71
2.19.1	Random spore analysis.....	72
2.19.2	Tetrad analysis	72
2.20	Protein methods.....	72
2.20.1	Protein isolation from <i>S. pombe</i>	72
2.20.2	Bradford assay.....	73
2.20.3	Immunoprecipitation.....	74
2.20.4	SDS-PAGE.....	74
2.20.4.1	Coomassie staining	75
2.20.4.2	Western Blot.....	75
2.21	Chromatin-Immunoprecipitation	76
2.21.1	Multiplex-PCR.....	79

2.21.2	qPCR.....	80
2.22	Microscopy.....	81
2.22.1	Microscopy of fixed cells	81
2.22.1.1	Immunofluorescence.....	81
2.22.1.2	DAPI staining	82
2.22.2	Live cell imaging.....	83
2.22.3	Quantification.....	84
2.23	Statistics	85
2.24	Replicates	85
3	Results.....	86
3.1	Asp1-generated inositol pyrophosphates influence MT-associated proteins.....	86
3.1.1	Asp1-generated IP ₈ influences the growth of deletion strains of MT-associated proteins	87
3.1.1.1	Lower-than-wild-type IP ₈ -levels rescue the temperature-sensitivity of <i>cut7^{ts}</i> strains ..	92
3.2	Asp1-generated IP ₈ regulates chromosome segregation in <i>S. pombe</i>	95
3.2.1	Chromosome segregation errors are increased without Asp1-generated IP ₈	95
3.2.2	Cells without Asp1-generated IP ₈ depend on a functional SAC.....	97
3.2.3	Higher-than-wild-type IP ₈ -levels increase chromosome transmission fidelity.....	99
3.2.3.1	Higher-than-wild-type IP ₈ -levels reduce aberrant segregation phenotypes.....	99
3.2.3.2	Higher-than-wild-type IP ₈ -levels increase the transmission fidelity of a non-essential minichromosome	103
3.3	Modifications of the Asp1 protein	105
3.4	Asp1-generated IP ₈ alters the kinetochore composition in <i>S. pombe</i>	107
3.4.1	The effect of cellular IP ₈ -levels on the Sim4-kinetochore-subcomplex.....	107
3.4.1.1	Plasmid-borne expression of <i>asp1¹⁻³⁶⁴</i> and <i>asp1³⁶⁵⁻⁹²⁰</i> affects the growth of Sim4-complex mutant strains	107
3.4.1.2	Plasmid-borne expression of <i>asp1¹⁻³⁶⁴</i> increases chromosome missegregation of the <i>mal2-1^{ts}</i> strain	110
3.4.1.3	<i>asp1³⁶⁵⁻⁹²⁰</i> expressed on a plasmid increases Mal2-1-GFP kinetochore targeting..	112
3.4.1.4	Plasmid-expression of <i>asp1¹⁻³⁶⁴</i> decreases Mal2-GFP kinetochore targeting.....	114
3.4.1.5	Mal2-GFP kinetochore targeting is increased in an <i>asp1^{D333A}</i> strain and reduced in an <i>asp1^{H397A}</i> strain	115
3.4.1.6	Asp1-generated IP ₈ affects Mal2-GFP kinetochore targeting in mitosis.....	120
3.4.1.7	Asp1-generated IP ₈ mediates its function at the kinetochore interface	123
3.4.1.8	Asp1 co-immunoprecipitates with Fta2-GFP	126
3.4.1.9	Higher-than-wild-type IP ₈ -levels reduce missegregation in the <i>mis15-68^{ts}</i> strain	128
3.4.1.10	Plasmid-borne expression of <i>asp1³⁶⁵⁻⁹²⁰</i> reduces Mis15-68-GFP kinetochore localization	130
3.4.1.11	<i>mis15-68^{ts}-gfp</i> interacts genetically with <i>asp1</i>	132
3.4.1.12	<i>mis15⁺-gfp</i> genetically interacts with <i>asp1</i>	133
3.4.1.13	Dad1-GFP KT localization is reduced in <i>mal2-1^{ts}</i> and <i>mis15-68^{ts}</i> backgrounds..	135
3.4.2	Mal2 and Mis15 act in an opposed manner	137
3.4.2.1	<i>mis15⁺</i> overexpression increases missegregation in a <i>mal2-1^{ts}</i> strain	137
3.4.2.2	<i>mis15⁺</i> overexpression reduces Mal2-GFP kinetochore targeting	139
3.4.2.3	(<i>mal2⁺ + fta2⁺</i>) overexpression reduces Mis15-68-GFP kinetochore targeting	140
3.4.2.4	(<i>mal2⁺ + fta2⁺</i>) overexpression leads to an aberrant phenotype in a non-tagged wild-type and a <i>mis15⁺-gfp</i> strain.....	141

3.4.3	The effect of Asp1-generated IP ₈ on the NMS-kinetochore-subcomplex	146
3.4.3.1	IP ₈ influences the growth of NMS-complex mutant strains.....	146
3.4.3.2	Expression of <i>asp1</i> ¹⁻³⁶⁴ or <i>asp1</i> ³⁶⁵⁻⁹²⁰ does not affect growth of an <i>spc7-23^{ts}-gfp</i> strain	149
3.4.3.3	Ndc80-GFP kinetochore targeting is reduced with non-physiological IP ₈ -levels	150
3.4.3.4	High cellular IP ₈ -levels re-stabilize the aberrant spindle of the <i>ndc80-21^{ts}</i> strain.....	151
3.4.4	Interdependencies among kinetochore proteins	154
3.4.4.1	Excess Ndc80, Mal2 and Mis15 does not influence the growth of specific KT mutant strains	154
3.5	First characterization of interaction partners of the Asp1 protein	156
3.5.1	Phenotypic analysis of <i>SPCC594.01Δ</i> , <i>hpm1Δ</i> and <i>SPBC725.03Δ</i> strains	156
3.5.2	The effect of IP ₈ on the <i>mis15-68^{ts}</i> strain is not dependent on the presence of Hpm1 or SPBC725.03.....	158
3.6	Met10 and Asp1: A link between mitosis and mitochondria?	160
3.6.1	Characterization of Met10 protein function.....	160
3.6.2	Met10 in mitosis.....	161
3.6.3	Plasmid-borne <i>met10⁺</i> expression reduces the growth of <i>mal2-1^{ts}</i> and <i>mis15-68^{ts}</i> strains	163
3.6.4	Mal2-GFP partially localizes to mitochondria in an <i>asp1</i> ¹⁻³⁶⁴ strain background	164
3.7	A new approach for a minichromosome loss assay	166
4	Discussion	168
4.1	Asp1-generated IP ₈ modulates Sim4-complex composition	168
4.2	Variations in cellular IP ₈ -levels and the fidelity of chromosome segregation	174
4.3	What's the use?	182
5	Appendix	184
6	Table of figures	190
7	References	192
8	Publications	206
9	Acknowledgments	207
10	Statutory Declaration	208

Abbreviations

amp	ampicillin
ble	bleomycin
bp	base pairs
C-terminus	carboxy-terminus
CHX	cycloheximide
DNA	desoxyribonucleinacid
<i>E. coli</i>	<i>Escherichia coli</i>
GFP	green fluorescent protein
dH ₂ O	distilled water
ddH ₂ O	double distilled water
dNTPs	deoxynucleotides
EtOH	ethanol
fwd	forward
g	gram
h	hours
hyg	hygromycin
kb	kilo base pairs
kDa	kilo Dalton
kan	kanamycin
L	liter
M	molar
mA	milliampere
min	minute

mg	milligram
ml	milliliter
mM	millimolar
μg	microgram
μl	microliter
μM	micromolar
ms	milliseconds
n	number
nm	nanometer
OD	optical density
ORF	open reading frame
PCR	polymerase chain reaction
pH	potential of hydrogen
pmol	pikomole
x ^R	resistance
rev	reverse
rpm	rounds per minute
RT	room temperature
U	units
V	volume
Δ	deletion

Zusammenfassung

Genomische Instabilität, welche zu Aneuploidie, d. h. dem Zugewinn oder Verlust ganzer Chromosomen, führt, führt im Allgemeinen zur reduzierten Fitness eines Organismus, oder sogar zum Zelltod. Aneuploidie ist assoziiert mit zahlreichen schwerwiegenden Erkrankungen, wie der Ausbildung von Tumoren, und kann von fehlerhaften mitotischen Prozessen verursacht werden. In Eukaryoten wird Chromosomensegregation vom Kinetochorkomplex unterstützt und überwacht, welcher auf dem Zentromerchromatin von Chromosomen assembliert und diese mit der mitotischen Spindel verbindet. In unserem Modellorganismus, der Spalthefe *Schizosaccharomyces pombe*, besteht der Kinetochor aus mehreren großen Subkomplexen mit mehr als 60 Proteinen.

Diese Thesis stellt einen neuen Modulator mitotischer Mechanismen vor: die Inositol Pyrophosphate (IPPs). Diese hoch-energetischen Moleküle werden von der hochkonservierten zwei-Domänen Vip1 Inositolpolyphosphat Kinase-Familie produziert: die N-terminale Kinasedomäne von Asp1 generiert das spezifische IPP IP_8 , während die C-terminale Pyrophosphatasedomäne IP_8 als Substrat nutzt, welches sie hydrolysiert.

Durch die Nutzung verschiedener Asp1-Varianten war es mir möglich, Mitose in Zellen mit unterschiedlichen IP_8 -Leveln zu analysieren. Ich konnte zeigen, dass Asp1-generiertes IP_8 die Komposition des Sim4-Kinetochor-Subkomplexes, über dessen Komponenten Mal2 und Fta2, moduliert. In Zellen ohne IP_8 war die Menge an kinetochorlokalisiertem Mal2 und Fta2 erhöht, während das Gegenteil in Zellen gefunden wurde, welche höhere IP_8 -Level als der Wildtyp aufwiesen. Diese Modulation ist wahrscheinlich ein direkter Effekt, vermittelt durch eine Modifikation von Fta2 durch IP_8 . Eine andere Komponente des Sim4-Komplexes, Mis15, zeigte einen anderen Phänotyp. Die Kinetochorlokalisierung von Mis15 in Stämmen ohne IP_8 war reduziert. Sim4-Komplex-Proteine können demnach, ihr Verhalten bei Variationen in zellulären IP_8 -Leveln betreffend, in Untergruppen aufgeteilt werden. Eine Modulation der Kinetochorlokalisierung durch IP_8 konnte auch für andere *S. pombe* Kinetochorkomplexe gefunden werden. Es wurde bereits vorher gezeigt, dass IP_8 die Dynamik und Stabilität der Spindel moduliert. In dieser Arbeit habe ich nach Mikrotubuli-assoziierten Proteinen gesucht, die in diese Änderungen der Spindeldynamik involviert sind. Ich habe das Kinesin Cut7 als Teil eines Funktionsweges identifiziert, welcher von IP_8 beeinflusst wird. Zellen mit niedrigeren IP_8 -Leveln, als unter wildtypischen Bedingungen, zeigten eine erhöhte Lokalisierung von Cut7 an der Spindelmitte, was vermutlich zu einer veränderten Spindeldynamik beiträgt.

Modulationen der mitotischen Spindel und der Lokalisation von Kinetochorproteinen durch IP_8 beeinflusste die Zuverlässigkeit der Chromosomensegregation. Die Abwesenheit von IP_8

reduzierte die Zuverlässigkeit der Chromosomensegregation. Zellen mit höheren IP_8 -Leveln, als im Wildtyp, zeigten einen optimierten Chromosomensegregationsprozess. Somit ist die enzymatische Funktion von Asp1 ein bedeutender Regulator der Mitose in *S. pombe*.

Summary

Genome instability resulting in aneuploidy, i.e. the gain or loss of entire chromosomes, in general leads to reduced fitness of an organism or even cell death. Aneuploidy is associated with numerous severe diseases such as the formation of solid tumors and can be caused by erroneous mitotic processes. Chromosome segregation in eukaryotes is powered and monitored by the kinetochore complex which assembles on the centromeres of chromosomes and connects them to the mitotic spindle. In our model organism the fission yeast *Schizosaccharomyces pombe* the kinetochore consists of several large subcomplexes of more than 60 proteins.

This work presents a new modulator of mitotic mechanisms: the inositol pyrophosphates (IPPs). These high-energy molecules are generated by the highly conserved dual domain Vip1 inositol polyphosphate kinase family: the N-terminal kinase domain of Asp1 generates the specific IPP IP_8 , while the C-terminal pyrophosphatase domain uses IP_8 as substrate which it hydrolyzes.

By using different Asp1 variants I was able to analyze mitosis in cells with different IP_8 -levels. I found that Asp1-generated IP_8 modulated the composition of the Sim4-kinetochore-subcomplex via its components Mal2 and Fta2. In cells without IP_8 the amount of kinetochore localized Mal2 and Fta2 increased, while the opposite was found with higher-than-wild-type IP_8 levels. This modulation is possibly a direct effect mediated via a modification of Fta2 by IP_8 . Another member of the Sim4-complex, Mis15, showed a different phenotype as its kinetochore targeting was reduced in IP_8 -less strains. The Sim4-complex proteins can therefore be divided in subgroups regarding their behavior upon variations in cellular IP_8 -levels. IP_8 mediated kinetochore targeting was also observed for other *S. pombe* kinetochore subcomplexes. It had been demonstrated previously that IP_8 modulates spindle dynamics and stability. In this work I screened for microtubule-associated proteins that are involved in these dynamic changes. I identified the kinesin Cut7 as part of a pathway that is affected by IP_8 . Cells with lower-than-wild-type IP_8 -levels showed an enhanced localization of Cut7 to spindle midzones, which is probably a cause for altered microtubule dynamics.

Modulation of the spindle and kinetochore targeting by IP_8 affected chromosome segregation fidelity. The absence of IP_8 reduced chromosome transmission fidelity, while higher-than-wild-type IP_8 -levels optimized the chromosome segregation process. Thus, Asp1 enzymatic function is therefore a major regulator of mitosis in *S. pombe*.

1 Introduction

1.1 Chromosome segregation and diseases

The faithful segregation of genetic material during cell division is crucial for the fitness and survival of each organism. In eukaryotes this requires a precise duplication and transmission of the chromosomes during meiosis and mitosis. Therefore these processes are well orchestrated and closely monitored to maintain genome stability.

Errors in chromosome segregation can lead to an unequal distribution of the genetic material which gives rise to daughter cells that have lost or gained an entire chromosome. This occurrence of an abnormal chromosome number is called aneuploidy (Torres et al., 2008). Aneuploid cells have altered gene expression and protein levels which lead to a reduced cell fitness or even cell death (Rutledge and Cimini, 2016; Torres et al., 2007).

If aneuploidy occurs during meiosis, the following fertilization results in monosomies or trisomies within the embryo. In most cases this leads to spontaneous abortions as the embryo is not viable (Witters et al., 2011).

A well-known example for the occurrence of aneuploidy during meiosis resulting in a viable embryo is trisomy 21 (Down syndrome), in which three copies of chromosome 21 are present (Petersen and Mikkelsen, 2000). The only monosomy described that leads to a viable human embryo is Turner syndrome. Women suffering from the Turner syndrome have a single copy of the X-chromosome which leads, amongst other things, to infertility (Legro, 2012).

If aneuploidy occurs during mitosis this results in daughter cells with an abnormal chromosome content. Such chromosomal instability (CIN) is correlated with a number of diseases like cancer and the Alzheimer's disease (Giam and Rancati, 2015; Zekanowski and Wojda, 2009). Aneuploidy is a hallmark of cancer cells and is found in most solid tumors (Duesberg et al., 2006; Hanahan and Weinberg, 2011; Thompson and Compton, 2011). This facilitation of tumor formation is discussed to be a result of gene expression imbalances (Gordon et al., 2012).

Furthermore aneuploidy has been linked to several neurodegenerative diseases like Alzheimer's disease and schizophrenia (Kingsbury et al., 2006) as well as to the process of aging. It has been described that an insufficiency of the mitotic regulator BubR1 in mice accelerated the aging process while increased expression reduced aneuploidy events and extended the lifespan (Baker et al., 2013; Baker et al., 2004).

The research of the underlying mechanisms that lead to aneuploidy is therefore an important and often discussed topic in modern research as it harbors the potential to understand and counteract widely spread severe diseases.

1.2 *Schizosaccharomyces pombe* as a model organism

The fission yeast *Schizosaccharomyces pombe* (*S. pombe*) is a popular model organism to study processes in eukaryotic cells. *S. pombe* is a haploid organism that has ~ 5000 genes and the genome is fully sequenced (Yanagida, 2002). This gives the opportunity to study the effect of specific genes and their gene products on cellular processes and makes it possible to introduce targeted mutations, epitope tags or deletions into the genome. Furthermore this yeast is able to maintain autonomous plasmids that can be used to analyze its behavior upon expression of genes of interest (Forsburg, 1993; Hoffman et al., 2015).

S. pombe is normally a unicellular organism that displays rod-shaped cells and divides by medial fission which results in two identical daughter cells. The generation time of *S. pombe* in full media is with 2.5 h very short and therefore it is possible to work with a high number of cells and obtain results in a short time (Forsburg and Rhind, 2006).

1.2.1 Mitotic processes are conserved among eukaryotes

Mitotic processes, like kinetochore (KT) assembly, the morphology of the mitotic spindle and the segregation of chromosomes, can be analyzed in *S. pombe* and the obtained results then transferred to higher eukaryotes as the components of chromosome segregation are highly conserved.

The structure and function of the regional centromeres of *S. pombe* is conserved while the sequence differs from that in other organisms (Buscaino et al., 2010; Clarke et al., 1986). In addition to the centromere chromatin also the KT proteins are highly conserved and analysis of their functions might lead to new insights into the role of their human orthologs (Przewloka and Glover, 2009).

Mitosis is one stage of the *S.pombe* cell cycle that will be introduced on the following pages.

1.2.2 Mitosis is part of the *S. pombe* cell cycle

The cell cycle of *S. pombe* can be divided into 4 phases: G1-, S-, G2- and M-phase. G1, S and G2 phase together are called interphase.

The G1 and G2 phases are the “gap” phases. In these gap phases the cell controls if all requirements for the progression into the next cell cycle phase are met. The transition from G1 to S phase and G2 to M phase is therefore tightly controlled. If nutrients are limited the cells can exit the cell cycle during the G1 phase and enter the G0 phase (Su et al., 1996).

After the G1 phase the cell enters into the S (synthesis)-phase in which chromosomes are replicated. The G1 phase of *S. pombe* is short and cells enter into S-phase before cytokinesis is finished (Gomez and Forsburg, 2004). After the S-phase follows the G2 phase.

The G2 phase is the second gap phase and the main growth phase within the *S. pombe* cell cycle. This phase makes up 70 % of the whole cell cycle. The progression from the G2 phase to the M (mitosis)-phase is tightly controlled and requires a certain cell size as well as the activity of cyclins and Cdc2 (Forsburg and Nurse, 1991).

Once the cell enters into M-phase the genetic material is distributed (Gould and Nurse, 1989; Nurse, 1990; Nurse et al., 1976). An overview of the *S. pombe* cell cycle is shown in Figure 1-1.

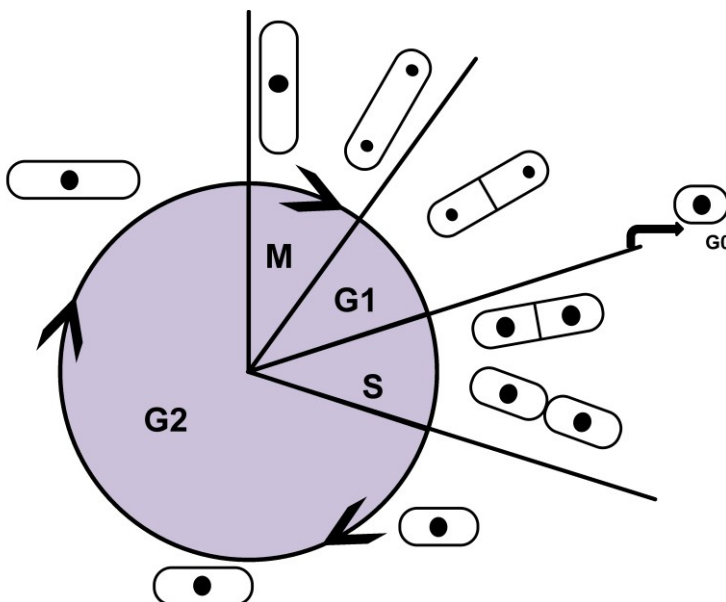


Figure 1-1 The *S. pombe* cell cycle.

The cell cycle is sub-divided in 4 phases: The G1 phase from which cells enter either G0 (stationary phase) or S (synthesis)-phase. After DNA replication the cells enter the main growth phase G2 in which they spend 70 % of the cell cycle before progressing into the M (mitosis)-phase in which the chromosomes are separated.

1.3 Mitosis in *S. pombe*

The entry into the M-phase of the cell cycle is controlled by the G2/M checkpoint. Progression into mitosis requires the activity of the Cdc2 kinase, a completed DNA replication and a critical cell size of $\sim 14 \mu\text{m}$ (Nurse and Thuriaux, 1980; Rowley et al., 1992; Turner et al., 2012).

S. pombe undergoes a closed mitosis which means that the nuclear envelope remains intact throughout this process. Once all requirements for G2/M phase transition are met the duplicated spindle pole bodies (SPBs) enter into the nuclear envelope via a fenestra. Situated there both SPBs are initiating the formation of microtubules (MTs) within the nucleus and separate to form the mitotic spindle (Figure 1-2 A-B (Ding et al., 1997; Hagan and Hyams, 1988)).

The mitotic spindle consists of two different kinds of MTs. The first ones being pole-to-pole MTs that span from one SPB to the other. These MTs overlap in an antiparallel fashion at their plus-ends. The function of the second shorter type of MTs is to attach to the chromosomes (Tanaka and Kanbe, 1986; Tolic-Norrelykke et al., 2004).

S. pombe has three linear duplicated chromosomes that condense upon entry into mitosis and are located in the middle of the nucleus during metaphase, the so-called metaphase plate. The short spindle MTs emerging from the SPBs are binding to these chromosomes (Figure 1-2 C; (Hayles and Nurse, 1989)). Once the sister chromosomes are correctly attached to the MTs the cell enters into anaphase A. This transition to anaphase A is dependent on the anaphase promoting complex (APC) which becomes active if correct attachments of sister chromosomes to spindle MTs have been established. The activated APC catalyzes reactions that lead to the degradation of Securin, which is then not inhibiting Separase any longer and this initiates the separation of the sister chromatids (Lorca et al., 1992; McLean et al., 2011).

The depolymerization of the spindle MTs bound to kinetochores (KT MTs) then transports the sister chromatids to the opposite SPBs (Figure 1-2 D). After the chromatids reach the SPBs the pole-to-pole MTs start polymerizing at their interdigitating plus-ends and push the SPBs to the opposite cell ends during anaphase B (Figure 1-2 E; (Mallavarapu et al., 1999; Nabeshima et al., 1998)). Once the chromosomes are distributed the spindle breaks down and cytokinesis takes place (Figure 1-2 F; (Marks et al., 1986)).

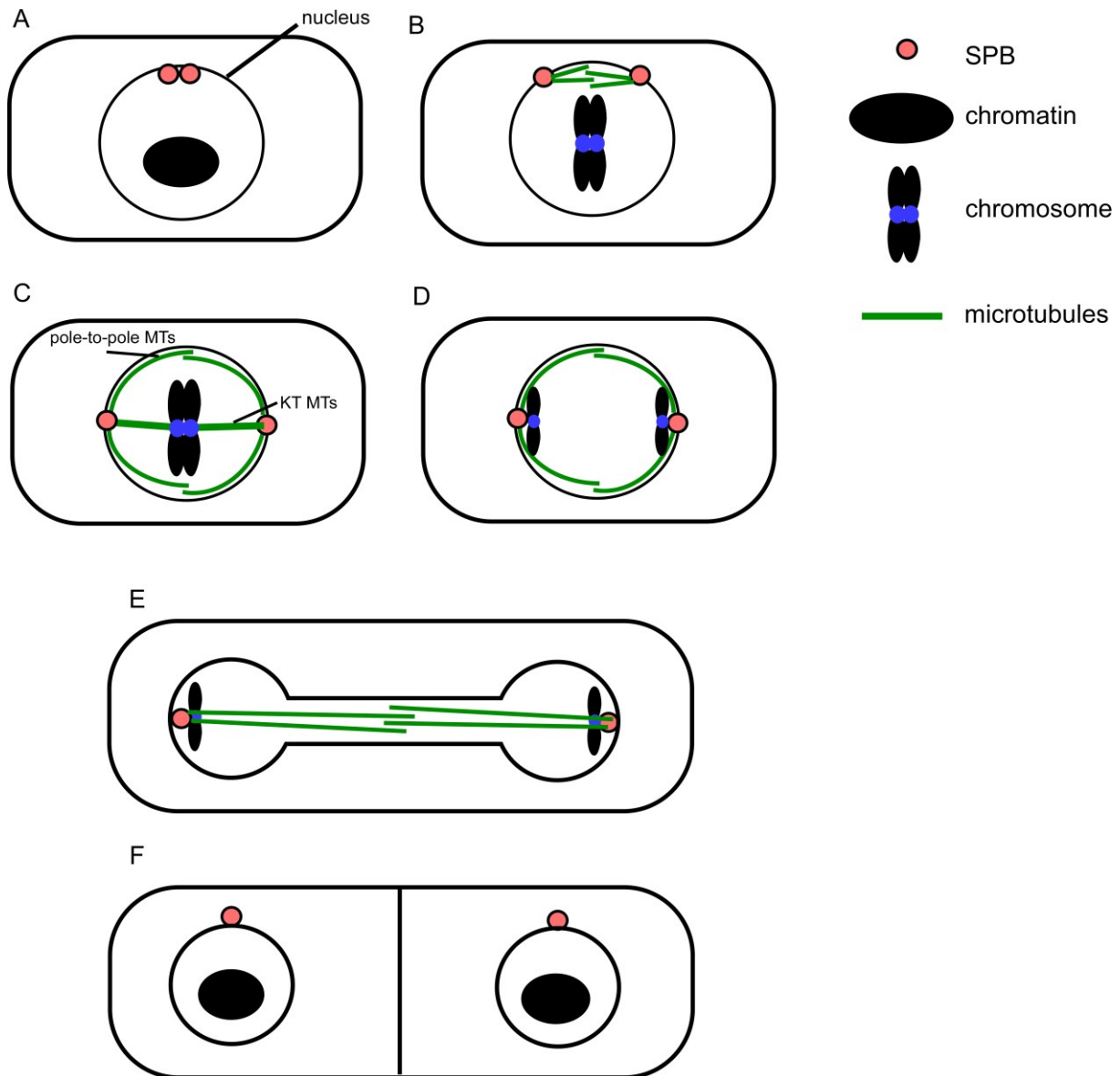


Figure 1-2 Mitosis in *S. pombe*.

A: Upon entry into mitosis the SPBs (spindle pole bodies) are duplicated and settle into the nuclear envelope. The DNA is not condensed yet. **B:** The SPBs start to initiate MT formation and slide to the opposite sides of the nucleus (prometaphase). The DNA gets condensed. **C:** The chromosomes locate to the metaphase plate. As an example only one chromosome pair is shown. Two kinds of MTs emerge from the SPBs. Pole-to-pole MTs that interdigitate at their plus-ends and KT MTs that bind to the chromosomes. The cell remains in that phase until correct attachments between the chromosomes and the KT MTs are established (metaphase). **D:** The sister chromatids are separated and the KT MTs depolymerized. The sister chromatids are transported to opposite SPBs (anaphase A). **E:** The pole-to-pole MTs start polymerizing at their plus-ends which are located at the spindle midzone where the MTs overlap. This elongation pushes the SPBs to opposite cell ends (anaphase B). **F:** After the distribution of the sister chromatids the mitotic spindle breaks down. The SPBs are transported back to the cytoplasm and septum formation and cytokinesis occur. This results in two identical daughter cells.

1.3.1 Mitosis is orchestrated and requires several structures

Mitosis is a complex process that requires several components to work together to ensure an accurate order of events. The mitotic spindle has to build up, connect to chromosomes and distribute them. The KT has to be assembled on the centromere chromatin as a basis for MT attachment and the centromere of each chromosome has to be structurally defined (Carbon and Clarke, 1990; Clarke and Carbon, 1980; Page and Snyder, 1993; Pluta et al., 1995).

In the following chapters I will introduce the components of mitosis required for the understanding of the result section of the thesis in more detail.

1.3.1.1 The mitotic spindle

The mitotic spindle is composed of α - and β -tubulin heterodimers and MT-associated proteins. The minus-end of the MTs is embedded in the SPB while the plus-end marks the growing end. The plus-end of MTs is highly dynamic and undergoes growth and shrinkage episodes (Galjart, 2010; Mitchison and Kirschner, 1984; Toda et al., 1984). The mitotic spindle of *S. pombe* consists of ~ 12-16 pole-to-pole MTs that overlap at their plus-ends and 2-4 short MTs that become attached to each KT of the chromosomes (Ding et al., 1993; Mallavarapu et al., 1999; McCully and Robinow, 1971).

1.3.1.1.1 The mitotic spindle goes through different spindle phases

In the course of mitosis the depolymerization of KT MTs is essential for the separation of the sister chromatids to the SPBs while the polymerization of the pole-to-pole MTs distributes the separated chromatids to the cell ends. To exert these functions the spindle goes through three different phases during mitosis (Mallavarapu et al., 1999; Nabeshima et al., 1998).

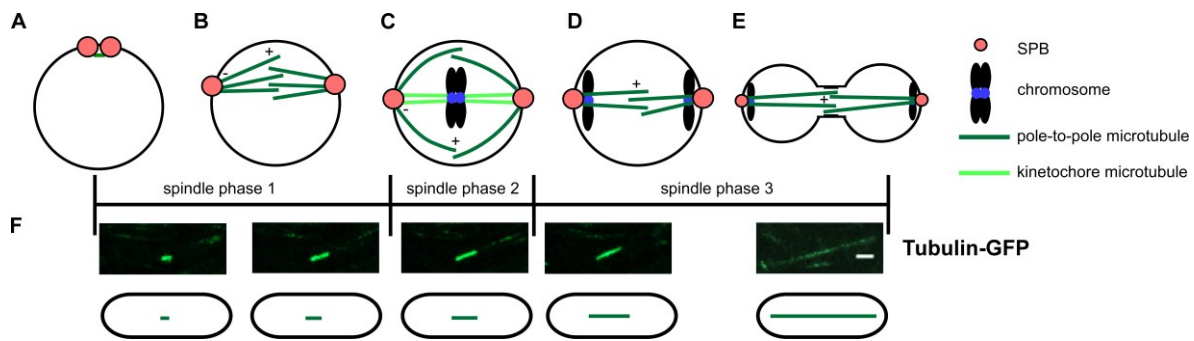


Figure 1-3 Mitotic spindle phases in *S. pombe*.

A: The mitotic spindle is formed between the two separating SPBs. **B:** The spindle rapidly elongates to a length of 1.5 μm through polymerization of the MTs at their plus-ends. The minus-ends are located at the SPBs. **C:** During phase 2 the spindle length stays constant at 1.5-3 μm . The KT MTs attach to the chromosomes over the KTs (2-4 MTs/ KT) while the pole-to-pole MTs interdigitate at their plus-ends. This stage marks metaphase (only two pole-to-pole MTs are shown as an example). **D:** The KT MTs are depolymerized and the sister chromatids are separated to the SPBs. The pole-to-pole MTs keep the spindle at a constant length (anaphase A). **E:** Upon start of spindle phase 3 the pole-to-pole MTs polymerize at their plus-ends and elongate to a length of up to 15 μm . The generated force drives the SPBs apart. **F:** Exemplary live cell microscopy pictures of the morphology of the spindle in the mitotic spindle phases. The spindle was visualized via expression of *SV40::atb2⁺-gfp*. Scale bar= 2 μm .

In spindle phase 1 the spindle is formed and rapidly elongates to a length of $\sim 1.5 \mu\text{m}$ (Figure 1-3 A-B). Spindle phase 2 is characterized by a spindle of a length between 1.5 and 3 μm which stays at a constant length for a specific time depending on temperature. In this phase the KT-MT attachments are established and the sister chromatids are separated to the opposite SPBs. Therefore this spindle phase represents the metaphase and anaphase A spindle (Figure 1-3 C) (Mallavarapu et al., 1999; Nabeshima et al., 1998). The binding of the KT MTs to the KTs during spindle phase 2 is stochastic which leads to erroneous connections of different types (Figure 1-4) (Musacchio and Salmon, 2007).

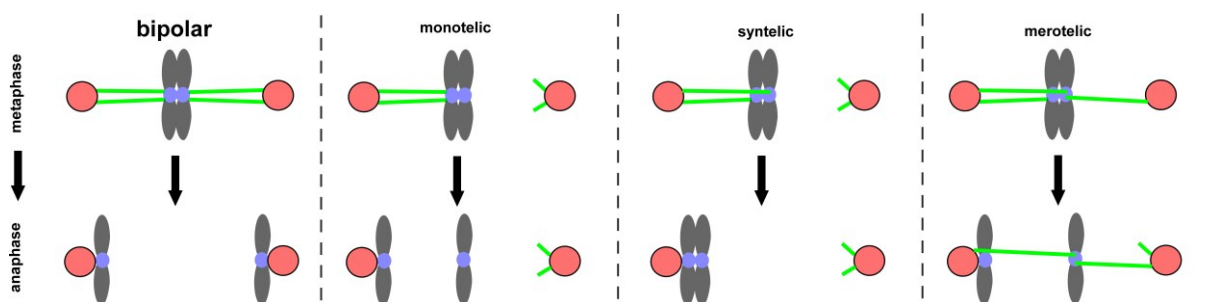


Figure 1-4 Errors in the establishment of KT-MT attachments and their consequences.

Establishing correct bipolar attachments during metaphase leads to a proper segregation of the sister chromatids in anaphase. Monotelic: one chromatid is not attached to KT MTs and is either left on the metaphase plate or segregates with its sister chromatid. Syntelic: Both sister chromatids are attached to the KT MTs emerging from one SPB and segregate to the same SPB during anaphase. Merotelic: A sister chromatid is attached to MTs from both SPBs. During anaphase it is pulled to both SPBs resulting in a draw with the chromatid left on the equator.

These kinds of attachment errors occur frequently and are corrected until bipolarity is established. If monotelic attachments exist one of the KTs is unattached. This condition recruits spindle assembly checkpoint (SAC) proteins that prevent the cell from entering anaphase A until all KT-MT connection errors are corrected (Kadura and Sazer, 2005; Rudner and Murray, 1996). In syntelic and merotelic attachment states no unbound KTs are found, but the tension between the sister chromatids is not bipolar. Such an unequal tension has been proposed to spatially bring the incorrect attached KTs in close vicinity to the centromere localized CPC (chromosomal passenger complex) subunit Aurora B kinase (Ark1 in *S. pombe*) which dissolves the connections (Gregan et al., 2011; Petersen et al., 2001). Merotelic attachments that are sensed via an unequal tension between the sister chromatids can still be corrected in anaphase B where spindle elongation is slower if merotelic attachments exist which can lead to spindle collapses if they are not detected (Courtheoux et al., 2009). KT-MT attachments are constantly disrupted by phosphorylation of different proteins at the KT interface by the Aurora B kinase. This disruption leads to unattached KTs that can be connected again until bipolarity is completed (Leverson et al., 2002; Vader et al., 2006).

When bipolarity is established the sister chromatids are segregated in anaphase A. Once they reach the SPBs, spindle phase 3 starts. This spindle phase is again marked by rapid elongation of the spindle to a length of up to 15 μm (Figure 1-3 D-E) (Mallavarapu et al., 1999; Nabeshima et al., 1998).

The dynamics and stability that the spindle MTs require to go through this spindle phases in a coordinated way is mediated by a number of MT-associated proteins.

1.3.1.1.2 Microtubule-associated proteins are required for spindle dynamics

The dynamic behavior of MTs is regulated by a multitude of MT-associated proteins that control the dynamics and stability of interphase and spindle MTs. These proteins range from MT stabilizing and destabilizing proteins and MT plus-end associated proteins (+TIPs) over motor proteins, so-called kinesins, to MT severing proteins (Maiato et al., 2004).

In the following chapter I will specifically introduce the proteins used in this thesis.

Alp14 and Dis1 are localized at MT plus-ends, belong to the TOG/XMAP protein family and are MT stabilizers and polymerases which promote MT assembly (Al-Bassam and Chang, 2011; Matsuo et al., 2016; Nabeshima et al., 1995). In order to function as a polymerase Alp14 forms a homo dimer that is able to bind soluble $\alpha\beta$ -tubulin dimers (Al-Bassam et al.,

2012; Garcia et al., 2001). Alp14 associates with MT plus-ends independent of the +-TIP protein Mal3 but its localization to cytoplasmic MTs and the mitotic spindle depends on Alp7 (*S. pombe* ortholog of the human transforming acid coiled-coil protein (TACC)) (Al-Bassam et al., 2012; Sato et al., 2004). During mitosis Alp14 is found at the periphery of KT in metaphase in a MT dependent manner and in anaphase it associates with the SPBs. Mutations in the *alp14*⁺ gene lead to an abnormal mitotic spindle and chromosome missegregation (Garcia et al., 2002a; Garcia et al., 2001).

Dis1 on the other hand associates to growing MT plus-ends autonomously but its recruitment is enhanced by an interaction with Mal3 (Matsuo et al., 2016; Nabeshima et al., 1995). Like Alp14 also Dis1 localizes to KT during mitosis but the KT association of that protein does not depend on MTs but is enhanced by the presence of MTs (Nakaseko et al., 2001). Dis1 has a known second function as a MT bundling protein that bundles MTs in a parallel orientation in addition to its function as a polymerase (Roque et al., 2010). It furthermore has been shown that Dis1 and Alp14 independently bind to the KT protein Ndc80, which is part of the NMS-complex, and therefore are crucial proteins for the establishment of KT-MT attachments (Hsu and Toda, 2011; Tang et al., 2013).

Klp5 and Klp6, kinesin-8 family proteins, are MT destabilizing proteins and are the balancing force to Alp14 and Dis1. They are plus-end directed motor proteins and upon reaching the plus-end they promote MT depolymerization (Gergely et al., 2016; West et al., 2001). During mitosis Klp5 and Klp6 form a heterodimer which localizes to spindle midzones and can also be found in the KT periphery. Located there they present the major inward pulling force within the mitotic spindle (Syrovatkina et al., 2013). Klp5 and Klp6 are required for anaphase A onset. The Klp5/6 dimer has been proposed to play a role in the capture of unaligned chromosomes by the spindle MTs and/or the generation of tension within the spindle (Garcia et al., 2002a; Gergely et al., 2016). Earlier it has been shown that both proteins are also important for chromosome alignment (Sanchez-Perez et al., 2005; West et al., 2002). Therefore a deletion of *klp5*⁺ and *klp6*⁺ results in a decreased chromosome stability and an elevated number of lagging chromosomes (a chromosome that trails behind the SPB) (Garcia et al., 2002b; Gergely et al., 2016).

Another kinesin of *S. pombe* is Pkl1. Pkl1 belongs to the kinesin-14 family and is, like dynein, a minus-end directed motor protein (Furuta et al., 2008; Pidoux et al., 1996). This is a special characteristic of those proteins, as most kinesins display plus-end directed motor activity. Pkl1 localizes to the mitotic spindle where it is important for spindle length control as the absence of *pkl1*⁺ leads to a reduction in spindle length (Pidoux et al., 1996; Troxell et al., 2001). Furthermore Pkl1 has been found to transport spindle anchoring factors to the SPBs where they bind γ -tubulin and anchor the MT minus-ends (Yukawa et al., 2015). Located at

the SPBs Pkl1 is important for SPB organization and upon *pkl1*⁺ deletion MT protrusions from the SPBs can be observed that lead to misplaced chromosomes during mitosis causing a cut phenotype in which the DNA is left at the cell equator and divided by the septum during cytokinesis (Syrovatkina and Tran, 2015). Pkl1 is the antagonist of the kinesin-5 Cut7 and opposes the spindle forces generated by that motor protein (Pidoux et al., 1996).

Cut7 is a plus-end directed motor protein (Pidoux et al., 1996; Troxell et al., 2001). However, it has been shown recently that Cut7 can change its direction and has bidirectional motility which is caused by a crowding of other motor proteins on the MT (Britto et al., 2016; Edamatsu, 2014). During mitosis Cut7 localizes predominantly to the SPBs and in anaphase cells also to the spindle midzone (Hagan and Yanagida, 1992). At the SPBs it binds to γ -tubulin which inhibits Pkl1 binding and antagonizes its function in SPB organization and nucleation (Olmsted et al., 2014). Localized at spindle MTs Cut7 mediates the interdigitation during spindle formation and elongation which stabilizes the mitotic spindle in prometaphase and anaphase. A loss of functional Cut7 therefore leads to aberrant spindle phenotypes like v-shaped spindles and is lethal (Hagan and Yanagida, 1990, 1992). Cut7 furthermore acts antagonistic to Klp5/Klp6 as it is the major contributor for outward pushing forces within the spindle (Syrovatkina et al., 2013). The balance of these forces is of utmost importance. A loss of functional Cut7 leads to decreased spindle elongation forces. As a consequence the tension at the KT is reduced and the KT-MT attachments are in proximity to the Aurora kinase Ark1 which might disrupt those attachments. This mechanism is necessary for the correction of merotelic attachments that can, uncorrected, lead to lagging chromosomes. It has been shown that an inhibition of Cut7 can reduce the amount of these merotelic attachments (Choi and McCollum, 2012). Moreover, Cut7 can be recruited directly to KTs via the SAC member Mad1 and located there it promotes chromosome bi-orientation and gliding (Akeru et al., 2015).

Ase1 is a MT bundling protein that localizes autonomously to overlapping MTs (Janson et al., 2007; Loiodice et al., 2005). Localized there it organizes interphase MTs into bundles. During mitosis Ase1 is localized at the spindle during metaphase and predominantly to the spindle midzone in anaphase (Loiodice et al., 2005). Located at the spindle midzone it stabilizes the spindle during the elongation in anaphase B and cooperates with Cut7 to separate the SPBs (Rincon et al., 2017). Therefore it is the second major outward pushing force within the spindle that opposes the inward force generated by Klp5/Klp6 (Syrovatkina et al., 2013). A loss of Ase1 leads to spindle collapses during elongation in anaphase B resulting in a reduced genome stability. Those collapsing spindles have found to be related to uncorrected merotelic KT-MT attachments that cause unequal tensions within the spindle. This led to the conclusion that the tension and stability generated by Ase1 is essential for the correction of

these erroneous KT-MT connections (Courtheoux et al., 2009). Furthermore Ase1 is required for the completion of cytokinesis as a loss of that protein leads to cytokinesis and septation defects (Loiodice et al., 2005; Yamashita et al., 2005).

All of the proteins introduced mediate their function during mitosis and are important for a proper sequence of events during that process as they regulate the dynamics of the spindle and the attachment of spindle MTs to KTs.

1.3.1.2 The structure of centromere chromatin

Binding of the spindle MTs to the chromosomes requires an attachment site on each chromosome. This site is the so-called centromere chromatin region. The centromere chromatin region forms the foundation for the assembly of the KT complex which then serves as a connector between the spindle MTs and the chromosomes during mitosis. Such a centromere chromatin can be found in all eukaryotes and is essential for a proper segregation of genetic material (Clarke and Carbon, 1985; Steiner and Henikoff, 2015).

1.3.1.2.1 Centromere chromatin as the foundation of KT assembly

Centromere chromatin is the foundation for KT assembly in eukaryotes and contains a core DNA region which is flanked by outer domains. However, even though the function of centromere chromatin regions is conserved there are structural differences in centromere chromatin organization between organisms and several types of centromeres have been described: Point centromeres (*S. cerevisiae*), regional centromeres (*S. pombe*), satellite centromeres (humans) and holocentromeres (*C. elegans*) (Steiner and Henikoff, 2015).

I will shortly introduce the central features of these different types of centromeres. Human centromeres are described in more detail as they are regional centromeres and share common features with the *S. pombe* centromere, like several sites for the binding of KT MTs via the KT.

The inner regions of these centromeres share a common feature: H3 nucleosomes are partially replaced by CENP-A nucleosomes, while canonical H3 nucleosomes are present in the outer domains. CENP-A (humans) is a specific histone H3 variant which is highly conserved and has with Cse4 and Cnp1 homologs in *S. cerevisiae* and *S. pombe*, respectively (Clarke and Carbon, 1985; Cottarel et al., 1989; Palmer et al., 1987; Schalch and Steiner, 2016).

Point centromeres of *S. cerevisiae*: these centromeres are small and build up of three conserved elements that span 125 bp of DNA: CDE I, CDE II and CDE III. The CDE II domain is the central domain of the centromere, which is marked by only one Cse4 containing nucleosome. During mitosis only one MT binds to each centromere (Cottarel et al., 1989; Pluta et al., 1995; Yamagishi et al., 2014).

Regional satellite centromeres in humans: Opposed to point centromeres regional centromeres are not defined by a specific DNA sequence but by epigenetic mechanism (Willard, 1990; Yamagishi et al., 2014). With up to 5 Mb in size they are much larger than *S. cerevisiae* centromeres. Their central regions are made up of α satellite tandem repeats with monomers of a size of 171 bp. The monomers are organized into several higher order repeats that span the centromeres in a head-to-tail fashion over a length of 1-4 Mb. Like the CDEII domain in *S. cerevisiae* also the CEN region in humans is marked by CENP-A containing nucleosomes interspersed between canonical H3 nucleosomes (Aldrup-Macdonald and Sullivan, 2014; Palmer et al., 1987). Opposed to point centromeres satellite centromeres contain several CENP-A nucleosomes. The incorporation of CENP-A at the centromeres is mediated by the histone chaperone HJURP and the Mis16 and Mis18 proteins (Foltz et al., 2009). CENP-A loading occurs once during the cell cycle: in the early G1 phase (Foltz et al., 2006; Fujita et al., 2007; Musacchio and Desai, 2017). A feature of CENP-A containing nucleosomes is that they are forming less tightly packed chromatin. This rather open chromatin structure allows the binding of inner KT proteins like CENP-C or CENP-N which then recruit other inner as well as outer KT members. Thus, the central centromere regions are the point of KT assembly (McKinley et al., 2015; Tanaka et al., 2009). The KTs then serve as a binding platform for ~ 20 MTs per centromere (Yamagishi et al., 2014). The regions flanking the central domain contain only H3 nucleosomes and the histones are methylated at position H3K9 which leads to heterochromatin formation (so-called pericentric heterochromatin). The pericentric heterochromatin has several functions: it inhibits the spreading of the centromere region, leads to a transcriptional silencing of these regions and is also required for the recruitment of proteins like cohesin that mediate the cohesion between sister chromatids (Aldrup-Macdonald and Sullivan, 2014; Steiner and Henikoff, 2015; Verdaasdonk and Bloom, 2011). This regions usually remain condensed throughout the cell cycle (Pluta et al., 1995).

Holocentromeres of *C. elegans*: Holocentromeres have dispersed centromeric regions along the entire chromosome. This leads to an attachment of MTs to KTs along the entity of the chromosome (Albertson and Thomson, 1982). However, it was demonstrated that the sites of KT assembly are favorably marked by the histone H3 variant HCP-3 and resemble point centromeres (Steiner and Henikoff, 2014).

As I worked with *S. pombe* in the course of this thesis I will introduce the centromere chromatin of *S. pombe* in detail.

1.3.1.2.2 Centromere chromatin in *S. pombe* is the point of KT assembly

The centromeres of *S. pombe* are regional centromeres that span 40-100 kb of DNA. They are organized in several domains. The central core (*cnt*) with a size of 4-7 kb is flanked by inverted repeats, the innermost repeats (*imr*) and the outer repeats (*otr*) (Pidoux and Allshire, 2005; Polizzi and Clarke, 1991). An overview of the centromere region of *S. pombe* is shown in Figure 1-5.

The *cnt* regions contain non-repetitive DNA sequences but the central core regions of chromosome 1 and 3 (*cen1/3*) share a common 3.3 kb sequence (Takahashi K et al., 1992). The *cnt* and *imr* regions together are called central core region and have a size of ~ 15 kb (Figure 1-5).

Within that region Cnp1 (CENP-A-like) containing nucleosomes are incorporated and interspersed with H3 nucleosomes. Like in humans more than one Cnp1 nucleosome can be found in the central core region (Figure 1-5). For *S. pombe* a number of 15 Cnp1 containing nucleosomes per centromere has been proposed (Lando et al., 2012; Takahashi et al., 2000). The incorporation of Cnp1 nucleosomes is mediated by the fission yeast HJURP homolog Scm3 which is recruited to centromeres via the Mis16-Mis20 complex (Hayashi et al., 2014; Hayashi et al., 2004; Subramanian et al., 2014; Williams et al., 2009). Furthermore it has been shown that the centromere localization of Cnp1 depends on Sim4-complex KT proteins, like Mal2 or Mis6 (Pidoux and Allshire, 2005). In contrast to humans loading of Cnp1 nucleosomes to *S. pombe* centromeres occurs in the late G2 phase of the cell cycle. During mitosis the Cnp1 nucleosomes are then distributed to the daughter cells and stay stable in number during G1 and S phase (Lando et al., 2012).

Also in *S. pombe* a specific chromatin structure can be found in the central core region, which is transcriptionally silent, like the central domains of all centromeres, but not defined by heterochromatin. It has been proposed that the transcriptional silencing of the central core region is caused by an occupation of that region by KT proteins and not heterochromatin formation (Pidoux and Allshire, 2005). Like in humans, the fission yeast KT assembles upon the central core region where it serves as an attachment site for 2-4 spindle MTs during mitosis (Yamagishi et al., 2014) (Figure 1-5).

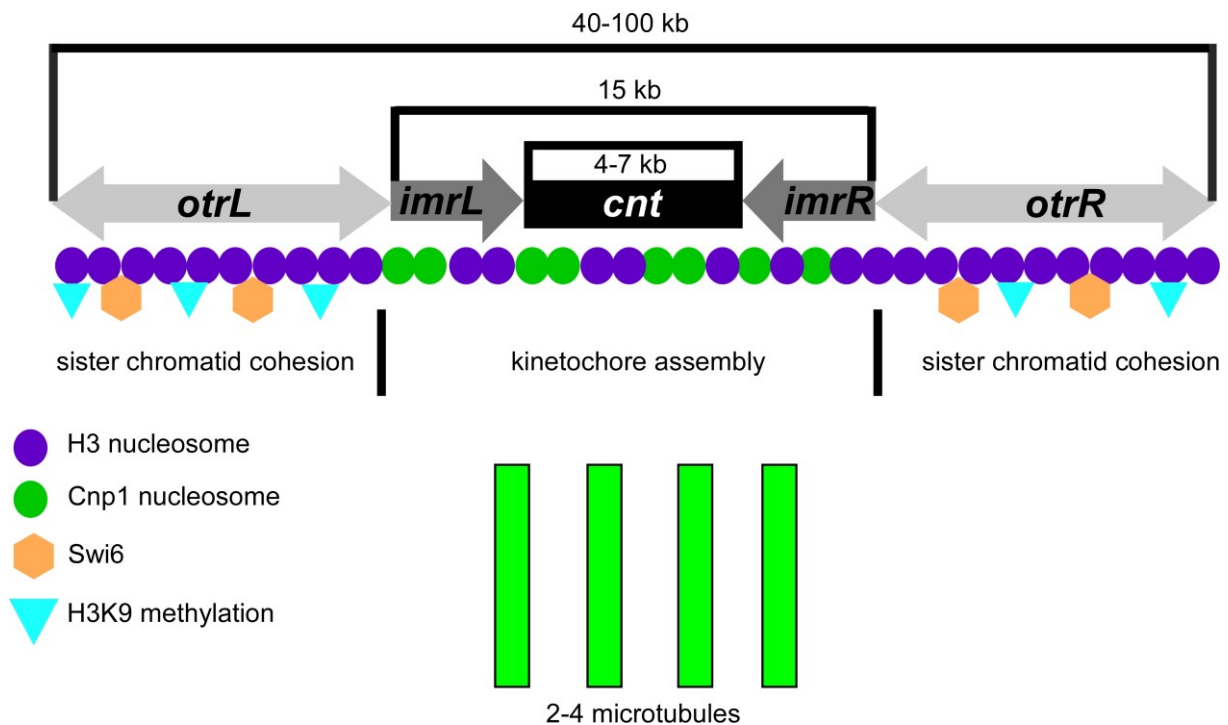


Figure 1-5 The centromere of *S. pombe*.

Schematic representation of the *S. pombe* centromere. The 4-7 kb *cnt* region is flanked by the innermost repeats (*imr*). Together they build the central core region with a size of ~ 15 kb. This region is defined by Cnp1 containing nucleosomes interspersed between H3 nucleosomes. This region has a specific chromatin structure and is the basis of KT assembly. The KT then serves as the platform for the binding of 2-4 spindle MTs per centromere. The central core region is flanked by the outer repeats (*otr*). These regions contain H3 nucleosomes with a heterochromatin typical H3K9 methylation. Swi6 is recruited to the *otr* regions where it is responsible for the recruitment of cohesin and therefore the establishment and maintenance of sister chromatid cohesion.

The outer repeat (*otr*) regions that flank the central core domain show a heterochromatin structure that is underacetylated and carries histones with an H3K9 methylation (Figure 1-5). Due to the heterochromatin formation this region is not transcribed (Pluta et al., 1995; Polizzi and Clarke, 1991). The formation of the heterochromatin is mediated by non-coding transcripts from the *otr* repeats which are processed to siRNAs (small interfering RNAs). These siRNAs start a pathway that leads to the recruitment of Clr4, a histone H3-specific methyltransferase, which methylates H3 at position K9 (Ekwall and Ruusala, 1994; Rea et al., 2000). This leads to the recruitment of the chromodomain protein Swi6 which recruits cohesin (Durand-Dubief and Ekwall, 2008; Ekwall, 2004) (Figure 1-5). The cohesin localized at the centromeres mediates the cohesion of the sister chromatids and is therefore crucial for proper chromosome segregation (Gartenberg, 2009; Heck, 1997).

The central core region of the centromere, the *cnt* and *imr* regions, are then the basis for the assembly of the KT-complex.

1.3.1.3 The KT-complex is assembled on centromere chromatin

The centromere chromatin described in Chapter 1.3.1.2.2 is the foundation for the assembly of the KT-complex. The KT is a large multiprotein complex consisting of ≥ 60 proteins in the budding yeast *Saccharomyces cerevisiae* and even ≥ 100 proteins in humans (Fukagawa, 2004; McAinsh et al., 2003). Assembled on the centromere chromatin it is involved in the maintenance of centromere chromatin structure and serves as a bridge between the chromosomes and the KT MTs (McAinsh and Meraldi, 2011; Subramanian et al., 2014; Takahashi et al., 2000).

The KT consists of several subcomplexes that are highly conserved between yeast and humans and almost all components have functional homologs in these organisms (Roy et al., 2013).

In *S. pombe* there are four subcomplexes within the KT: the Mis16/Mis20-, Sim4-, NMS- and DASH-complexes (Figure 1-6). The constitutive components are localized to KTs throughout the cell cycle while other components are transiently localizing to KTs. Constitutive components are the Sim4- and NMS-subcomplexes while the DASH-complex (except from the protein Dad1) and several MT-associated proteins, like Alp14, Dis1, Klp5, Klp6 and Mal3 are transiently recruited in mitosis. The Mis16-Mis20-complex on the other hand delocalizes in mid-mitosis (Fleig et al., 1996; Hayashi et al., 2014; Hayashi et al., 2004; Jin et al., 2002; Kerres et al., 2004; Liu et al., 2005; Pidoux et al., 2003).

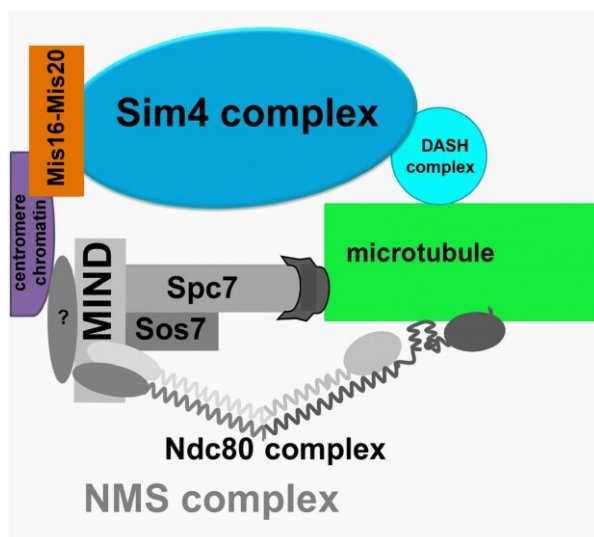


Figure 1-6 Overview of the *S. pombe* KT sub-complexes and their positioning.

The Mis16-Mis20-complex associates to centromere chromatin and recruits the Sim4-complex. The Sim4-complex is responsible for the KT localization of the DASH-complex that connects the Sim4-complex to spindle MTs. The NMS-complex is localization independent of the Sim4-complex and directly connects to MTs.

In the following chapters I will introduce the *S. pombe* KT subcomplexes in more detail.

1.3.1.3.1 The Mis16-Mis20-complex interacts with the Sim4-complex to promote KT integrity

Mis16 and Mis18 form a complex and were identified as proteins that are essential for faithful chromosome segregation. Localization studies showed that Mis16 and Mis18 are enriched in the nuclear chromatin region throughout the cell cycle and are associated with KTs, except from a delocalization during mid-mitosis (Hayashi et al., 2004). The Mis16/Mis18 complex is essential for the incorporation of Cnp1 in the centromere region and known for the recruitment of the Sim4-complex proteins Mis6, Mis15 and Mis17 (others have not been tested) (Hayashi et al., 2004). Recently, two additional members of this complex have been identified: Mis19 (Eic1) and Mis20 (Eic2) (Subramanian et al., 2014). Mis19 and Mis20 have orthologs in other fission yeasts, but not in other organisms. They showed the same localization pattern as Mis16 and Mis18 with a delocalization from KTs in mid-mitosis. Furthermore, functional Mis19 is necessary to recruit the Sim4-complex components Mis6, Fta7, Mal2 and Cnl2 (Subramanian et al., 2014). Moreover it was shown that Mis19 localization is greatly dependent on Mal2 and partially dependent on Mis16, Mis18 and Scm3, but independent of Mis12, Cnp1, Mis6 and Mis20. Mis20 localization depended on all tested proteins (Mis18, Mis16, Scm3, Cnp1, Mis12 and Mis6). A model has been proposed in which Mis19 serves as a connector between Mis18 and Mis16 to which also Mis20 is recruited. The formed complex is then responsible for Cnp1 incorporation at the centromeres and interacts with Sim4-complex proteins to promote KT integrity (Hayashi et al., 2014; Subramanian et al., 2014).

1.3.1.3.2 The Sim4-complex is a constitutive KT-subcomplex

The Sim4-KT sub-complex consists of 12 proteins which were identified via biochemical purification: Sim4, Mal2, Mis6, Mis15, Mis17, Cnl2, Fta1, Fta2, Fta3, Fta4, Fta6 and Fta7 (Liu et al., 2005; Shiroiwa et al., 2011). This complex is highly conserved (CCAN in humans) as almost all Sim4-complex members have orthologues in humans (Cheeseman and Desai, 2008; Shiroiwa et al., 2011). The Sim4-complex is bound to the KT over the Mis16-Mis20-complex and promotes Mis19 and Mis20 KT targeting (Subramanian et al., 2014). It is then constitutively localized at the KT throughout the cell cycle (Hayashi et al.,

2004). Known localization dependencies exist between Mal2 and Fta2, as well as Mis6/Mis15/Mis17 (Hayashi et al., 2004; Kerres et al., 2006) (Figure 1-7).

All members of the Sim4-complex, except Fta6, are essential and therefore a deletion of the genes encoding for these proteins leads to inviability (Kim et al., 2010). Further characterization of these proteins has been done using temperature-sensitive (ts) mutant strains in which the gene products are not functional at high temperatures. However, the analysis of the functions and interdependencies of Sim4-complex members is still not well characterized.

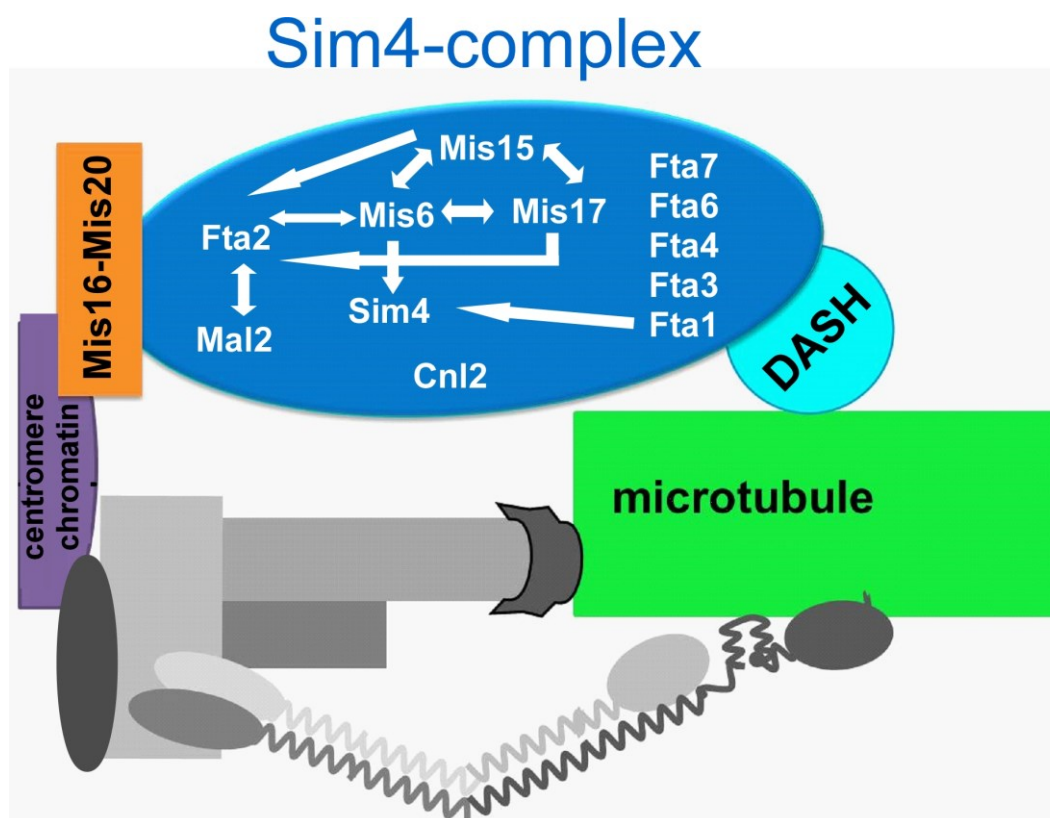


Figure 1-7 The *S. pombe* Sim4-complex members.

The *S. pombe* Sim4-complex contains 12 proteins and is localized to KT's over the Mis16-Mis20 complex. Arrows indicate known localization dependencies (Hayashi et al., 2004; Kerres et al., 2006; Pidoux et al., 2003; Tanaka et al., 2009).

The Sim4 (CENP-K in humans) protein is essential for faithful chromosome segregation. It has been shown that Mis6 (CENP-I in humans), another Sim4-complex member, is required for Sim4 KT localization and together they play an important role in Mad2 and therefore SAC recruitment (Pidoux et al., 2003; Saitoh et al., 2005).

Mis6 was first identified in a screen for proteins that caused chromosome missegregation if their function was disrupted (Takahashi et al., 1994). Mis15 (human CENP-N), and Mis17

(human CENP-U) were identified later (Hayashi et al., 2004). These three proteins are localization interdependent and also interact physically (Hayashi et al., 2004). It has been proposed that these three proteins are involved in the deacetylation-acetylation cycle of histones within the centromere chromatin (Shiroiwa et al., 2011). However, even though Mis6, Mis17 and Mis15 are thought to be closely related the way and timing in which they exert their functions differs.

Mis6 is essential for the maintenance of centromere chromatin structure, correct spindle morphogenesis and the positioning of chromosomes (Saitoh et al., 1997). Apart from Mis15 and Mis17, Mis6 localization is also dependent on the functional Fta2 (CENP-P) protein and *f_{ta2}⁺* overexpression led to synthetic lethality in a *mis6-302^{ts}* strain (Kerres et al., 2006). Furthermore, Mis6 was found to exert its function during the G1/S transition of the cell cycle (Saitoh et al., 1997; Takahashi et al., 2000).

Mis17 is highly phosphorylated in *S. pombe* showing that it is a target for possible post-translational modification within the Sim4-complex. A mutation of this protein led to a defect of histone H3 recruitment to centromeres (Shiroiwa et al., 2011). Opposed to Mis6, which is required in G1/S phase, Mis17 acts during mitosis after being hyperphosphorylated in G1/S phase (Saitoh et al., 1997; Shiroiwa et al., 2011; Takahashi et al., 2000).

The proteins Fta1, Fta3, Fta4, Fta6, Fta7 and Cnl2 are not further characterized yet. The only known fact is that they localize to KTs throughout the cell cycle (Liu et al., 2005; Shiroiwa et al., 2011) and that Fta1 interacts with Cnp3, the fission yeast CENP-C homolog, and is essential for faithful chromosome segregation (Tanaka et al., 2009).

Mis15 (CENP-N) is essential for normal chromosome segregation and is localized to KTs throughout the cell cycle. The localization of Mis15 depends on the Sim4-complex members Mis6 and Mis17. Furthermore a physical interaction of Mis15 with Mis6 and Mis17 has been shown (Hayashi et al., 2004).

As the Mal2 and Fta2 proteins were regularly used in this thesis these proteins are introduced in greater detail.

1.3.1.3.2.1 Mal2 and Fta2 are closely related proteins within the Sim4-complex

Mal2 is essential for chromosome segregation and is conserved in humans (CENP-O) (Fleig et al., 1996; Foltz et al., 2006). Mal2 is localized at the KT throughout the cell cycle and therefore associated with the central region of centromeres. It is required for maintenance of the centromere chromatin structure and mutations in the *mal2⁺* gene lead to massive

chromosome missegregation due to nondisjunction of the sister chromatids. Mal2 function is also crucial for the morphogenesis of the mitotic spindle as a mutation of the *mal2⁺* gene leads to an elongated metaphase spindle (Fleig et al., 1996; Jin et al., 2002). A mutation in the *fta2⁺* gene leads to aberrant segregation phenotypes showing the importance of the Fta2 (CENP-P) protein for the chromosome segregation process. A non-functional Fta2 protein leads to unequally or partially segregated DNA or DNA that stays highly condensed at the cell equator while the spindle elongates. This indicates a defect in KT-MT attachments (Kerres et al., 2006). Furthermore it has been shown that Fta2-GFP KT localization depends on a functional Mis15 protein (Jakopec, 2006). Mal2 and Fta2 interact and are localization interdependent. Overexpression of Mal2 suppresses the phenotype of an *fta2^{ts}* strain and vice versa. This implicates a closely related function of these proteins (Kerres et al., 2006).

1.3.1.3.2.2 The CCAN-complex in humans

The Sim4-complex is known in humans as the CCAN (c̄onstitutive c̄entromere āssociated n̄etwork)-complex and almost all Sim4-complex members have orthologues within that complex (Table 1-1).

The CCAN-complex is further divided into functional subgroups. They are categorized into the CENP-O-, CENP-N/L- and CENP-H- complexes (Cheeseman and Desai, 2008; McAinsh and Meraldi, 2011; McClelland et al., 2007; Musacchio and Desai, 2017) (Table 1-1).

Sim4-complex protein	CCAN ortholog	CCAN sub-groups
Mal2	CENP-O	CENP-O-complex
Fta2	CENP-P	
Mis17	CENP-U	
Fta7	CENP-Q	
Fta1	CENP-L	CENP-N/L-complex
Mis15	CENP-N	
Mis6	CENP-I	CENP-H-complex
Sim4	CENP-K	
Fta3	CENP-H	
Fta4	(CENP-U)	
Fta6	-	No human ortholog
Cnl2	-	

Table 1-1 Sim4-complex members are conserved and have orthologues in the CCAN-complex.

1.3.1.3.3 The DASH-complex connects the Sim4-complex to spindle MTs

Other than the Sim4-complex the DASH-complex is a transient KT complex that only localizes at the KTs during mitosis. It consists of 10 members: Ask1, Dam1, Spc19, Spc34, Duo1, Dad1, Hos2 (Dad2), Dad3, Dad4 and Hos3 (Hsk3). The DASH-complex is conserved in yeast and essential in *S. cerevisiae* but not in *S. pombe* and all of its components are localization interdependent and dependent on Dad1 (Liu et al., 2005; Sanchez-Perez et al., 2005).

The Dad1 protein is the only DASH-complex member that localizes to KTs throughout the cell cycle. At the KT interface it closely interacts with Sim4-complex proteins and it was shown that Dad1 KT localization depends on Fta2, Mal2 and Mis6 (Kerres et al., 2006; Sanchez-Perez et al., 2005).

The DASH-complex serves as the connector between the Sim4-complex and the spindle MTs (Coffman et al., 2011; Miranda et al., 2005). Although the DASH-complex is binding also unattached KTs the binding gets stronger if MTs are attached (Saitoh et al., 2008). This anchoring of KTs to MTs is believed to be essential to retrieve unclustered chromosomes during mitosis. The DASH-complex attaches the KTs to depolymerizing MT plus-ends which transports unaligned chromosomes back to the SPBs. At the SPBs the chromosomes can be coupled to polymerizing MTs again which transport them to the metaphase plate (Franco et al., 2007; Gachet et al., 2008).

Therefore the DASH-complex is one of the KT-complexes that make direct contact to spindle MTs. The second KT-subcomplex that binds to KT MTs is the NMS-complex.

1.3.1.3.4 The NMS-complex establishes connections at the KT-MT interface

The third KT subcomplex is the NMS (Ndc80-MIND-Spc7)-complex which consists of 10 proteins (Jakopce et al., 2012; Liu et al., 2005). This complex is conserved among eukaryotes and known in humans as the KMN network. It serves as the major connector between the KT and the spindle MTs (Cheeseman et al., 2006; Obuse et al., 2004) (Figure 1-8).

All the NMS-complex components of *S. pombe* are essential, KT localized throughout the cell cycle and play an important role in proper chromosome segregation. A loss of function of NMS-complex proteins leads to several different aberrant chromosome segregation and

mitotic spindle phenotypes (Goshima et al., 1999; Hsu and Toda, 2011; Jakopec et al., 2012; Kerres et al., 2007).

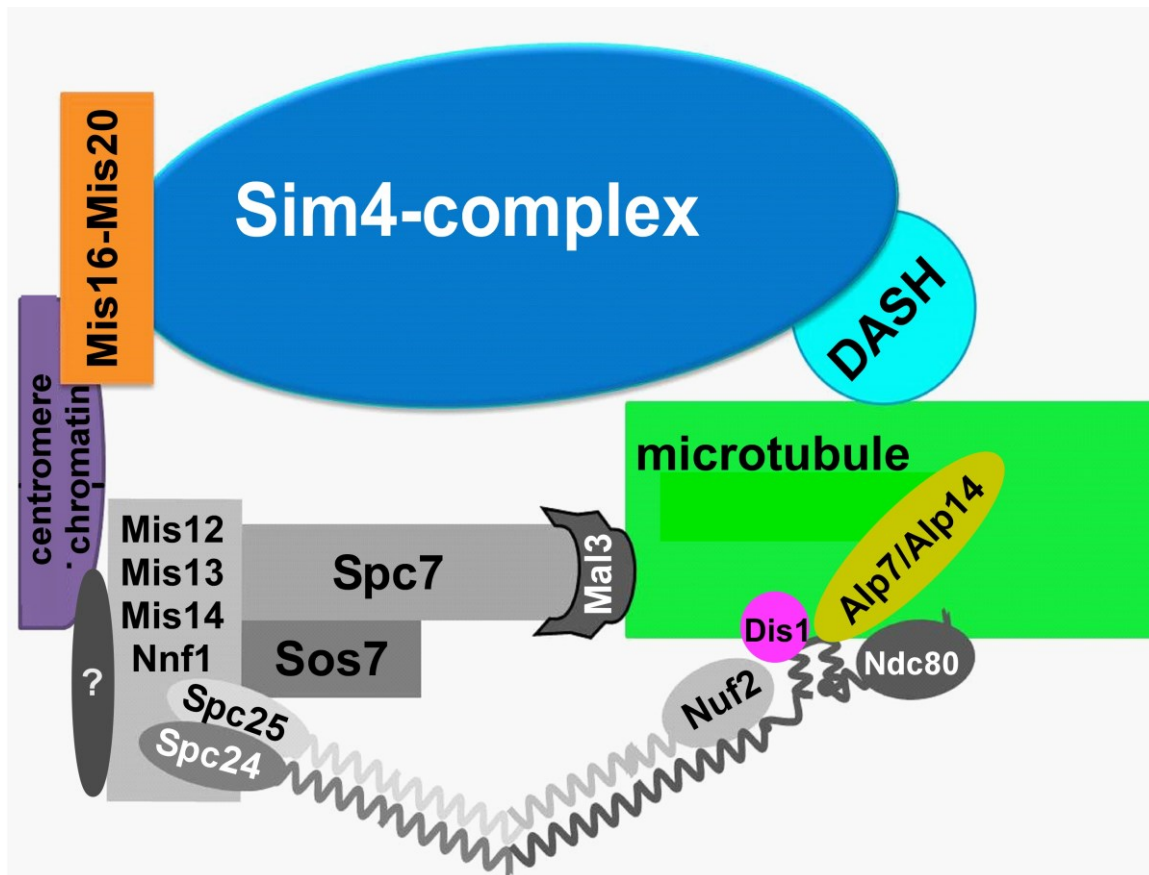


Figure 1-8 The *S. pombe* NMS-complex.

Shown is a schematic overview of the NMS-complex of *S. pombe*. The four component MIND-complex serves as a connector between the Spc7- and Ndc80-complexes and links them to the centromere. The two component Spc7-complex is directly interacting with the KT-MTs over the Mal3 protein. The Ndc80-complex is connected to the MIND-complex via Spc24/Spc25. Ndc80 directly interacts with the MT lattice and makes additional contact via the Dis1 protein and the Alp7/Alp14-complex.

1.3.1.3.4.1 The MIND-complex is the foundation of the NMS-complex

One sub-complex within the NMS-complex is the MIND-complex which contains the Mis12, Mis13, Mis14 and Nnf1 proteins (Figure 1-8; (Liu et al., 2005)). The MIND-complex has been shown to be the basis for the KT localization of the Spc7- and Ndc80-complexes (Jakopec et al., 2012; Kerres et al., 2007). The MIND-complex has been argued to be KT targeted independently of Cnp1 and also not to be involved in Cnp1 incorporation at the centromeres (Takahashi et al., 2000). How exactly the KT loading of the MIND-complex works remains unknown.

However, for the human Mis12 protein an interaction with the heterochromatin component HP1 has been shown (Obuse et al., 2004). Recently it has furthermore been published that human Mis12 KT localization depends on the CCAN members CENP-H/I and K (Kim and Yu, 2015).

The Mis12 protein has further been shown to be important for spindle integrity and chromosome segregation but not sister chromatid separation (Goshima et al., 1999). For the Mis13 protein it was demonstrated that it is needed to recruit condensin to centromeres (Nakazawa et al., 2008).

1.3.1.3.4.2 The Spc7-complex attaches to MTs via Mal3

The second NMS-subcomplex is the Spc7/ Sos7-complex that consists of these two proteins (Figure 1-8; (Jakopec et al., 2012)). Spc7 interacts with the plus-end associated protein Mal3 and therefore directly connects the KT to the spindle MTs. This interaction is necessary to maintain spindle integrity and influences the dynamics of MT plus-ends (Kerres et al., 2007). Furthermore it has been proposed that after Spc7 attaches correctly to MTs over Mal3 the Dis2, Klp5 and Klp6 proteins are recruited to the MT-tip which causes silencing of the SAC and MT depolymerization that transports the sister chromatids to the SPBs (Meadows et al., 2011).

Spc7 is also a target for phosphorylation at the KT interface by Ark1 which disrupts KT-MT attachments (Koch et al., 2011). Spc7 can also be phosphorylated by Mph1, a kinase that is part of the SAC, which leads to a recruitment of SAC proteins like Mad1, Mad2, Bub1 and Bub3 (Shepperd et al., 2012; Yamagishi et al., 2012).

The Spc7 protein is involved in the KT localization of other NMS-complex members (Kerres et al., 2007). Interestingly, it has also been shown that the KT targeting of the Sim4-complex protein Fta2 depends on Spc7, while that of other Sim4-components (Mal2, Mis6, Sim4) and the Dad1 protein does not. Furthermore it was demonstrated that Spc7 genetically interacts with the Sim4-complex member Mal2 (Kerres et al., 2007). These findings suggest a crosstalk between the Spc7- and Sim4-complexes.

The second Spc7-complex protein, Sos7, physically interacts with Spc7 and these proteins are localization interdependent. While Spc7 connects to MTs directly, Sos7 serves as a stabilizer of this MT binding. Like Spc7 also Sos7 depends on the MIND-complex member Mis12 in terms of localization but is independent from Sim4-complex proteins (Jakopec et al., 2012).

1.3.1.3.4.3 The Ndc80-complex contacts MT-associated proteins

The Ndc80-complex consists of the four proteins Spc24, Spc25, Nuf2 and Ndc80. The structure of that complex has been extensively studied in humans. The Spc24 and Spc25 proteins form dimers and are linked to the MIND-complex. They are connected to the Ndc80 and Nuf2 proteins, respectively, which have a specific coil structure (Figure 1-8; (Ciferri et al., 2007)). The Ndc80 protein is directly binding to MTs via the CH (calponin-homology) domain at its N-terminus. This binding is stabilized by the MT-associated protein Dis1 which is recruited to a specific loop region within the Ndc80 protein (Hsu and Toda, 2011). Apart from Dis1 also the Alp7/Alp14 protein complex binds to the loop region of Ndc80. This interaction additionally stabilizes the established KT-MT attachments (Figure 1-8; (Tang et al., 2013)). Ndc80 is furthermore phosphorylated by the Aurora B kinase which disrupts the KT-MT bindings and might correct erroneous attachments (Alushin et al., 2010; Ciferri et al., 2007; Deluca et al., 2011). Upon binding of Ndc80 to Alp7 the Dis2, Klp5 and Klp6 proteins are recruited which support the depolymerization of the MTs and therefore the transport of the sister chromatids to the SPBs (Tang and Toda, 2015). A functional Ndc80 protein is therefore crucial for spindle integrity and a stable mitotic spindle (Hsu and Toda, 2011).

In addition to proteins that stabilize the KT-MT linkage the Ndc80 protein also recruits SAC members. It was shown that the hairpin region of Ndc80 is a platform for Mph1 recruitment which leads to the recruitment of other SAC members like Mad1-3, Bub1 and Bub3 (Chmielewska et al., 2016).

Like the Spc7-complex, the Ndc80-complex depends on MIND to be KT localized. However, the Spc7- and Ndc80-complexes are not localization interdependent (Jakopec et al., 2012; Kerres et al., 2007). Recently it has also been shown that in humans the Ndc80-complex is recruited to centromeres via CENP-C and can also directly interact with the CCAN member CENP-T (Rago et al., 2015).

Until the KT-MT attachments are established in a bipolar fashion, mediated by the MT-associated and KT proteins introduced in the preceding chapter, the cells stay in metaphase. This ensures that anaphase A entry only occurs if bipolarity is established. This process is monitored by the SAC.

1.3.1.4 The SAC monitors entry into anaphase A

The SAC is the guardian of mitosis. Its activity blocks entry into anaphase A until bipolar KT-MT attachments are established. This process is crucial to avoid chromosome missegregation events and therefore the development of aneuploidy.

The SAC network is made up of the proteins Mph1, Mad1, Mad2, Mad3, Bub1 and Bub3 (Musacchio and Salmon, 2007). Those proteins are concentrated on unattached KTs and block the activity of the APC/C (APC/ cyclosome) (Figure 1-9; (Cleveland et al., 2003; Kops and Shah, 2012)). The APC/C is an E3 ubiquitin ligase that regulates the progression from metaphase to anaphase A and the mitotic exit. The major role of SAC proteins is to inhibit the activation of the APC/C in metaphase until bipolarity is established (Acquaviva and Pines, 2006; Peters, 2006). To fulfill this function SAC members are hierarchically recruited to unattached KTs (Heinrich et al., 2012). The basis of this recruitment is the Aurora B kinase Ark1. Ark1 is part of the CPC (chromosomal passenger complex) that also contains the proteins Pic1, Nbl1 and Bir1 and its function is crucial to maintain SAC signaling. To mediate this function Ark1 is localized at KTs during metaphase and at the spindle midzone during anaphase B (Levenson et al., 2002; Petersen et al., 2001). Localized at the KT the Ark1 kinase phosphorylates several proteins that are involved in processes like chromosome compaction (condensin component Cnd2), heterochromatin formation (histone H3) and KT-MT attachments (KT protein Spc7) (Koch et al., 2011). Mediated through Ark1 the Mph1 kinase is recruited to KTs where it acts upstream of other SAC members (He et al., 1998; Heinrich et al., 2012). Mph1 is recruited to the hairpin region of the KT protein Ndc80. This brings Mph1 in close proximity to its phosphorylation target Spc7 (Chmielewska et al., 2016). The phosphorylation of Spc7 leads to the recruitment of other SAC components (Figure 1-9; (Rischitor et al., 2007; Shepperd et al., 2012; Yamagishi et al., 2012)). The Mad2/Mad3 complex then associates with Cdc20 and the APC/C and block its activation and therefore entry into anaphase A (Figure 1-9; (Peters, 2006; Sczaniecka et al., 2008)).

It has been shown that DASH- and Sim4-complex members are required for Mad2 localization to unattached KTs and that it even physically interacts with the Sim4-complex protein Mis6 (Saitoh et al., 2005; Saitoh et al., 2008).

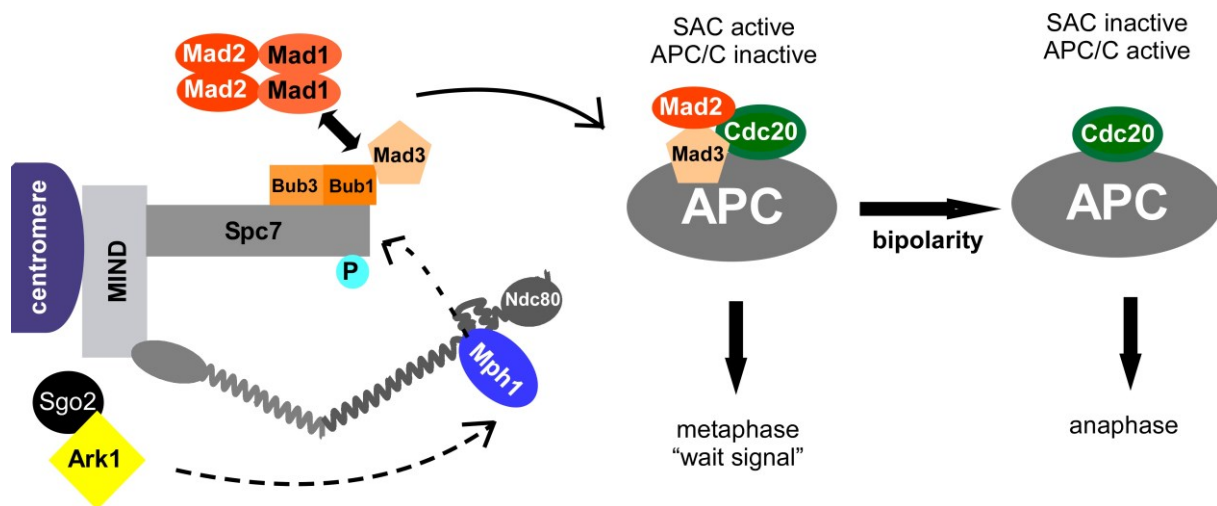


Figure 1-9 Model of the activation of the SAC in *S. pombe*.

SAC activation requires a localization of the Aurora B kinase Ark1 to KT. Ark1 recruits the Mph1 protein which is proposed to bind to Ndc80 and phosphorylate the KT protein Spc7. A phosphorylation of Spc7 enhances its interaction with the Bub1 and Bub3 proteins which recruit Mad3. These three proteins are required to localize Mad1/Mad2 complexes to the KT interface. Mad2 and Mad3 form a complex with the APC/C co-activator Cdc20 which inactivates the APC/C and keeps the cells in metaphase until bipolar KT-MT attachments are established. After bipolarity is achieved the SAC is inactivated and the APC/C can be activated by Cdc20 which leads to the entry into anaphase A. Model modified from (Chmielewska et al., 2016).

The SAC is activated in the presence of unattached KTs. How syntelic and merotelic attachments are corrected before entry into anaphase A is still a matter of debate. However, it has been proposed that upon changes in KT tension the Aurora B kinase Ark1 can reach KTs and disrupt the KT-MT attachment via phosphorylation. Upon establishment of bipolarity the KTs are pulled out of Auroras reach and the KT-MT attachments stay stable. Once bipolarity is established the SAC is inactivated and cells progress through mitosis (Meadows et al., 2011; Vanoosthuyse and Hardwick, 2009).

As mitochondria and their distribution will be important for several results in the results section of this thesis I will briefly introduce the role of mitochondria in mitosis.

1.3.2 Mitochondria and mitosis

During the process of mitosis not only genetic material in form of chromosomes has to be equally divided between the two daughter cells. Also cell organelles have to be separated to ensure the survival of the emerging cells. One of these organelles, mitochondria, are the energy sources within the cell.

In interphase cells, mitochondria form a tubular network which displays dynamic movements like the division or fusion of those structures. The tubular mitochondrial structures partially co-localize with the cytoskeleton which supports their dynamics. In *S. pombe* this mitochondrial movement depends on MTs (Berger and Yaffe, 1996). It was shown that this movement is driven by a coupling of mitochondria to MTs (Yaffe et al., 1996). It has been demonstrated that the MT plus-end associated protein Peg1 as well as Mmb1 are important to couple mitochondria to MTs and both proteins are essential for mitochondrial movements (Chiron et al., 2008; Fu et al., 2011). It has been argued that motor proteins are involved in the mitochondrial movements but recently it was proposed that the distribution is rather mediated in a passive motor-independent way that relies on MT dynamics (Berger and Yaffe, 1996; Li et al., 2015) (Figure 1-10).

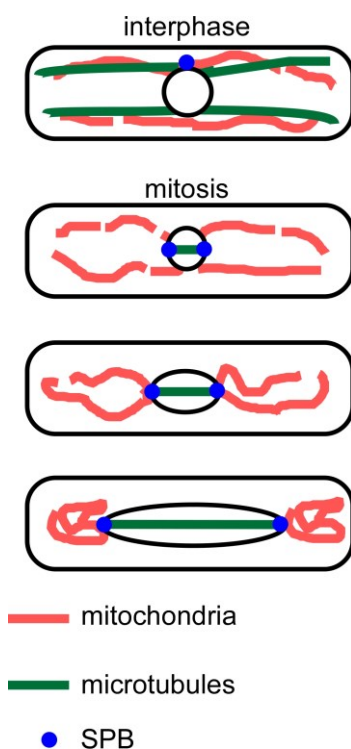


Figure 1-10 Mitochondrial distribution depends on MTs.

The dynamics of mitochondria are mediated by MT-associated proteins. This interaction is responsible for the movement as tubular structures in interphase cells. During mitosis the mitochondria are associated with SPBs. That ensures the segregation of mitochondria and affects both mitochondrial and spindle positioning.

During mitosis mitochondria associate with SPBs to ensure their segregation. This interaction is mediated by Mto1 which was suggested to mediate a binding of mitochondria to the cytoplasmic site of the SPBs (Kruger and Tolic-Norrelykke, 2008). Furthermore it has been shown that this interaction not only affects mitochondrial movements during mitosis, but that the association of mitochondria with the SPBs is crucial for the positioning of the mitotic spindle, as a loss of this association leads to an increased spindle rotation. It was proposed that mitochondria and the mitotic spindle are interdependent in terms of positioning during mitosis (Kruger and Tolic-Norrelykke, 2008) (Figure 1-10).

During my PhD thesis I analyzed the effects of inositol-pyrophosphates (IPPs) on KT-composition, chromosome segregation and spindle integrity. Therefore I will introduce these high-energy molecules in the following Chapter.

1.4 Inositol-pyrophosphates: production and significance

IPPs are high-energy molecules conserved in eukaryotes that regulate a number of cellular processes in several organism ranging from regulation of telomere length and resistance to salt-stress in *S. cerevisiae* (Dubois et al., 2002; Saiardi et al., 2005; York et al., 2005) to the jasmonate defense in *A. thaliana* (Laha et al., 2015) and the interferon response in humans (Pulloor et al., 2014). Our lab could furthermore identify a role of IPPs in regulation of the dimorphic switch in *S. pombe* and identified Asp1 as a modulator of the MT cytoskeleton in fungi (Pöhlmann and Fleig, 2010; Pöhlmann et al., 2014). Recently a role of IPPs in the sensing of cellular inorganic phosphates (Pi) has been proposed, which leads to an altered regulation of phosphate homeostasis (Wild et al., 2016).

The basic structure of IPPs is an inositol ring that is fully phosphorylated and in addition carries pyrophosphate groups at specific positions within the ring structure. These molecules are generated by two different kinases: IP₆ kinases and the highly conserved VIP1 inositol polyphosphate kinases (from here on out called VIP1 kinases) (Draskovic et al., 2008; Fridy et al., 2007; Lin et al., 2009; Mulugu et al., 2007; Saiardi et al., 1999). These enzymes catalyze the reactions from IP₆ to one of the IP₇ isomers: 5- or 1-IP₇ and further to 1,5-IP₈ ((Wilson et al., 2013); Figure 1-11).

Humans have three IP₆ kinases (IP6K1-3) which are catalyzing the reaction of IP₆ to 5-IP₇ *in vitro* and *in vivo* (Draskovic et al., 2008). The *S. cerevisiae* IP₆ kinase, Kcs1, also catalyzes the reaction of IP₆ to 5-IP₇ (Saiardi et al., 1999; Saiardi et al., 2001). IP₆ kinases can furthermore use IP₇ as a substrate to generate IP₈ (Figure 1-11; (Draskovic et al., 2008)).

The IP₇ generated by IP₆ kinases is then used as a substrate by VIP1 kinases to generate IP₈. Furthermore these enzymes can use IP₆ as a substrate to generate IP₇ (Fridy et al., 2007; Ingram et al., 2003; Mulugu et al., 2007; Thota and Bhandari, 2015). Members of the family of VIP1 kinases are conserved enzymes in yeast (VIP1 in *S. cerevisiae* and Asp1 in *S. pombe*) as well as in humans (PPIP5K1 and PPIP5K2). The structure of these enzymes is marked by two domains. An N-terminal ATP-grasp kinase domain and a C-terminal histidine acid phosphatase like domain. The kinase domain of these proteins is responsible for the generation of IPPs (Mulugu et al., 2007; Pöhlmann et al., 2014; Weaver et al., 2013). For human PPIP5K2 it was shown *in vitro* that it can use IP₆ and 5-IP₇ as substrates to generate 1-IP₇ or 1,5-IP₈, but that it has higher affinity to 5-IP₇ ((Wang et al., 2011; Weaver et al., 2013); Figure 1-11).

The function of the C-terminal domain was not identified until recently. It was already demonstrated in (Pöhlmann et al., 2014) that the C-terminal domain of *S. pombe* Asp1 negatively influenced the IP₇ amount generated by the Asp1 protein *in vitro*. Recently the pyrophosphorylation activity of the C-terminal domain has been demonstrated for *S. pombe* Asp1 *in vivo* and human PPIP5Ks *in vitro* ((Marina Pascual-Ortiz, unpublished data; (Gu et al., 2017; Wang et al., 2015); Figure 1-11)). Therefore it can be stated that VIP1 kinases are bifunctional enzymes. The *in vivo* data obtained by Marina Pascual-Ortiz will be introduced in more detail in the following Chapter (Page 39).

In vitro studies of (Wang et al., 2015) demonstrated that the Asp1 pyrophosphatase domain specifically dephosphorylates the 1-diphosphate group of both 1-IP₇ and 1,5-IP₈. Furthermore the authors showed that the pyrophosphatase activity of *S. pombe* Asp1 is negatively regulated by binding of a [2Fe-2S]²⁺-cluster to specific cysteine residues *in vitro*. Moreover, it has been demonstrated *in vitro* that the human VIP1 kinases PPIP5K1 and PPIP5K2 also have phosphorylation activities and dephosphorylate the 1-diphosphate group. PPIP5K2 shows a higher pyrophosphorylation activity than PPIP5K1 and both enzymes show a higher affinity towards 1,5-IP₈ than 1-IP₇. The authors demonstrated additionally that inorganic Pi inhibits the pyrophosphatase activity of human PPIP5Ks (Gu et al., 2017).

However, the mechanism of the regulation of the activity of the two domains is still under extensive research.

Another protein group, apart from VIP1 kinases, that can dephosphorylate IPPs, even though not specific, is that of diphosphoinositol-phosphate phosphohydrolases (DIPPs) ((Figure 1-11); (Wilson et al., 2013)).

The cellular levels of IP₆ in yeast and mammalian cells lie between 15-60 μM while IP₇ concentrations are with 0.5-5 μM lower. IP₈ levels are only found to be 10-20% of those of IP₇

in mammalian cells, while they are much higher in *S. pombe* (Ingram et al., 2003; Shears et al., 2011). The levels of 1-IP₇ in yeast and mammalian cells are with 0.05 μM very low and the two major pools of IPPs consist of 5-IP₇ and 1,5-IP₈ instead which indicates that the pathway over 5-IP₇ is favored in terms of IP₈ production *in vivo* (Gu et al., 2017; Lin et al., 2009)(Figure 1-11). Hence the main pool of IP₈ is generated from 5-IP₇ by VIP1 kinases as could recently also be shown for *S. pombe* Asp1 *in vivo* ((Figure 1-11) Marina Pascual-Ortiz; unpublished data).

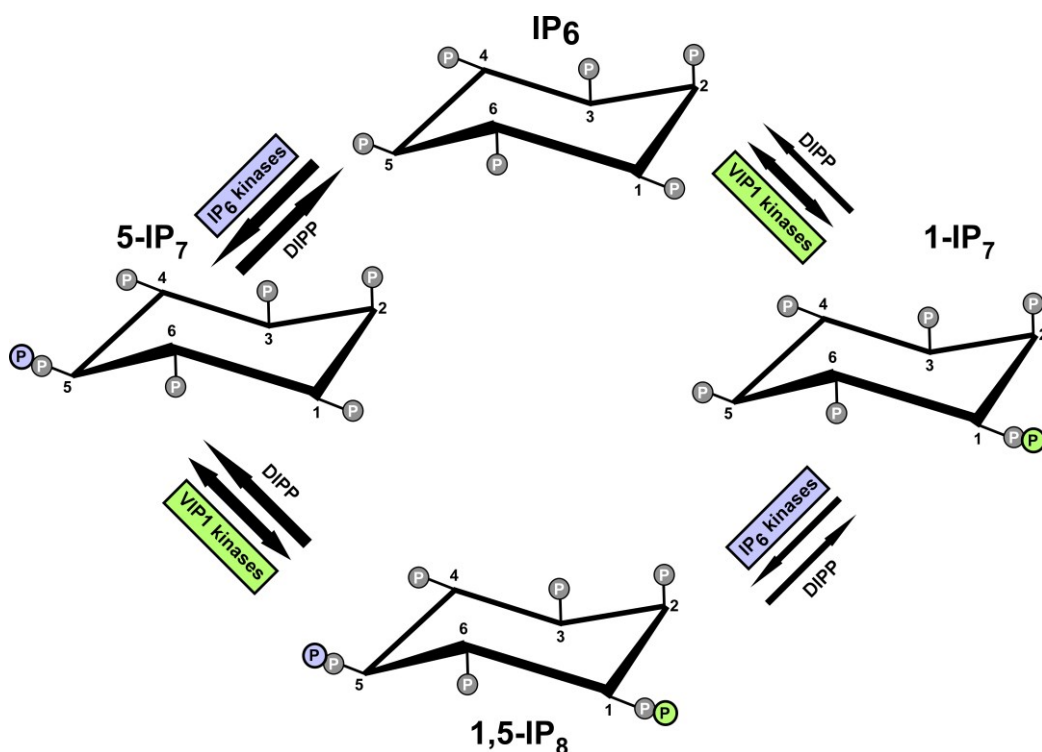


Figure 1-11 The generation of IPPs.

IP₆ is used as a substrate by IP₆- and VIP1 kinases to generate 5- or 1-IP₇, respectively. The produced isomer of IP₇ is converted into 1,5-IP₈. For this reaction VIP1 kinases use 5-IP₇ as a substrate, while IP₆ kinases use 1-IP₇. The pathway over 5-IP₇ to 1,5-IP₈ is the major pathway proposed to exist *in vivo*. IPPs can be dephosphorylated by DIPP. Recently it has been demonstrated that the pyrophosphatase domain of human and *S. pombe* VIP1 kinases can dephosphorylate 1-IP₇ and 1,5-IP₈.

It has been shown that IPPs can mediate their various cellular functions via two possible modes of action: pyrophosphorylation of a protein at a former phosphorylated serine residue (Bhandari et al., 2007; Saiardi et al., 2004) or direct binding to a target protein (Lee et al., 2007).

Such a modification is involved in the regulation of numerous cellular processes. It has been published that binding of Vip1 generated IP₇ to Pho81 is inhibiting the Pho80-Pho85 complex

and affects the response to phosphate starvation in *S. cerevisiae* (Lee et al., 2007). Another role of IPPs is in phosphate homeostasis regulation, which links them to the synthesis of the energy storage molecule poly-P (Auesukaree et al., 2005; Azevedo and Saiardi, 2017; Gerasimaite et al., 2017). It has been demonstrated that this regulation is mediated by a binding of IPPs to SPX domain containing proteins in *S. cerevisiae* (Wild et al., 2016). Furthermore, it has been shown that a binding of IP_8 to the Ask1-COI1-JAZ complex induces the jasmonate response in *Arabidopsis thaliana* (Laha et al., 2015).

A regulation of cellular processes by IPPs via pyrophosphorylation of a protein target was shown for human AP3B1, a protein involved in the release of HIV particles (Azevedo et al., 2009) and IRF3, which is regulating the interferon response (Pulloor et al., 2014). Moreover, Asp1-generated IPPs in *S. pombe* modulate the function of the mitotic spindle and chromosome segregation fidelity ((Topolski et al., 2016) and this thesis).

This underlines the significance of IPPs for a large number of cellular processes in different organisms and the importance of deciphering their exact mechanisms to get a better understanding of their modes of function.

As I worked with the VIP1 kinase of *S. pombe*, Asp1, I will introduce this protein in more detail.

1.4.1 Asp1 in *S. pombe*

Asp1 is the *S. pombe* VIP1 inositol polyphosphate kinase (Feoktistova et al., 1999; Mulugu et al., 2007). Like all members of this family it contains a specific dual-domain structure that includes a C-terminal kinase domain and an N-terminal pyrophosphatase domain. When I started my PhD thesis the function of Asp1 in terms of generating IPPs had only been analyzed *in vitro*. *In vitro* the kinase domain can generate IP_7 from IP_6 while the N-terminal phosphatase domain was shown to reduce the amount of IP_7 generated by Asp1 if it was present in the samples (Pöhlmann et al., 2014). Therefore Asp1 is a bifunctional enzyme.

Moreover, it was found that the resistance against the microtubule destabilizing drug thiabendazol (TBZ) was increased *in vivo* for Asp1 variants that generated more IPPs *in vitro*. Therefore the TBZ-resistance of *S. pombe* cells served as an *in vivo* readout for their cellular IPP-levels.

The bifunctional enzymatic function of Asp1 was recently verified by Marina Pascual-Ortiz, who studied the IPP-levels of *S. pombe* *in vivo* (unpublished data). For a better

understanding of the upcoming data I will shortly introduce the results obtained by Marina Pascual-Ortiz.

In vivo measurement of IP₆- to IP₈-levels was performed in strains expressing different *asp1*-variants and in these strains different IP₇ and IP₈ amounts were detected (Marina Pascual-Ortiz; unpublished data).

In addition to the wild-type (*asp1*⁺), an *asp1*^{D333A} strain was used. The Asp1^{D333A} protein carries a point mutation in the catalytic center of the kinase domain which abolishes the enzymatic function. The second endogenous *asp1*-variant used was *asp1*^{H397A}. The Asp1^{H397A} protein has a single amino acid exchange within the pyrophosphatase domain. This point mutation abolished the pyrophosphatase activity (Figure 1-12 A).

Furthermore, two plasmid-expressed *asp1*-variants were used. The first one was the kinase domain of *asp1*: *asp1*¹⁻³⁶⁴. The second one was the pyrophosphatase domain: *asp1*³⁶⁵⁻⁹²⁰ (Figure 1-12 A).

IP₇- and IP₈-levels generated by the Asp1 variants used were measured using HPLC. For this *S. pombe* cells were radiolabeled with [³H] inositol. Thereby, IPPs generated *in vivo* can be traced. In the HPLC elution profile a peak for every inositol polyphosphate species, namely IP₆, IP₇ and IP₈, was detected. To compare the IP₈-levels generated by different Asp1 variants to the levels generated by the wild-type (Asp1⁺) the cpm (counts per minute) values for IP₈ were normalized to IP₆ and the total amount of inositol polyphosphates labeled. As an example, the HPLC elution profile of the wild-type strain is shown in Figure 1-12 B.

The *asp1*^{D333A} expressing strain did not generate IP₈, while the *asp1*^{H397A} expressing strain generated 1.6-fold higher IP₈-level compared to the wild-type *asp1*⁺ strain (Figure 1-12 C).

Expression of *asp1*¹⁻³⁶⁴ (kinase domain) in an *asp1*⁺-background increased the cellular IP₈-levels 2.6-fold. Expression of *asp1*³⁶⁵⁻⁹²⁰ (pyrophosphatase domain) had the opposite effect. IP₈-levels were decreased (Figure 1-12 A; C).

Hence, the *in vivo* IP₈-output of different *asp1*-variants deviated from the wild-type levels of these molecules. The above presented *asp1*-variants were used in the course of this work.

After the analysis of the enzymatic function of Asp1 *in vivo* it was demonstrated that the IPPs generated by Asp1 are IP₈. Therefore also previously obtained results were due to an alteration of IP₈-levels.

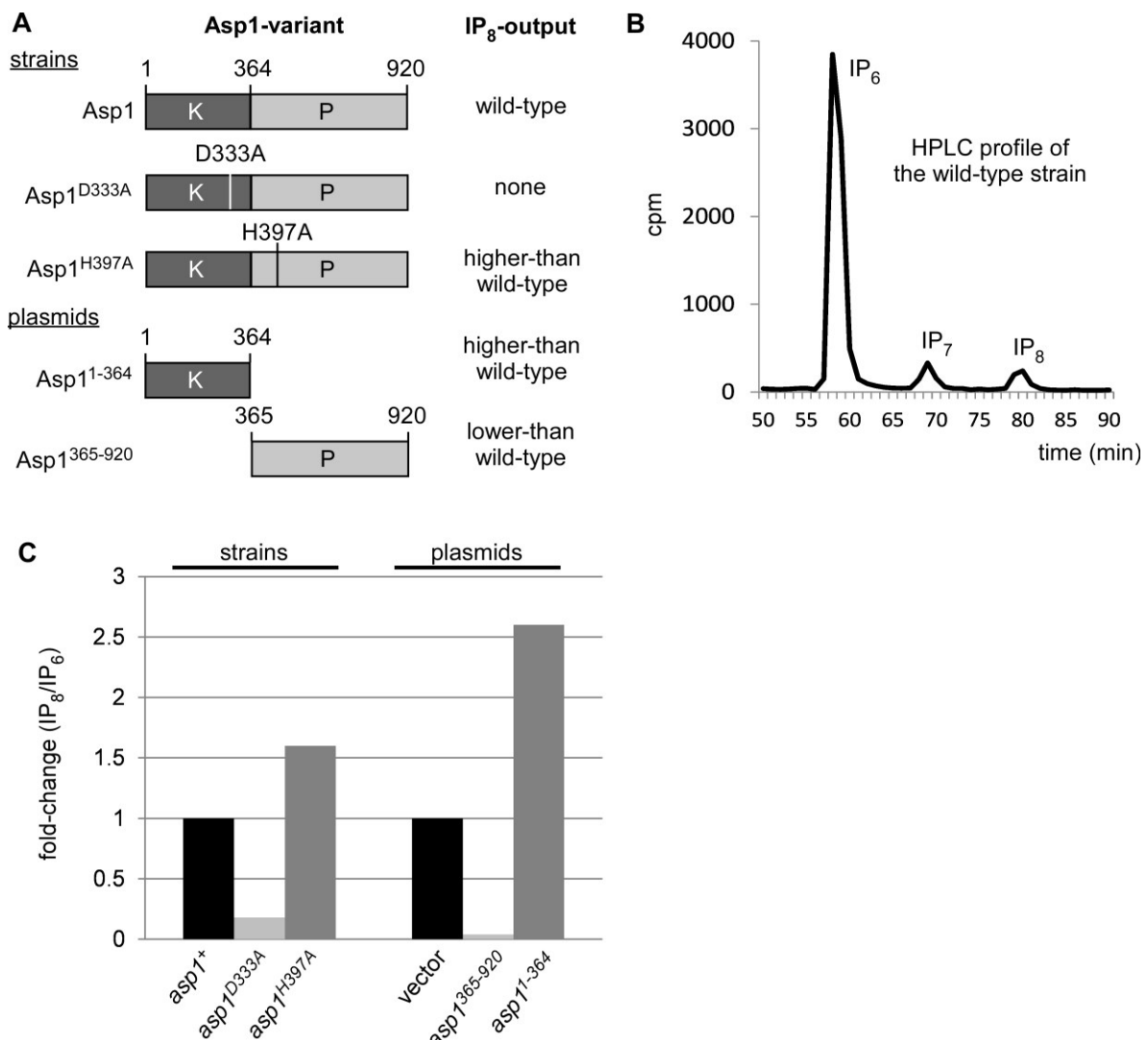


Figure 1-12 Cellular IP₈-levels are altered via expression of different *asp1*-variants.

A: Diagrammatic representation of the Asp1 protein variants used in this work and their *in vivo* IP₈-output. Top: *asp1*-variant strains encoding the indicated Asp1 proteins: Asp1, Asp1^{D333A} or Asp1^{H397A}. Bottom: plasmid-expressed *asp1*-variants: Asp1¹⁻³⁶⁴ (kinase domain) or Asp1³⁶⁵⁻⁹²⁰ (pyrophosphatase domain). **B:** HPLC elution profile of inositol polyphosphates from a wild-type strain. *S. pombe* cells were radiolabeled with [³H] inositol and cell lysates were separated using anion-exchange HPLC. **C:** Diagram of the fold-change of IP₈/IP₆ in the *asp1*-variants shown in A (cpm = counts per minute). Data from B and C kindly provided by Marina Pascual-Ortiz (unpublished).

1.4.1.1 Asp1-generated IP₈ regulates interphase microtubules and the mitotic spindle

It was shown in our lab that IP₈ is a modulator of the interphase MT cytoskeleton as well as the mitotic spindle (Pöhlmann et al., 2014; Topolski et al., 2016). An overview of the effects of IP₈ on these structures is shown in Figure 1-13. The absence of Asp1-generated IP₈ led to an increase in interphase MT dynamics and a decrease in stability. The early mitotic spindle

was aberrant in cells without Asp1-generated IP_8 in its overlap zone and frequently the spindle collapsed. Like for interphase MTs, higher dynamics could be observed also for the spindle MTs as spindle phases 1 and 3 were shorter than in cells with wild-type IP_8 -levels. The duration of spindle phase 2 however, in which bipolarity is established, was prolonged in the absence of Asp1-generated IP_8 . For cells with higher-than-wild-type IP_8 -levels it was found that the interphase MTs are less dynamic as in cells with wild-type levels of these molecules. Thus, the interphase MTs displayed a higher stability which was also found for the mitotic spindle. Spindle phase 2 was shortened in these cells compared to the wild-type, possibly indicating that these cells establish bipolar KT-MT attachments faster (Pöhlmann et al., 2014; Topolski et al., 2016).

IP_8 -levels	effect on interphase MTs	effect on spindle MTs
none	disorganized interphase MTs increased MT growth rate increased number of catastrophe events increased MT length reduced pausing time at cell tips	thin spindle midzone spindle collapses prior to chromosome segregation accelerated spindle elongation in spindle phases 1 and 3 SAC dependent delay of anaphase A (longer spindle phase 2)
higher-than wild-type	decreased MT shrinkage rate decreased number of catastrophe events increased MT length increased pausing time at cell tips	stable spindle midzones faster entry into anaphase A (shorter spindle phase 2)

Figure 1-13 Effects of Asp1-generated IP_8 on interphase MTs and the mitotic spindle.

Without Asp1-generated IP_8 interphase MTs were disorganized and showed accelerated MT dynamics that led to less stable MTs. Also the mitotic spindle was unstable but showed faster dynamics. Only spindle phase 2 was prolonged without Asp1-generated IP_8 . In cells with higher-than-wild-type IP_8 -levels the MTs in interphase were less dynamic but displayed a higher stability. The same was found for the mitotic spindle. Only spindle phase 2 was accelerated in the presence of higher-than-wild-type IP_8 -levels.

Thus, Asp1-generated IP_8 influences MTs in interphase and mitosis and is crucial for their stability and dynamics.

As part of my PhD work, I furthermore demonstrated that IP_8 regulates chromosome transmission fidelity. This part of my PhD work has been published: (Topolski et al., 2016).

1.5 Aim of this work

The aim of this work was to decipher the role of Asp1-generated IP₈ in the regulation of mitotic processes: in particular KT architecture, possible targets of IP₈ at the mitotic spindle and the effect of these high-energy molecules on chromosome transmission fidelity.

In the first part of this thesis I wanted to investigate if the regulation of spindle dynamics via IP₈ were linked to a MT-associated target of these molecules. Furthermore I set out to identify a possible pathway by which IP₈ modulates spindle dynamics.

Secondly I wanted to elucidate the influence of variations in cellular IP₈-levels on chromosome transmission fidelity and analyze if a modification of the Asp1 protein is affecting its role in this process.

In the third part the goal was to uncover the underlying mechanism of the effect of IP₈ on chromosome segregation. Therefore the influence of Asp1-generated IP₈ on the composition of the Sim4-KT-complex was studied. Furthermore it should be deciphered if compositional changes in Sim4-complex structure are localization and timing dependent. In the course of these experiments it was tested if different KT subcomplexes show the same reaction to changes in cellular IP₈-levels and if there are interdependencies among KT proteins.

Lastly, I set out to characterize interaction partners of the Asp1 protein to further narrow down the possible mode of action of Asp1. During these experiments I discovered a new link between the Asp1 protein, mitochondria and the KT-complex.

2 Material and Methods

2.1 Equipment

Electroporation	Gene Pulser Xcell BIO-RAD
qPCR	ABI PRISM 7000 Sequence Detection System
PCR	MJ Research PTC-200/ BIO-RAD C1000 Thermal Cycler
Microscopy	Zeiss Spinning Disc-Confocal microscope Nikon Eklipse Ti microscope Zeiss Axiovert microscope
Tetrad analysis	Singer MSM System 300 Singer Instruments
Cell lysis	Precellys24 Peqlab
DNA measurements	Nanodrop 2000c Peqlab
Blotting	Biometra Fastblot
Sonification	Bandelin Sonoplus
Gel documentation	Intas/ LTF
OD measurement	Photometer Eppendorf
Centrifugation	Biofuge Hereaus/ Multifuge X3R Thermo Scientific
Incubators	Infors/ Binder/ Hereaus

2.2 Chemicals

Chemical	Manufacturer
4',6-diamidino-2-phenylindole (DAPI)	Roche
4-(2-hydroxyethyl)-1-piperazineethanesulfonic acid (HEPES)	ROTH
3-(N-morpholino) propanesulfonic acid (MOPS)	Fluka
Acrylamid solution Rotiphorese-Gel 30; 37,5:1	ROTH
Adenine	Sigma Aldrich
Agarose	Biozym
Alanine	AppliChem
Ammonium sulfate ((NH ₄) ₂ SO ₄)	ROTH
Ampicillin	Sigma Aldrich
APS	Merck

Arginine	AppliChem
Aspartic acid	ROTH
β -glycerophosphate	AppliChem
Bacto Agar	BD
Bacto Malt extract	BD
BCIP	Sigma Aldrich
Biotin	Sigma Aldrich
Boric acid (H_3BO_3)	Sigma Aldrich
Bromophenol blue	AppliChem
BSA	Sigma Aldrich
Calcium chloride dihydrate ($\text{CaCl}_2 \times 2 \text{H}_2\text{O}$)	Grüssing
Calcium pantothenate	ROTH
Calcium sulphate dihydrate ($\text{CaSO}_4 \times 2 \text{H}_2\text{O}$)	ROTH
Carrier DNA	Sigma Aldrich
Chloroform	Fisher
Citric acid	AppliChem
Complete protease inhibitor	Roche
Coomassie Brilliant Blue	Serva
Copper sulfate pentahydrate ($\text{CuSO}_4 \times 5 \text{H}_2\text{O}$)	Sigma Aldrich
Cycloheximide	Sigma Aldrich
Cysteine	ROTH
Dimethylformamide (DMF)	Fisher
Dimethylsulfoxide (DMSO)	Merck
Dithiothreitol (DTT)	ROTH
Disodium hydrogen phosphate (Na_2HPO_4)	ROTH
Dorfmanite ($\text{Na}_2\text{HPO}_4 \times 2\text{H}_2\text{O}$)	ROTH
Ethanol	Chemical storage HHU
Ethylenediaminetetraacetic acid (EDTA)	AppliChem
Ethylene glycol bis-(aminoethyl ether) (EGTA)	Sigma Aldrich
Genetecin sulfate (G418)	Merck
Glucose	ROTH

Glutamic acid	Sigma Aldrich
Glutamine	ROTH
Glycerol	Fisher
Glycine	VWR
Histidine	Sigma Aldrich
Hydrochloric acid (HCl)	Sigma Aldrich
Hygromycin	Invivogen
Inositol	Sigma Aldrich
Iron (III) chloride hexahydrate ($\text{FeCl}_3 \times 6\text{H}_2\text{O}$)	Sigma Aldrich
Isoleucine	ROTH
Isopropanol	Chemical storage HHU
Kanamycin	Life Technologies
Lanoline	Sigma Aldrich
Leucine	AppliChem
Lithium acetate (LiAc)	ROTH
Lithium chloride (LiCl)	Merck
Lysine	Sigma Aldrich
Manga sulphate (MnSO_4)	Sigma Aldrich
Magnesium chloride hexahydrate ($\text{MgCl}_2 \times 6 \text{H}_2\text{O}$)	ROTH
Magnesium sulphate (MgSO_4)	Sigma Aldrich
Magnesium sulphate heptahydrate ($\text{MgSO}_4 \cdot 7\text{H}_2\text{O}$)	Grüssing
Methanol	Chemical storage HHU
Methionine	ROTH
Milk powder	ROTH
Molbdenum oxide (MoO_3)	Sigma Aldrich
Nicotinic acid	Sigma Aldrich
Nitro blue tetrazolium chloride (NBT)	Serva
Nonoxynol 40 (NP-40)	Sigma Aldrich
p-nitrophenylphosphate	Sigma Aldrich
Paraformaldehyde	Sigma Aldrich
Paraffine	Caesar & Loretz

para amino benzoic acid	Sigma Aldrich
Peptone	BD
Phenol-chloroform	ROTH
Phenylalanine	TCI
Phenylmethylsulfonyl fluoride (PMSF)	Serva
Phleomycin	Invivogen
Piperazine-N, N'-bis-(2-ethanesulfonic acid) (PIPES)	Sigma Aldrich
Polyethylene glycol (PEG)	Sigma Aldrich
Poly-L-lysine	Sigma Aldrich
Potassium acetate (KAc)	Grüssing
Potassium chloride (KCl)	ROTH
Potassium hydroxide (KOH)	Grüssing
Potassium iodide (KI)	Sigma Aldrich
Potassium phthalate monobasic	Sigma Aldrich
Proline	ROTH
Serine	ROTH
Sodium azide (NaN_3)	Sigma Aldrich
Sodium chloride (NaCl)	Fisher
Sodium citrate	AppliChem
Sodium deoxycholate	Sigma Aldrich
Sodium fluoride (NaF)	Sigma Aldrich
Sodium hydroxide (NaOH)	AppliChem
Sodium lauryl sulfate (SDS)	Sigma Aldrich
Sodium orthovanadate	Sigma Aldrich
Sodium pantothenic acid	Sigma Aldrich
Sodium phosphate	Sigma Aldrich
Sodium sulfate (Na_2SO_4)	Merck
Sorbitol	ROTH
Tetramethylethylene diamine (TEMED)	Merck
Thiabendazole	Sigma Aldrich
Thiamine	Sigma Aldrich

Threonine	ROTH
Tris(hydroxymethyl)aminomethane (Tris)	Honeywell
Triton X 100	AppliChem
Tryptone	BD
Tryptophane	ROTH
Tryosine	ROTH
Tween	AppliChem
Uracil	Sigma Aldrich
Valine	ROTH
Vaseline	Caesar & Loretz
Yeast extract	BD
Yeast nitrogen base	BD
Zinc sulfate heptahydrate ($\text{ZnSO}_4 \times 7 \text{H}_2\text{O}$)	Sigma Aldrich

2.3 Antibodies

Antibody	Manufacturer	Application	Dilution
<u>First antibodies:</u>			
monoclonal α -GFP	Roche	Western blot	1:1000; mouse
α - γ -tubulin	Sigma Aldrich	Western blot	1: 10000; mouse
α -GAPDH	Sigma Aldrich	Western blot	1:3000; mouse
anti-actin	Abersham	Western blot	1:4000; mouse
α -Asp1	K. Gould Lab	Western blot	1:100000; rabbit
α -Tat1 (tubulin)	(Woods et al., 1989)	IF	1:5
α -GFP A11122	Molecular Probes	ChIP	-
<u>Secondary antibodies:</u>			
α -mouse IgG	Promega	Western blot	1:7500
α -rabbit IgG	Promega	Western blot	1:7500
α -mouse Alexa Fluor®488	Molecular Probes	IF	1:200

Beads:

Protein A agarose beads	Roche	ChIP
α -GFP μ MACS beads	Miltenyi	IP

2.4 Enzymes and PCR-Kits

Enzyme/ PCR-Kit	Manufacturer
GoTaq qPCR Master Mix	Promega
Q5 High-Fidelity DNA polymerase	New England Biolabs
QuikChange II Site-Directed Mutagenesis Kit	Agilent
Taq DNA polymerase	Roche
EcoRI	Thermo Scientific
HindIII	Thermo Scientific
PacI	New England Biolabs
SmaI	Thermo Scientific
XhoI	Thermo Scientific
β -Glucuronidase	Roche
Lallzyme	Lallemand
Proteinase K	AppliChem
Zymolyase	Seikagaku
Taq DNA Polymerase	produced in the lab

2.5 Kits

Plasmid Midi Kit	Qiagen
Gel Extraction Kit Qiaquick	Qiagen

2.6 Other materials

Material	Manufacturer
Cover slips	Knittel Glas
Electroporation cuvettes	Sarstedt
Eppendorf tubes	Eppendorf
Falcon tubes	Sarstedt
Glass beads	ROTH
Immersion oil	Zeiss
PVDF membrane	VWR
MitoTracker Red CMXRos	Molecular Probes
Mounting solution Vectashield	Vector
μMAC columns	Miltenyi
Object slides	Diagonal
Petri dishes	Sarstedt
Pipet tips	Sarstedt
qPCR tubes and lids	Applied Biosystems
Whatman paper	VWR

2.7 Oligonucleotides

Number	Sequence 5' to 3'	Application
16	CTAGACTGAAAGAGCAACTGGA	verification <i>mal2⁺-gfp</i> tag fwd
98	GATAATGGACCTGTTAATCGA	sequencing backbone 270 fwd
99	ATCGTAATATGCAGCTTGAAT	sequencing backbone 270 rev
162	CAGCTCTAGCTGAATAGC	<i>ura4-v-5⁻-r</i>
217	AACAATAAACACGAATGCCTC	<i>cnt1</i> ChIP
218	ATAGTACCATGCGATTGTCTG	<i>cnt2</i> ChIP
219	GGCTACCAGCATTGTTATTCATAACC	<i>imr1</i> ChIP
221	CACATCATCGTCGTACTION	<i>otr1</i> ChIP
222	GATATCATCTATATTTAATGACTACT	<i>otr2</i> ChIP
223	AATGACAATTCCTCACTAGCC	<i>fbp1</i> ChIP

224	ACTTCAGCTAGGATTCACCTGG	fbp2 ChIP
228	GGATATATGTATTCTTGCACCTC	imr3 ChIP
261	ACGTGTCTTGTAGTTCCC	verification <i>gfp</i> tags fwd 1
302	CCTCGACATCATCTGCCC	verification <i>rpl42</i> ^(P56Q) / <i>SPCC594.01Δ</i> fwd 2
304	GGATGTATGGGCTAAATG	verification <i>SPCC594.01Δ</i> fwd 1
347	TAGATGATTCTAATGCTGCC	sequencing 1096
519	CGAAAGTTTGGAAATAGAAATC	sequencing 1232
520	GACTCTGAGGCAATTTGAGA	verification <i>asp1</i> mutations rev
547	GCATCACCTTCACCCTCTCC	verification <i>mis15</i> ⁺ - <i>gfp</i> fwd
608	CCTCTAAGATATCAATTGCG	sequencing 1231
672	GTCAGTCGTATGTGATTGC	verification <i>asp1</i> ^{D333A} fwd
673	GTCGGAGTCCTGCGTGC	verification <i>asp1</i> ^{H397A} fwd
694	TGCATTTACAATGCTTGGA	verification <i>rpl42</i> ⁺ <i>kan</i> fwd
777	CACCGGATTCAGTCGTCACCTC	verification <i>gfp</i> tags fwd 2
778	GATCCTGGTATCGGTCTGCG	verification <i>asp1</i> ¹⁻³⁶⁴ fwd
843	GAAAAACCCTAGCAGTACTGGCAAGGGA GACATTCCTTTTATTAATTAATGTAAACAG G	<i>asp1</i> in 270 fwd
948	GACAACCTGTTTAGCGTGTGCG	verification <i>aps1Δ</i> fwd
949	TGCTGGAATATATGCTGTACC	verification <i>aps1Δ</i> rev
1004	AATCTCATTCTCACTTTCTGACTTATAGTC GCTTTGTTAAATGATTCAAATGCAAGTCA	<i>asp1</i> in 270 rev
1005	AAAAACCCTAGCAGTACTGGCAAGGGAG ACATTCCTTTTATTATTTGTATAGTTCATC CA	<i>asp1-gfp</i> variants in 270 fwd
1408	CGCACTTAACTTCGCATCTG	sequencing <i>rpl42</i> plasmids 1
1421	AGTTCATCTTCCCAAAGGTTTATTCCTGT TAACATTAATCGGATCCCCGGGTTAATTA A	<i>asp1-gfp</i> variants in 270 rev
1423	TTATGATAATGCTGCTCG	verification <i>asp1</i> ¹⁻³⁶⁴ rev
1486	CGAAAACCGAGGACCTCTGC	sequencing GBP
1640	TTAAGTTGGGTAACGCCAGGG	sequencing <i>rpl42</i> plasmids 2
1677	GGGACAATTCAACGCGTCTG	<i>rpl42</i> ^(P56Q) veri fwd 1
1745	AAACCGGATTATCAACTGTATGTACGG GATGGGCTTGTCTACAAAGGCAGGAAA GTCTCGGACAACAAGAGATTAACCGGATC CCCGGGTTAATTA	tagging <i>mis15-68-gfp</i> fwd
1746	ATCGAATTAATCGTATTCATTATAAAAGTA CATTCCAACCTGCAGCGTGTATTTTTTACA GTGCGGATATTTAGCATGTCCGAATTCGA GCTCGTTTAAAC	tagging <i>mis15-68-gfp</i> rev
1747	TATTACTCTTGATCATGACT	verification <i>mis15-68-gfp</i> rev 1
1791	GAAGAAGGATGATGGTGCT	verification <i>mis15-68-gfp</i> rev 2
1825	CCCAAATCCAACCGTGAGAAGATG	act fwd qChIP
1826	CCAGAGTCCAAGACGATACCAAGTG	act rev qChIP
1827	CAGACAATCGCATGGTACTATC	cen1/3 fwd qChIP
1828	AGGTGAAGCGTAAGTGAGTG	cen1/3 rev qChIP
1852	GGAAACAGCTATGACCATG	sequencing <i>rpl42</i> plasmids 3
1857	GAAGAGTGGAAATCCCGAAGC	verification <i>mis15</i> ⁺ - <i>gfp</i> rev
1913	CCCATCCAAGGTTGCTGAACTATACGATA C	<i>asp1</i> ^{S674A} mutagenesis fwd
1914	GTATCGTATAGTTCAGCAACCTTGATGG	<i>asp1</i> ^{S674A} mutagenesis rev

	G	
2000	CCCATCCAAGGTTGAGGAACTATACGATAC	<i>asp1</i> ^{S674E} mutagenesis fwd
2001	GTATCGTATAGTTCCTCAACCTTGGATGGG	<i>asp1</i> ^{S674E} mutagenesis rev
2018	AGTCACGACGTTGTA AACGACGGCCAGTGCCAAGCTTGCAAATTTACTACAATAATTTT	cloning <i>rpl42</i> ⁺ in 222 fwd
2019	CGACTCTAGAGGATCCCCGGGTACCGAGCTCGAATTCGTA CTCTCGCTATTTTACGCTGT	cloning <i>rpl42</i> ⁺ in 222 rev
2034	AGGCTATTAATGCTGGGCTG	verification <i>met10</i> ⁺ - <i>gfp</i> rev 2
2039	TACCTTTAGCCAAACACCCTGGTACGCTAGTAAAAGACCGTATTTTGGAGAGGTAAAAGGGCCAAAGAGATCCTTGGAAGGCGCGCCACTTCTAAATAA	<i>SPCC594.01Δ</i> fwd
2040	CACAAAAAAGAGCAGTATTCGACGATACAAGACAAACCGCCATTAAGTCTAAAGAACA AAAAACAGGCCTAAATAATCGGAATTGAGCTCGTTTTAAAC	<i>SPCC594.01Δ</i> rev
2041	TTCTGGATTAAGAGAGGGG	verification <i>SPCC594.01Δ</i> rev 1
2042	AGGAACGATGATAGCTTCGG	verification <i>SPCC594.01Δ</i> rev 2
2062	AATCTCATTCTCACTTTCTGACTTATAGTCGCTTTGTTAAATGCAAGATTCTTCTCTTA	<i>ndc80</i> ⁺ in 270 fwd
2063	CCGCGGGGGCCCTACTGCAGGGCGCGCCTCGCGAGTCGACTTACAGTTCCGAACGAGATA	<i>ndc80</i> ⁺ in 270 rev
2078	GCGTAAAATAGCGAGAGTACGAATTCGAGCTCGGTACCCGATGGGTAAAAGCCTGAACT	cloning <i>rpl42</i> ⁺ <i>hyg</i> ^R in 222 fwd
2079	CATGATTACGCCAAGCTTGCATGCCTGCAAGTTCGACTCTATTATTCCTTTGCCCTCGGAC	cloning <i>rpl42</i> ⁺ <i>hyg</i> ^R in 222 rev
2080	GGTGGTCAAACCTAAGCAGGTTTTCCACAAAG	sequencing <i>rpl42</i> plasmids 4; mutagenesis fwd
2081	CTTGTGGAAAACCTGCTTAGTTTGACCACAC	mutagenesis <i>rpl42</i> ^(P56Q) rev
2082	CAAGGGTTTAGCAGAGAACTTTATGCTGTCGAGTTCCTAATCACCACCATCTAACCATCACTTATAAAAAGTATCAAAAATGGTGAACTTCCCAAGAC	insertion <i>rpl42</i> ^(P56Q) fwd
2083	AACAAATTTAGCAATTGAACAAGCGAACCCTTAGTTTTGCAAGGGAATTGTACACGTCGTACGCAGAAAAACAAGAACGTACGTTGCTTTAGTACCAAAA	insertion <i>rpl42</i> ^(P56Q) fwd
2139	GCAGTTATGATGAGCCAGTCGATGCTCGCAAGATCATTGAACAATGGAAGGAAGAGCGTCGTTTTGTCATCGAAGTTTACCGGATCCCCGGGTTAATTAA	tagging <i>met10</i> ⁺ - <i>gfp</i> fwd
2140	GGCATTGTCACAACCTAATGTGTAATAAACCTGAAAAGGTTTTAAATGAGTTTGATTGACATCTCCTTCTATAAGCTGAATTCGAGCTCGTTTTAAAC	tagging <i>met10</i> ⁺ - <i>gfp</i> rev
2141	GAGAAGAGTATCTGTATGGT	verification <i>met10</i> ⁺ - <i>gfp</i> rev 1
2142	AATCTCATTCTCACTTTCTGACTTATAGTC	<i>met10</i> ⁺ in 270 fwd

	GCTTTGTTAAATGGTTGCTACTGATTCTTC	
2143	CCGCGGGGGCCCTACTGCAGGGCGCGC CTCGCGAGTCGACCTAGTAACTTCGATG ACAA	<i>met10</i> ⁺ in 270 rev
2148	CCGAAGCTGATCCTGTCTCC	sequencing <i>met10</i> 1
2149	TCCTCCATCGCACCAGATGA	sequencing <i>met10</i> 2
2171	CAAGTACAGCGTAAAATAGCGAGAGTAC GAATTCGAGCTCCAGTATAGCGACCAGC ATTC	recloning <i>rpl42 hyg</i> in 222 1
2172	AGCATATTTGATGCTTTAGTGACATGGAG GCCAGAATAC	recloning <i>rpl42 hyg</i> in 222 2
2173	GTATTCTGGGCCTCCATGTCACTAAAGCA TCAAATATGCT	recloning <i>rpl42 hyg</i> in 222 3
2174	CGCCAAGCTTGCATGCCTGCAGGTGCAC TCTACGGGTACCCTTTTATAAACTCATTGA AG	recloning <i>rpl42 hyg</i> in 222 4
2212	CGATGGTAACAACACTAGTGAT	<i>rpl42</i> ^(P56Q) veri rev 2/ sequencing
2213	CGATTTATCTGGTACTGCAA	<i>rpl42</i> ^(P56Q) veri rev 1
2217	AGTTCATCTTCCCAAAGGTTTATTCCTGT TAACATTAATATGGATCAAGTCCAACCTGG T	cloning <i>asp1</i> -GBP variants fwd
2218	ATTGCTTTTAAATATTTAATTTTCATCGTTT TTTAATTAACAGTATAGCGACCAGCATTCC	cloning <i>asp1</i> -GBP variants rev
2221	TTTGAAAAAAGATTTCGTTTTTCAACATT TACCATCTCATTAAAGCTGAGCTGCCAAGG TATATACATACTTCATCGAATAAATTTACT ACAATAATTTT	insertion <i>rpl42</i> ⁺ locus kan + ble fwd
2222	TACAATCTAGAATTTCAAATAAAATATTA TTTAAACAAAAAGCAAGCAAATCATTTA ACAGTTATGTCTATGGTCGCGACATGGAG GCCAGAATAC	insertion <i>rpl42</i> ⁺ locus rev
2224	AATCTCATTCTCACTTTCTGACTTATAGTC GCTTTGTTAAATGGATCAAGTCCAACCTGG T	cloning GBP fwd
2241	CACATTTGTCAGCATGTTAACTAAGATAAA AGTAATCAAACAAGTACAGCGTAAAATAG CGAGAGTACGAATTCGAGCTCCAGTATAG CGACCAGCATTCC	marker change <i>rpl42</i> ⁺ locus kan to ble rev
2242	AGAACTCGACCGCTCCGGCG	veri <i>rpl42</i> ⁺ locus fwd
2243	GCAGCACATTATTCGGGGGG	veri <i>rpl42</i> ⁺ locus rev
2286	GTATCAAAGTATAGATATCA	verification <i>mph1Δ</i> rev

2.8 Plasmids

Number	Name, genes and markers	Application
148	pREP3X- <i>mal2</i> ⁺ - <i>LEU2</i> , <i>Amp</i> ^R , <i>nmt1</i> ⁺ promoter	expression vector
177	<i>KLG 1153</i> - <i>GFP</i> - <i>kan</i> ^R cassette	template <i>gfp kan</i> ^R cassette
264	pREP3x - <i>mph1</i> ⁺ , <i>nmt1</i> ⁺ promoter (Sazer Lab)	expression vector
270	pJR2-3XL - <i>LEU2</i> , <i>Amp</i> ^R , <i>nmt1</i> ⁺ promoter	expression vector, cloning backbone
272	pJR1-41XL - <i>LEU2</i> , <i>Amp</i> ^R , <i>nmt41</i> promoter	expression vector, cloning backbone

286	pJR2-41XU - <i>ura4⁺</i> , <i>Amp^R</i> , <i>nmt41</i> promoter	expression vector, cloning backbone
421	pFA6a-hphMX6 (10 μ l of \sim 100 ng/ μ l) (Hygromycin resistance) (Bahler et al., 1998)	template 1173
422	pFA6a-bleMX6 (10 μ l of \sim 100 ng/ μ l) (Phleomycin resistance) (Bahler et al., 1998)	marker change <i>rpl42⁺</i>
503	pJR2-3X L- <i>fta2⁺</i> - <i>LEU2</i> , <i>Amp^R</i> , <i>nmt1⁺</i> promoter	expression vector
553	pJR2-3XL- <i>sim4⁺</i> - <i>LEU2</i> , <i>Amp^R</i> , <i>nmt1⁺</i> promoter	expression vector
672	pJR2-3XL- <i>asp1^{1-364aa}</i> - <i>LEU2</i> , <i>Amp^R</i> , <i>nmt1⁺</i> promoter (York)	expression vector
754	pREP4XU- <i>fta2⁺</i> - <i>gfp</i> - <i>ura4⁺</i> , <i>Amp^R</i> , <i>nmt1⁺</i> promoter	expression vector
770	pJR2-3XL- <i>asp1¹⁻³⁶⁴</i> - <i>GFP</i> - <i>LEU2</i> , <i>Amp^R</i> , <i>nmt1⁺</i> promoter	expression vector
815	pJR2-3XL- <i>mal2⁺</i> - <i>fta2⁺</i> - <i>LEU2</i> , <i>Amp^R</i> , two <i>nmt1⁺</i> promoters	expression vector
875	<i>asp1⁺</i> - <i>kan^R</i> in pBsk ⁺	template mutagenesis
882	pJR2-3XL- <i>asp1⁺</i> - <i>LEU2</i> , <i>Amp^R</i> , <i>nmt1⁺</i> promoter	expression vector
883	pJR2-3XL- <i>asp1^{D333A}</i> - <i>LEU2</i> , <i>Amp^R</i> , <i>nmt1⁺</i> promoter	expression vector
884	pJR2-3XL- <i>asp1^{H397A}</i> - <i>LEU2</i> , <i>Amp^R</i> , <i>nmt1⁺</i> promoter	expression vector
887	pJR2-3XL- <i>asp1⁺</i> - <i>gfp</i> - <i>LEU2</i> , <i>Amp^R</i> , <i>nmt1⁺</i> promoter	expression vector
916	pJR2-3XL- <i>asp1^{365-920aa}</i> - <i>LEU2</i> , <i>Amp^R</i> , <i>nmt1⁺</i> promoter	expression vector
1035	pJR2-41XL- <i>mis15⁺</i> - <i>LEU2</i> , <i>Amp^R</i> , <i>nmt41</i> promoter	expression vector
1064	pJR2-3XL- <i>mis15⁺</i> - <i>LEU2</i> , <i>Amp^R</i> , <i>nmt1⁺</i> promoter	expression vector
1078	pFA6a-GBP-mCh-hyg (Dodgson et al., 2013)	template <i>gbp::mcherry hyg^R</i> cassette
1096	pBsk ⁺ - <i>asp1^{S674A}</i> :: <i>kan^R</i> - site directed mutagenesis S674A	template <i>asp1^{S674A}</i>
1099	pJR2-3XL- <i>asp1^{S674A}</i> - <i>LEU2</i> , <i>Amp^R</i> , <i>nmt1⁺</i> promoter	expression vector
1143	pJR2-3XL- <i>asp1^{S674A}</i> - <i>gfp</i> - <i>LEU2</i> , <i>Amp^R</i> , <i>nmt1⁺</i> promoter	expression vector
1152	pBsk ⁺ - <i>asp1^{S674E}</i> :: <i>kan^R</i> - site directed mutagenesis S674E	template <i>asp1^{S674E}</i>
1153	pUR19- <i>rpl42⁺</i> -locus	template 1156
1156	pUR19- <i>rpl42⁺</i> -locus- <i>kan^R</i>	template <i>rpl42⁺</i> -locus
1157	pJR2-3XL- <i>asp1^{S674E}</i> - <i>LEU2</i> , <i>Amp^R</i> , <i>nmt1⁺</i> promoter	expression vector
1167	pJR2-3XL- <i>ndc80⁺</i> - <i>LEU2</i> , <i>Amp^R</i> , <i>nmt1⁺</i> promoter	expression vector
1168	pJR2-3XL- <i>asp1^{S674E}</i> - <i>gfp</i> - <i>LEU2</i> , <i>Amp^R</i> , <i>nmt1⁺</i> promoter	expression vector
1173	pUR19- <i>rpl42⁺</i> -locus- <i>hyg^R</i>	template 1181
1181	pUR19- <i>rpl42^(P56Q)</i> -locus- <i>hyg^R</i>	template <i>rpl42^(P56Q)</i>
1208	pJR2-3XL- <i>SPCC584.01c</i> - <i>LEU2</i> , <i>Amp^R</i> , <i>nmt1⁺</i> promoter	expression vector
1227	pJR2-3XL- <i>asp1⁺</i> - <i>gbp::mCherry hyg^R</i> - <i>LEU2</i> , <i>Amp^R</i> , <i>nmt1⁺</i> promoter	expression vector
1229	pJR2-3XL- <i>gbp::mCherry hyg^R</i> - <i>LEU2</i> , <i>Amp^R</i> , <i>nmt1⁺</i> promoter	expression vector
1231	pJR2-3XL- <i>asp1^{D333A}</i> - <i>gbp::mCherry hyg^R</i> - <i>LEU2</i> ,	expression vector

	<i>Amp^R, nmt1⁺</i> promoter	
1232	pJR2-3XL- <i>asp1^{H397A}-gfp::mCherry</i> <i>hyg^R - LEU2, Amp^R, nmt1⁺</i> promoter	expression vector

2.9 Strains

2.9.1 *S. pombe* strains

Number	Genotype	Origin
40	<i>ade6-M210, leu1-32, h⁻</i>	U. Fleig
103	<i>ade6-M210, leu1-32, ura4-D6, mini-chromosome Ch¹⁶ [ade6-M216], h⁻</i>	Yanagida (10.2.2)
229	<i>cut7-446, leu1-32, h⁻</i>	I. Hagan 138
230	<i>cut7-24, leu1-32, h⁻</i>	I. Hagan 136
302	<i>pk11Δ::his3⁺, ade6-210, leu1-32, ura4-Dx, his3Δ, h⁻</i>	U. Fleig
518	<i>fta2-gfp::kan^R, ade6-210, leu1-32, ura4-D6, h⁻</i>	U. Fleig
547	<i>mal2-1-gfp::kan^R, ade6-M210, leu1-32, ura4-D18, h⁻</i>	U. Fleig
605	<i>his3-D1, ade6-M210, leu1-32, ura4-D18, h⁻</i>	K. Gould 425
845	<i>sim4-193, arg3-D4, ade6-210, his3-D1, ura4-D18, leu1-32, h⁺</i>	R. Allshire FY5231
852	<i>mal2-1, leu1-32, ade6-M210, ura4-D18, h⁻</i>	U. Fleig
974	<i>dad1-gfp::kan^R, leu1-32, ura4-D18, h⁺</i>	J. Millar
1027	<i>spc7-30::his3⁺, his3-D1, ade6-M216, leu1-32, ura4-D18, h⁺</i>	U. Fleig
1028	<i>spc7-23::his3⁺, his3-D1, ade6-M216, leu1-32, ura4-D18, h⁺</i>	U. Fleig
1029	<i>spc7-24::his3⁺, his3-D1, ade6-M216, leu1-32, ura4-D18, h⁺</i>	U. Fleig
1048	<i>fta2-291::his3⁺, his3⁻, leu1-32, ura4-D18, ade6-M210, h⁻</i>	U. Fleig
1058	<i>mal2⁻-gfp::kan^R, ade6-M210, leu1-32, ura4-Dx, his3-D1, h⁻</i>	U. Fleig
1065	<i>mis15-68, leu1-32, ura4-D18, ade6-M210, h⁻</i>	U. Fleig
1066	<i>mis15-68, leu1-32, ura4-D18, ade6-M210, h⁺</i>	U. Fleig
1067	<i>mis17-362, his-D1, leu1-32, ura4-D18, ade6-M210, h⁺</i>	U. Fleig
1122	<i>fta2-291::his3⁺, mal2-gfp::kan^R, leu1-32, ura4-, ade6-M210, his3-Dx, h⁻</i>	U. Fleig
1156	<i>asp1Δ::kan^R, his3-D1, ade6-M216, leu1-32, ura4-D18, h⁻</i>	U. Fleig
1244	<i>spc7-23-gfp::kan^R::his3⁺, his3-D1, ade6-M216, leu1-32, ura4-D18, h⁺</i>	U. Fleig
1503	<i>mis6-302, leu1⁻, ura⁻, ade⁻, h⁺</i>	M. Yanagida
1505	<i>mis12-537, leu1-32, ura⁻, his⁻, ade⁻, h⁻</i>	M. Yanagida
1511	<i>asp1^{D333A}::kan^R, his3-D1, ade6-M210, leu1-32, ura4-D18, h⁺</i>	U. Fleig
1577	<i>mal2-1, ade6-M210, leu1-32, ura4-D18, h⁻</i>	U. Fleig
1579	<i>asp1^{H397A}::kan^R, his3-D1, ade6-M210, leu1-32, ura4-D18, h⁺</i>	U. Fleig
1648	<i>ase1Δ::kan^R, leu1-32, ura⁻, h⁻</i>	U. Fleig
1687	<i>cut7-gfp::kan^R, cut12-CFP::nat^R, leu1, ura4, h⁻</i>	FY17673 (YGRC)
1929	<i>sos7-178::his3⁺, ade6-Mx, leu1-32, ura4-D18, his3-D1, h⁺</i>	U. Fleig
2118	<i>sad1-mCherry::kan^R, leu1, h⁻</i>	YGRC

2156	<i>leu1-32::SV40::atb2⁺-gfp[LEU2], his3-D1, h⁻</i>	U. Fleig
2163	<i>alp14Δ::kan^R, leu1-32, ura4, his3, h⁺</i>	U. Fleig
2237	<i>ndc80-21::kan^R, leu1, ura4, h⁻</i>	T. Toda KSH060
2242	<i>sad1-mCherry::kan^R, asp1^{D333A}::kan^R, LacI-GFP::his7⁺, LacO-repeat::lys1⁺, h⁻</i>	U. Fleig
2249	<i>sad1-mCherry::kan^R, LacI-gfp::his7⁺, LacO-repeat::lys1⁺, ura4-D18, leu1-32 h⁻</i>	U. Fleig
2252	<i>mis14-634, leu1⁻, h⁻</i>	FY20040 (YGRC)
2254	<i>nuf2-3::ura4⁺, leu1-32, ade6-M210, lys1⁻, ura4-D18, h⁻</i>	FY15680 (YGRC)
2279	<i>asp1^{H397A}::kan^R, leu1-32::SV40::atb2⁺-gfp[LEU2], h⁻</i>	U. Fleig
2280	<i>asp1^{D333A}::kan^R, leu1-32::SV40::atb2⁺-gfp[LEU2], his3-D1, h⁻</i>	U. Fleig
2337	<i>leu1-32::SV40::atb2⁺-gfp[LEU2], asp1^{D333A}::kan^R, mph1Δ::ura4⁺, ura4-D18</i>	U. Fleig
2338	<i>leu1-32::SV40::atb2⁺-gfp[LEU2], mph1Δ::ura4⁺, ura4-D18</i>	U. Fleig
2345	<i>mal2⁺-gfp::kan^R, asp1^{H397A}::kan^R leu1-32, ura4-18, his3-D1, h</i>	U. Fleig
2346	<i>mal2⁺-gfp::kan^R, asp1^{D333A}::kan^R leu1-32, ura4-18, his3-D1, h</i>	U. Fleig
2367	<i>sad1-mCherry::kan^R, asp1^{H397A}::kan^R LacI-gfp::his7⁺, LacO-repeat::lys1⁺, ura4-D18, leu1-32 h⁻</i>	U. Fleig
2369	<i>mal2^{T185P, K198R, L213R}::his3⁺ (mal2-30) his3-D1, ade6-M2xx, leu1-32, ura4-D18, h</i>	U. Fleig
2370	<i>fta2-gfp::kan^R asp1^{H397A}::kan^R, ade6-M210, leu1-32, ura4-D18, h</i>	U. Fleig
2372	<i>fta2-gfp::kan^R asp1^{D333A}::kan^R, his3-D1, ade6-M210, leu1-32, ura4-D18, h</i>	U. Fleig
2421	<i>klp5::kan^R, leu1, ura4, h⁻</i>	AR001 (NK07) T. Toda
2422	<i>klp6::kan^R, leu1, ura4, his2/7, h⁺</i>	AR018 T. Toda
2435	<i>alp14Δ::kan^R, leu1-32, ura4⁻, ade6-M210, h⁻</i>	U. Fleig
2478	<i>mis15-gfp [ura4⁺], leu1, ura4, h⁻</i>	FY10468 (M. Yanagida; (YGRC))
2490	<i>asp1^{D333A}::kan^R, mis15-gfp [ura4⁺], ura4-D18, leu1-32, h⁺</i>	This study
2491	<i>asp1^{H397A}::kan^R, mis15-gfp [ura4⁺], ura4-D18, leu1-32, ade6-M210, h⁻</i>	This study
2519	<i>mis15-68-gfp::kan^R ade6-M210, leu1-32, ura4-D18, h⁻</i>	This study
2520	<i>asp1^{H397A}::kan^R mph1Δ::ura4⁺. leu1-32::SV40-atb2⁺-gfp[LEU], ura4-D18, h⁻</i>	This study
2531	<i>mal2-1 mis15-68, leu1-32, ura4-D18, ade6-M210, h⁻</i>	This study
2532	<i>mal2-1 mis15-68, leu1-32, ura4-D18, ade6-M210, h⁺</i>	This study
2536	<i>mal2-1 dad1-gfp::kan^R, leu1-32, ade6-M210, ura4-D18, h⁺</i>	This study
2537	<i>mis15-68 dad1-gfp::kan^R, leu1-32, ura4-D18, ade6-M210, h⁺</i>	This study
2578	<i>asp1^{D333A}::kan^R, mis15-68-gfp::kan^R his3?, ade6-M210, leu1-32, ura4-D18, h⁻</i>	This study
2579	<i>asp1^{D333A}::kan^R, mis15-68-gfp::kan^R his3?, ade6-M210, leu1-32, ura4-D18, h⁺</i>	This study
2585	<i>hpm1Δ::"gfp"::kan^R, ade6-M210, leu1-32, h⁻</i>	U. Fleig
2587	<i>SPBC725.03Δ::"gfp"::kan^R, ade6-M210, leu1-32, h⁻</i>	U. Fleig
2605	<i>hpm1Δ::"gfp"::kan^R, mis15-68, leu1-32, ade6-M210, ura4-D18, h⁺</i>	This study

2622	<i>mal2^{F77L;V111A}::his3⁺ (mal2-10) his3-D1, ade6-M2xx, leu1-32, ura4-D18, h⁺</i>	U. Fleig
2627	<i>mph1Δ::ura4⁺, LacI-gfp::his7⁺, LacO-repeat::lys1⁺, sad1-mCherry::kan^R, leu1-32, ura4-Dx, lys1-131, h⁻</i>	This study
2628	<i>asp1^{H397A}::kan^R, mph1Δ::ura4⁺, ura4-Dx, leu1-32, lys1-131, his7-366, LacI-gfp::his7⁺, LacO-repeat::lys1⁺, sad1-mCherry::kan^R, h⁻</i>	This study
2646	<i>asp1^{D333A}::kan^R, mph1Δ::ura4⁺, LacI-gfp::his7⁺, LacO-repeat::lys1⁺, sad1-mCherry::kan^R, lys1-131, ura4-Dx, leu1-32, h⁻</i>	This study
2647	<i>SPBC725.03Δ::gfp⁺::kan^R, mis15-68, leu1-32, ura4-D18, ade6-M210, h⁺</i>	This study
2686	<i>SPCC594.01Δ::kan^R, his3-D1, ade6-M210, leu1-32, ura4-D18, h⁻</i>	This study
2728	<i>ndc80-21::kan^R, leu1-32::SV40::atb2⁺-gfp [LEU2], ura4-D18, h⁻</i>	This study
2733	<i>ndc80⁺-GFP::ura4⁺ sad1⁺::DsRed-LEU2 ade6-M216, ura4-D18, leu1-32, h⁹⁰</i>	FY15690 (YGRC)
2734	<i>ndc80⁺-gfp::ura4⁺ ade6-M216, ura4-D18, leu1-32, his3-D1, h⁺</i>	This study
2747	<i>asp1^{H397A}::kan^R, ndc80-21::kan^R, leu1-32::SV40::atb2⁺-gfp [LEU2], his3-D1, ade6-M210, leu1-32, ura4-D18, h⁻</i>	This study
2749	<i>asp1^{H397A}::kan^R ndc80⁺-gfp::ura4, his3-D1, leu1-32, ura4-D18, h⁻</i>	This study
2761	<i>asp1^{D333A}::kan^R, ndc80⁺-gfp::ura4⁺, his3-D1, ade6-, leu1-32, ura4-D18, h⁺</i>	This study
2795	<i>SPCC584.01c-gfp::kan^R, his3-D1, ade6-M210, leu1-32, ura4-D18, h⁻</i>	This study
2796	<i>SPCC584.01c-gfp::kan^R, his3-D1, ade6-M210, leu1-32, ura4-D18, h⁺</i>	This study
2855	<i>rpl42^(P56Q)::hyg^R, his3-D1, ade6-M210, leu1-32, ura4-D18, h⁻ (Cycloheximide resistant)</i>	This study
2908	<i>cox4-rfp:LEU2 ade6-M210 leu1-32 ura4-D18 h⁻</i>	Tran 2011 (PT. 1651)
2929	<i>rpl42^(P56Q)::hyg^R, ade6-M210, (Cycloheximide resistant), Yanagida mini-chromosome Ch¹⁶[ade6-M216], h⁻</i>	This study
2954	<i>mal2⁺-gfp::kan^R, asp1¹⁻³⁶⁴::kan^R, ade6-, leu1-32, ura4-Dx, his3-D1, h⁺</i>	This study
2960	<i>rpl42^(P56Q)::hyg^R, ade6-M210, (Cycloheximide resistant), Yanagida mini-chromosome Ch¹⁶[ade6-M216Δ::rpl42⁺-kan^R](CHX sensitive), h⁻</i>	This study
2962	<i>sad1-mCherry::kan^R SPCC584.01c-gfp::kan^R, his3-D1, ade6-M210, leu1-32, ura4-D18, h⁺</i>	This study
2968	<i>cox4-rfp:LEU2 mal2⁺-gfp::kan^R leu1-32, ura4-Dx his3-D1, h⁺</i>	This study
2969	<i>cox4-rfp:LEU2 mal2⁺-gfp::kan^R, asp1¹⁻³⁶⁴::kan^R, leu1-32, ura4-Dx, his3-D1, h⁺</i>	This study
2992	<i>rpl42^(P56Q)::hyg^R, ade6-M210, (Cycloheximide resistant), Yanagida mini-chromosome Ch¹⁶[ade6-M216Δ::rpl42⁺-ble^R](CHX sensitive), h⁻</i>	This study
3009	<i>mal2-1-GFP::kan^R, leu1-32, ura4-D18, ade6-M210, h⁻</i>	This study

YGRC: Yeast Genetic Resource Center; Japan

2.9.2 *S. cerevisiae* strains

Strain	Genotype	Origin
CenPK	<i>Mata, leu2-3, 112, ura3-52, trp1-289, his3Δ1, MAL2-8c, SUC2</i>	AG Hegemann

2.9.3 *E. coli* strains

Strain	Genotype	Origin
XL1-blue	<i>recA1, lac⁻, endA1, gyrA46, thi, hsdR17, supE44, relA1, F' [proAB⁺, lac^q, lacZΔM15, Tn (tet^r)]</i>	Stratagene

2.10 Media and cultivation

2.10.1 *S. pombe* media

Full medium (YE5S)

10 g	Yeast extract
20 ml	Histidine (7.5 mg/ ml)
20 ml	Leucine (7.5 mg/ ml)
150 ml	Adenine (2.7 mg/ ml adenine hemisulfate)
75 ml	Uracil (2 mg/ ml)
20 ml	Lysine (7.5 mg/ ml)
1515 ml	dH ₂ O
2 L	

Media was prepared and autoclaved. For solid media 20 g/ L Bacto agar was added. After autoclavation separately autoclaved glucose was added to an end concentration of 3 %.

Minimal medium (MM)

5.5 g	Na ₂ HPO ₄ x 2H ₂ O
6 g	Potassium phthalate monobasic
2 g	Glutamic acid
40 ml	Saltstock
2 ml	Vitaminestock
0.2 ml	Mineralstock
1760 ml	dH ₂ O
2 L	

Media was prepared and autoclaved. For solid media 20 g/ L Bacto agar was added. After autoclavation separately autoclaved glucose was added to an end concentration of 4 %. Depending on the application the media was supplemented with the following aminoacids: arginine, leucine, lysine, histidine, uracil and adenine (end concentration: 75 µg/ ml) (Moreno et al., 1991).

Saltstock

21.4 g	MgCl ₂ x 6H ₂ O
0.29 g	CaCl ₂ x 2H ₂ O
20 g	KCl
0.8 g	Na ₂ SO ₄
ad 400 ml	dH ₂ O

Stock solution was autoclaved and stored at 4°C.

Vitaminestock

1 g	Sodium pantothenic acid
10 g	Nicotinic acid
10 g	Inositol
10 mg	Biotin
ad 1 L	dH ₂ O

Stock solution was autoclaved and stored at 4°C.

Mineralstock

5 g	H ₃ BO ₃
4 g	MnSO ₄
4 g	ZnSO ₄ x 7H ₂ O
2 g	FeCl ₂ x 6H ₂ O
4 g	MoO ₃
1 g	KI
4 g	CuSO ₄ x 5H ₂ O
10 g	Citric acid
ad 1 L	dH ₂ O

Stock solution was autoclaved and stored at 4°C.

The following additives were added to YE5S or MM media after autoclavation if necessary:

Additive	Purpose	Storage
5 µg/ ml thiamine (stock 10 mg/ ml in ddH ₂ O)	Regulation of expression of genes under control of <i>nmt</i> -promoters	RT
TBZ (stock 10 mg/ ml in DMF)	Screening for TBZ-sensitivity	-20°C
100 µg/ ml G418 (Geneticin disulfate in ddH ₂ O)	Screening for <i>kan^R</i> marker	4°C

The media was cooled down to ~ 50°C before addition (Moreno et al., 2000).

Malt medium

30 g	Bacto malt extract
75 mg	Histidine
75 mg	Leucine
75 mg	Adenine
75 mg	Uracil
1 L	dH ₂ O

The pH was adjusted with 10 M NaOH to 5.5 prior to autoclaving. For solid media 20 g/ L Bacto agar was added.

2.10.2 *S. cerevisiae* media

Synthetic defined media (SD)

1.7 g	Yeast nitrogen base
5 g	Ammonium sulfate
2 g	Drop-out mix
900 ml	dH ₂ O

The pH was adjusted with 10 M NaOH to 5.5 prior to autoclaving. For solid media 20 g/ L Bacto agar was added. After autoclavation separately autoclaved glucose was added to an end concentration of 2 %.

Drop-out mix

0.2 g	para amino benzoic acid
0.5 g	Adenine
2 g each	Alanine, arginine, aspartic acid, cysteine, lysine, methionine, phenylalanine, proline, glutamine, glutamic acid, histidine, inositol, isoleucine, serine, threonine, tyrosine, uracil, valine

Depending on the application the media was additionally supplemented with leucine (75 µg/ ml) or tryptophan (50 µg/ ml).

Full medium (YPD)

20 g	peptone
10 g	Bacto yeast extract
2 ml	Adenine (2.7 mg/ ml adenine hemisulfate)
4 ml	Tryptophane (5 mg/ ml)
1 L	dH ₂ O

For solid media 27 g/ L Bacto agar was added. After autoclavation separately autoclaved glucose was added to an end concentration of 4 % (Kaiser et al., 1994).

2.10.3 *E.coli* media

Lysogeny broth medium (LB)

10 g	Tryptone
5 g	Bacto yeast extract
5 g	NaCl
1 L	dH ₂ O

For solid media 20 g/ L Bacto agar was added. After autoclavation separately autoclaved glucose was added to an end concentration of 4 %.

Depending on the application the media was supplemented with ampicillin (50 µg/ ml) or kanamycin (12.5 µg/ ml).

2.11 DNA preparations

2.11.1 DNA preparation from *S. pombe*

Genomic DNA was isolated using the following protocol (Moreno et al., 1991):

- Overnight culture grown in 8 ml YE5S at the required temperature.
- Centrifugation for 5 min at 3000 rpm followed by resuspending of the cells in 1 ml SP1 with 25 mg freshly added Zymolyase.
- Incubation for 45 min at 37°C. Formation of spheroplasts checked under the microscope.
- Centrifugation for 5 min at 6000 rpm.
- Pellet resuspended in 450 µl 5x TE.

- Addition of 50 μ l 10 % SDS. 5 min incubation at RT.
- Addition of 150 μ l 5 M KAc. Incubation for 10 min on ice.
- Centrifugation for 10 min at 13000 rpm. Supernatant transferred to fresh tube.
- Addition of 1 V isopropanol. Centrifugation for 3 min at 13000 rpm.
- Pellet washed with 500 μ l 70 % EtOH.
- Pellet resuspended in 250 μ l 5x TE with 2 μ l freshly added RNase (10 mg/ ml).
- Incubation for 20 min at 37°C.
- Addition of 2 μ l 10 % SDS and 2 μ l 5 mg/ ml Proteinase K.
- Incubation for 1 h at 55°C.
- Phenol-chloroform extraction (1:1 V) followed by chloroform-extraction (1:1 V). Centrifugation for 8 min at 13000 rpm. Upper fraction transferred to fresh tube.
- Addition of 1:10 V 3 M NaAc pH 5.1 and 2.5:1 V 96 % EtOH.
- Centrifugation for 30 min at 13000 rpm.
- Pellet washed with 500 μ l 70 % EtOH.
- Centrifugation for 10 min at 13000 rpm.
- Pellet resuspended in 30 μ l 1x TE.

SP1		5x TE	
1.2 M	Sorbitol	50 mM	Tris pH 8
50 mM	Sodium citrate	5 mM	EDTA pH 8
50 mM	Sodium phosphate	50 mM	Sodium phosphate
40 mM	EDTA	40 mM	EDTA
pH was adjusted to 5.6. Buffer was stored at RT.		Buffer was stored at RT.	

2.11.2 DNA preparation from *S. cerevisiae*

Plasmid DNA was isolated using the following protocol (alkaline lysis method; modified from: (Birnboim and Doly, 1979)):

- Overnight culture grown in 5 ml SD at 30°C.
- Centrifugation of 2 ml of culture for 5 min at 3500 rpm.
- Cells washed twice with 2 ml dH₂O.
- Pellet resuspended in 0.5 ml P1.
- Addition of 0.5 ml P2. Inverted 4-6 times.
- Addition of ~ 2/3 volume glass beads.

- Lysis of cells in Precellys (2x 2000 U for 20 sec). Cells kept on ice.
- Centrifugation for 2 min at 2000 rpm.
- 1 ml supernatant transferred into fresh tube.
- Addition of 0.5 ml P3. Inverted 4-6 times.
- Incubation on ice for 10 min.
- Centrifugation for 15 min at 13000 rpm.
- 750 μ l supernatant transferred into a fresh tube, addition of 1 V isopropanol. Vortexed.
- Centrifugation for 30 min at 13000 rpm.
- Pellet washed with 70 % EtOH. Pellet air-dried.
- DNA resuspended in 20 μ l dH₂O.

P1	
50 mM	Tris/ HCl pH 8
100 mM	EDTA
100 μ g/ ml	RNase

Buffer was stored at 4°C.

P2	
200 mM	NaOH
1 %	SDS

Buffer was stored at RT.

P3	
3 M	Potassium acetate pH 5.5

Buffer was stored at RT.

2.11.3 DNA preparation from *E. coli*

Mini-Preparation (alkaline lysis method (Maniatis et al., 1989)):

- Overnight culture grown in 2 ml LB + required antibiotic (amp or kan) at 37°C.
- Centrifugation of 1.5 ml culture for 1 min at 13000 rpm.
- Supernatant discarded and pellet resuspended in 250 μ l P1.
- Addition of 250 μ l P2. Inverted 4-6 times.
- Incubation for 5 min at RT.
- Addition of 250 μ l P3. Inverted 4-6 times.
- Incubation for 5 min on ice.
- Centrifugation for 10 min at 13000 rpm.

- 700 μ l supernatant transferred into fresh tube.
- Addition of 1 V isopropanol. Vortexed.
- Centrifugation for 10 min at 13000 rpm.
- Pellet washed with 70 % EtOH and air-dried.
- Pellet resuspended in 100 μ l dH₂O, incubation for 15 min at 65°C. Vortexed.
- 3 μ l solved DNA used for restriction enzyme analysis.

For higher DNA yields a Qiagen Midi Kit was used according to manufacturers instructions.

2.11.4 DNA sequencing

Sequences of cloned plasmids or constructed strains were verified via GATC Sanger sequencing. The samples were prepared according to the protocol of the GATC Biotech Sanger sequencing service.

2.12 Transformation

2.12.1 Transformation in *S. pombe*

The LiAc method (Okazaki et al., 1990) was used for transformation of *S. pombe* cells. The protocol was modified if PCR products were transformed to achieve an endogenous homologous recombination (Fennessy et al., 2014).

- Overnight cultures were grown in 100-200 ml YE5S at 25°C or 30°C.
- Centrifugation of 1×10^8 cells/ transformation for 3 min at 3500 rpm.
- Cells washed with 0.1 M LiAc pH 4.9. Centrifugation for 3 min at 3500 rpm.
- Cells resuspended in 70 μ l 0.1 M LiAc/ transformation.
- Incubation for 1 h at 25°C or 30°C.
- Addition of 0.5 μ g plasmid DNA or PCR-product + 2 μ l carrier DNA (10 mg/ ml) for endogenous homologous recombination.
- Addition of 290 μ l 50% PEG₄₀₀₀. Resuspended carefully.
- Incubation for 1 h at 25°C or 30°C.
- Heat-shock for 15 min at 43°C.
- Samples cooled down for 2 min at RT.
- Centrifugation for 5 min at 3500 rpm.

- Cells resuspended in 1 ml YE5S (MSL-N for endogenous homologous recombination).
- Incubation for at least 1 h at 25°C or 30°C (16 h for endogenous homologous recombination).
- Cells washed twice with 1 ml dH₂O.
- Centrifugation in between for 2 min at 3000 rpm.
- Cells resuspended in 1 ml dH₂O.
- 1x 50 µl and 1x 100 µl plated on selective plates.

1x MSL-N

10 g	Glucose
2 g	Arginine
1 g	KH ₂ PO ₄
0.1 g	NaCl
0.2 g	MgSO ₄ x 7H ₂ O
0.1 g	CaSO ₄ x 2 H ₂ O
500 µg	Boric acid
50 µg	CuSO ₄ x 5H ₂ O
100 µg	KI
200 µg	FeCl ₃ x 6H ₂ O
500 µg	MnSO ₄ x 4H ₂ O
150 µg	MoO ₃
400 µg	ZnSO ₄ x 7H ₂ O
10 µg	Biotin
100 µg	Calcium pantothenate
1 mg	Nicotinic acid
1 mg	Meso-inositol
1 L	dH ₂ O

Medium was stored on RT (Egel et al., 1994).

2.12.2 Transformation in *S. cerevisiae*

The LiAc method was used for transformation of *S. cerevisiae* cells (Gietz R.D., 2006).

- Overnight cultures grown in 5 ml YPD at 30°C.
- 50 ml YPD were inoculated with the overnight culture to an OD₆₀₀ of 0.1-0.2.

- Incubation on shaker at 30°C for 4-5 h.
- OD was measured.
- Centrifugation at 3500 rpm for 5 min.
- Cells washed with 25 ml dH₂O and resuspended in 1 ml 0.1 M LiAc pH 8.4-8.9.
- Centrifugation for 10 sec at 13000 rpm. Supernatant discarded.
- Cells resuspended at 2 x 10⁹ cells/ ml in 0.1 M LiAc pH 8.4-8.9.
- 50 µl/ transformation centrifuged for 10 sec at 13000 rpm. Supernatant discarded.
- Addition of:
 - 240 µl 50 % PEG₃₃₅₀
 - 36 µl 1 M LiAc pH 8.4-8.9
 - 50 µl boiled cold carrier DNA (2 mg/ ml)
 - 34 µl DNA diluted in dH₂O
- Vortexed until pellet dissolved.
- Incubation at 30°C for 30 min.
- Heat-shock at 42°C for 30 min.
- Centrifugation for 10 sec at 13000 rpm. Supernatant discarded.
- Pellet resuspended in 200 µl dH₂O. 10 % and 90 % plated on plasmid-selective plates.

2.12.3 Transformation in *E. coli*

2.12.3.1 1' Transformation in *E. coli*

The protocol was modified from (Golub, 1988):

- DMSO-competent cells thawed on ice.
- Addition of 0.5-1 µg DNA to 3 µl cells.
- Heat-shock at 42°C for 1 min.
- Addition of 100 µl LB. Cells plated.

2.12.3.2 Electroporation in *E. coli*

The protocol was modified from (Dower et al., 1988):

- Electro-competent cells thawed on ice.
- Addition of 1-5 µl plasmid DNA (for plasmid isolation from *S. cerevisiae* diluted in 200 µl dH₂O).

- Sample transferred to electroporation cuvette.
- Sample electroporated at 2.1 kV, 200 Ω , 25 μ F.
- Addition of 1 ml LB to the cuvette.
- Transferred to tube.
- Incubation for 1 hour at 37°C with shaking.
- Centrifugation for 2 min at 13000 rpm. Discard supernatant.
- Pellet resuspended in 200 μ l LB. Vortexed.
- 10 % and 90 % plated on selective media.

2.13 Serial dilution patch test

- Overnight cultures grown in 5 ml YE5S or plasmid-selective media. In case of plasmid expression of a gene under control of *nmt*-promoters one culture was grown with and one without thiamine for 24 h at the required temperature.
- Dilution of every culture to 2×10^6 cells/ ml. Dilution series with 2×10^5 , 2×10^4 , 2×10^3 cells/ ml was prepared.
- 5 μ l of each dilution patched on the required media.

2.14 Survival rate

- Overnight cultures grown in 5 ml plasmid-selective media. One culture was grown with and one without thiamine for 24 h at the required temperature to regulate the expression via the *nmt1*⁺-promoter.
- Certain number of cells plated on plasmid-selective plates.
- Growing colonies counted after several days of incubation at the required temperature.

2.15 Minichromosome loss assay

The minichromosome loss assay was done based on the color assay published in (Niwa et al., 1989).

- Overnight cultures grown in 20 ml MM - adenine - leucine. Cultures were grown once with and once without thiamine at 25°C.
- 30×1000 cells were plated on MM - leucine + 5 μ g/ ml adenine + thiamine or MM - leucine + 5 μ g/ ml adenine - thiamine plates.

- Incubation for 10 days at 25°C.
- White, sectored and red colonies were counted.

2.16 PCR

2.16.1 Colony-PCR

Colony-PCR was used to verify markers, mutations or deletions in *S. pombe* strains. A cell suspension was used as template for the reaction.

Reaction mix		Cycler program	
10 µl	Cell suspension	94°C	10 min
12.8 µl	ddH ₂ O	35 cycles:	
3 µl	10x Taq buffer	94°C	1 min
1.5 µl	4 mM dNTPs	T _A	2.5 min
1.8 µl	25 mM MgCl ₂	72°C	1 min/ kb
0.3 µl	50 mM primer 1		
0.3 µl	50 mM primer 2	72°C	7 min
0.3 µl	Taq polymerase	T _A depended on amplified fragment.	

2.16.2 Taq-PCR

Taq-PCR was used to verify markers, mutations or deletions of *S.pombe* strains. Isolated genomic DNA or plasmid DNA was used as a template (Maniatis et al., 1989).

Reaction mix		Cycler program	
1 µl	DNA (100 µg plasmid/ 1 µg genomic DNA)	94°C	5 min
35.5 µl	ddH ₂ O	35 cycles:	
5 µl	10x Taq buffer	94°C	1 min
2.5 µl	4 mM dNTPs	T _A	1 min
3 µl	25 mM MgCl ₂	72°C	1 min/ kb
1 µl	50 mM primer 1		
1 µl	50 mM primer 2	72°C	7 min
		T _A depended on amplified fragment.	

1 μ l	Taq polymerase
-----------	----------------

2.16.3 Q5-PCR

Q5 High-Fidelity DNA polymerase from New England Biolabs was used for the amplification of fragments that were used for the cloning of plasmids or endogenous homologous recombination. PCR reaction mix and cycler program as given in the manual.

2.16.4 Site-directed mutagenesis

Site directed mutagenesis was performed using the QuikChange II Site-Directed Mutagenesis Kit from Agilent. Reaction mix and cycling program were used as given in the QuikChange II Site-Directed Mutagenesis Kit protocol.

2.17 Cloning

DNA fragments used for cloning were amplified using the Q5 High-Fidelity DNA polymerase. Vectors were linearized with a compatible restriction enzyme. The linearized vector and the PCR product were co-transformed in the *S. cerevisiae* strain CenPK for homologous recombination. Plasmid DNA was isolated from *S. cerevisiae* and electroporated in *E. coli* XL1 blue cells. Plasmid DNA was isolated from *E. coli* and used for restriction analysis. If the restriction showed the correct fragments the sample was sequenced (GATC Sanger sequencing).

Plasmids cloned in the course of this work:

Plasmid Nr.	Backbone + enzyme	PCR-product: template; primer; fragment size
1096	mutagenesis p875	primer: 1913 + 1914
1099	270 + SmaI	template: p1096; primer: 843 + 1004; fragment: 2483 bp
1152	mutagenesis p875	primer: 2000 + 2001
1153	222 + EcoRI	template: gDNA; primer: 2018 + 2019; fragment: 1211 bp
1156	1173 + EcoRI	template: p177 primer: 2171 + 2172 fragment: 1300 bp
1157	270 + SmaI	template: p1152; primer: 843 + 1004; fragment: 2483 bp
1167	270 + XhoI	template: gDNA 40; primer: 2062 + 2063; fragment 2047 bp
1168	1157 + PaeI	template: p177; primer: 1005 + 1421; fragment: 800 bp
1173	1153 + BamHI	template 1: p421 primer: 2171 + 2172 fragment:

		1638 bp template 2: gDNA primer: 2173 + 2174 fragment: 411 bp
1181	mutagenesis p1173	primer: 2080 + 2081
1208	270 + XhoI	template: gDNA 40; 2142 + 2143; 3000 bp
1227	882 + PaeI	template: p1078 ; primer: 2217 + 2218; fragment: 3018 bp
1229	270 + PaeI	template: p1078 ; primer: 2218 + 2224; fragment: 3018 bp
1231	883 + PaeI	template: p1078 ; primer: 2217 + 2218; fragment: 3018 bp
1232	884 + PaeI	template: p1078 ; primer: 2217 + 2218; fragment: 3018 bp

2.18 Strain construction

For mutations, deletions and epitope tags the cassette that was inserted in the genome was amplified using the Q5 High-Fidelity DNA polymerase. The PCR product was transformed into *S. pombe* cells and the transformants selected for the inserted marker. To verify the insertion of the cassette colony PCR was performed.

For deletion of SPCC594.01 the whole ORF was replaced with the *kan^R* marker. For the introduction of *rpl42^(P56Q)* the whole *rpl42⁺* ORF was replaced with a cassette containing the *rpl42^(P56Q)* allele and a *hyg^R* marker. For the insertion of *CHX^S* on Ch16 the *ade6-M216* ORF was replaced with a cassette carrying the *rpl42⁺* locus (containing 349 bp flanking region in front of and 351 bp flanking region behind the ORF (Roguev et al., 2007)) and the *kan^R* marker. For GFP epitope tags the stop codon of the tagged gene was deleted and the *gfp::kan^R* cassette inserted in frame at the C-terminus of the gene.

Strain	PCR-product: template; primer; fragment size	Modified strain
2519	template: p177; primer: 1745 + 1746; fragment: 2557 bp	1065
2686	template: p177; primer: 2039 + 2040; fragment: 1700 bp	605
2795	template: p177; primer: 2139 + 2140; fragment: 2500 bp	605
2855	template: p1181; primer: 2082 + 2083; fragment: 2803 bp	605
2929	template: p1156; primer: 2221 + 2222; fragment: 2740 bp	2855
2992	template: p422; primer: 2222 + 2241; fragment: 1082 bp	2960

Verification PCRs performed for strain constructions:

Mutation, deletion or tag	Primer	T _A	Fragment size
<i>mis15-68-gfp</i> 1	261 + 1747	54°C	628 bp
<i>mis15-68-gfp</i> 2	777 + 1791	57°C	898 bp
<i>SPCC594.01Δ</i> 1	304 + 2041	50°C	512 bp
<i>SPCC594.01Δ</i> 2	302 + 2042	50°C	449 bp
<i>met10⁺-gfp</i> 1	261 + 2141	45°C	662 bp
<i>met10⁺-gfp</i> 2	777 + 2034	45°C	665 bp
<i>rpl42</i> ^(P56Q) 1	2212 + 302	50°C	1342 bp
<i>rpl42</i> ^(P56Q) 2	2213 + 1677	50°C	600 bp
<i>rpl42⁺</i> locus on Ch16	694 + 2081	55°C	705 bp
<i>rpl42⁺</i> locus on Ch16 marker exchange	2242 + 2243	50°C	551 bp

2.19 Mating

Matings were performed to obtain double mutant strains or strains with specific marker combinations:

- Strains were mixed in 15 µl dH₂O and patched on a malt plate.
- Incubation for 2-3 days at 25°C until tetrads had developed.
- Tetrads used for random spore or tetrad analysis.

The genotypes of the strains were analyzed with the following methods:

<u>Genotype</u>	<u>Verification method</u>
prototrophy/ auxotrophy	selection on selective MM
ade6-M210/ ade6-M216	red color on MM with 5 µg/ ml adenine
<i>kan^R</i> cassette	growth on G418 plates
fluorescent tags	visual confirmation using a fluorescence microscope
mating type	test mating with strains with a known mating type
temperature-sensitivity	no growth at high temperatures (34°C - 36°C)

Verification PCRs were performed for selected matings:

Mutation, deletion or tag	Primer	T _A	Fragment size
<i>asp1</i> ^{D333A}	520 + 672	58°C	1150 bp
<i>asp1</i> ^{H397A}	520 + 673	58°C	959 bp
<i>mph1Δ</i>	162 + 2286	50°C	1300 bp
<i>aps1Δ</i>	948 + 949	56.5°C	2551 bp

<i>mis15⁺-gfp</i>	547 + 1857	57°C	1295 bp
<i>mis15-68-gfp</i> 1	261 + 1747	54°C	628 bp
<i>mis15-68-gfp</i> 2	777 + 1791	57°C	898 bp
<i>met10⁺-gfp</i>	261 + 2141	45°C	662 bp
<i>asp1¹⁻³⁶⁴</i>	778 + 1423	55°C	1133 bp
<i>mal2⁺-gfp</i>	16 + 302	54°C	255 bp

2.19.1 Random spore analysis

For random spore analysis the tetrads were mixed with 20 µl of 1:10 β-glucuronidase and 980 µl dH₂O. The mixture was incubated overnight at 25°C. The spores were washed twice with 1 ml dH₂O and 2x 500 and 2x 1000 spores were plated on YE5S plates or marker selective plates.

2.19.2 Tetrad analysis

Cell material of a mating sample was resolved in 100 µl dH₂O and pipetted on a YE5S plate. A micromanipulator was used to pick tetrads on specific positions on a grid. After several hours of incubation at 36°C the asci opened and the four spores of each tetrad were separated. After several days of incubation at 25°C the spores formed colonies whose genotype was determined.

2.20 Protein methods

2.20.1 Protein isolation from *S. pombe*

Protein extracts of *S. pombe* strains were isolated using the following protocol. All buffers were kept at 4°C and all centrifugation steps were performed at 4°C.

- Overnight cultures were grown in YE5S or MM with the required supplements.
- 2x10⁸ cells were centrifuged for 5 min at 3500 rpm. Supernatant discarded.
- Cells resuspended in 5 ml Stop buffer.
- Centrifugation for 5 min at 3500 rpm. Supernatant discarded.
- Cells resuspended in the remaining Stop buffer.
- Centrifugation for 5 min at 10000 rpm. Supernatant discarded.
- Addition of 500 µl HB15 buffer and ~ 1 tube of glass beads.
- Lysis of cells in Precellys (1x5000 U for 10 sec). Twice. Cells kept on ice.
- Tube was pierced with a heated needle and placed on a new tube.
- Centrifugation for 30 sec at 3000 rpm. Pierced tube discarded.

- Centrifugation for 30 min at 13000 rpm. Supernatant transferred to fresh tube.
- Centrifugation for 30 min at 13000 rpm. Supernatant transferred to fresh tube.
- Samples were stored at -20°C or used for immunoprecipitation.

Stop buffer		HB15 buffer	
150 mM	NaCl	25 mM	MOPS
10 mM	EDTA	60 mM	β -glycerophosphate
1 mM	NaN ₃	15 mM	p-nitrophenylphosphate
50 mM	NaF	15 mM	MgCl ₂
pH was adjusted to 8. Buffer was stored at 4°C.		15 mM	EGTA
		1 mM	DTT
		0.1 mM	Sodium orthovanadate
		1 %	Triton X 100
		1 mM	PMSF
		1 tablet	Complete protease inhibitor
		Buffer was stored at 4°C.	

The OD of the samples was measured after incubation with Bradford solution. The protein extracts were diluted with HB15 buffer to the OD of the sample with the lowest value. Samples were prepared for SDS-PAGE analysis:

Sample preparation	
32.5 μ l	Protein extracts
12.5 μ l	4x SDS loading buffer
5 μ l	1 M DTT

The samples were boiled for 10 min at 100°C before they were loaded on a 10 % SDS-gel.

2.20.2 Bradford assay

- Protein extracts were diluted 1:800 in ddH₂O in a total volume of 800 μ l.
- Addition of 200 μ l Bradford solution. Vortexed.
- 10 min of incubation at RT.
- Measurement of the OD at a wavelength at 595 nm.
- Protein samples were diluted to the lowest OD at 595 nm to obtain similar protein amounts.

2.20.3 Immunoprecipitation

- Addition of 50 μ l μ MACS GFP-beads to 250 μ l protein extract. Vortexed.
- Incubation for 60 min on ice or at 4°C overnight.
- Required μ MACS columns equilibrated with 200 μ l HB15 buffer.
- IP sample pipetted on the columns.
- Washed 8x with 200 μ l HB15 buffer.
- Addition of 20 μ l pre-warmed (100°C) elution buffer. 5 min incubation.
- Elution 2x with 50 μ l pre-warmed (100°C) elution buffer.
- Samples analyzed on an SDS-PAGE (10 %).

2.20.4 SDS-PAGE

In all experiments 10 % SDS gels were used. The gels were prepared the following:

Stacking gel		Resolving gel	
1.5 ml	Acrylamid solution	6.7 ml	Acrylamid solution
2.5 ml	4x stacking gel buffer	5 ml	4x resolving gel buffer
6 ml	dH ₂ O	8.3 ml	dH ₂ O
100 μ l	APS	200 μ l	APS
15 μ l	TEMED	20 μ l	TEMED

Gels were stored at 4°C.

4x stacking gel buffer		4x resolving gel buffer	
960 ml	0.5 M Tris/ HCl Ph 6.8	960 ml	0.5 M Tris/ HCl Ph 8.8
40 ml	10 % SDS	40 ml	10 % SDS

Buffer was stored at RT.

Buffer was stored at RT.

SDS-PAGE was performed in running buffer at 100 V until the samples reached the resolving gel. Afterwards the voltage was increased to up to 200 V.

Running buffer	
0.05 M	Tris
0.2 M	Glycine
0.1 %	SDS

The gel was used for a Coomassie staining or a Western blot analysis.

2.20.4.1 Coomassie staining

- SDS gel was placed in H₂O and heated in a microwave for 30 sec at 600 Watt. Shaking for several minutes.
- Step 1 repeated.
- Addition of Coomassie solution. Heated in a microwave for 30 sec at 600 Watt
- Washed with H₂O several hours or overnight.
- Pictures were taken.

Coomassie solution

60-80 mg	Coomassie Brilliant Blue G-250
35 mM	HCl
1 L	dH ₂ O

2.20.4.2 Western Blot

- SDS gel placed on an equilibrated PVDF membrane.
- Both placed between two Whatman papers soaked with transfer buffer.
- Transfer performed for 30 min at 300 mA using a blotting machine.
- Membrane blocked for 1 h in 3 or 5 % milk powder in PBS + 0.1 % Tween at RT.
- Incubation with 1. antibody overnight at 4°C on a wheel.
- Membrane washed 2x briefly, 1x 15 min and 3x 5 min with PBS + 0.1 % Tween.
- Incubation with 2. antibody for 4-6 h at RT while shaking.
- Membrane washed 2x briefly, 1x 15 min and 3x 5 min with PBS + 0.1 % Tween.
- Detection with DIG P3 + NBT/BCIP until signals appeared.

Transfer buffer

5.8 g	Tris
2.9 g	Glycine
3.7 ml	10 % SDS
200 ml	Methanol
ad 1L	dH ₂ O

Buffer was stored at RT.

Detection buffer (DIG P3)

0.1 M	Tris/ HCl pH 9.5
0.1 M	NaCl
50mM	MgCl ₂
ad 1L	dH ₂ O

Buffer was stored at RT.

DIG P3 + NBT/BCIP		10x PBS	
20 ml	DIG P3	80 g	NaCl
66 μ l	BCIP (stock 0.25 g in 10 ml DMF)	14.4 g	Na ₂ HPO ₄
66 μ l	NBT (0.5 g in 10 ml 70 % DMF)	2.4 g	KH ₂ HPO ₄
Buffer was freshly supplemented with NBT/BCIP before detection.		2 g	KCl
		ad 1L	dH ₂ O
		pH was adjusted with 10 M NaOH. Buffer was stored at RT.	

After the signals appeared the membrane was documented via scanning. For quantifications of relative protein levels the band intensities were measured using the ImageJ software. The values obtained for the protein of interest were normalized against the intensity value measured for the control protein. The normalized value for the wild-type situation was set as 1. The normalized values for the other conditions were divided by the wild-type value for the ratios of protein levels.

2.21 Chromatin-Immunoprecipitation

Chromatin-immunoprecipitation (ChIP) was performed to analyze the association of Mal2-GFP with the centromere regions of chromosomes 1 and 3. This experiment served as a read-out of Mal2-GFP KT localization.

ChIP was performed with the following protocol modified from (Karig, 2004):

- Overnight cultures were grown in 200 ml plasmid-selective MM for 28 h at 30°C (transformants for metaphase arrest) or sterile filtered MM (strains) with all amino acids at 25°C
- Cultures were grown to a density of 5×10^6 – 1×10^7 cells/ ml for the metaphase arrest
- Cultures were grown to an OD of 0.4-0.8 for *mal2⁺-gfp* expressing strains
- Cells were fixed with 3 % PFA (3 g PFA in 10 ml YE5S with 0.3 ml 10 M NaOH resolved at 65°C; cooled down to RT)
- The cultures were incubated for 30 min at 25°C while shaking
- Fixed cells were transferred to a falcon tube and centrifuged for 5 min at 3500 rpm at 4°C. Supernatant discarded.
- Washed twice with 20 ml cold 1x PBS.

- Cells were resuspended in 20 ml PEMS buffer with 0.4 mg/ ml Zymolyase 100 T (transformants) or 50 mg/ ml Lallzyme (strains).
- Incubation for 30-45 min at 37°C.
- The digestion was verified by mixing some cells with 10 % SDS on an object slide followed by microscopy. Around 80 % of the cells formed protoplasts.
- Samples washed twice with 10 ml PEMS.
- Pellets resuspended in 1 ml PEMS and twice 500 µl divided to two fresh tubes (one sample for experiment without antibody; one sample for experiment with antibody).
- Centrifugation for 1 min at 4000 rpm. Supernatant discarded.
- Pellets frozen at – 20°C.
- Pellets were thawed and resuspended in 400 µl cold Lysis buffer containing 1:100 complete protease inhibitor cocktail and 2 mM PMSF (prepared fresh).
- Samples were sonicated twice for 6 sec at 10 % using a sonicator. Cells were kept on ice in between the two sonification steps and for transport.
- Centrifugation for 5 min at 15000 rpm at 4°C. Supernatant transferred to fresh tube.
- Centrifugation for 10 min at 15000 rpm at 4°C. Supernatant transferred to fresh tube.
- Addition of 25 µl Protein A Agarose and incubation for 1-2 h at 4°C on a wheel.
- Centrifugation for 5 min at 8000 rpm at 4°C. Supernatant transferred to fresh tube. Duck bill tip used to get all the supernatant off the beads.
- 40 µl of the supernatant was frozen at – 20°C as input control.
- Addition of 25 µl Protein A Agarose and 2 µl antibody (α-GFP; Molecular Probes; A11122). Incubation overnight at 4°C on a wheel.
- Centrifugation for 5 min at 8000 rpm at RT. Supernatant discarded.
- Addition of 1 ml Lysis buffer.
- Incubation for 5 min on a wheel at RT. Centrifugation for 2 min at 8000 rpm at RT. Supernatant discarded.
- Addition of 1 ml Lysis buffer with 0.5 M NaCl.
- Incubation for 5 min on a wheel at RT. Centrifugation for 2 min at 8000 rpm at RT. Supernatant discarded.
- Addition of 1 ml Wash buffer.
- Incubation for 5 min on a wheel at RT. Centrifugation for 2 min at 8000 rpm at RT. Supernatant discarded.
- Addition of 1 ml TE buffer.
- Incubation for 5 min on a wheel at RT. Centrifugation for 2 min at 8000 rpm at RT. Supernatant discarded. Duck bill used to get all the supernatant off the beads.
- Addition of 250 µl TES to beads and 210 µl TES to previously frozen input samples.

- Incubation at 65°C in a waterbath overnight.
- Centrifugation for 1 min at 8000 rpm. Supernatant transferred to fresh tube. Beads discarded.
- Addition of 450 µl TE + 30 µl freshly prepared 10 mg/ ml Proteinase K.
- Incubation for 4 h at 37°C while shaking.
- Addition of 600 µl Phenol-chloroform. Vortexed. Centrifugation 8 min at 13000 rpm at RT.
- Upper fraction transferred to a fresh tube.
- Addition of 600 µl chloroform. Vortexed. Centrifugation 8 min at 13000 rpm at RT.
- Upper fraction transferred to a fresh tube.
- Addition of 1:10 V 3 M NaAc pH 5.5 and 2.5:1 V 96 % EtOH. Vortexed.
- Incubation on dry ice for 1 h.
- Centrifugation for 30 min at 15000 rpm at 4°C. Supernatant discarded.
- Pellets air-dried.
- Pellets resolved in 30 µl TE (IP) or 300 µl TE (input).
- Samples stored at - 20°C and used for conventional ChIP multiplex PCR or qPCR.

PEMS	
100 mM	PIPES pH 7
1 mM	MgCl ₂
1 mM	EDTA
1.2 M	Sorbitol

Buffer was stored at RT.

Lysis buffer	
50 mM	HEPES-KOH pH 7.5
140 mM	NaCl
1 mM	EDTA
1 %	Triton X 100
0.1%	Sodium deoxycholate

Buffer was stored at RT.

Lysis buffer + NaCl	
50 mM	HEPES-KOH pH 7.5
500 mM	NaCl
1 mM	EDTA
1 %	Triton X 100
0.1%	Sodium deoxycholate

Buffer was stored at RT.

Wash buffer	
10 mM	Tris/ HCl pH 8
250 mM	LiCl
1 mM	EDTA
0.5 %	NP-40
0.5%	Sodium deoxycholate

Buffer was stored at RT.

TE buffer		TES buffer	
10 mM	Tris/ HCl pH 8	50 mM	Tris/ HCl pH 8
1 mM	EDTA	10 mM	EDTA
Buffer was stored at RT.		1 %	SDS
		Buffer was stored at RT.	

2.21.1 Multiplex-PCR

For the multiplex PCR a mastermix was prepared and 6 μ l DNA of each sample was added.

Reaction mix		Cycler program	
2 μ l	10x PCR buffer (+Mg)	94°C	4 min
1 μ l	25 mM MgCl ₂	30 cycles:	
2 μ l	2.5 mM dNTPs	94°C	30 sec
1.5 μ l	4 mM dNTPs	55°C	30 sec
1 μ l	cnt1 primer (10 pmol/ μ l)	72°C	1 min
1 μ l	cnt2 primer (10 pmol/ μ l)		
1 μ l	imr1 primer (5 pmol/ μ l)	72°C	5 min
1 μ l	imr3 primer (5 pmol/ μ l)		
1 μ l	otr1 primer (30 pmol/ μ l)		
1 μ l	otr2 primer (30 pmol/ μ l)		
1 μ l	fbp1 primer (5 pmol/ μ l)		
1 μ l	fbp2 primer (5 pmol/ μ l)		
0.1 μ l	Taq polymerase (5 U/ μ l Roche)		
3 μ l	ddH ₂ O		

The PCR products were separated on a 1.5 % agarose gel. A picture of the gel was taken. For quantification of the enrichment of the *cnt* and *imr* regions the intensity of each band in the gel was measured using the ImageJ software. Within each lane the band intensities of the PCR products for the *cnt* and *imr* regions were normalized to the PCR product for the endogenous *fbp* control region. The values obtained for the ChIP samples were further compared to the same value obtained for the input control. This value then represents the % enrichment.

2.21.2 qPCR

For the qPCR reaction as analysis of the ChIP experiments the GoTaq qPCR Master Mix from Promega was used. The reaction mix was prepared as given in the GoTaq qPCR Master Mix protocol. 2 µl CXR reference dye were added to each reaction tube.

The cycling program was performed as given in the GoTaq qPCR Master Mix protocol.

As template 5 µl of a 1:10-1:50 dilution of the ChIP samples were used. The dilution used was the same within one experimental setup and was decided after analyzing the DNA amount in the input samples on a 1.5 % agarose gel.

For each sample two PCR reactions were performed. One with primers 1827 + 1828 for amplification of a 133 bp fragment within the central region of centromeres 1 and 3 (cen1/3) and one with primers 1825 + 1826 for amplification of a 134 bp fragment within the *act1*⁺ locus on chromosome 2 (Choi et al., 2012; Subramanian et al., 2014).

Quantification of the enrichment of cen1/3 over act was performed as follows (Haring et al., 2007):

- 1) Calculation of the ΔC_t values for the cen1/3 and act reactions:

$$\Delta C_t = C_t IP - (C_t input - \log(10; 2))$$

Served to calculate the differences in enrichment of cen1/3 and *act1*⁺ products between the input and IP sample.

- 2) Calculation of the % input values for the cen1/3 and act reactions:

$$\% input = (2^{\Delta C_t})$$

Transformation of the value from step 1) as a percentage value.

- 3) Calculation of the % enrichment cen1/3 over act:

$$enrichment\ cen1/3\ over\ act = \frac{(\% input\ cen1/3)}{(\% input\ act)}$$

Served to calculate the percentage of the enrichment of the cen1/3 region in the IP compared to the input normalized to the enrichment of the *act* locus in the IP compared to the input.

2.22 Microscopy

Microscopy was either performed with fixed cells (fixed with 96 % EtOH or 3 % PFAS) or living cells.

2.22.1 Microscopy of fixed cells

2.22.1.1 Immunofluorescence

Immunofluorescence was performed to visualize the mitotic spindle with a TAT1 (α -tubulin) antibody. For immunofluorescence (IF) experiments the following protocol was used (Hagan and Hyams, 1988):

- Overnight cultures were grown in 50 ml plasmid selective MM (transformants) or MM with all supplements (strains) at 25°C.
- $\sim 7.5 \times 10^7$ cells were mixed with 1 V YE5S + 2.4 M Sorbitol. Shaked for 5 min at 25°C.
- Cells fixed with 1:6 V 30 % PFAS (3 g PFA in 8 ml YE5S + 1.2 M Sorbitol. Addition of 60 μ l 10 M NaOH. Dissolved at 65°C. Cooled down to RT.)
- Tube inverted quickly.
- Incubation for 5 min at 25°C.
- Incubation for 30 - 90 min on a wheel at RT.
- Centrifugation for 3 min at 3500 rpm. Supernatant discarded (PFA waste).
- Pellet resuspended in 1 ml 1x PEM.
- Sample washed 3x with 1 ml 1x PEM. Centrifugation steps: 1 min at 4000 rpm.
- Cells resuspended in 1 ml 1x PEMS + 20 μ l Zymolyase (10 mg/ ml; 100 T) or 10 μ l Lallzyme (500 mg/ ml).
- Incubation for 8-30 min at 37°C. Incubation stopped if 50 % of the cells formed spheroblasts. Tested via microscopy after the addition of 10 % SDS to the digestion.
- Centrifugation for 1 min at 4000 rpm. Supernatant discarded.
- Addition of 1 ml 1x PEMS + 1 % Triton X 100. Incubation for 2 min at RT.
- Sample washed 3x with 1 ml 1x PEM. Centrifugation steps: 1 min at 4000 rpm.
- Pellet resuspended in 1 ml PEMBAL.
- Incubation for 1.5 h on a wheel at RT.
- Centrifugation for 1 min at 4000 rpm. Supernatant discarded.
- Addition of 50 μ l 1. antibody (TAT1) diluted in PEMBAL.
- Incubation overnight on a wheel at RT.
- Sample washed 3x with 1 ml 1x PEMBAL. Centrifugation steps: 1 min at 4000 rpm.

- Pellet resuspended in 150 μ l 2. Antibody (Alexa Fluor®488) diluted in PEMBAL.
- Incubation for 5-6 h on a wheel at RT.
- Sample washed 1x with 1 ml 1x PEMBAL and 1x with 1 ml 1x PBS. Centrifugation steps: 1 min at 4000 rpm.
- The samples were used for DAPI staining.

PEM		PEMS	
100 mM	PIPES	1 V	PEM
1 mM	EGTA	1 V	1.2 M Sorbitol (autoclaved)
1 mM	MgSO ₄	Buffer was stored at RT.	
0.5 %	NP-40		
0.5%	Sodium deoxycholate		

pH was adjusted to 6.9 with acidic acid.
Buffer was autoclaved and stored at RT.

PEMBAL	
100 mM	PEM
1 %	BSA
0.1 %	NaN ₃
100 mM	Lysine hydrochloride

Buffer was sterile filtered and stored at 4°C.

2.22.1.2 DAPI staining

DAPI staining was performed to visualize the DNA. The following protocol was used (after IF only steps 8-11 were performed):

- Overnight culture grown in 5 ml MM medium.
- Centrifugation of 1.5 ml culture for 1 min at 4000 rpm.
- Eppi shifted 180°C. Centrifugation for 1 min at 4000 rpm. Supernatant discarded.
- Centrifugation for 1 min at 4000 rpm. Supernatant discarded completely.
- Pellet resuspended in 30 μ l ddH₂O.
- Addition of 70 μ l ice cold 96 % EtOH while vortexing.
- Samples washed twice with 1 ml 1x PBS. Centrifugation for 1 min at 4000 rpm.
- Pellet resuspended in 90 μ l 1x PBS + 10 μ l DAPI (1 μ g/ ml).

- Incubation for 3 min at RT in darkness.
- Centrifugation for 1 min at 4000 rpm. Supernatant discarded completely.
- Pellet resuspended in 50 μ l 1x PBS.

The samples were either stored at 4°C or prepared for microscopy. For this purpose 35 μ l of the stained cells were pipetted on a cover slip covered with poly-L-lysine. 5 μ l mounting solution were used to prepare the object slide. The cover slip was sealed with nail polish. The analysis of the signals was done using a Zeiss Axiovert microscope or a Nikon Eklipse Ti microscope.

2.22.2 Live cell imaging

Live cell imaging was performed to analyze fluorescence signal intensities and the localization or the dynamics of epitope tagged proteins. For live cell imaging the cultures were grown in live fluorescence media (LFM). Depending on the application the cells were grown in volumes between 5 ml and 200 ml of LFM.

LFM		Pre-mix	
20 ml	Pre-mix	5.5 g	Na ₂ HPO ₄ x 2 H ₂ O
20 ml	Glucose (40 g/ ml sterile filtered)	6 g	Potassium hydrogene phthalate
8 ml	Saltstock	2 g	Glutamic acid
400 μ l	Vitaminestock	100 ml	ddH ₂ O
40 μ l	Mineralstock	Pre-mix was sterile filtered and stored at 4°C.	
300 ml	ddH ₂ O		

LFM was stored at 4°C.

If transformants were used for the microscopy analysis the following supplements were added:

4 ml	Histidine (7.5 mg/ ml)
4 ml	Arginine (7.5 mg/ ml)
15 ml	Adenine (2.7 mg/ ml adenine hemisulfate)
15 ml	Uracil (2 mg/ ml)
4 ml	Lysine (7.5 mg/ ml)

In case of analysis of strains 4 ml leucine (7.5 mg/ ml) were additionally added.

Samples were prepared using the following protocol:

- 1-5 ml of cell culture was transferred to a fresh tube and centrifuged for 1 min at 3500 rpm. Tube shifted 180°C. Centrifugation for 1 min at 3500 rpm.
- 980 µl supernatant discarded. Cells resuspended in the leftover LFM.
- 50 µl 100°C warm MM medium containing agarose was pipetted on an object slide to generate an agarose pad.
- 2 µl of cell suspension were pipetted on the agarose pad.
- After several minutes a cover slip was placed on the agarose pad and it was sealed with VALAP (pre-heated on 100°C).

The medium for the agarose pads was prepared using LFM + 2 % agarose. The agarose was dissolved in the medium and aliquots prepared and stored at RT. VALAP was prepared by dissolving vaseline, paraffin and lanolin and mixing them in a 1:1:1 ratio. 1 ml aliquots of VALAP were stored at RT (Tran et al., 2004).

To additionally stain mitochondria MitoTracker Red CMXRos from Molecular Probes was used according to the protocol included for the staining.

The object slides were used for microscopy with a Zeiss Spinning Disc-Confocal microscope. Pictures were taken with a Rolera EM-C² (QImaging) camera. Pictures were analyzed and edited with the Zen2011 blue software (Zeiss). The pictures were taken at the temperature indicated in the figure legends. Laser intensities as given in the figure legends. For each channel an exposure time of 400 ms was used. Pictures were taken in a range from 15-50 stacks with a diameter of 0.5 µm. In the pictures shown the stacks were projected to one plane with the function “maximum intensity projection” (MIP).

2.22.3 Quantification

The dynamics of fluorescence markers and the cell length were analyzed using the Zen2011 blue and Axiovision softwares (Zeiss).

For the quantification of fluorescence signal intensities the samples were prepared in parallel under the same conditions. Furthermore the pictures were taken back to back without changing the settings of the microscope, the temperature chamber or the microscopy software.

For each sample pictures with 50 z-stacks were taken and the 15 stacks showing the cell layer were cut out using the Zen2011 (Zeiss) software. The digital editing of all samples within one experimental set was performed equally. The picture was then used to generate a

MIP picture. MIPs were exported as .tiff files. The .tiff files were opened in the Adobe Photoshop software to generate greyscale pictures.

The greyscale pictures were opened with the ImageJ software. With this software a specific square surrounding the GFP signal was measured and the background (measured with a square of the same size) then subtracted. The obtained value was the AU (arbitrary unit) value for the fluorescence signal intensity. For each picture a .zvi file was exported in addition. That file was opened with the Axiovision software (Zeiss) where the length of each cell was measured.

2.23 Statistics

Frequencies of characteristics (for example missegregation events) were compared using a χ^2 test.

Absolute numbers were compared with the students t-test type 2 or 3 with 2 tails.

Statistics were calculated with Microsoft Excel.

2.24 Replicates

If not indicated otherwise each experiment has been performed once.

3 Results

3.1 Asp1-generated inositol pyrophosphates influence MT-associated proteins

A former member of our lab, Dr. Boris Topolski, previously demonstrated that Asp1-generated inositol-pyrophosphates (IP₈) influenced the dynamics of the mitotic spindle. In particular he found that without Asp1-generated IP₈, in an *asp1*^{D333A} strain, the spindle midzone is weakened leading to a breakage of short spindles. In contrast in the *asp1*^{H397A} strain (more Asp1-generated IP₈ than in the wild-type) the opposite was observed (Figure 1-12 (p. 41); Figure 1-13 (p. 42)). Furthermore he showed that all three mitotic spindle phases were altered in *asp1*^{D333A} and *asp1*^{H397A} strains compared to the wild-type situation. Spindle phases 1 and 3, where the spindle elongates, were accelerated in *asp1*^{D333A} cells. Spindle phase 2, where bipolar kinetochore-microtubule (KT-MT) attachments are established, on the other hand was prolonged in *asp1*^{D333A} cells in a spindle assembly checkpoint (SAC) dependent manner. The opposite was found for an *asp1*^{H397A} strain. This strain progressed through spindle phase 2 faster than the wild-type strain (Figure 1-13 (p. 42); (Topolski et al., 2016)). At this stage the Asp1 in mitosis project was taken over by me. Several of the experiments performed by Dr. Boris Topolski were repeated by me to obtain data suitable for a publication (Supplementary Figure 1; Supplementary Figure 2; Supplementary Figure 3 (p. 186)). In addition I showed that the SAC is not active in *asp1*^{H397A} cells. These data have been published (Topolski et al., 2016) and I am one of the joined first authors.

With the previously obtained results two questions emerged, that I tried to answer in the course of my work:

- 1) Which are the targets that mediate the effect of IP₈ on the mitotic spindle or microtubules (MTs) in general?
- 2) Is chromosome transmission fidelity altered in strains with different Asp1-generated IP₈-levels?

3.1.1 Asp1-generated IP₈ influences the growth of deletion strains of MT-associated proteins

The first question to be answered was if Asp1-generated IP₈ modulated specific MT-associated proteins.

An Asp1-variant was identified as a suppressor of the TBZ-sensitivity of a *mal3-1* mutant strain (Pöhlmann and Fleig, 2010). However, the role of Asp1 as a regulator of MT dynamics was independent of Mal3 (Pöhlmann and Fleig, 2010; Pöhlmann et al., 2014). Mal3 is the *S. pombe* homolog of the +-tip associated EB1 protein and is responsible for the MT association of other +-TIPs, such as Tip1 or Tea2 (Beinhauer et al., 1997; Busch and Brunner, 2004; Busch et al., 2004). As Asp1 function was independent of the presence of Mal3 it was unlikely that proteins directly recruited by Mal3 to MT plus-ends were targets of IP₈. Therefore I analyzed proteins that were associated with MTs independently of Mal3.

A multitude of MT-associated proteins is involved in the regulation of MT- and spindle dynamics. An overview of the proteins used in the following experiments is shown in Figure 3-1:

The strains were chosen because upon deletion or mutation they show similar phenotypes to those observed for *mal3-1* or *mal3Δ* strains.

Klp6, a kinesin-8 family protein, is a plus-end directed motor protein that acts as a dimer with Klp5. They destabilize MTs and generate inward pulling forces at the mitotic spindle (Syrovatkina et al., 2013; West et al., 2001). Pkl1 is the *S. pombe* kinesin-14: a minus-end directed motor protein that anchors MTs to the SPB (Pidoux et al., 1996; Yukawa et al., 2015). Cut7, kinesin-5, is a plus-end directed motor protein that opposes Pkl1 function and is essential for stabilization of interdigitating MTs during spindle formation and elongation (Hagan and Yanagida, 1990; Pidoux et al., 1996). Ase1 is a MT bundling protein that localizes to interdigitating interphase- and spindle MTs and stabilizes them (Loiodice et al., 2005). Alp14 is a member of the TOG/XMAP family which localizes to MT plus-ends and stabilizes them as well (Garcia et al., 2001).

Detailed information about the roles of these proteins can be found in Chapter 1.3.1.1.2 (p. 17).

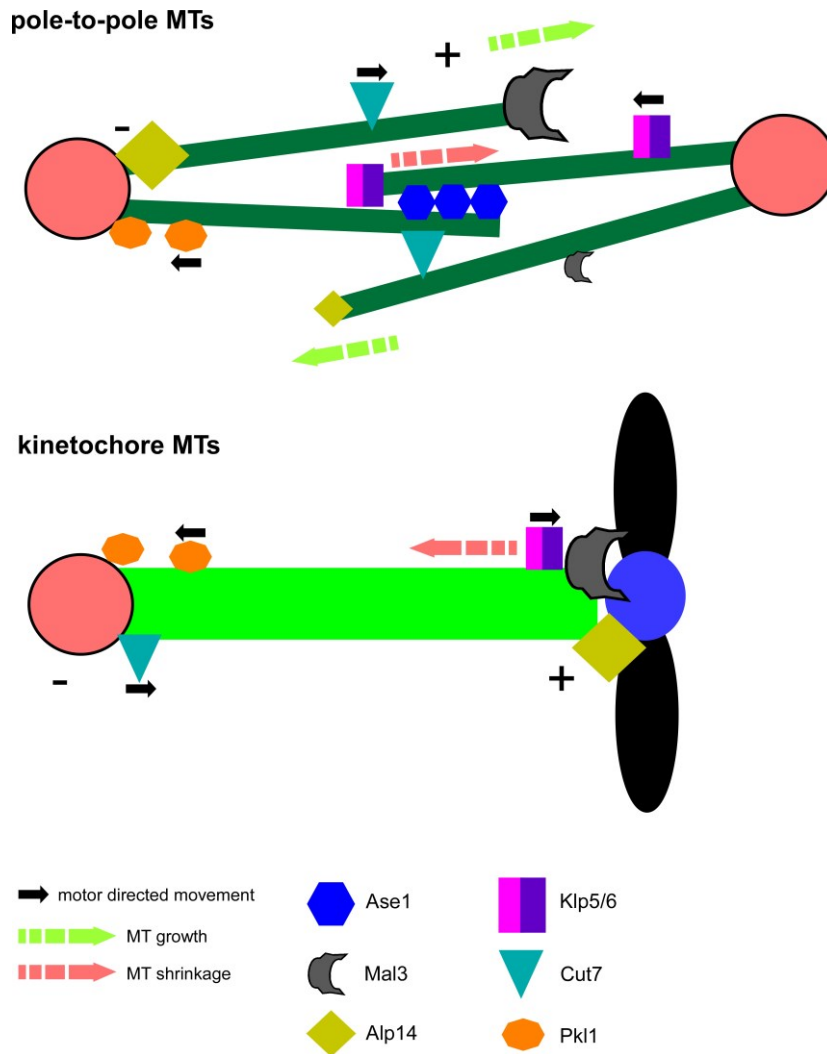


Figure 3-1 Functions of the analyzed proteins in MT- and spindle dynamics.

Ase1 is a MT-cross-linking factor that bundles and stabilizes MTs. Mal3 is a +-TIP that is required for MT growth. Alp14 is a plus-end associated MT polymerase. Klp5/Klp6 depolymerize and destabilize MTs and generate inward pulling spindle forces. Cut7 is a plus-end directed motor protein that generates outward pushing forces, is localized to the SPBs and interdigitating MTs and stabilizes forming and elongating spindles. Pkl1 opposes Cut7 and is a minus-end directed motor protein that is involved in SPB organization.

First I tested if the influence of Asp1-generated IP_8 on MT dynamics depended on these MT-associated proteins. To this end deletion strains of genes encoding for these proteins were analyzed regarding their growth behavior under different cellular IP_8 -levels. For this purpose *asp1*¹⁻³⁶⁴ or *asp1*³⁶⁵⁻⁹²⁰ were plasmid expressed in these strains under the control of the no message in thiamine (*nmt1*⁺) -promoter. The *nmt1*⁺ promoter is repressible by thiamine, but low expression occurs even in presence of thiamine.

Higher- or lower-than wild-type IP_8 -levels had no effect on the growth of a wild-type strain on media without TBZ. However, higher-than-wild-type IP_8 -levels via expression of *asp1*¹⁻³⁶⁴

increased the TBZ-resistance of a wild-type strain. Lower-than-wild-type IP₈-levels via *asp1*³⁶⁵⁻⁹²⁰ expression led to an increased TBZ-sensitivity (Figure 3-2 A).

As a rescue of TBZ-sensitivity was also observed for the *mal3-1* strain and this effect was independent of the presence of Mal3 it was concluded that a screening for TBZ-sensitivity is not a suitable method for analysis (Pöhlmann and Fleig, 2010; Pöhlmann et al., 2014). Therefore the effect of *asp1*¹⁻³⁶⁴ and *asp1*³⁶⁵⁻⁹²⁰ expression on the growth of these strains was assayed under conditions without TBZ.

First the effect of IP₈ on the growth of a *klp6Δ* strain was analyzed. Under low expression conditions no influence on the growth of that strain with either *asp1*¹⁻³⁶⁴ or *asp1*³⁶⁵⁻⁹²⁰ expression was detected. It was observed that while high expression of *asp1*¹⁻³⁶⁴ had no effect on growth lower-than-wild-type IP₈-levels via expression of *asp1*³⁶⁵⁻⁹²⁰ slightly reduced the growth of that strain. The same effect was observed for a *klp5Δ* strain (Figure 3-2 B; Supplementary Figure 4 A (p. 186)).

Next a *pk11Δ* strain was used. This deletion mutant showed no change in growth with low expression of *asp1*¹⁻³⁶⁴ or *asp1*³⁶⁵⁻⁹²⁰ compared to the vector control. High expression of *asp1*¹⁻³⁶⁴ still had no effect while with *asp1*³⁶⁵⁻⁹²⁰ expression a reduction in growth was observed (Figure 3-2 C).

In an *ase1Δ* strain low expression of *asp1*¹⁻³⁶⁴ or *asp1*³⁶⁵⁻⁹²⁰ had no effect on growth compared to the vector control. High expression of *asp1*¹⁻³⁶⁴ led to a slightly better growth while expression of *asp1*³⁶⁵⁻⁹²⁰ caused synthetic lethality (Figure 3-2 D).

The *alp14Δ* strain with low expression of *asp1*¹⁻³⁶⁴ or *asp1*³⁶⁵⁻⁹²⁰ showed no changes in growth compared to the vector control. The same was found for high expression of *asp1*¹⁻³⁶⁴ while expression of *asp1*³⁶⁵⁻⁹²⁰ caused synthetic lethality (Figure 3-2 E).

Hence, lower-than-wild-type IP₈-levels had an effect on the growth of all deletion strains of MT-associated proteins assayed and the effect observed was most severe in *alp14Δ* and *ase1Δ* strains.

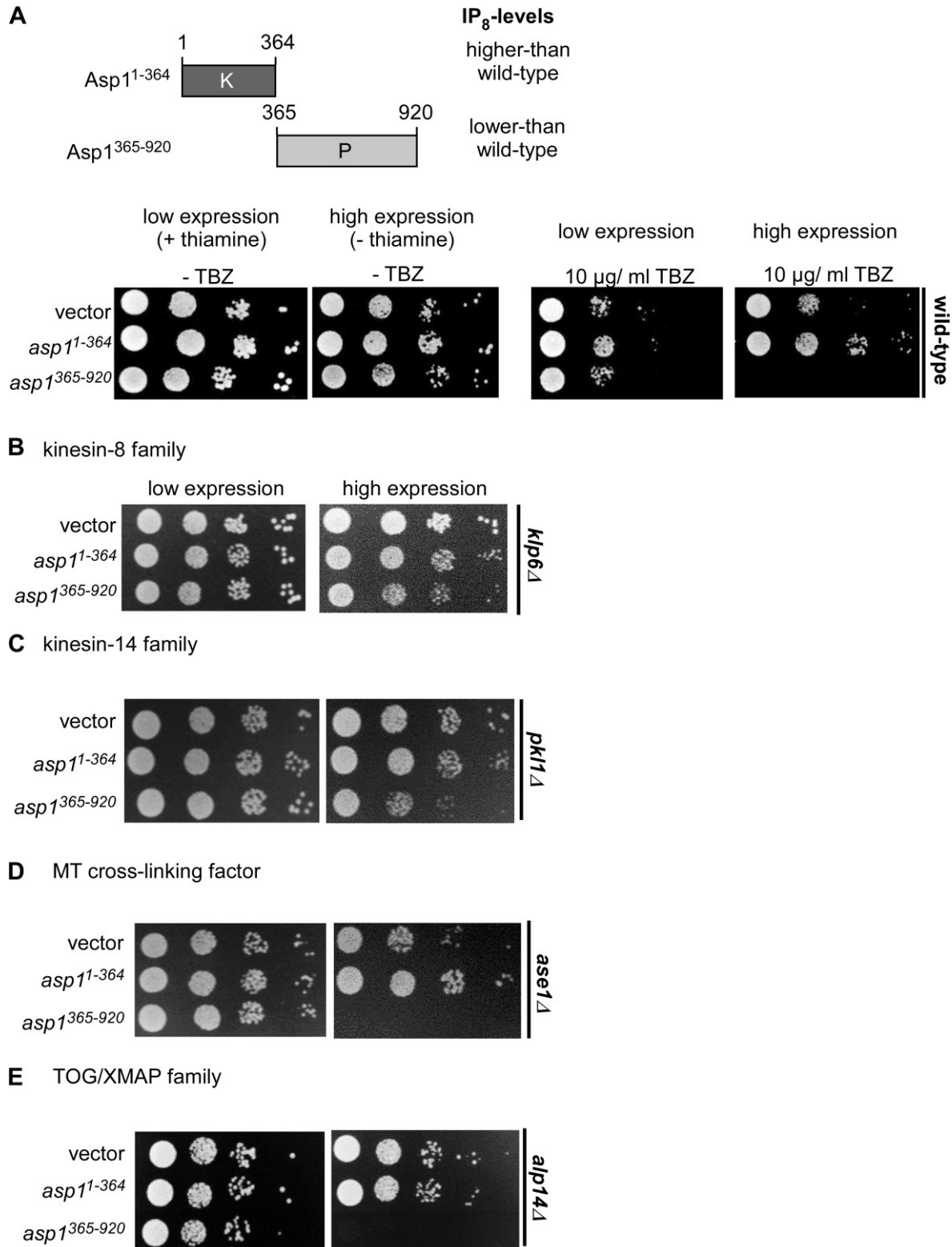


Figure 3-2 Asp1-generated IP₈ affects the growth of deletion strains of MT-associated proteins.

A-E: Asp1 variants used depicted at the top. Serial dilution patch tests (10^4 - 10^1 cells) of the indicated strains transformed with a vector control, *asp1*¹⁻³⁶⁴ or *asp1*³⁶⁵⁻⁹²⁰ on plasmids. An overview of the *asp1* variants used is shown at the top. Transformants were grown under plasmid-selective conditions in media with (low expression) or without (high expression) thiamine for 4-6 days at 25°C. Examples out of at least 3 transformants/ plasmid and strain are shown. Parts B and C of this figure have been published: (Topolski et al., 2016).

The effects of lower- and higher-than-wild-type IP₈-levels on the growth of mutant strains of MT-associated proteins are summarized in Table 3-1.

Influence of IP₈ on microtubule mutant strains				
Temperature	25 °C		28 °C	
Expression	<i>asp1¹¹⁻³⁶⁴</i>	<i>asp1³⁶⁵⁻⁹²⁰</i>	<i>asp1¹¹⁻³⁶⁴</i>	<i>asp1³⁶⁵⁻⁹²⁰</i>
Deletion/ Mutant				
<i>klp5Δ</i>	-	↓	X	X
<i>klp6Δ</i>	-	↓	X	X
<i>ase1Δ</i>	↑	↓↓	X	X
<i>alp14Δ</i>	-	↓↓	X	X
<i>pk11Δ</i>	-	↓	X	X
<i>cut7-446^{ts}</i>	-	-	-	↑

Table 3-1 The effect of variations in IP₈-levels on the growth of deletion or mutant strains of MT-associated proteins.

↑ rescue of growth, ↓ reduced growth, - no effect, X not determined.

Lower-than-wild-type IP₈-levels via *asp1³⁶⁵⁻⁹²⁰* expression caused synthetic lethality in an *alp14Δ* strain. This indicated that the Alp14 protein is essential if lower-than-wild-type IP₈-levels were present in the cell. To check if the same was true for the absence of Asp1-generated IP₈ I tested if a double mutant of *alp14Δ* and endogenously expressed *asp1^{D333A}* was viable. I found that compared to the single mutants (*asp1^{D333A}* and *alp14Δ*) the *asp1^{D333A} alp14Δ* strain showed an increased TBZ-sensitivity, but the strain was viable and showed no severe growth defect under conditions without TBZ (Figure 3-3).

Thus, Alp14 did not become essential without Asp1-generated IP₈ but was essential if the cellular levels of these molecules were lower-than-wild-type.

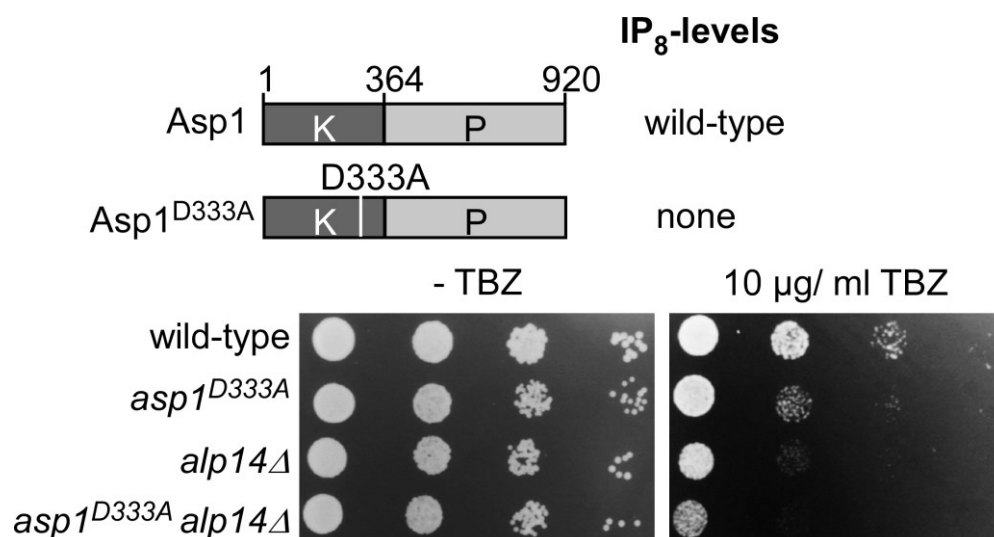


Figure 3-3 Absence of Asp1-generated IP₈ does not induce synthetic lethality in an *alp14*Δ strain.

Asp1 variants used are depicted at the top. Serial dilution patch tests (10^4 - 10^1 cells) of the indicated strains. Strains were incubated on YE5S plates with the indicated concentration of TBZ for 4 days at 25 °C.

3.1.1.1 Lower-than-wild-type IP₈-levels rescue the temperature-sensitivity of *cut7*^{ts} strains

Lower-than-wild-type IP₈-levels reduced the growth of both *klp6*Δ and *pk1*Δ strains. Klp6 and Pkl1 have opposing functions to the kinesin-5 Cut7 (Edamatsu, 2014; Hagan and Yanagida, 1992; Pidoux et al., 1996). Therefore it was interesting to test if different cellular IP₈-levels affected the growth of a temperature-sensitive (ts) *cut7* strain.

Ts mutants are able to grow at a permissive temperature (such as 25°C). At a semi-permissive temperature they show limited growth and no growth at the restrictive temperature (Ben-Aroya et al., 2010; Bonatti et al., 1972). Restrictive temperatures vary for different mutant strains and experimental conditions.

In my experiments I used the *cut7-446*^{ts} and *cut7-24*^{ts} strains (Hagan and Yanagida, 1990). These strains have different mutations within the *cut7*⁺ gene, but the position and character of the mutations is not known. The *cut7-446*^{ts} and *cut7-24*^{ts} strains were transformed with the vector control or *asp1*¹⁻³⁶⁴ or *asp1*³⁶⁵⁻⁹²⁰ expressed on a plasmid. For the TBZ-sensitivity of *cut7-446*^{ts} and *cut7-24*^{ts} strains a variation in cellular IP₈-levels had the same effect than in the wild-type strain (data not shown). Strikingly, the ts phenotype of the *cut7-446*^{ts} and *cut7-24*^{ts} strains was rescued with lower-than-wild-type IP₈-levels. High expression of *asp1*³⁶⁵⁻⁹²⁰ enabled the *cut7-446*^{ts} strain to grow at temperatures up to 28°C (Figure 3-4 A, right panel; Supplementary Figure 4 B (p. 186)). Assessment of the survival rate of

transformants of the *cut7-446^{ts}* strain with either a vector control or the *asp1³⁶⁵⁻⁹²⁰* plasmid showed that with high expression of *asp1³⁶⁵⁻⁹²⁰* the percentage of surviving cells at 28°C increased from 15.2 (vector) to 57.8 % (Figure 3-4 B).

As one phenotype of *cut7-446^{ts}* and *cut7-24^{ts}* mutant strains is a loss of Cut7^{ts} localization to the spindle midzone but not the spindle ends after a 3 h shift to 36°C (Hagan and Yanagida, 1992) I tested if Cut7-GFP localization was affected by high expression of *asp1³⁶⁵⁻⁹²⁰*. For this purpose a *cut7⁺-gfp* strain was transformed with either the vector control or an *asp1³⁶⁵⁻⁹²⁰* plasmid. To analyze the localization pattern of Cut7-GFP in those transformants videos were taken at 30°C and the changes in Cut7-GFP localization were tracked and quantified (Figure 3-4 C). In transformants expressing *asp1³⁶⁵⁻⁹²⁰* the Cut7-GFP fluorescence signal along the spindle was in general increased compared to transformants with the vector control (short spindles: spindle ends: vector: 108 arbitrary units (AU);, *asp1³⁶⁵⁻⁹²⁰*:140 AU; spindle midzone: vector: 22 AU, *asp1³⁶⁵⁻⁹²⁰*: 42 AU; long spindles: spindle ends: vector: 41 AU, *asp1³⁶⁵⁻⁹²⁰*: 56 AU; spindle midzone: vector: 31 AU, *asp1³⁶⁵⁻⁹²⁰*: 54 AU). Therefore, instead of analyzing the signal intensity as such, I analyzed the distribution of Cut7-GFP between the midzone and ends of the spindle to check for a possible spatial shift in localization with lower-than-wild-type IP₈-levels.

First I analyzed the Cut7-GFP localization pattern for short spindles (2-3.5 μm) that represent metaphase spindles and therefore mitotic spindle phase 2. The ratio of fluorescence signal at the spindle midzone compared to the spindle ends was 0.2 for the vector control. More Cut7-GFP was present on the spindle midzone compared to the spindle ends with high expression of *asp1³⁶⁵⁻⁹²⁰* with an increase in the ratio to 0.3 (Figure 3-4 D). The same tendency was observed for long spindles of a length between 3.5-8.5 μm. Those represent anaphase B spindles. The ratio of Cut7-GFP fluorescence signal at the spindle midzone compared to the spindle ends was 0.9 for the vector control. 1.3 was measured with high expression of *asp1³⁶⁵⁻⁹²⁰* (Figure 3-4 E; F).

Therefore, the rescue of the *cut7-446^{ts}* phenotype with lower-than-wild-type IP₈-levels might be caused by an increased localization of Cut7 protein to the spindle midzones.

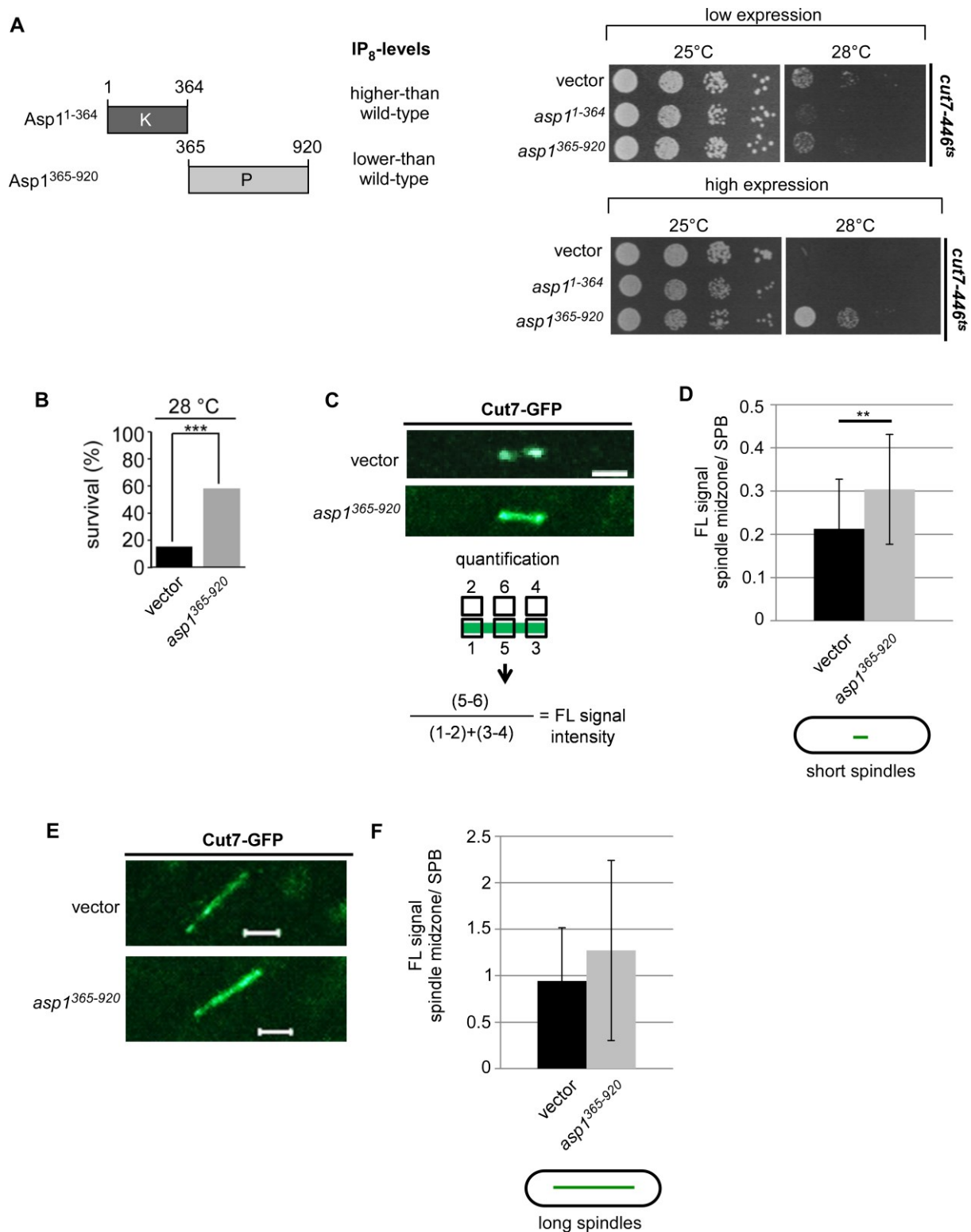


Figure 3-4 More Cut7-GFP is recruited to the spindle midzones with lower-than-wild-type cellular IP₈-levels.

A: Left: Asp1-variants used in this figure. Right: Serial dilution patch tests (10^4 - 10^1 cells) of the *cut7-446^{ts}* strain transformed with a vector control, *asp1*¹⁻³⁶⁴ or *asp1*³⁶⁵⁻⁹²⁰ expressed on plasmids. Transformants were grown under plasmid-selective conditions in media with or without thiamine for 7 days at the indicated temperatures. Examples of one out of 6 transformants/ plasmid are shown. **B:** Diagram of the survival rate of selected transformants as used in A. Transformants were pre-grown in plasmid selective media without thiamine (high expression) and 1000 cells/ transformant were plated. After incubation at 28°C colony formation was assayed. (Figure legend continued on the next page).

C: Quantification of the fluorescence signal of Cut7-GFP at the spindle midzone of short spindles (2-3.5 μm). Photomicrographs of *cut7⁺-gfp* cells transformed with a vector control or *asp1³⁶⁵⁻⁹²⁰* are shown. Scale bar= 2 μm . For relative signal intensity the fluorescence signal at the spindle midzone was normalized against the background (square 5 – square 6). This value was divided by the fluorescence intensity at spindle ends normalized against the background and summed up (square 1 – square 2 and square 3 – square 4). **D:** Diagram of the ratio of fluorescence signal intensity at the spindle midzone compared to the ends of short spindles (2-3.5 μm) calculated as in C. (n= 30/ transformant; **: $p \leq 0.01$, two-sample-t-test). **E:** Photomicrographs of *cut7⁺-gfp* cells transformed with a vector control or *asp1³⁶⁵⁻⁹²⁰*. Long spindles are shown. Scale bar= 2 μm . **F:** Diagram of the ratio of fluorescence signal intensity at the spindle midzone compared to the ends of long spindles (3.5-8.5 μm spindle phase 3; anaphase B) calculated as in C. (n= 30/ transformant). Part B of this figure has been published: (Topolski et al., 2016). Videos taken by Dr. Visnja Jakopec using a Zeiss Spinning Disc-Confocal microscope. Videos taken at 30°C.

3.2 Asp1-generated IP₈ regulates chromosome segregation in *S. pombe*

The above results gave a hint towards an answer for the first question I had: if IP₈ has a MT-associated protein as a target. Even though no definite target was identified I found a pathway that was affected by Asp1-generated IP₈ and involved the Cut7 protein.

The next question was if the changes in MT dynamics by IP₈ and the pathway identified in the section above were crucial for chromosome segregation processes. Therefore I next addressed the question if variations in cellular IP₈-levels had consequences in form of alterations in chromosomal segregation and therefore survivability of *S. pombe* cells.

3.2.1 Chromosome segregation errors are increased without Asp1-generated IP₈

First I tested if chromosome transmission fidelity required Asp1-generated IP₈. For this purpose the segregation of chromosome 1 sisters in cells with wild-type IP₈-levels and in an *asp1^{D333A}* strain, without Asp1-generated IP₈ was analyzed.

In this approach two fluorescence markers were tracked in living cells. The SPB component Sad1 was tagged with mCherry so that the SPBs could be traced during mitosis (Hagan and Yanagida, 1995). Further the *cen1-GFP* system was used to track the centromeres of chromosome 1 sisters. In this system GFP-LacI is expressed from the *his7⁺* locus and is tethered to LacO repeats integrated at the *lys1⁺* locus near the centromere of chromosome 1 (Tatebe et al., 2001). With this experimental setup the distribution of chromosome 1 sisters was observed in living cells with different IP₈-levels. Two major abnormal phenotypes were observed. Lagging chromosomes were observed, in which one *cen1-GFP* signal lags behind the SPB but in the end the chromosomes were equally distributed. This phenotype was

found in 3 % of the cells of a *sad1-mCherry cen1-gfp* strain with wild-type IP_8 -levels while 97 % of the cells showed normal segregation (Figure 3-5 A, top panel; B).

Furthermore missegregation events were found, where both *cen1-GFP* signals were distributed to the same daughter cell. The missegregation events were further subdivided: 1) cells that showed two separate *cen1-GFP* signals at one point during the segregation process and 2) *cen1-GFP* signals that never separated, indicating that a nondisjunction event occurred. An example for each phenotype is depicted in Figure 3-5 A, bottom panel.

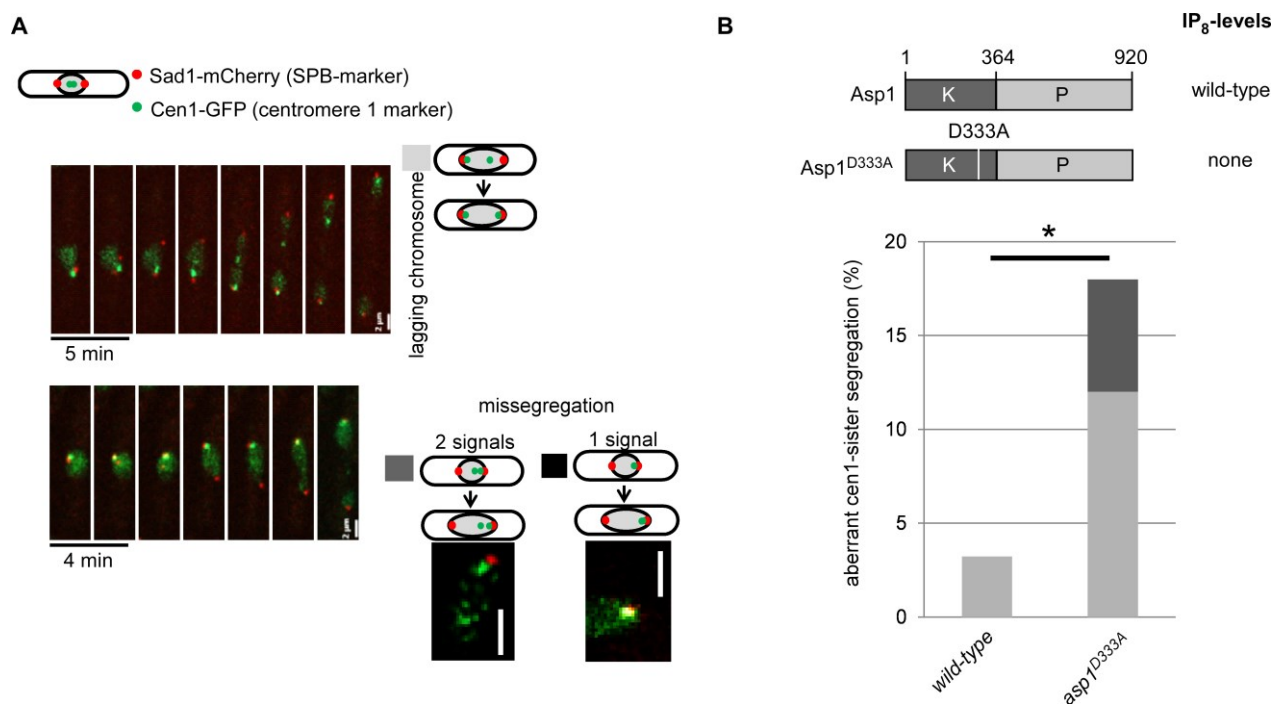


Figure 3-5 Faithful chromosome segregation requires Asp1-generated IP_8 .

A: Live cell microscopy of a strain expressing *sad1-mCherry* to visualize the SPBs and *cen1-GFP* to visualize the centromeres of chromosome 1 sisters. Cells were pre-grown at 25°C for 24 h in live fluorescence media (LFM; p.83). Pictures were taken at 25°C. Time between images: 5 min or 4 min, respectively. Scale bar: 2 μ m. First row: Cell showing a lagging chromosome. Second row: Left: Cell showing chromosome missegregation. Right: Example for two distinguishable *cen1-GFP* signals during the missegregation process or *cen1-GFP* signals that did not separate. Examples shown in photomicrographs show an *asp1^{D333A}* strain with an additional mutation that made the system more sensitive. The features of that strain will be further described in Figure 3-6. Example for missegregation with two distinguishable *cen1-GFP* signals shows an *asp1^{D333A}* strain. Example for missegregation with one *cen1-GFP* signal shows an *asp1^{D333A}* strain with an additional mutation. **B:** Asp1-variants used are depicted at the top. Diagrammatic illustration of the percentage of aberrant *cen1-GFP* segregation as shown on the left in the indicated strains. Wild-type: 3 % lagging chromosomes (n= 62), *asp1^{D333A}*: 6 % missegregation with two distinguishable *cen1-GFP* signals, 12 % lagging chromosomes (n= 34), (*: $p \leq 0.05$, χ^2 -test). The results in this figure have been published in (Topolski et al., 2016).

More aberrant segregation phenotypes were observed for the *asp1^{D333A} sad1-mCherry cen1-gfp* strain in which only 82 % of the cells showed a normal segregation phenotype while 18 % of the cells distributed chromosome 1 sister aberrantly (Figure 3-5 B).

Thus, Asp1-generated IP_8 was required for a normal segregation process.

3.2.2 Cells without Asp1-generated IP₈ depend on a functional SAC

It was known that an *asp1*^{D333A} strain showed a mitotic delay (Topolski et al., 2016). Such a mitotic delay can be caused by the spindle assembly checkpoint (SAC p. 33) that keeps cells in metaphase and delays anaphase onset until bi-orientation is established (Rudner and Murray, 1996). The delay of anaphase onset in *asp1*^{D333A} cells was indeed caused by an activation of that checkpoint (Topolski et al., 2016). Therefore I next checked if the *asp1*^{D333A} strain depended on a functional SAC to reduce abnormal segregation phenotypes. The SAC component Mph1 acts upstream of other SAC members and is crucial for a recruitment of the checkpoint components to unattached KTs (He et al., 1998; Heinrich et al., 2012). The segregation phenotypes of chromosome 1 sisters in *mph1*Δ and *asp1*^{D333A} *mph1*Δ strains were assayed. In these strains the SAC was deactivated because of the absence of Mph1.

Growth analysis of a *sad1-mCherry cen1-gfp* strain versus an *mph1*Δ *sad1-mCherry cen1-gfp* strain showed an increased TBZ-sensitivity for the latter. The TBZ-sensitivity of an *asp1*^{D333A} *mph1*Δ *sad1-mCherry cen1-gfp* strain was higher than that of the *mph1*Δ strain indicating that in *asp1*^{D333A} cells KT-MT attachments were defective and required an active SAC (Figure 3-6 A, bottom panel).

Microscopic analysis of the segregation behavior of chromosome 1 sisters in these strains revealed that the *mph1*Δ *sad1-mCherry cen1-gfp* strain showed normal segregation in 91.5 % and aberrant segregation phenotypes in 8.5 % of the cells (Figure 3-6 B). An *asp1*^{D333A} *mph1*Δ *sad1-mCherry cen1-gfp* strain showed a higher amount of abnormal chromosome segregation. 25 % of cells showed aberrant mitosis. 8 % of the cells distributed their chromosome 1 sisters unequally while 17 % of mitotic cells showed a lagging chromosome (Figure 3-6 B).

Thus, the aberrant chromosome segregation phenotypes observed for cells without Asp1-generated IP₈ were increased in an *mph1*Δ background, showing that these cells depended on a functional SAC. As another prominent phenotype of the *asp1*^{D333A} strain is a breakage of the mitotic spindle (Topolski et al., 2016) the amount of spindle breaks in an *asp1*^{D333A} background with a functional or non-functional SAC was analyzed. It was found that the amount of breaking spindles was not altered by SAC depletion (data not shown).

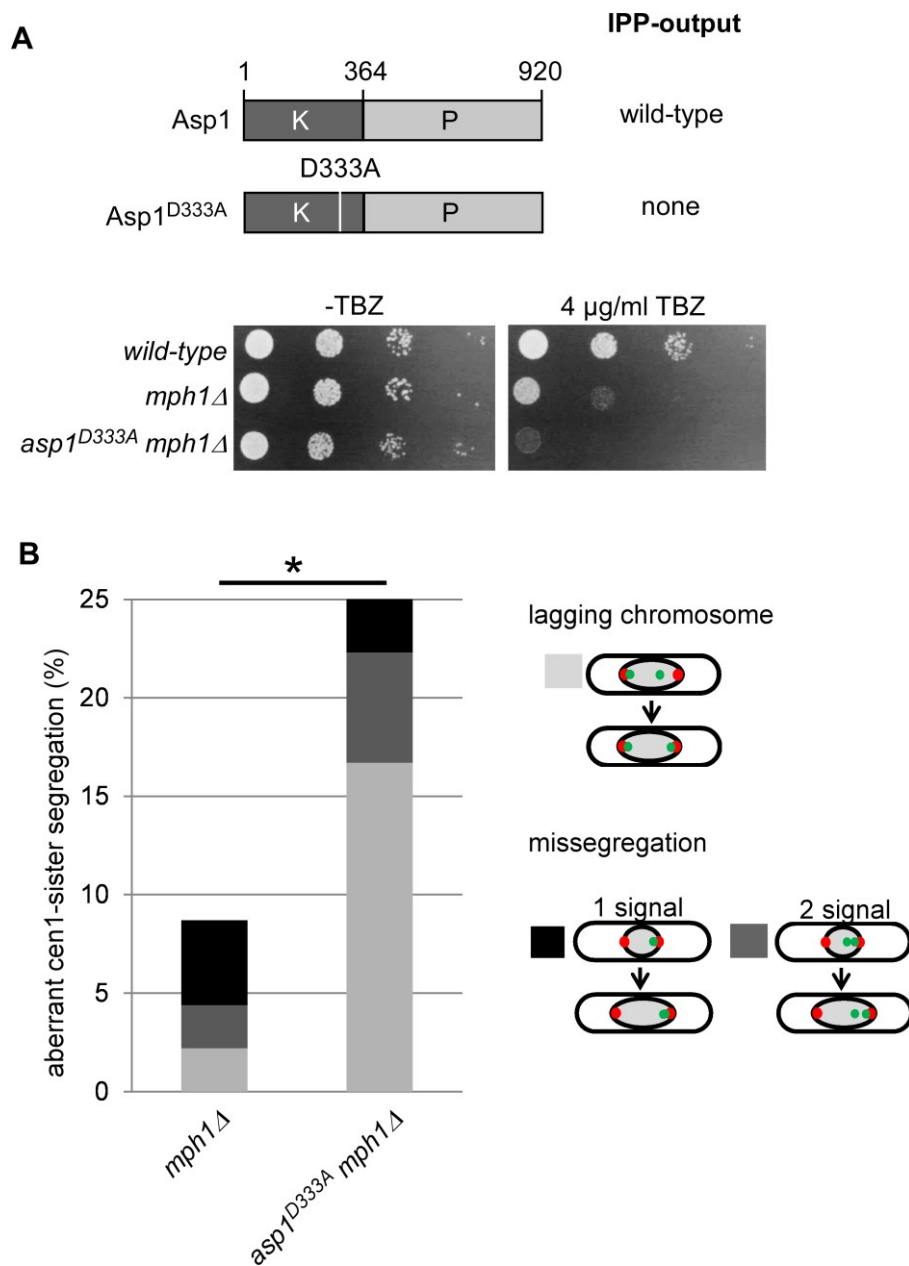


Figure 3-6 Aberrant segregation phenotypes increase in the absence Asp1-generated IP_s in an *mph1*Δ strain background.

A: Asp1-variants used are depicted at the top. Serial dilution patch tests (10^4 - 10^1 cells) of the indicated strains expressing *sad1-mCherry* and *cen1-gfp*. Strains were patched on YE5S with 4 μg/ml or without TBZ (-TBZ) and incubated at 25°C for 3 days (performed by Eva Walla). **B:** Diagrammatic illustration of the percentage of aberrant cen1-GFP segregation as depicted on the right in the indicated strains. *mph1*Δ: 2 % lagging chromosomes, 2.5 % missegregation with two distinguishable cen1-GFP signals, 4 % missegregation with one cen1-GFP signal (n = 46), *asp1*^{D333A} *mph1*Δ 17 % lagging chromosomes, 5 % missegregation with two distinguishable cen1-GFP signals, 3 % missegregation with one cen1-GFP signal (n = 36). (*: p ≤ 0.05, χ^2 -test). The results in this figure have been published in (Topolski et al., 2016).

3.2.3 Higher-than-wild-type IP₈-levels increase chromosome transmission fidelity

Next I tested if higher-than-wild-type IP₈-levels had the opposite effect on chromosome transmission fidelity.

Preliminary results from Dr. Boris Topolski showed that a wild-type strain and an *asp1*^{H397A} strain (higher-than-wild-type IP₈-levels) showed no aberrant segregation phenotypes in an immunofluorescence experiment (Topolski, 2013). As the number of abnormal chromosome segregation therefore seemed to be very low another approach was used to analyze the occurrence of aberrant segregation phenotypes under these conditions in more detail.

3.2.3.1 Higher-than-wild-type IP₈-levels reduce aberrant segregation phenotypes

To analyze chromosome segregation in living cells with higher-than-wild-type IP₈-levels live cell imaging was performed.

Compared to the *sad1-mCherry cen1-gfp* strain with wild-type IP₈-levels the amount of lagging chromosomes was reduced from 3 % to 1.7 % in *asp1*^{H397A} *sad1-mCherry cen1-gfp* cells. Missegregation events were not detected for either strain (Figure 3-7).

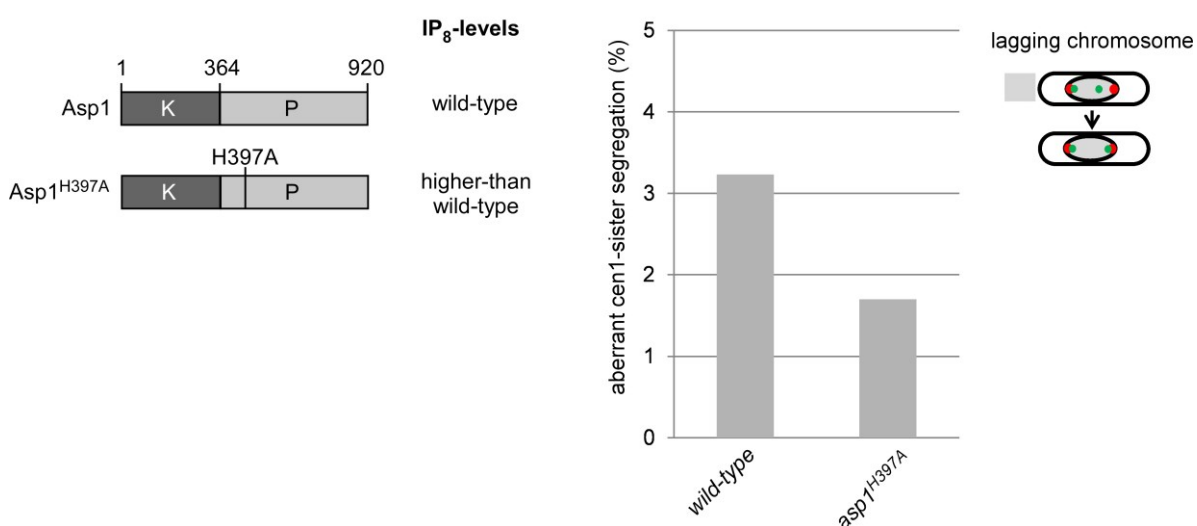


Figure 3-7 Higher-than-wild-type IP₈-levels slightly reduce aberrant segregation phenotypes.

Asp1-variants used are depicted on the left. Diagrammatic illustration of the percentage of aberrant *cen1*-GFP segregation as depicted on the right in the indicated strains: wild-type 3.23 (n = 62), *asp1*^{H397A} 1.72 (n = 58). The results in this figure have been published in (Topolski et al., 2016).

This result indicated that *asp1^{H397A}* cells made fewer errors in the segregation of chromosome 1 sisters than cells with wild-type IP₈-levels but due to the low level of chromosome segregation errors in the wild-type strain this result was not significant.

To get better numbers, the experiment was repeated in SAC depleted cells. Growth analysis of the strains used revealed that the *asp1^{H397A} mph1Δ* strain was less TBZ-sensitive than the *mph1Δ* strain (Figure 3-8 A, bottom panel).

To assess if this effect was due to a reduced amount of aberrant segregation phenotypes in an *asp1^{H397A}* background, *mph1Δ* and *asp1^{H397A} mph1Δ* cells expressing SV40::*atb2⁺-gfp* (α-tubulin-GFP (Bratman and Chang, 2007)) were fixed and stained with DAPI to visualize the DNA. The *asp1^{H397A}* strain showed normal chromosome segregation in 91 % of mitotic cells analyzed. 9 % of cells showed a mitotic spindle with part of the DNA located at one spindle end while the other was still present between the cell equator and the opposite spindle end (Figure 3-8 B), indicating defective KT-MT attachments. An *mph1Δ* strain showed aberrant segregation phenotypes in 19 % of the cells (Figure 3-9 B). 16 % of the *asp1^{H397A} mph1Δ* double mutant cells showed aberrant segregation phenotypes which was a slight reduction compared to the *mph1Δ* strain (Figure 3-8 B).

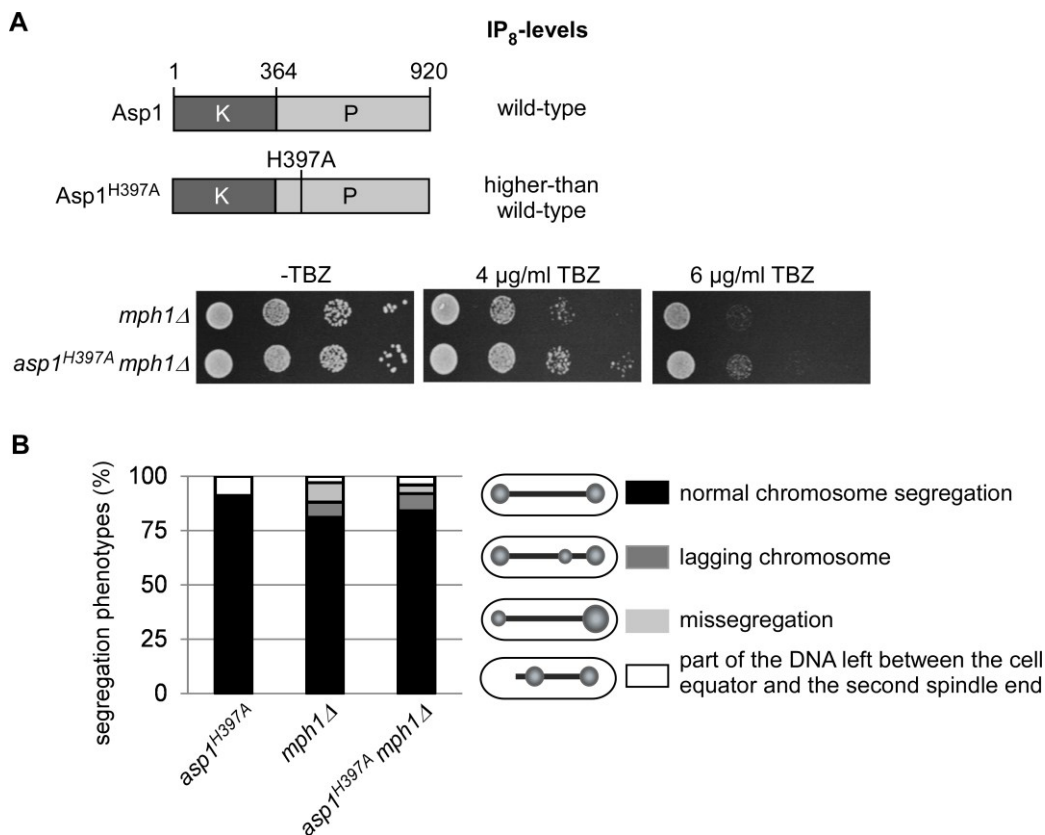


Figure 3-8 Higher-than-wild-type IP₈-levels slightly reduce missegregation events in an *mph1Δ* background.

(Figure legend continued on the next page).

A: Asp1-variants used are depicted at the top. Serial dilution patch tests (10^5 - 10^1 cells) of the indicated strains. Strains were patched on MM with all supplements without TBZ (-TBZ) or with 4 μ g/ml, 6 μ g/ml and incubated at 25°C for 4 days. **B:** Diagram of the segregation defects in the indicated strains endogenously expressing SV40::*atb2*⁺-*gfp*. Strains were grown overnight in MM with all supplements at 25°C. Cells were fixed with 96 % EtOH. Chromosome missegregation was analyzed via DAPI staining. Phenotypes observed are indicated on the right. *asp1*^{H397A}: 9 % with part of the DNA left at the cell equator; *mph1* Δ : 7 % lagging chromosomes, 9 % missegregation, 3 % with part of the DNA left at the cell equator, *asp1*^{H397A} *mph1* Δ : 8 % lagging chromosomes, 4 % missegregation, 4 % with part of the DNA left at the cell equator n= 100/ strain.

Thus, with higher-than-wild-type IP₈-levels aberrant segregation phenotypes in cells with depleted SAC activity (*mph1* Δ) were slightly reduced. To further analyze the effect of higher-than-wild-type IP₈-levels on chromosome segregation the segregation behavior of chromosome 1 sisters in living cells was scored using *sad1-mCherry cen1-gfp* strains. Growth analysis of the *sad1-mCherry cen1-gfp* strains showed that the *mph1* Δ single mutant strain was slightly more TBZ-sensitive than the *asp1*^{H397A} *mph1* Δ double mutant strain (Figure 3-9 A, bottom panel). Microscopic analysis of these strains showed that the *mph1* Δ *sad1-mCherry cen1-gfp* strain revealed aberrant segregation phenotypes in 8 % of the cells (Figure 3-9 B). If *asp1*^{H397A} was present the total amount of aberrant segregation phenotypes was similar with 9 %. However, the type of aberrant segregation phenotypes was altered. Missegregation events were reduced from 6.5 (*mph1* Δ) to 2.5 %. The percentage of lagging chromosomes increased from 2.2 (*mph1* Δ) to 7.5 % (Figure 3-9 B, left).

I additionally determined the missegregation events in *mph1* Δ *sad1-mCherry cen1-gfp* and *asp1*^{H397A} *mph1* Δ *sad1-mCherry cen1-gfp* strains in media with TBZ in the hope to sensitize the system. In the presence of TBZ the total amount of aberrant segregation phenotypes in *mph1* Δ *sad1-mCherry cen1-gfp* cells increased to 24 %. Lagging chromosomes were detected in 16 %, missegregation in 8 % of the cells (Figure 3-9 B, right). Only 17 % of *asp1*^{H397A} *mph1* Δ *sad1-mCherry cen1-gfp* cells showed aberrant segregation phenotypes (15 % lagging chromosomes, 2 % missegregation) (Figure 3-9 B, right). This result indicated that in cells with higher-than-wild-type IP₈-levels fewer faulty KT-MT attachments were present.

In line with this hypothesis I found that the average distance between a lagging chromosome 1 sister and the SPB was decreased from 2.2 (*mph1* Δ *sad1-mCherry cen1-gfp*) to 1.79 μ m with higher-than-wild-type IP₈-levels (*asp1*^{H397A}). This indicated that faulty KT-MT-attachments that lead to lagging chromosomes were corrected before the distance between the centromere and the SPB increased to a high extend (Figure 3-9 C).

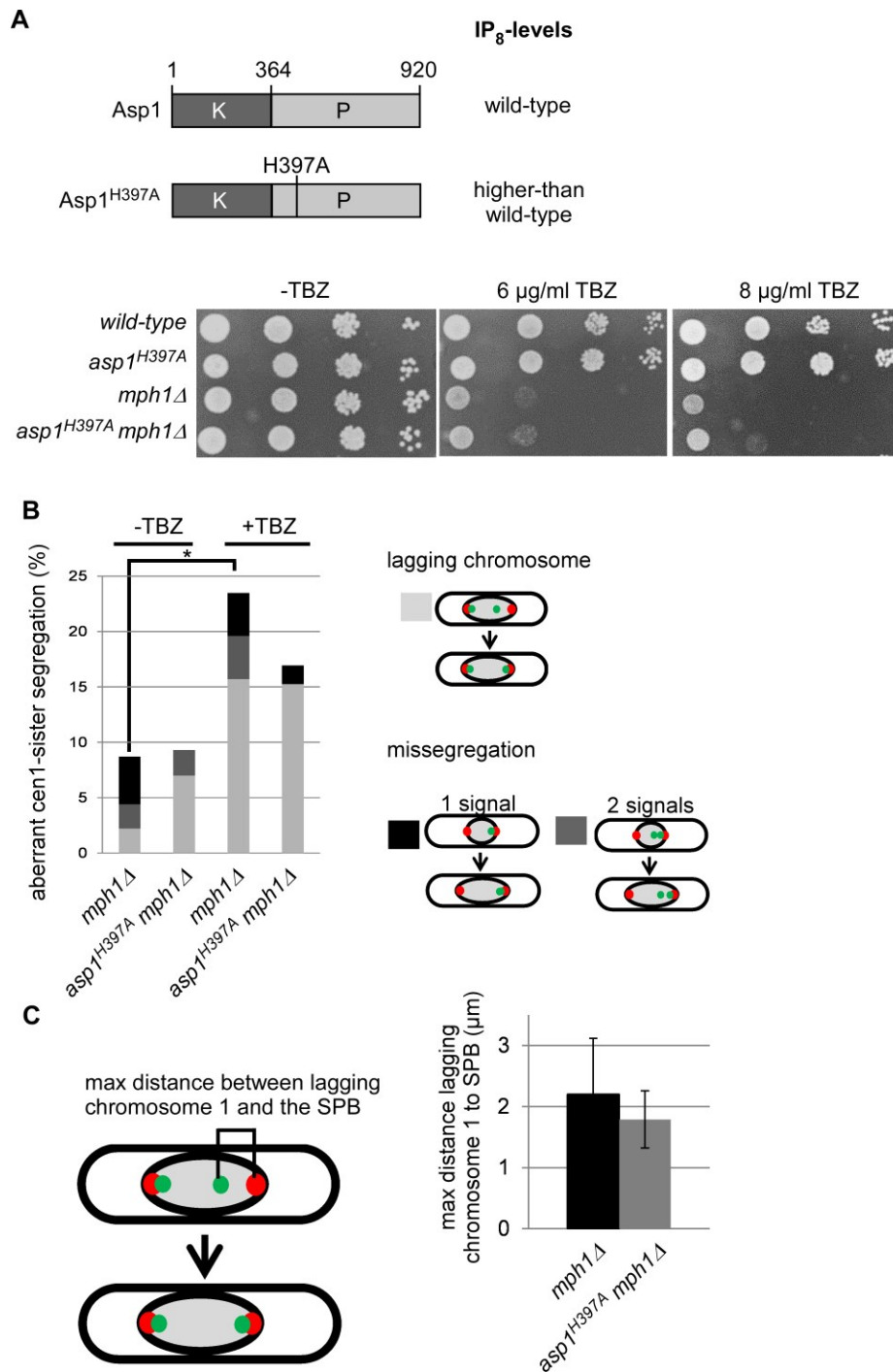


Figure 3-9 Higher-than-wild-type IP₈-levels reduce missegregation events in SAC-less cells.

A: Asp1-variants used are depicted at the top. Serial dilution patch tests (10^4 - 10^1 cells) of the indicated strains expressing *sad1-mCherry* and *cen1-gfp*. Strains were patched on YE5S with 6 or 8 µg/ml or without TBZ (-TBZ) and incubated at 25°C for 5 days (performed by Eva Walla). **B:** Diagram for the percentage of aberrant cen1-GFP segregation in the indicated strains in absence (-TBZ) or with addition of 5 µg/ml TBZ to the overnight culture (+TBZ): -TBZ: *mph1Δ*: 2 % lagging chromosomes, 2.5 % missegregation with two distinguishable cen1-GFP signals, 4 % missegregation with one cen1-GFP signal (n = 46), *asp1^{H397A} mph1Δ* 7 % lagging chromosomes, 2.5 % missegregation with two distinguishable cen1-GFP signals (n = 44); +TBZ: *mph1Δ*: 16 % lagging chromosomes, 4 % missegregation with two distinguishable cen1-GFP signals, 4 % missegregation with one cen1-GFP signal (n = 51), *asp1^{H397A} mph1Δ*: 15 % lagging chromosomes, 2 % missegregation with one cen1-GFP signal (n = 59). **C:** Diagram of the average of the maximal distance of chromosome 1 to the SPB it is lagging behind under +TBZ-conditions. *mph1Δ* 2.2 (n = 7), *asp1^{H397A} mph1Δ* 1.79 (n = 9). The results in Part B of this figure have been published in (Topolski et al., 2016).

3.2.3.2 Higher-than-wild-type IP₈-levels increase the transmission fidelity of a non-essential minichromosome

In the last chapter, I analyzed the segregation behavior of an endogenous chromosome in the presence of different IP₈-levels. The effects observed were moderate, thus I used another system to analyze the effect of variations in IP₈-levels on chromosome transmission fidelity. Namely, a non-essential minichromosome loss assay. This assay gives a more sensitive read-out for chromosome loss as the minichromosome loss rate is 10-times higher than that of an endogenous chromosome (Niwa et al., 1989).

The strain used carried apart from the three *S. pombe* chromosomes a 550 kb non-essential minichromosome, named Ch16. Presence of Ch16 in the cell gave rise to white colonies on limited amount of adenine medium. A loss of Ch16 during the growth of the colony resulted in a white/pink sector colony. The amount of sector colonies therefore gave a read-out of how stable Ch16 was segregated (Niwa et al., 1989). To analyze the effect of IP₈ on Ch16 loss the assay strain was either transformed with a vector control, *asp1*¹⁻³⁶⁴ or *asp1*³⁶⁵⁻⁹²⁰ expressed on plasmids via the *nmt1*⁺-promoter. I found that under low expression conditions (with thiamine) 1.21 % of the analyzed colonies were sector. This number was decreased to 0.56 % with expression of *asp1*¹⁻³⁶⁴ and to 0.67 % with *asp1*³⁶⁵⁻⁹²⁰ expression (Figure 3-10 A, bottom left). Strikingly, with high expression of *asp1*¹⁻³⁶⁴ the percentage of sector colonies was reduced from 0.93 (vector control) to 0.05 % (Figure 3-10 A, bottom right). This was a 20-fold reduction in the loss of Ch16. Thus, higher-than-wild-type IP₈-levels massively increased the transmission fidelity of a non-essential minichromosome. With high expression of *asp1*³⁶⁵⁻⁹²⁰ an increase in sector colonies to 1.06 % was observed, indicating that lower-than-wild-type IP₈-levels increased Ch16 loss (Figure 3-10 A, bottom right).

To analyze the differences in expression of *asp1*¹⁻³⁶⁴ under low and high expression conditions, *asp1*¹⁻³⁶⁴-*gfp* was plasmid-expressed under the control of the *nmt1*⁺-promoter. Proteins extracted from transformants grown under low or high expression conditions were used for western blot analysis. Asp1¹⁻³⁶⁴-GFP was detected under high expression conditions (Figure 3-10 B, left panel). Under low expression conditions the blot had to be overloaded 6x to detect Asp1¹⁻³⁶⁴-GFP (Figure 3-10 B, right panel).

Thus, the Asp1¹⁻³⁶⁴ protein was present under low and high expression conditions. Therefore the effect observed in the minichromosome loss assay seemed to be dosage dependent.

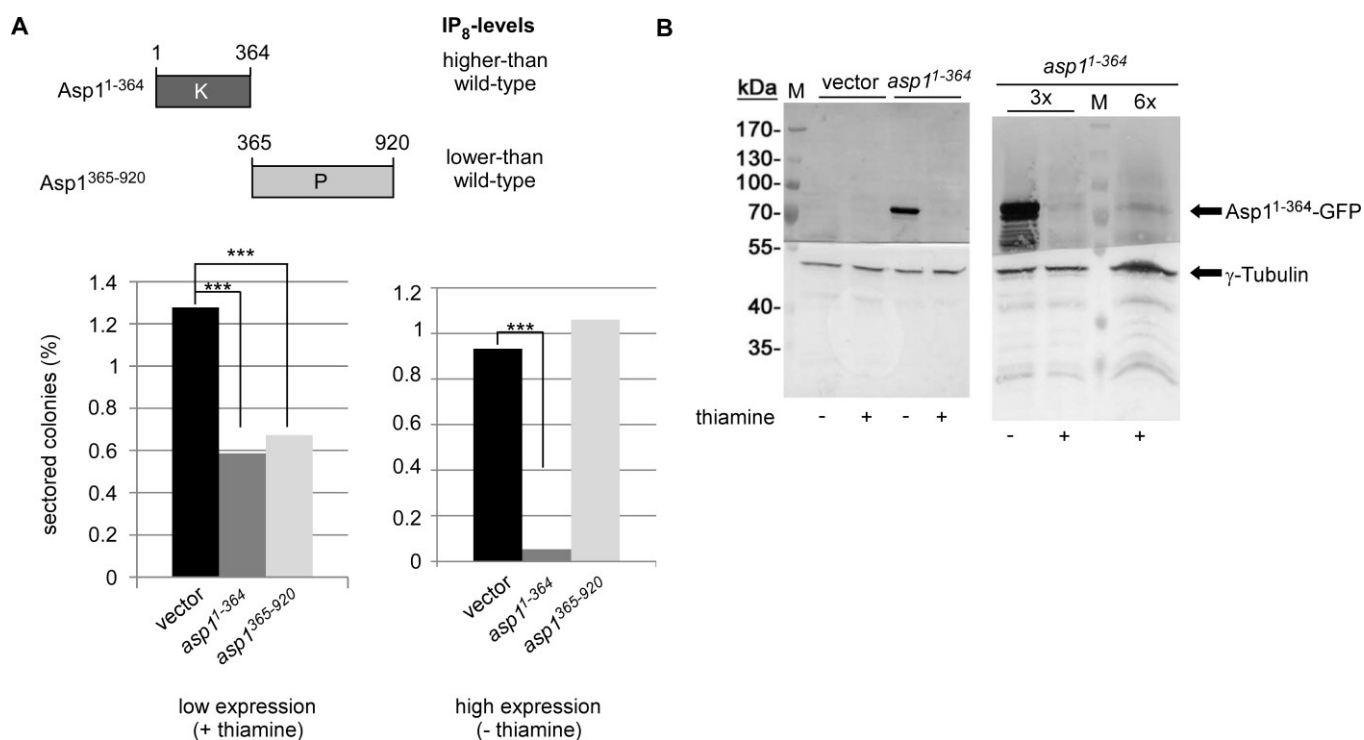


Figure 3-10 Higher-than-wild-type IP₈-levels reduce the loss of a non-essential minichromosome.

A: Asp1-variants used are depicted at the top. Diagrammatic illustration of the amount of sectoring which represents the loss of the Ch¹⁶ minichromosome. A Ch¹⁶ containing strain was transformed with a vector control, *asp1*¹⁻³⁶⁴ or *asp1*³⁶⁵⁻⁹²⁰ under the control of the *nmt1*⁺-promoter. Transformants were plated on plasmid-selective MM with a limited amount of adenine and with or without thiamine resulting in either low (+ thiamine) or high (- thiamine) expression of *asp1*¹⁻³⁶⁴ or *asp1*³⁶⁵⁻⁹²⁰. The amount of sectoring was assayed after 10 days at 25°C. For + thiamine: control 1.21 (n= 19411); *asp1*¹⁻³⁶⁴ 0.56 (n= 10075); *asp1*³⁶⁵⁻⁹²⁰ 0.67 (n= 14874). For -thiamine: control 0.93 (n= 21582); *asp1*¹⁻³⁶⁴ 0.05 (n= 21488); *asp1*³⁶⁵⁻⁹²⁰ 1.06 (n= 12945); (***: p ≤ 0.001). **B:** Western blot analysis of Asp1¹⁻³⁶⁴-GFP in cultures with (+ thia) or without (- thia) thiamine. Transformants were grown 24 h at 30°C in plasmid selective media before proteins were extracted. Left: Detection of Asp1¹⁻³⁶⁴-GFP (69 kDa) and γ-Tubulin (50 kDa). Right: Blot overloaded 3x and 6x to visualize Asp1¹⁻³⁶⁴-GFP expression in presence of thiamine. The result for *asp1*¹⁻³⁶⁴ plasmid expression in Part A and Part B have been published: (Topolski et al., 2016).

3.3 Modifications of the Asp1 protein

In the above experiments I demonstrated that Asp1-generated IP₈ influenced chromosome segregation. However, it remained unclear how the function of Asp1 was regulated to mediate the observed effects at the right time and in the right location. Therefore, it was interesting to analyze if the function of the Asp1 protein was modulated during mitosis to induce the effects that led to an optimized chromosome segregation process.

(Koch et al., 2011) showed that Asp1 was phosphorylated by the aurora kinase Ark1 at the serine at position 674 during mitosis. This residue lies within the pyrophosphatase domain of the Asp1 protein (Figure 3-11 A). To test if this modification was important for the function of Asp1 two plasmid-expressed *asp1* mutants were generated. The first was *asp1*^{S674A} which was a phosphodead mutant. The second one was *asp1*^{S674E} which was a phosphomimicking mutation. The functionality of these variants was tested in a patch test experiment. To this end *asp1*⁺, *asp1*^{S674A} and *asp1*^{S674E} were plasmid-expressed under control of the *nmt1*⁺-promoter in an *asp1*Δ strain. All three proteins rescued the TBZ-sensitivity of that strain if expressed at low or high levels (Figure 3-11 B).

To exclude the possibility that the proteins induced the same effect on the growth behavior of the *asp1*Δ strain but were expressed at different levels an additional Western Blot analysis was performed. Proteins of an *asp1*Δ strain transformed with a vector control or *asp1*⁺-*gfp*, *asp1*^{S674A}-*gfp* or *asp1*^{S674E}-*gfp* expressed on plasmids were extracted. All protein extracts contained similar levels of proteins as analyzed on a 10 % SDS-gel stained with Coomassie blue (Figure 3-11 C, left panel). Western Blot analysis of these protein extracts was performed using an α-GFP antibody to detect the *asp1*-*gfp* constructs. While for the vector control there was no band detected with an α-GFP antibody a strong band was observed for the transformants expressing *asp1*⁺-*gfp*, *asp1*^{S674A}-*gfp* or *asp1*^{S674E}-*gfp* on plasmids. Quantification of the band intensity normalized to the γ-tubulin control showed that these *asp1* variants were expressed at similar levels (Figure 3-11 C, right panel).

Thus, the modification of the serine residue at position 674 was not affecting Asp1 function.

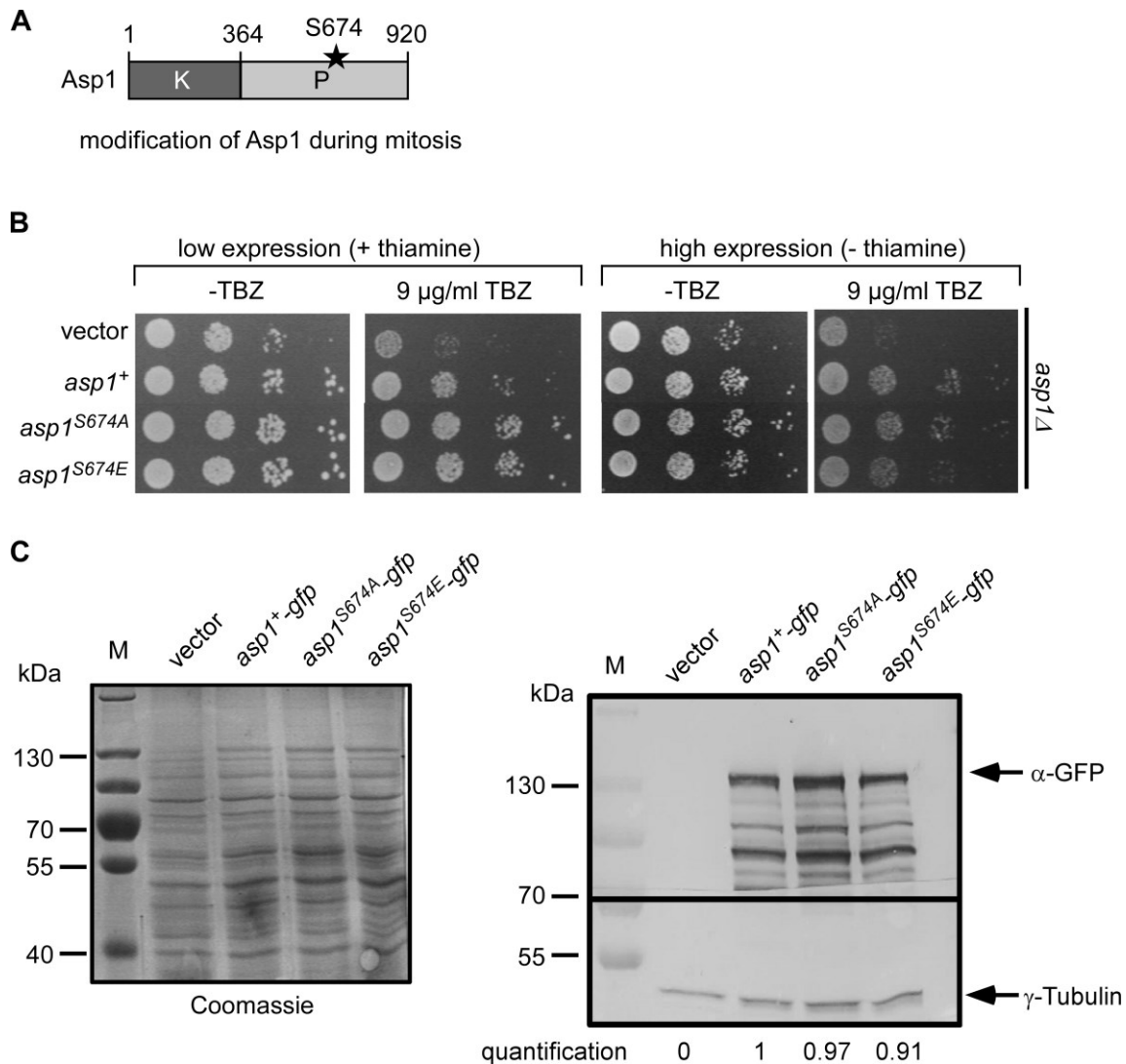


Figure 3-11 Modification of the residue S674 is not important for Asp1 function.

A: Schematic overview of a modification of the Asp1 protein. The serine on position 674 within the pyrophosphatase domain is phosphorylated by Ark1 during mitosis (modification indicated as star) (Koch et al., 2011). **B:** Serial dilution patch tests (10^4 - 10^1 cells) of *asp1*Δ transformed with a vector control, *asp1*⁺, *asp1*^{S674A} or *asp1*^{S674E} expressed on a plasmid via the *nmt1*⁺-promoter. Transformants were grown under plasmid-selective conditions on media with or without thiamine and without or with TBZ for 12 days at 25°C. **C:** Protein expression analysis for the Asp1^{S674} variants. Left: Coomassie staining for whole cell protein extracts of an *asp1*Δ strain transformed with vector control, *asp1*⁺-gfp, *asp1*^{S674A}-gfp and *asp1*^{S674E}-gfp. Transformants were grown 24 h under plasmid selective conditions in thiamine-free media before proteins were extracted. Equal amounts of proteins were loaded on a 10 % SDS-gel and stained with Coomassie blue. Right: Western blot analysis of the protein extracts used on the left. Top: Detection of Asp1-GFP, Asp1^{S674A}-GFP and Asp1^{S674E}-GFP (132 kDa) with an α-GFP antibody. Middle: Detection of γ-Tubulin (50 kDa) using an α-γ-Tubulin antibody. Bottom: Quantification of the GFP signal for the Asp1 variants detected in Western Blot analysis. The band intensity of GFP was normalized against the γ-Tubulin bands. *asp1*⁺-gfp measurement was set to 1.

3.4 Asp1-generated IP₈ alters the kinetochore composition in *S. pombe*

We have shown that Asp1-generated IP₈ influenced chromosome transmission fidelity and the formation of the mitotic spindle (Chapter 3.2 p. 95 (Topolski et al., 2016)). However, for precise chromosome transmission an interplay between spindle MTs and the kinetochore (KT) is required. Thus the question arose if Asp1-made IP₈ affected the function of the kinetochore.

3.4.1 The effect of cellular IP₈-levels on the Sim4-kinetochore-subcomplex

I therefore analyzed if Asp1-generated IP₈ influenced KT proteins. Preliminary data of Boris Topolski (2013) showed that IP₈-levels might affect members of the Sim4-KT-sub-complex. The Sim4-complex contains 12 different proteins (Liu et al., 2005; Shiroiwa et al., 2011). Within the Sim4-complex Mal2 and Fta2, as well as Mis6/Mis17/Mis15 show localization dependency (Hayashi et al., 2004; Kerres et al., 2006). More information about the Sim4-complex can be found in Chapter 1.3.1.3.2 (p. 25).

3.4.1.1 Plasmid-borne expression of *asp1*¹⁻³⁶⁴ and *asp1*³⁶⁵⁻⁹²⁰ affects the growth of Sim4-complex mutant strains

To screen the effect of variations in cellular IP₈-levels on Sim4-complex proteins ts mutant strains were used.

A well characterized member of the Sim4-complex is the essential Mal2 protein (Fleig et al., 1996; Jin et al., 2002). In the *mal2-1^{ts}* mutant strain the Mal2-1 protein shows no KT localization at the restrictive temperature. This leads to a massive amount of chromosomal missegregation, an elongated metaphase spindle, and lethality (Jin et al., 2002; Kerres et al., 2006). The *mal2-1* mutant strain was transformed with either *asp1*¹⁻³⁶⁴ or *asp1*³⁶⁵⁻⁹²⁰ expressed on a plasmid via the *nmt1*⁺-promoter. Plasmid-expression of *asp1*¹⁻³⁶⁴ and *asp1*³⁶⁵⁻⁹²⁰ under low expression and high expression conditions had no effect on the growth of a wild-type strain (Figure 3-12 B). Low expression of *asp1*¹⁻³⁶⁴ had no effect on the growth of the *mal2-1^{ts}* strain, while *asp1*³⁶⁵⁻⁹²⁰ expression led to a slight rescue of the non-growth phenotype at 30°C.

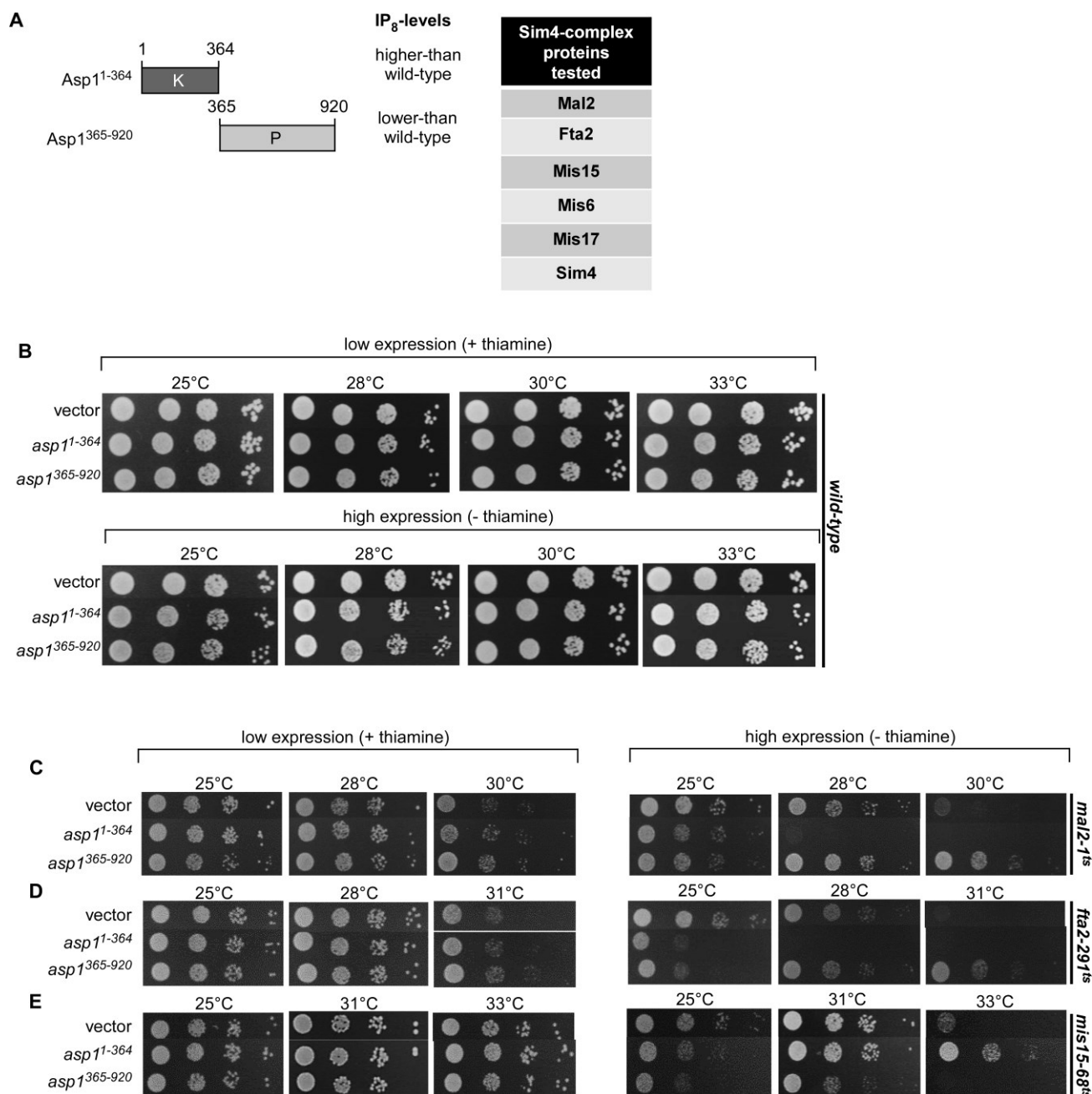


Figure 3-12 A change in cellular IP₈-levels influences the growth of Sim4-complex mutant strains.

A: Left: Asp1-variants used. Right: Members of the Sim4-complex that were tested in the screen. **B-E:** Serial dilution patch tests (10^4 - 10^1 cells) of the indicated strains transformed with a vector control, *asp1¹⁻³⁶⁴* or *asp1³⁶⁵⁻⁹²⁰* plasmids. Transformants were grown under plasmid-selective conditions in media with or without thiamine for 4-6 days at the indicated temperatures. The temperatures shown were selected to best demonstrate the differences in growth. Examples out of at least 2 (B) or 3 (C-E) transformants/ plasmid are shown. Patch test in B performed by Eva Walla.

On thiamine less media the *mal2-1^{ts}* strain transformed with a vector control could not grow at temperatures $\geq 30^\circ\text{C}$ (Figure 3-12 C). High expression of *asp1¹⁻³⁶⁴* inhibited colony formation already at 28°C . However, expression of *asp1³⁶⁵⁻⁹²⁰* on the other hand rescued the

ts phenotype of the *mal2-1^{ts}* strain and enabled it to grow at the restrictive temperature (30°C) (Figure 3-12 C). Thus, higher-than-wild-type IP₈-levels reduced the growth of the *mal2-1^{ts}* strain in a temperature dependent manner, while lower-than-wild-type levels rescued the ts phenotype.

I next analyzed if the effect of *asp1¹⁻³⁶⁴* and *asp1³⁶⁵⁻⁹²⁰* expression was also relevant for the Sim4-complex mutant strain *fta2-291^{ts}*. The growth of the *fta2-291^{ts}* mutant strain was not affected by low expression of *asp1¹⁻³⁶⁴* or *asp1³⁶⁵⁻⁹²⁰*. Without thiamine the strain transformed with a vector control was not able to grow at 31°C (Figure 3-12 D, left panel). Expression of *asp1¹⁻³⁶⁴* led to reduced growth at the permissive temperature (25°C) and was lethal at higher temperatures, while expression of *asp1³⁶⁵⁻⁹²⁰* led to the opposite effect and rescued the ts phenotype of the *fta2-291^{ts}* strain (Figure 3-12 D, right panel).

Thus, similar to the *mal2-1^{ts}* strain, the growth of the *fta2-291^{ts}* strain is rescued by lower-than-wild-type IP₈-levels and reduced with higher-than-wild-type IP₈-levels.

Interestingly, the Sim4-complex mutant strain *mis15-68^{ts}* showed the opposite phenotype. High expression of *asp1³⁶⁵⁻⁹²⁰* reduced the growth of the *mis15-68^{ts}* strain already at the permissive temperature compared to the vector control, while expression of *asp1¹⁻³⁶⁴* rescued the ts phenotype (Figure 3-12 E). Hence, the growth of the *mis15-68^{ts}* strain was rescued by higher-than-wild-type IP₈-levels and reduced by lower-than-wild-type IP₈-levels.

Analysis of the effect of *asp1¹⁻³⁶⁴* and *asp1³⁶⁵⁻⁹²⁰* expression on other Sim4-complex mutant strains was performed the results shown in Table 3-2. The growth of the *mis6-302^{ts}* and *mal2-10^{ts}* mutant strains was reduced by *asp1¹⁻³⁶⁴* expression while *asp1³⁶⁵⁻⁹²⁰* expression had the opposite effect. The growth of the *mal2-30^{ts}* and *mis17-362^{ts}* mutant strains was slightly reduced by expression of either *asp1¹⁻³⁶⁴* or *asp1³⁶⁵⁻⁹²⁰* under high expression conditions. The *sim4-193^{ts}* mutant strain showed a slight rescue of the ts phenotype with both *asp1¹⁻³⁶⁴* and *asp1³⁶⁵⁻⁹²⁰* expression (Supplementary Figure 5 (p. 187)).

Therefore, the growth of all analyzed Sim4-complex mutant strains was affected by changes in cellular IP₈-levels, albeit to varying degrees.

As the *mal2-1^{ts}*, *fta2-291^{ts}* and *mis15-68^{ts}* strains showed the clearest phenotypes with changing IP₈-levels, I analyzed the effect of these high-energy-molecules on these strains in more detail.

Influence of IP ₃ on growth of Sim4-complex mutants			
Category	Mutant	asp1 variant	
		asp1 ¹⁻³⁶⁴	asp1 ³⁶⁵⁻⁹²⁰
		growth phenotype	
1	<i>mal2-1^{ts}</i> <i>mal2-10^{ts}</i> <i>fta2-291^{ts}</i> <i>mis6-302^{ts}</i>	↓	↑
2	<i>mis15-68^{ts}</i>	↑	↓
3	<i>mal2-30^{ts}</i> <i>mis17-362^{ts}</i>	↓	↓
4	<i>sim4-193^{ts}</i>	↑	↑

Table 3-2 Effect of *asp1*¹⁻³⁶⁴ and *asp1*³⁶⁵⁻⁹²⁰ expression on Sim4-complex mutant strains.

There were four categories observed. ↑ growth defect partially rescued ↓ reduced growth. The arrow size indicates the strength of the effect.

3.4.1.2 Plasmid-borne expression of *asp1*¹⁻³⁶⁴ increases chromosome missegregation of the *mal2-1^{ts}* strain

How is this effect of *asp1*¹⁻³⁶⁴ and *asp1*³⁶⁵⁻⁹²⁰ expression on the growth of Sim4-complex mutants mediated?

The *mal2-1^{ts}* strain shows a high level of missegregation (Fleig et al., 1996) and thus I determined if chromosome segregation in this strain was affected by expression of the *asp1* variants. To this end an immunofluorescence experiment of the *mal2-1^{ts}* strain transformed with a vector control, *mal2*⁺, *asp1*¹⁻³⁶⁴ or *asp1*³⁶⁵⁻⁹²⁰ was performed. The mitotic spindle was visualized via antibody staining and the DNA stained with DAPI.

At 25°C the *mal2-1^{ts}* strain transformed with the vector control had 64 % mitotic cells with normal chromosome segregation where two equal DAPI signals were observed at the ends of the spindle (Figure 3-13 black bar). 16 % of the cells showed lagging chromosome(s) where three signals were detected on the mitotic spindle, two signals at the spindle ends and one in between. In 10 % of the cells missegregation was observed, where the amount of DNA at the spindle ends was unequal (lagging chromosomes and missegregation were grouped and are shown as a dark grey bar in Figure 3-13). Furthermore, 6 % of cells showed a DAPI signal that was detected in the middle of the spindle or the DNA was smeared along the spindle (Figure 3-13 light grey bar). The last observed phenotype was a possible non-disjunction in 4 % of the cells where the DAPI signal was only detectable at one spindle

end (Figure 3-13 white bar). Thus, 36 % of the *mal2-1^{ts}* cells transformed with the vector control showed aberrant segregation phenotypes (Figure 3-13 B).

Expression of the plasmid-encoded wild-type *mal2⁺* gene rescued the *mal2-1^{ts}* missegregation phenotype and reduced the amount of aberrant segregation events from 36 % (vector) to 12 % (Figure 3-13 B). Plasmid-borne expression of *asp1¹⁻³⁶⁴* led to a massive increase in abnormal segregation phenotypes to 60 %. While missegregation events were the same as for the vector control (10 %) an increase in lagging chromosomes to 23 % was observed. Furthermore, a massive increase of cells with smeared DNA along the spindle from 6 % (vector control) to 26 % was found. Hence, *asp1¹⁻³⁶⁴* expression in the *mal2-1^{ts}* strain enhanced the aberrant segregation phenotype of this mutant (Figure 3-13 B).

Plasmid expression of *asp1³⁶⁵⁻⁹²⁰* on the other hand led to an increase in chromosome segregation fidelity to 72 % at 25°C. Missegregation phenotypes were reduced to 6 % and lagging chromosomes to 10 % (Figure 3-13 B). Thus higher-than-wild-type IP₈-levels increased aberrant segregation phenotypes in the *mal2-1^{ts}* strain whereas lower-than-wild-type levels reduced them.

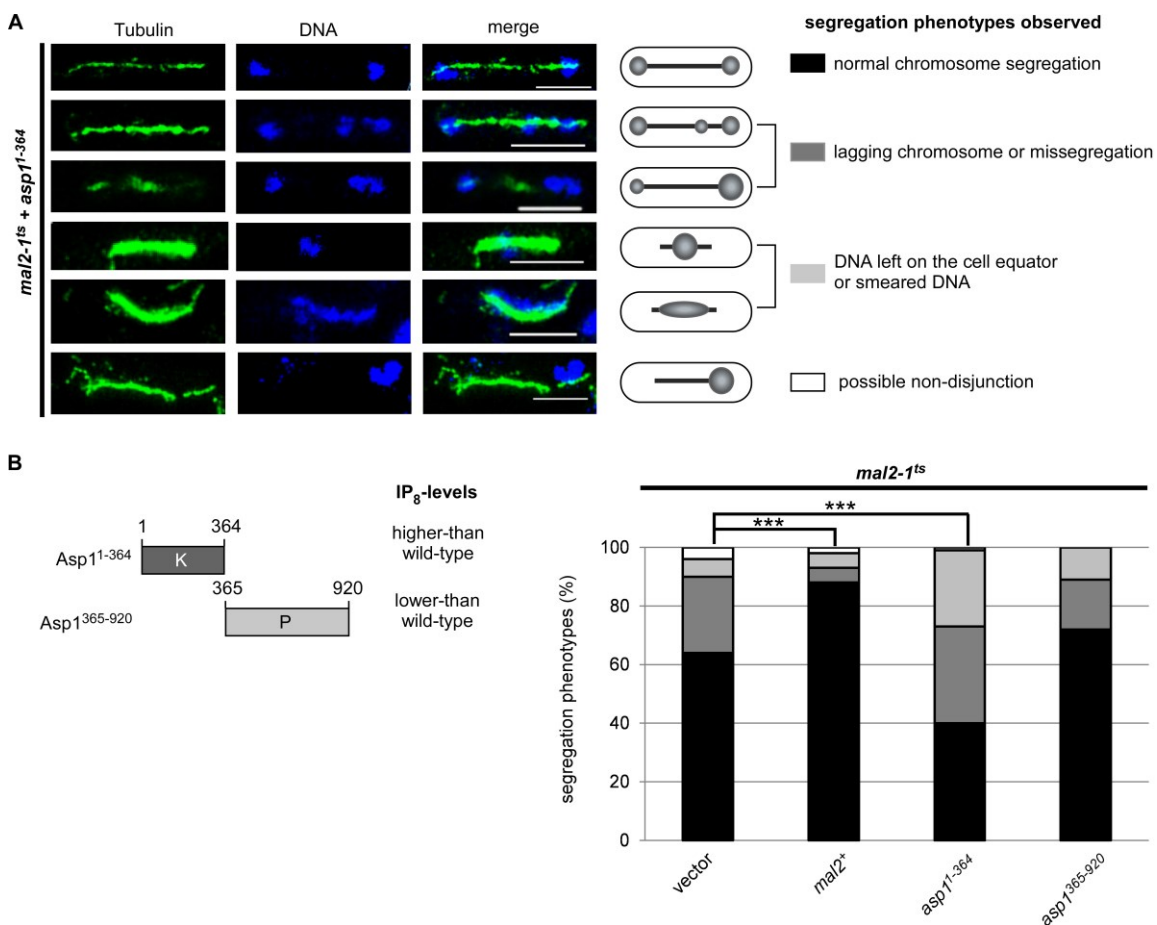


Figure 3-13 Plasmid-borne expression of *asp1¹⁻³⁶⁴* enhances aberrant segregation events in the *mal2-1^{ts}* mutant strain.

(Figure legend continued on the next page).

A: Immunofluorescence (α -TAT1 (tubulin) antibody) and DAPI staining of the *mal2-1^{ts}* strain transformed with a vector control, *asp1¹⁻³⁶⁴* or *asp1³⁶⁵⁻⁹²⁰* expressed on plasmids. Transformants were pre-grown at 25°C in plasmid selective media without thiamine (high expression conditions). Exemplary pictures of the observed phenotypes are shown. Black bar = proper segregation (DNA is equally distributed to the ends of the spindle), dark grey bar = lagging chromosome or unequally distributed DNA, light grey bar = the DNA left on the cell equator or smeared DNA, white bar = possible non-disjunction. Scale bar = 5 μ m. Pictures show the *mal2-1^{ts}* strain transformed with an *asp1¹⁻³⁶⁴* plasmid. Pictures were taken using a Nikon Eclipse Ti microscope with help of M.Sc. Corinna Braun. **B:** Left: Asp1-variants used. Right: Diagram of the phenotypes shown in A observed for the indicated transformants. n = 100/ plasmid; 2 transformants/ plasmid. (***: p \leq 0.005, χ^2 -test).

3.4.1.3 *asp1³⁶⁵⁻⁹²⁰* expressed on a plasmid increases Mal2-1-GFP kinetochore targeting

The Mal2-1 protein is defective in KT localization at high temperatures (30°C) (Jin et al., 2002). Hence, one possibility of how IP₈-levels might influence the growth of a *mal2-1^{ts}* strain might be Mal2-1 KT localization. To analyze whether the KT targeting of Mal2-1 was influenced by IP₈ we determined Mal2-1-GFP KT targeting with different IP₈-levels. The effect of *asp1¹⁻³⁶⁴* or *asp1³⁶⁵⁻⁹²⁰* expression in the *mal2-1^{ts}-gfp* strain was comparable to that of the *mal2-1^{ts}* strain (Figure 3-12 A; Figure 3-14 A, bottom panel). High expression of *asp1¹⁻³⁶⁴* reduced the amount of surviving *mal2-1^{ts}-gfp* cells at 28°C to 0.4 % compared to the vector control (8.3 %). High expression of *asp1³⁶⁵⁻⁹²⁰* increased the number of surviving cells to 34.5 % (Figure 3-14 B, right panel). Microscopic analysis of the Mal2-1-GFP KT signal in transformants expressing these *asp1* variants was performed.

I had noticed previously that in general the fluorescence signal intensity correlated with cell size (Figure 3-14 C). An increase in cell size correlated with an increased fluorescence signal intensity. This effect was not restricted to the Mal2-1-GFP signal, but was also seen for other fluorescent proteins (Supplementary Figure 6 (p. 187)). To minimize the influence of this effect on the analysis only cells with a size between 9-12 μ m were analyzed. That way a more homogenous population within the samples was analyzed.

Mal2-1-GFP fluorescence signals of *asp1³⁶⁵⁻⁹²⁰* expressing *mal2-1^{ts}-gfp* cells were found to be higher than in those transformed with the vector control (6.46 and 2.99 AU, respectively). High expression of *asp1¹⁻³⁶⁴* decreased the fluorescence signals of Mal2-1-GFP from 3 to 2.2 AU compared to the vector control (Figure 3-14 D; E).

Hence, high cellular IP₈-levels reduced the Mal2-1-GFP KT signal, while low levels increased it.

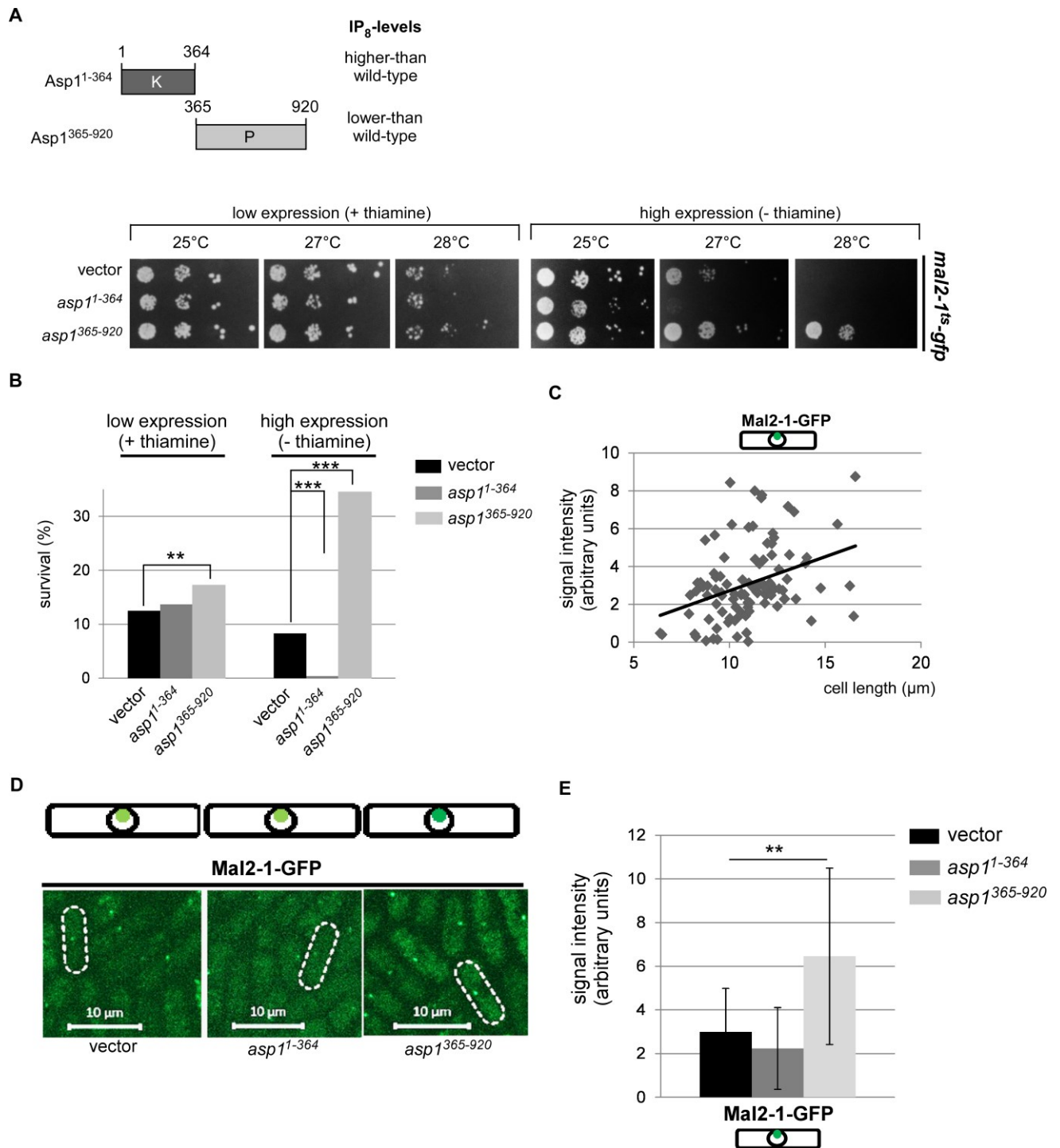


Figure 3-14 Mal2-1-GFP KT localization is affected by *asp1*¹⁻³⁶⁴ and *asp1*³⁶⁵⁻⁹²⁰ expression.

A: Top: Asp1-variants used. Bottom: Serial dilution patch tests (10^4 - 10^1 cells) of the *mal2-1^{ts}-gfp* strain transformed with a vector control, *asp1*¹⁻³⁶⁴ or *asp1*³⁶⁵⁻⁹²⁰ expressed on plasmids. Transformants were grown under plasmid-selective conditions in media with or without thiamine for 8 days at the indicated temperatures. The temperatures shown were selected to best demonstrate the differences in growth. Examples out of at least 5 transformants/ plasmid are shown. **B:** Diagrammatic illustration of the survival rate of the transformants used in A. Transformants were pre-grown overnight at 25°C and 1000 cells/ plasmid were plated on plasmid-selective media with or without thiamine. Plates were incubated at 28°C and the number of growing colonies counted. (**: $p \leq 0.01$; ***: $p \leq 0.005$, χ^2 -test). **C:** Diagram of correlation of Mal2-1-GFP signals and the cell size ($n = 100$). The trendline (black) shows an upward slope. (Figure legend continued on the next page.)

D: Top: Schematic overview of the Mal2-1-GFP fluorescence signal at the KT in the indicated transformants. Light green = weak signal; dark green = strong signal. Bottom: Live fluorescence microscopy pictures of the indicated transformants expressing *mal2-1^{ts}-gfp*. Transformants were pre-incubated for 24 h at 25°C in LFM (live fluorescence media) without leucine and without thiamine before they were patched on agarose pads. Pictures were taken at 20°C with 100 % laser intensity using a Zeiss Spinning Disc-Confocal microscope (pictures taken by Boris Topolski). Scale bar = 10 µm. **E:** Quantification of Mal2-1-GFP fluorescence signals. Pictures taken as in C for the indicated transformants: vector 2.99 AU (arbitrary units) ± 1.99; *asp1¹⁻³⁶⁴* 2.24 AU ± 1.87; *asp1³⁶⁵⁻⁹²⁰* 6.46 AU ± 4.04 (vector: n = 57; *asp1¹⁻³⁶⁴*: n = 47; *asp1³⁶⁵⁻⁹²⁰*: n = 55; **: p ≤ 0.01, two-sample-t-test).

3.4.1.4 Plasmid-expression of *asp1¹⁻³⁶⁴* decreases Mal2-GFP kinetochore targeting

As the localization of the Mal2-1-GFP protein was affected by cellular IP₈-levels I analyzed if this effect was also seen for the wild-type Mal2-GFP protein. Expression of *asp1¹⁻³⁶⁴* or *asp1³⁶⁵⁻⁹²⁰* had no effect on the growth of a *mal2⁺-gfp* strain (Figure 3-15 A, bottom panel). Microscopic analysis of the Mal2-GFP KT signal in these transformants showed that high expression of *asp1¹⁻³⁶⁴* reduced Mal2-GFP fluorescence signals at the KT from 18.8 (vector) to 15.9 AU. High expression of *asp1³⁶⁵⁻⁹²⁰* increased the Mal2-GFP signal compared to the vector control from 18.8 to 20.2 AU (Figure 3-15 B, C).

Thus, KT-targeting of Mal2-GFP was also affected inversely by IP₈-levels.

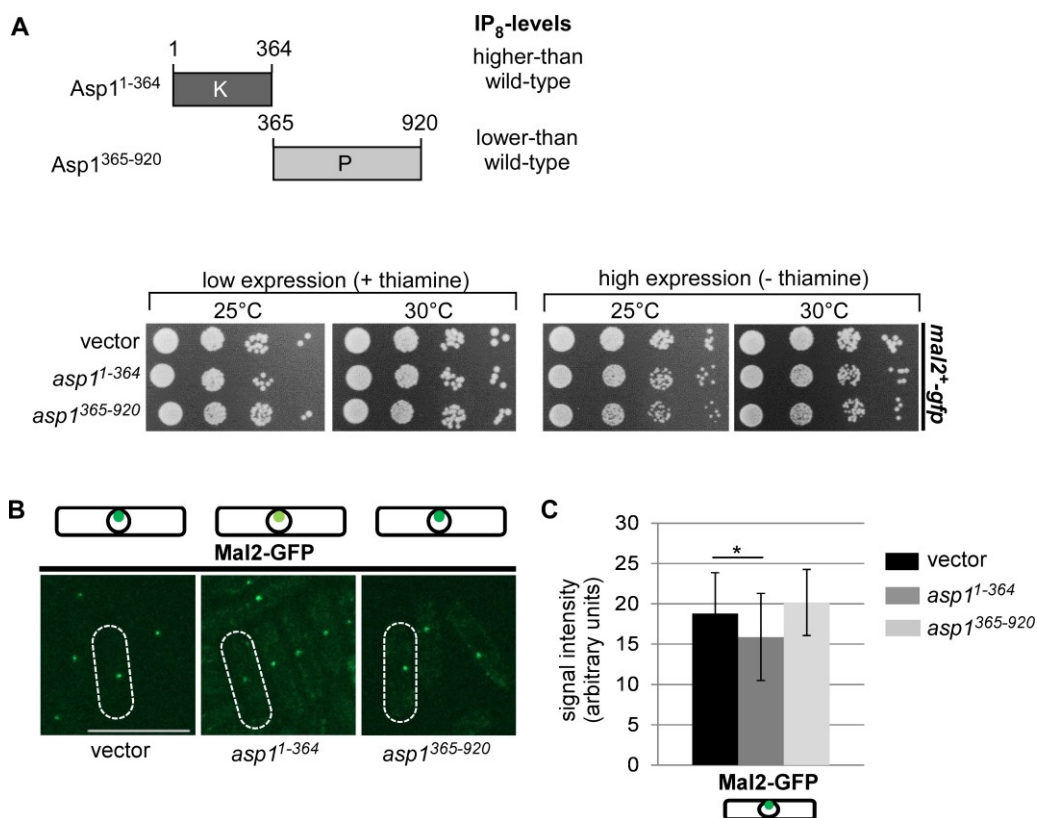


Figure 3-15 Mal2-GFP KT targeting is decreased in the presence of Asp1¹⁻³⁶⁴.

(Figure legend continued on the next page.)

A: Serial dilution patch tests (10^4 - 10^1 cells) of the *mal2⁺-gfp* strain transformed with a vector control, *asp1¹⁻³⁶⁴* or *asp1³⁶⁵⁻⁹²⁰* expressed on plasmids. Transformants were grown under plasmid-selective conditions in media with or without thiamine for 4 days at the indicated temperatures. **B:** Top: Schematic overview of the Mal2-GFP fluorescence signal at the KT in the indicated transformants. Light green = weak signal; dark green = strong signal. Bottom: Live fluorescence microscopy pictures of the indicated transformants expressing *mal2⁺-gfp*. Transformants were pre-incubated for 24 h at 25°C in LFM (live fluorescence media) without leucine and without thiamine before they were patched on agarose pads. Pictures were taken at 25°C with 40 % laser intensity using a Zeiss Spinning Disc-Confocal microscope. Scale bar = 10 μ m. **C:** Quantification of Mal2-GFP fluorescence signals. Pictures taken as in B for the indicated transformants: vector 18.8 AU \pm 5.1; *asp1¹⁻³⁶⁴* 15.9 AU \pm 6.2; *asp1³⁶⁵⁻⁹²⁰* 20.2 AU \pm 4.1 (vector: n = 42; *asp1¹⁻³⁶⁴*: n = 40; *asp1³⁶⁵⁻⁹²⁰*: n = 39; *: p \leq 0.05, two-sample-t-test).

3.4.1.5 Mal2-GFP kinetochore targeting is increased in an *asp1^{D333A}* strain and reduced in an *asp1^{H397A}* strain

Analysis of fluorescence signals in transformants plasmid-expressing *asp1* variants showed a heterogeneous population of signal intensities. This was due to possible differences of expression of these proteins. Therefore an analysis of the effect of proteins that are endogenously expressed was preferable.

Therefore, I determined Mal2-GFP KT localization in strains endogenously expressing *asp1^{D333A}* or *asp1^{H397A}* from the *asp1⁺* locus. Expression of *asp1^{H397A}* led to higher-than-wild-type IP₈-levels while *asp1^{D333A}* expressing strains cannot generate Asp1-generated IP₈ (Figure 1-12 (p. 39); Figure 3-16 A, top panel). As a negative control a *fta2-291^{ts} mal2⁺-gfp* strain was used as Fta2 and Mal2 are known to be localization dependent (Kerres et al., 2006). No difference was observed in growth of *asp1⁺ mal2⁺-gfp*, *asp1^{H397A}* and *asp1^{H397A} mal2⁺-gfp* strains (Figure 3-16 A, bottom panel). The *asp1^{D333A} mal2⁺-gfp* strain showed reduced growth compared to the single mutant strains. *fta2-291^{ts}* and *fta2-291^{ts} mal2⁺-gfp* strains showed reduced growth at 25°C and no growth at 32°C (Figure 3-16 A, bottom panel).

Microscopic analysis of Mal2-GFP KT signals in these strains showed that in the *asp1^{H397A}* strain Mal2-GFP KT localization was decreased compared to the wild-type (*asp1^{H397A}*: 9.4 AU; *asp1⁺*: 11.2 AU). For the *asp1^{D333A} mal2⁺-gfp* strain the opposite was observed. There was an increase at Mal2-GFP fluorescence signal at the KT from 11.2 (*asp1⁺*) to 15.1 AU (*asp1^{D333A}*). In the *fta2-291^{ts} mal2⁺-gfp* strain no KT fluorescence signal was detected (Figure 3-16 B; C). The same effect was also observed for the KT localization of Fta2-GFP. In the *asp1^{D333A} fta2⁺-gfp* strain the intensity of Fta2-GFP signal at the KT was increased from 6.1 (*asp1⁺*) to 7.5 AU. While in an *asp1^{H397A}* background a decrease from 6.1 (*asp1⁺*) to 4.3 AU was scored (Supplementary Figure 7 (p. 188)).

Hence, Mal2-GFP and Fta2-GFP showed higher KT fluorescence signals in the absence of Asp1-generated IP₈ and a reduced KT signal intensity with higher-than-wild-type levels of IP₈.

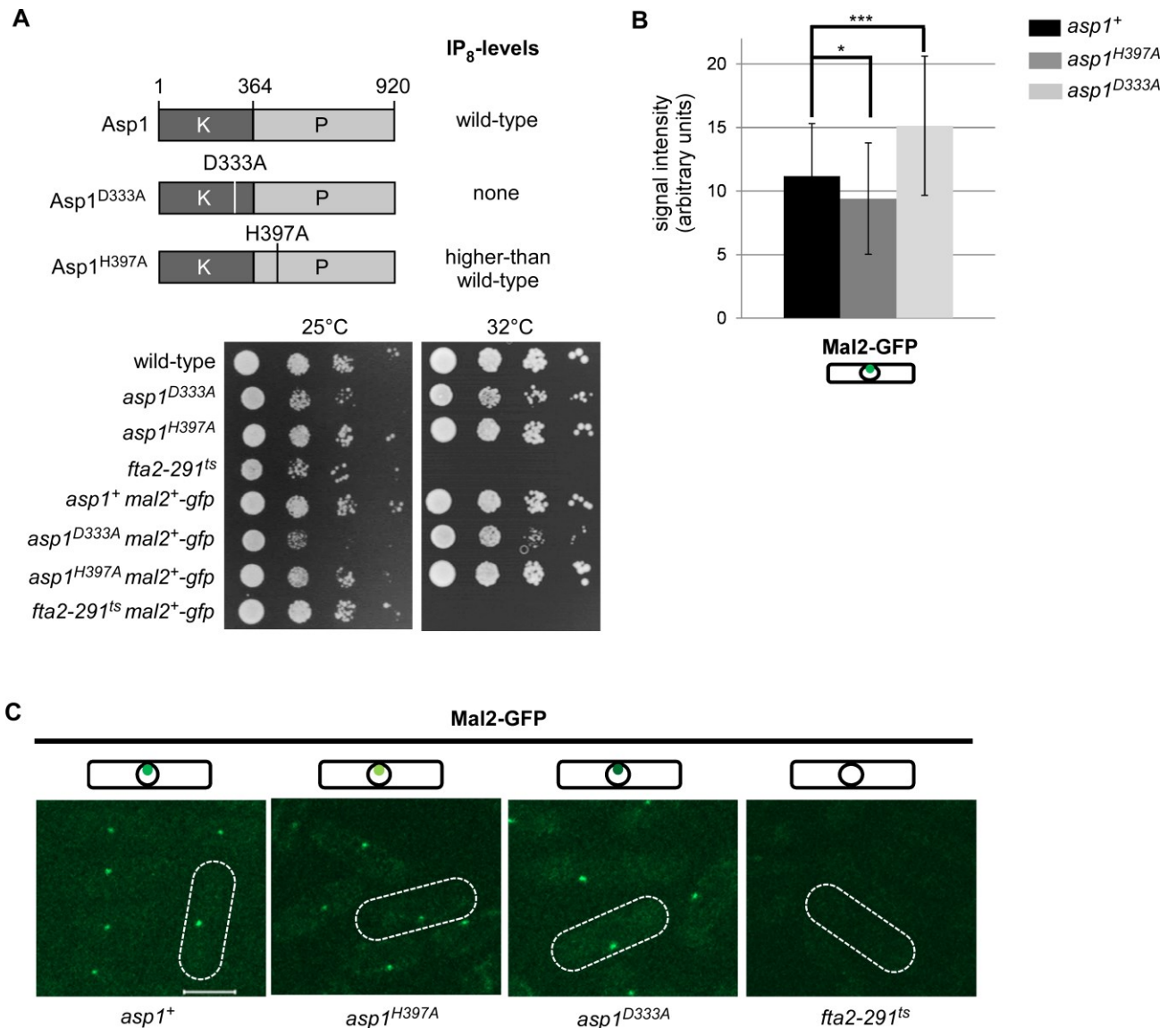


Figure 3-16 In an *asp1*^{D333A} strain the fluorescence signal of Mal2-GFP at the KT is increased.

A: Top: Asp1-variant strains used. Bottom: Serial dilution patch tests (10^4 - 10^1 cells) of the *mal2*⁺-*gfp* strains used. Strains were incubated on MM with all supplements for 5 days at the indicated temperatures. **B:** Quantification of Mal2-GFP fluorescence signals. Pictures taken as in C for the indicated strains: *asp1*⁺ 11.18 AU ± 4.1; *asp1*^{D333A} 15.14 AU ± 5.5; *asp1*^{H397A} 9.4 AU ± 4.4 (n = 66/ strain. *: p ≤ 0.05, ***: p ≤ 0.001, two-sample-t-test). **C:** Top: Schematic overview of the Mal2-GFP fluorescence signal at the KT in the indicated strains. Darker green = stronger signal. Bottom: Live fluorescence microscopy pictures of the indicated strains expressing *mal2*⁺-*gfp*. Strains were pre-incubated for 24 h at 25°C in LFM before they were patched on agarose pads. Pictures were taken at 25°C with 40 % laser intensity using a Zeiss Spinning Disc-Confocal microscope. Scale bar = 5 μm.

Mal2-GFP KT localization in *asp1*⁺, *asp1*^{D333A} and *asp1*^{H397A} backgrounds was further analyzed via chromatin immunoprecipitation (ChIP) in non-synchronous populations.

The centromeres of *S. pombe* span several kb of DNA. They are organized in several domains. The central core (*cnt*) is flanked by inverted repeats, the innermost repeats (*imr*) and the outer repeats (*otr*) (Pidoux and Allshire, 2005). The *cnt* regions contain non-repetitive DNA sequences but the central core regions of chromosome 1 and 3 (cen1/3) share a common sequence (Takahashi K et al., 1992). An overview of the centromere and more detailed information can be found in Chapter 1.3.1.2.2 (p. 20). The Mal2-GFP KT protein is associated with the central region of that centromere chromatin: *cnt* and *imr* as shown in Figure 3-17 A, bottom panel (Jin et al., 2002; Polizzi and Clarke, 1991). Therefore, those regions are then enriched in the PCR analysis of ChIP samples.

Mal2-GFP was associated with the *cnt* and *imr* regions in a *mal2*⁺-*gfp* strain. In an *asp1*^{H397A} *mal2*⁺-*gfp* strain the amount of precipitated centromere chromatin was decreased to 0.4-fold for the *cnt* and 0.8-fold for the *imr* region compared to the *asp1*⁺ strain (set at 1) (Figure 3-17 B; C). In an *asp1*^{D333A} *mal2*⁺-*gfp* strain the opposite was observed. The precipitated centromere chromatin was increased 3.5-fold for the *cnt* and 4-fold for the *imr* regions compared to the wild-type (Figure 3-17 B; C).

To exclude the possibility that the higher amount of Mal2-GFP associated with the centromere region is due to higher levels of Mal2-GFP protein in the strains used for the ChIP an immunoprecipitation of Mal2-GFP with following Western Blot analysis was performed. Mal2-GFP protein levels were comparable in *asp1*⁺, *asp1*^{H397A} and *asp1*^{D333A} backgrounds (Figure 3-17 D).

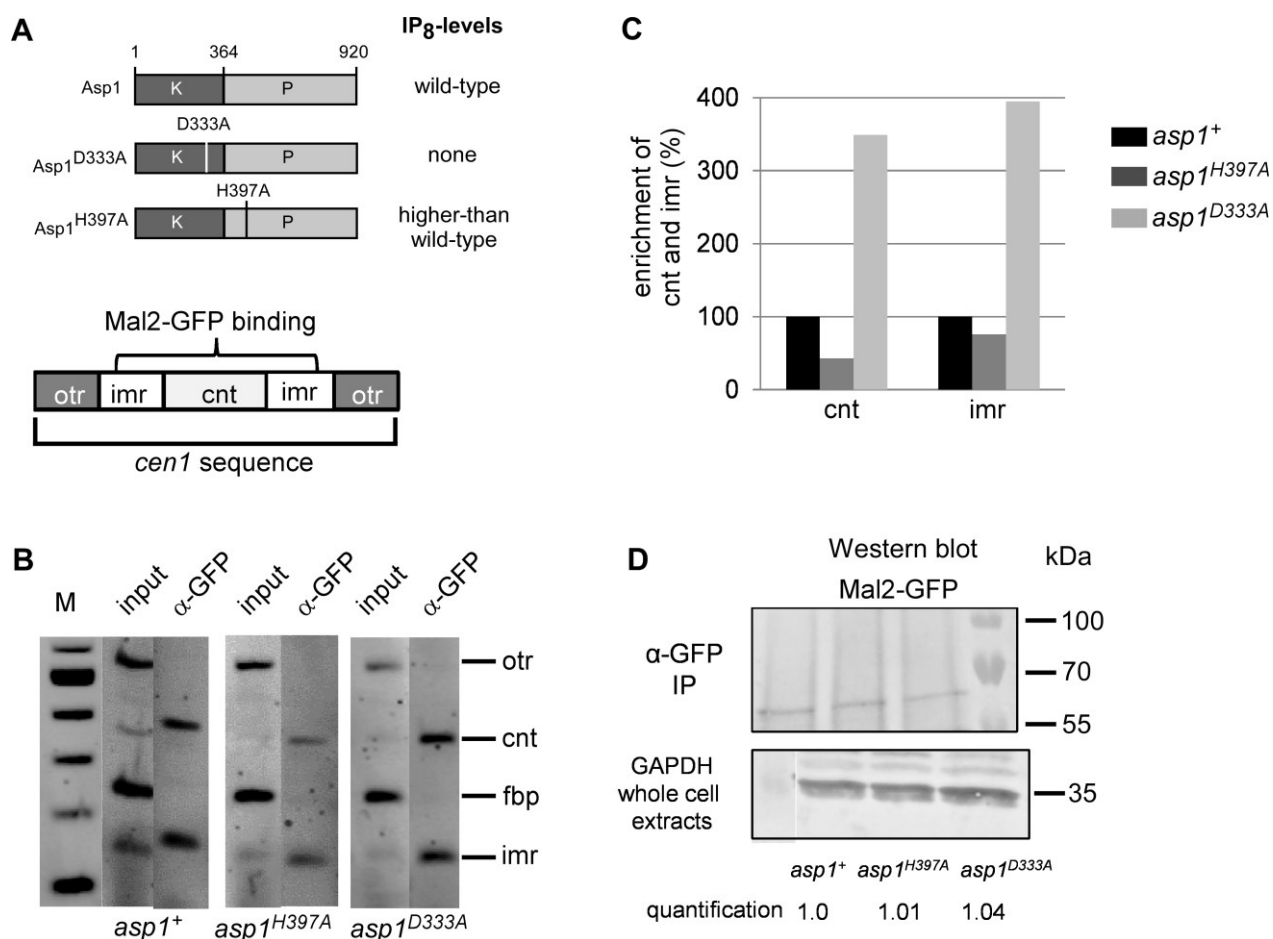


Figure 3-17 Mal2-GFP KT targeting is altered in *asp1*^{D333A} and *asp1*^{H397A} strains.

A: Top: Asp1-variants used. Bottom: Schematic overview of the association of Mal2-GFP with the centromeric DNA sequence of chromosome 1. **B:** Chromatin immunoprecipitation of Mal2-GFP in the indicated strains. For the precipitation an α -GFP antibody was used. Strains were grown in full media at 25°C overnight before fixation. ChIP samples were used for a multiplex PCR with primer pairs for each inner centromere region *cnt* and *imr*, the *otr* region (outmost repeats) and the *fbp* region (euchromatic control). PCR products were analyzed on a 1.5 % agarose gel. **C:** Quantification of the enrichment of the PCR products shown in B. Within a lane the band intensity for *cnt* and *imr* was normalized against that for *fbp*. To compare the enrichment of *cnt* and *imr* PCR products between strains the enrichment in the wild-type (*asp1*⁺) strain was set as 100 % for each strain. Enrichments for the gel shown: *asp1*^{H397A}: *cnt*: 43 %, *imr*: 76 %; *asp1*^{D333A} *cnt*: 349 %, *imr*: 395 %. **D:** Western blot analysis of Mal2-GFP immunoprecipitates (GFP-beads). Strains were grown overnight at 25°C before proteins were extracted. Top: Detection of Mal2-GFP (62 kDa) with an α -GFP antibody. Middle: Detection of GAPDH (36 kDa) with an α -GAPDH antibody. Bottom: Quantification of the Mal2-GFP signals detected in Western Blot analysis. The band intensity of Mal2-GFP was normalized against the GAPDH bands detected in the whole cell extract. *asp1*⁺ measurement was set to 1. Values shown are the average of two independent experiments.

Additionally, quantitative ChIP (qChIP) analysis of the *asp1* variant strains endogenously expressing *mal2*⁺-*gfp* was performed. The ChIP samples were analyzed using quantitative PCR. Here, enrichment of Mal2-GFP at the centromeres of chromosomes 1 and 3 (*cen1/3*) relative to the *act1*⁺ locus served as measurement for KT localization (Subramanian et al., 2014). An untagged *mal2*⁺ and *fta2-291*^{ts} *mal2*⁺-*gfp* strains served as negative controls.

As the *act1*⁺ locus served as a control in the qChIP experiment I first tested if actin levels in the *asp1*⁺, *asp1*^{D333A} and *asp1*^{H397A} strains endogenously expressing *mal2*⁺-*gfp* were equal. In Western blot analysis comparable levels of actin were detected in all three strains (Figure 3-18 A, bottom panel).

In the untagged strain the background enrichment of *cen1/3* relative to the *act1*⁺ locus was determined as 1.99 %. The quantification is explained in Chapter 2.21.2 (p. 80). For *fta2-291*^{ts} *mal2*⁺-*gfp* the enrichment of the *cen1/3* region relative to the *act1*⁺ locus was 33 % in accordance with previous results that mutant Fta2 reduces Mal2 KT targeting (Kerres et al., 2006). In an *asp1*⁺ *mal2*⁺-*gfp* strain the enrichment of the centromere region of chromosomes 1 and 3 normalized to the *act1*⁺ locus was 155 %. In an *asp1*^{H397A} *mal2*⁺-*gfp* strain the enrichment was 120 % whereas in the *asp1*^{D333A} strain it was 224 % (Figure 3-18 B).

Thus, higher cellular IP₈-levels result in a reduction of Mal2-GFP localized at the KT while no Asp1-generated IP₈ in the cell had the opposite effect.

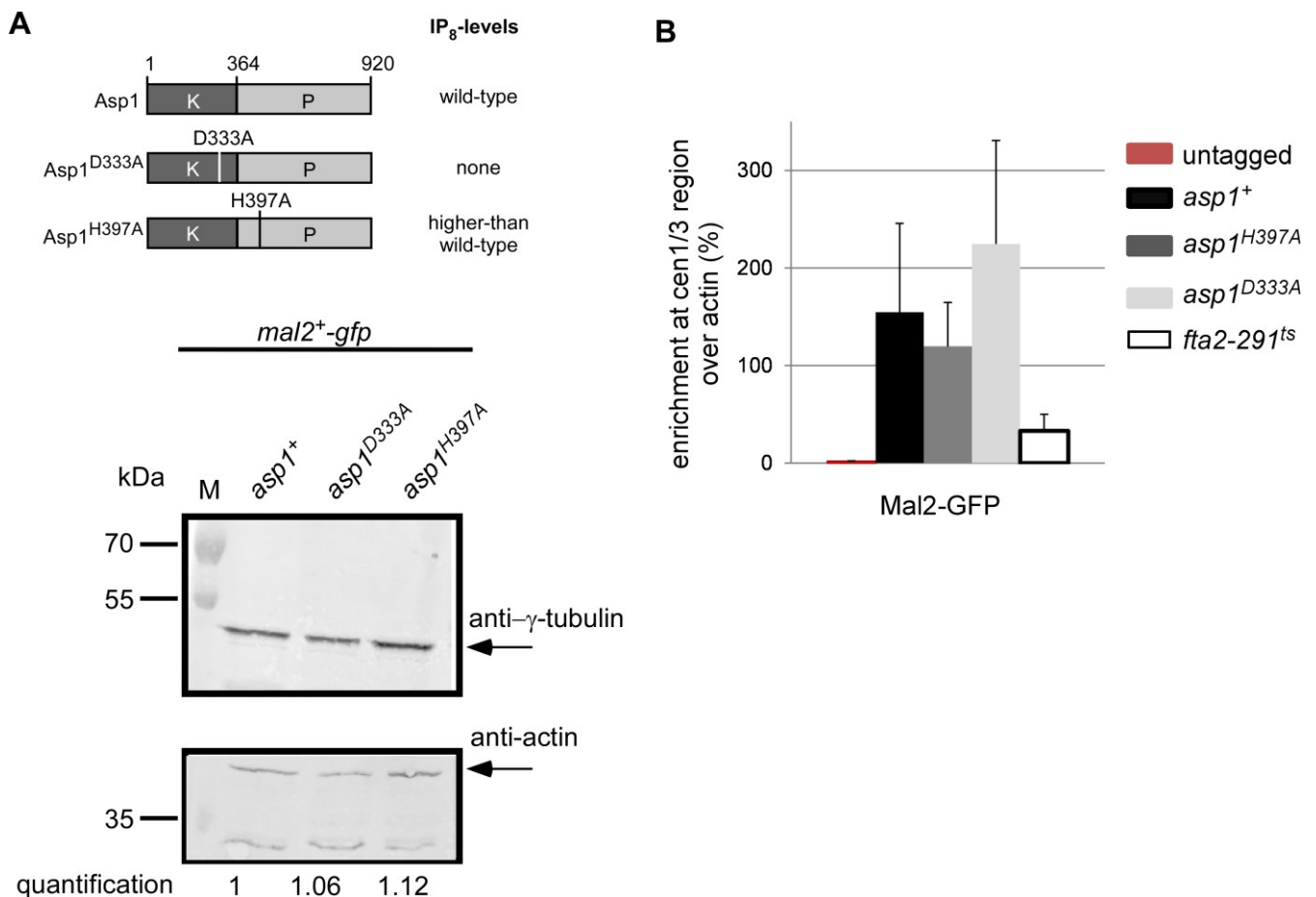


Figure 3-18 Mal2-GFP KT targeting is affected by IP₈-levels.

(Figure legend continued on the next page).

A: Top: Asp1 variants used. Bottom: Western blot analysis of whole cell extracts of *asp1* variant strains. Top: Detection of γ -Tubulin (50 kDa) using an anti-tubulin antibody. Bottom: Detection of actin (42 kDa) using an anti-actin antibody. Strains were incubated overnight at 25°C before proteins were extracted. Quantification: band intensities of actin were normalized to the intensities of γ -tubulin for the blot shown. Value in the *asp1⁺ mal2⁺-gfp* strain was set as 1. **B:** Quantitative ChIP experiment for the indicated strains. For the precipitation an α -GFP antibody was used. Strains were grown at 25°C overnight in MM with all supplements to an OD of 0.4-0.8 before fixation. Samples were used for a quantitative PCR reaction. The diagram shows the enrichment of *cen1/3* DNA relative to the *act1⁺* locus: untagged 1.99 ± 0.3 ; *asp1⁺* 154.67 ± 90.99 ; *asp1^{H397A}* 119.55 ± 45.01 ; *asp1^{D333A}* 224.83 ± 105.56 ; *fta2-291^{ts}* 33.03 ± 17.06 . Averages of duplicates (untagged and *fta2-291^{ts}*) or triplicates (*asp1⁺*, *asp1^{D333A}*, *asp1^{H397A}*) shown.

Hence, I showed via fluorescence microscopy and ChIP that Mal2-GFP KT targeting increased with higher-than-wild-type IP_8 -levels and decreased with lower-than-wild-type IP_8 -levels. For Fta2-GFP KT targeting the same was observed using fluorescence microscopy (Supplementary Figure 7 (p. 188)).

The observed effects are summed up in Figure 3-19.

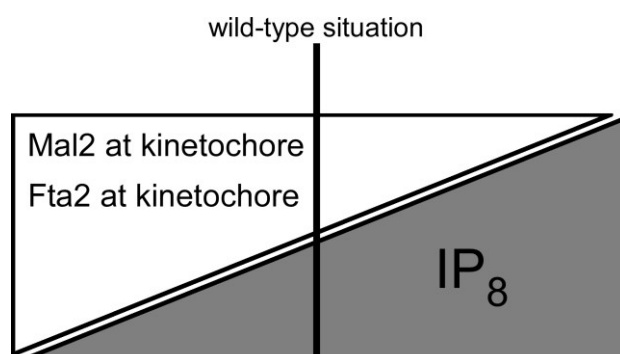


Figure 3-19 Schematic of the effect of Asp1-generated IP_8 on Mal2-GFP and Fta2-GFP KT targeting.

3.4.1.6 Asp1-generated IP_8 affects Mal2-GFP kinetochore targeting in mitosis

KT targeting of Mal2-GFP in non-synchronous populations was affected by IP_8 -levels. In those populations around 70 % of the cells are in the G_2 -phase of the cell-cycle, while only 10 % are undergoing mitosis (Gomez and Forsburg, 2004).

Microscopic analysis of Mal2-GFP fluorescence signals in mitotic cells of a non-synchronized population was performed. To this end fluorescence microscopy pictures of the cultures were taken and cells showing two clearly separated Mal2-GFP signals within one cell at a distance of 5-10.5 μ m (anaphase B (Nabeshima et al., 1998)) were analyzed. This was done in the

asp1⁺, *asp1*^{H397A} and *asp1*^{D333A} strains. With higher cellular IP₈-levels (*asp1*^{H397A}) the signal intensity was decreased from 10.1 (*asp1*⁺) to 8.9 AU while without Asp1-generated IP₈ (*asp1*^{D333A}) the fluorescence signal intensity was increased to 14.9 AU (Figure 3-20 A, bottom panel; B). These values were comparable to those obtained for interphase cells suggesting that IP₈ affects KT targeting during interphase and mitosis to the same extent.

Furthermore, I tested the Mal2-GFP KT targeting in cells arrested in metaphase via qChIP.

For this purpose the SAC-member *mph1*⁺ was overexpressed in *mal2*⁺-*gfp* *asp1* variant strains. Excess Mph1 results in a prolonged metaphase arrest with super condensed chromosomes (He et al., 1998). DAPI-staining of a transformant overexpressing *mph1*⁺ showed that the arrest was successful: In cells transformed with a vector control interphase cells (one DAPI signal in the middle) as well as mitotic cells (two divided DAPI signals) were observed. Around 50 % of cells overexpressing *mph1*⁺ showed condensed DNA signals in the cell middle (Figure 3-20 C).

Transformants of *asp1*⁺ *mal2*⁺-*gfp*, *asp1*^{D333A} *mal2*⁺-*gfp* and *asp1*^{H397A} *mal2*⁺-*gfp* overexpressing *mph1*⁺ were thus used for qChIP analysis.

The enrichment of the centromere region (*cen1/3*) relative to the *act1*⁺ locus in an *asp1*⁺ background was 436 %. In the *asp1*^{H397A} *mal2*⁺-*gfp* strain this enrichment was reduced to 242 % compared to the wild-type (*asp1*⁺). In the *asp1*^{D333A} *mal2*⁺-*gfp* strain the opposite effect was observed. This strain showed an increase of *cen1/3* enrichment from 436 % to 521 % (Figure 3-20 D). Therefore, the same influence of IP₈ on Mal2-GFP centromere association as in non-synchronous cells was detected. Note that the values for that qChIP experiment could not be compared to the values obtained for non-synchronous cultures as the experimental setup for overexpression of *mph1*⁺ required 28 h incubation at 30°C.

Hence, cellular IP₈-levels affected Mal2-GFP KT targeting also during metaphase.

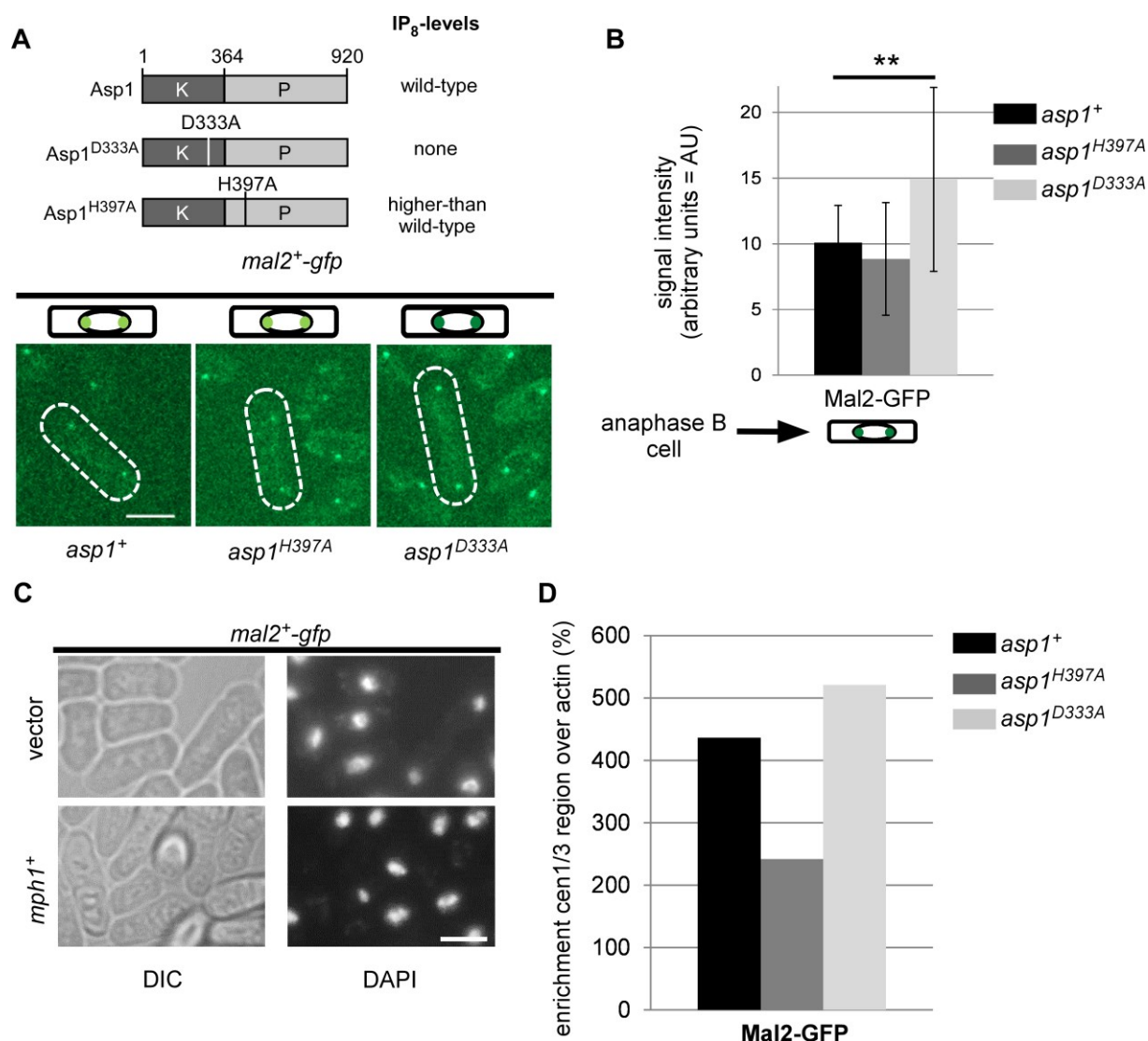


Figure 3-20 Mal2-GFP KT localization also depends on IP₈-levels during mitosis.

A: Top: Asp1 variants used. Middle: Schematic presentation of the Mal2-GFP fluorescence signal at the KT in anaphase B in the indicated strains. Darker green = stronger signal. Bottom: Live fluorescence microscopy pictures of the indicated strains expressing *mal2*⁺-*gfp*. Strains were pre-incubated for 24 h at 25°C in LFM before they were patched on agarose pads. Pictures were taken at 25°C with 40 % laser intensity using a Zeiss Spinning Disc-Confocal microscope. Scale bar = 5 μm. **B:** Quantification of Mal2-GFP fluorescence signals in anaphase B cells (two distinguishable Mal2-GFP signals at a distance of 5-10.5 μm). Pictures taken as in A for the indicated strains: *asp1*⁺ 10.1 AU ± 2.8; *asp1*^{H397A} 8.85 AU ± 4.3; *asp1*^{D333A} 14.9 AU ± 7 (n= 31/ strain; **: p ≤ 0.01, two-sample-t-test). **C:** Microscopy pictures of fixed *asp1*⁺ *mal2*⁺-*gfp* cells transformed with either a vector control or an *mph1*⁺-plasmid. Left: DIC pictures of transformants. Right: DAPI DNA-staining. Scale bar = 5 μm. Pictures taken with a Zeiss Axiovert Microscope. **D:** Quantitative ChIP experiment for transformants overexpressing *mph1*⁺. For the precipitation an α-GFP antibody was used. Transformants were grown for 28 h at 30°C in plasmid-selective media before fixation. Samples were used for a quantitative PCR reaction. Enrichment of cen1/3 DNA relative to the *act1*⁺ locus: *asp1*⁺ 436.55; *asp1*^{H397A} 242.19; *asp1*^{D333A} 520.95.

3.4.1.7 Asp1-generated IP₈ mediates its function at the kinetochore interface

Higher-than-wild-type IP₈-levels reduced the loss rate of a non-essential minichromosome, led to faster establishment of bipolar KT-MT-attachments and affected Mal2-GFP and Fta2-GFP KT targeting (Chapters 1.4.1.1, 3.2.3.2, 3.4.1.4; p.41, 103, 114). All these processes take place in the nucleus and therefore in proximity to the KT interface. Asp1 is generally localized throughout the cell, in the cytoplasm and the nucleus, and shows an enriched localization in the nucleus at lower temperatures (personal communication; data not shown). Therefore Asp1 is always present at the KT to some extent. However, we wanted to analyze a situation where Asp1 KT localization was concentrated.

To analyze the effect of IP₈ when Asp1 was concentrated at the KT, *asp1* variants were fused to *GBP* (GFP binding protein)-*mCherry* on a plasmid under control of the *nmt1*⁺-promoter (Chen et al., 2017; Dodgson et al., 2013; Rothbauer et al., 2008). This GBP-tag forces a fusion protein to a GFP-tagged protein. The *asp1-GBP-mCherry* plasmids were transformed into the wild-type and into a *mal2*⁺-*gfp* strain.

Asp1-GBP-mCherry co-localized with Mal2-GFP at the KT in transformants with low expression of *asp1*⁺-*GBP-mCherry* in a *mal2*⁺-*gfp* background (Figure 3-21 A; B).

Under low expression conditions all Asp1 variants used: Asp1-GBP-mCherry (wild-type IP₈-levels), Asp1^{D333A}-GBP-mCherry (no Asp1-generated IP₈) and Asp1^{H397A}-GBP-mCherry (higher-than-wild-type IP₈-levels) (Figure 3-21 C) co-localized with Mal2-GFP to the KT. Under high expression conditions the mCherry signal was detected throughout the cell (Supplementary Figure 8 (p. 188)). Further analysis was therefore performed using low expression conditions.

Low expression of the *GBP-mCherry* cassette alone or fused to an *asp1* variant slightly reduced the growth of a wild-type strain at 25°C and 36°C (Figure 3-21 D, top panel). In a *mal2*⁺-*gfp* strain a similar effect was observed, but the reduction in growth was stronger than in the wild-type. At 36°C expression of *asp1*^{H397A}-*GBP-mCherry* (higher-than-wild-type IP₈-levels) led to a clear reduction in growth (Figure 3-21 D, bottom panel).

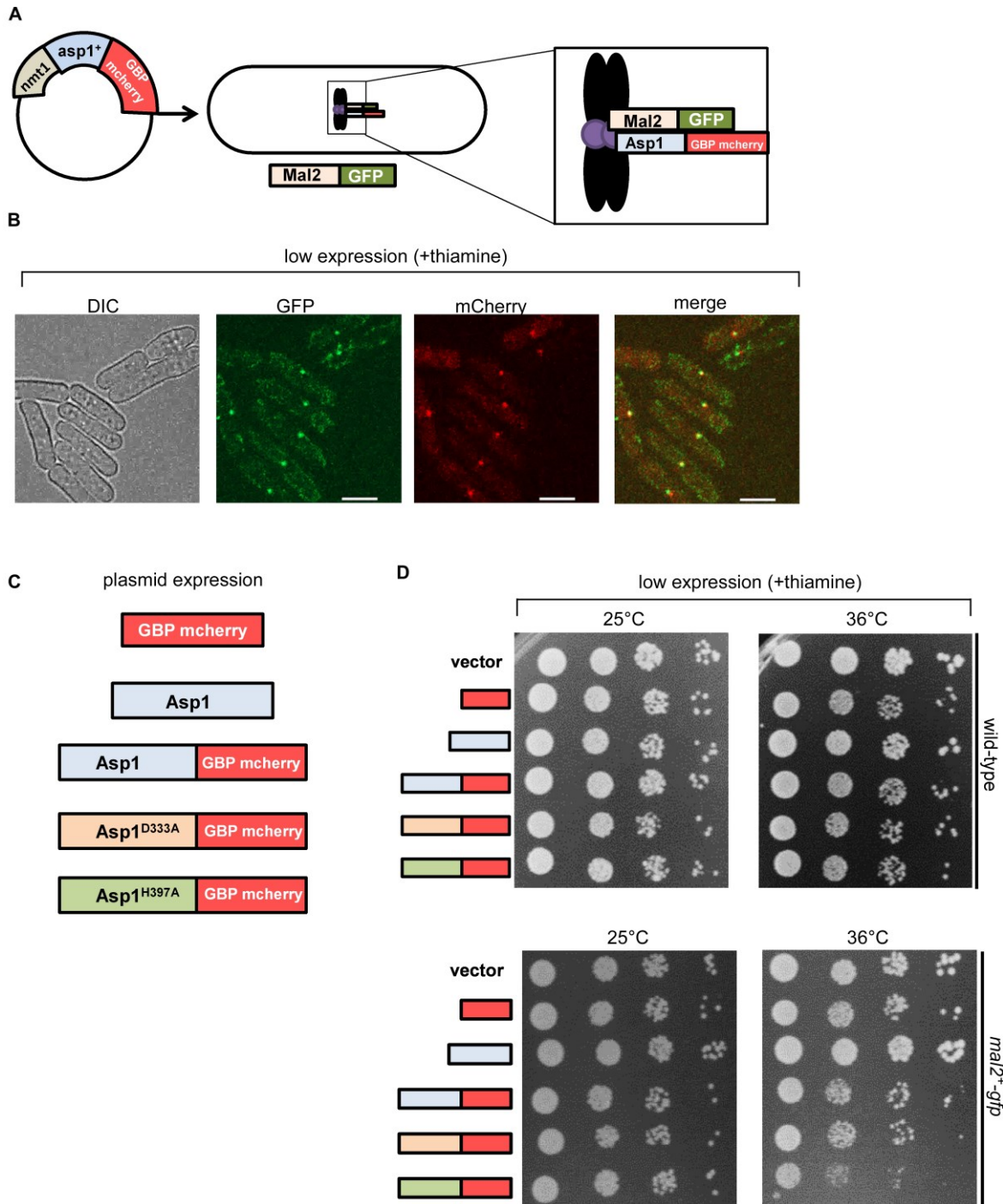


Figure 3-21 $Asp1^{H397A}$ present at the KT interface reduces the growth of a $mal2^{-}GFP$ strain.

A: Schematic overview over the GBP-GFP system used to force Asp1 proteins to Mal2-GFP at the KT interface. **B:** Live cell fluorescence microscopy pictures for $asp1^{+}$ -GBP-mCherry expressed in a $mal2^{-}$ -gfp strain. Left to right: DIC pictures, Mal2-GFP fluorescence signal (40 % laser intensity), Asp1-GBP-mCherry fluorescence signal (10 % laser intensity), merge for GFP and mCherry signals. Transformants were pre-grown overnight in LFM without leucine and with thiamine (low expression) at 25°C before they were patched on agarose pads. Pictures were taken at 25°C using a Zeiss Spinning Disc-Confocal microscope. Scale bar = 5 μ m. **C:** Overview of the Asp1-GBP-mCherry variants used in the assay. **D:** Serial dilution patch tests (10^4 - 10^1 cells) of wild-type (left) and $mal2^{-}$ -gfp (right) strains transformed with a vector control, GBP-mCherry, $asp1^{+}$, $asp1^{+}$ -GBP-mCherry, $asp1^{D333A}$ -GBP-mCherry or $asp1^{H397A}$ -GBP-mCherry expressed on plasmids. Transformants were grown under plasmid-selective conditions in media with thiamine (low expression) for 5 days at 25°C and 36°C.

Microscopic analysis of the transformants used in the patch test experiment was performed and Mal2-GFP KT signals were quantified. At high temperatures no specific KT localization of Asp1-GBP-mCherry variants was observed but a red signal was detected throughout the cells (data not shown). Therefore the quantification was performed for cultures incubated at 25°C.

Low expression of *asp1*⁺-GBP-mCherry reduced Mal2-GFP fluorescence signals at 25°C from 7.99 to 7 AU compared to the vector control. Expression of *asp1*^{D333A}-GBP-mCherry, caused a slighter reduction to 7.24 AU while *asp1*^{H397A}-GBP-mCherry (higher-than-wild-type IP₈-levels) decreased the Mal2-GFP signal at the KT to 5.86 AU (Figure 3-22).

It is noteworthy that a transformant expressing only *GBP-mCherry* showed an increased Mal2-GFP fluorescence signal compared to the empty vector (data not shown). Therefore this variant was not considered in the analysis as it was feasible that this transformant was compromised.

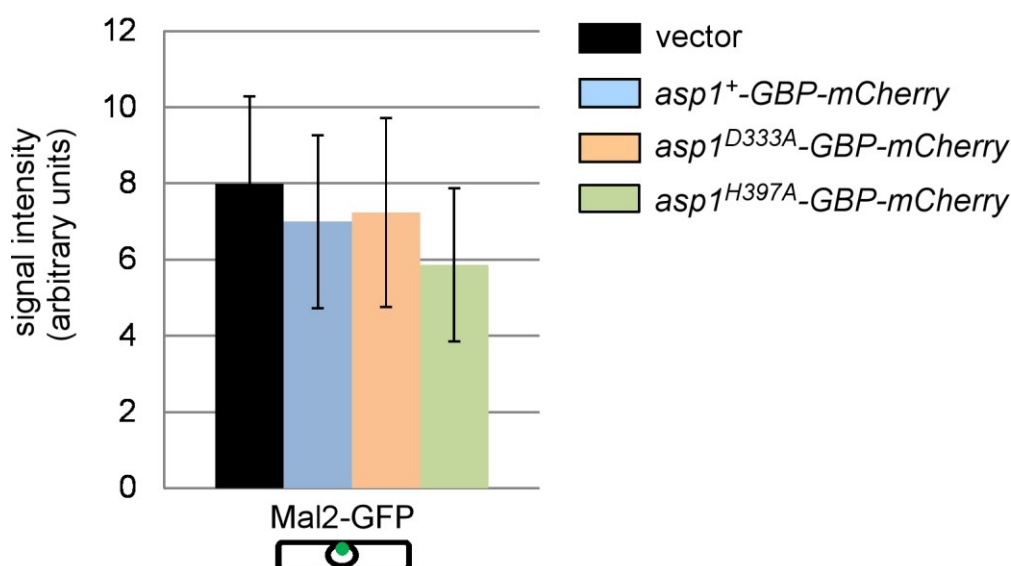


Figure 3-22 Expression of *asp1*^{H397A}-GBP-mCherry reduces Mal2-GFP fluorescence signals at the KT.

Quantification of Mal2-GFP fluorescence signals for the indicated transformants: vector control 7.99 AU ± 2.3 (n = 54); *asp1*⁺-GBP-mCherry 7.0 AU ± 2.27 (n = 56); *asp1*^{D333A}-GBP-mCherry 7.24 ± 2.48 (n = 67); *asp1*^{H397A}-GBP-mCherry 5.86 ± 2.01 (n = 35). Transformants were pre-grown overnight in LFM without leucine and with thiamine (low expression) at 25°C before they were patched on agarose pads. Pictures were taken at 25°C using a Zeiss Spinning Disc-Confocal microscope.

Thus, with increasing levels of IP₈ generated in proximity to the KT the amount of Mal2-GFP KT localization was decreased indicating that IP₈ mediates its function at the KT interface.

3.4.1.8 Asp1 co-immunoprecipitates with Fta2-GFP

The effect of IP₈ that was observed when the Asp1 protein was concentrated at the KT interface indicated that Asp1 might have a potential target or interaction partner that is KT associated.

Therefore I revisited online protein interaction databases to check for bioinformatic evidence of an interaction of Asp1 and Mal2 or another KT protein. I found that an interaction for Asp1 and the Sim4-complex member Fta2 was predicted (http://bahlerweb.cs.ucl.ac.uk/PInt/protint_index.htm).

To analyze if Asp1 and Fta2 indeed interacted *in vivo* I performed a co-immunoprecipitation experiment. In the experimental setup Fta2-GFP was precipitated using α -GFP beads and it was tested if Asp1 was co-immunoprecipitated.

As KT proteins are generally hard to detect in a Western Blot due to a low level of protein in the cells I chose an experimental setup where *fta2⁺-gfp* was overexpressed under control of the *nmt1⁺*-promoter in an *fta2⁺-gfp* strain.

Protein extracts were prepared for the wild-type strain, an *asp1* Δ strain, that served as a negative control, and the *fta2⁺-gfp* strain transformed with a vector control or the *fta2⁺-gfp* plasmid. The protein content of the extracts was determined in a Bradford analysis and equal amounts were analyzed on a 10 % SDS-gel stained with Coomassie blue. It was observed that similar levels of protein were present in the protein extracts (Figure 3-23 A). Equal protein amounts were then used for immunoprecipitation with α -GFP beads and the precipitation samples were used for Western Blot analysis (Figure 3-23 B).

It was observed that Fta2-GFP was not detectable in the protein extracts of the wild-type strain, the *asp1* Δ strain and the *fta2⁺-gfp* strain transformed with a vector control. Only for the protein extract of the *fta2⁺-gfp* strain transformed with the *fta2⁺-gfp* plasmid a band was detected at a size of 68 kDa. Also for the immunoprecipitation samples only the *fta2⁺-gfp* strain transformed with the *fta2⁺-gfp* plasmid expressed a detectable level of Fta2-GFP (Figure 3-23 B, top panel). The possibility that there was no protein present in the protein extracts was excluded as the control protein GAPDH was detectable at similar levels in all protein extracts (Figure 3-23 B, middle panel).

For the detection of Asp1 using a pre-cleaned α -Asp1 antibody a band was detected in the protein extracts of the wild-type and the *fta2⁺-gfp* strain transformed with a vector control or *fta2⁺-gfp*. For the protein extract of the *asp1* Δ strain no band appeared showing that the antibody did not produce a background signal (Figure 3-23 B, bottom panel).

In the immunoprecipitation samples for the wild-type and the *fta2⁺-gfp* strain transformed with a vector control no Asp1 protein was detected, while the *fta2⁺-gfp* strain transformed with *fta2⁺-gfp* showed a co-precipitation of Asp1 and Fta2-GFP (Figure 3-23 B).

Thus, Asp1 and Fta2-GFP co-precipitated in a co-immunoprecipitation experiment and might therefore interact *in vivo*.

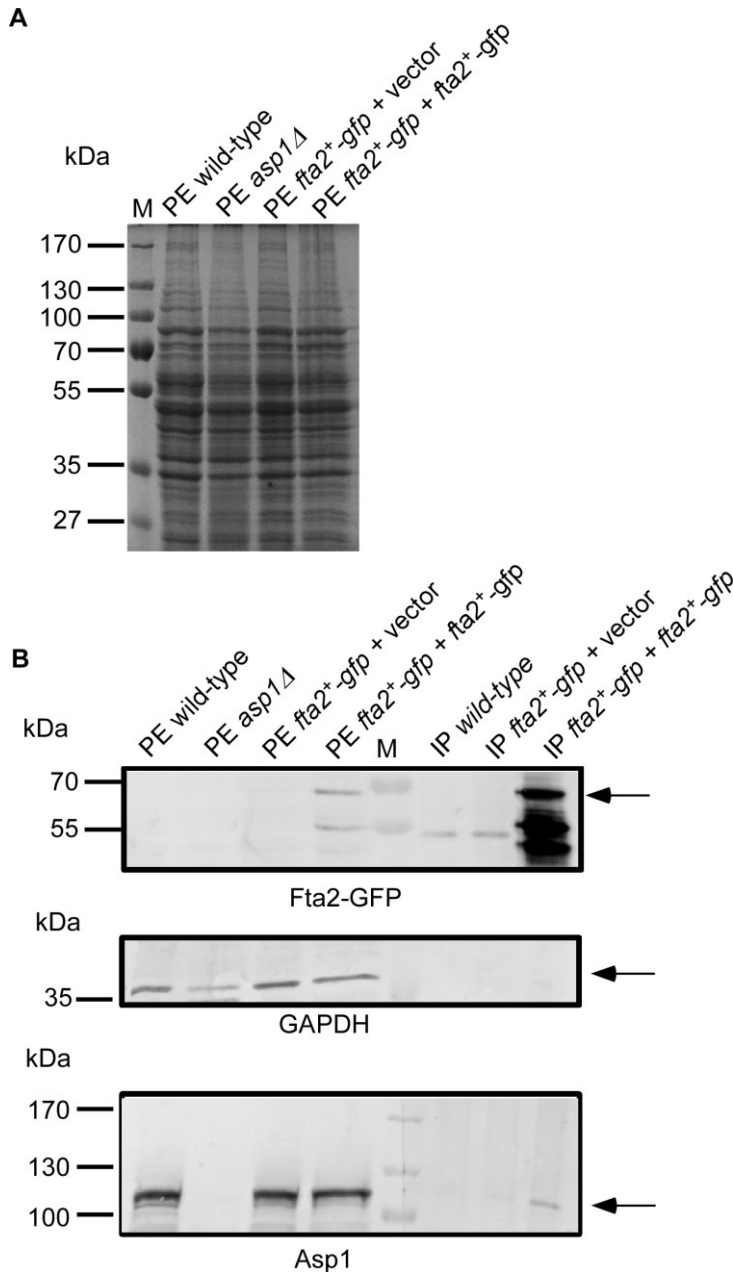


Figure 3-23 Asp1 co-immunoprecipitates with Fta2-GFP.

A: Coomassie staining for whole cell protein extracts of the indicated strains and transformants. Strains and transformants were grown at 25°C overnight in either MM with all supplements (strains) or MM without leucine and without thiamine (transformants) and whole cell protein extracts were prepared. Equal amounts of proteins were loaded on a 10 % SDS-gel and stained with Coomassie blue. **B:** Co-immunoprecipitation (IP) of Fta2-GFP transformed with a vector control or a plasmid overexpressing *fta2⁺-gfp* (under control of the *nmt1⁺*-promoter) and the Asp1 protein. Protein extracts (PE) of the wild-type and an *asp1*Δ strain served as positive and negative controls for the Asp1-antibody. For the immunoprecipitation equal amounts of proteins were used together with α-GFP beads. Western blot analysis of the immunoprecipitates: Top: Detection of Fta2-GFP (68 kDa) using an α-GFP antibody. Middle: Detection GAPDH (36 kDa) using an α-GAPDH antibody. Bottom: Detection of Asp1 (110 kDa) using an α-Asp1 antibody.

3.4.1.9 Higher-than-wild-type IP₈-levels reduce missegregation in the *mis15-68^{ts}* strain

As shown in Chapter 3.4.1 (p. 107) the *mis15-68^{ts}* strain showed the opposite phenotype to the *mal2-1^{ts}* strain as far as *asp1¹⁻³⁶⁴* or *asp1³⁶⁵⁻⁹²⁰* expression was concerned (Figure 3-12).

Thus I analyzed the *mis15-68^{ts}* strain phenotype in various IP₈-level backgrounds. Two strain backgrounds with higher-than-wild-type IP₈-levels were used: *asp1^{H397A}* and *aps1Δ* where the gene encoding for nudix hydrolase that degrades IP₇ and IP₈ *in vitro* had been deleted (Ingram et al., 2003) (Figure 3-24 A).

In contrast to the wild-type strain, the *mis15-68^{ts}* strain showed massively reduced growth at 32°C and did not grow at temperatures ≥ 33°C (Figure 3-24 B). For the *asp1^{H397A} mis15-68^{ts}* double mutant strain a rescue of the non-growth phenotype was observed at 32°C and limited growth was still detectable at 33°C. The same was observed for the *aps1Δ mis15-68^{ts}* strain (Figure 3-24 B).

Hence, an increase in cellular IP₈-levels by different means led to a partial rescue of the temperature-sensitivity of the *mis15-68^{ts}* strain.

The *mis15-68^{ts}* strain shows a high frequency (60 % of cells) of missegregation at the restrictive temperature (Hayashi et al., 2004). Therefore I analyzed the aberrant segregation phenotypes of the above mentioned strains albeit at 25°C. At 25°C *asp1^{H397A}* and *aps1Δ* single mutant strains had a low level of aberrant segregation phenotypes (7.4 % and 2.3 %, respectively; phenotypes shown in Figure 3-24 C). Please note, that this experiment was done in the very beginning of my PhD thesis. After gathering more experimental experience I think that the frequencies obtained in this experiment have to be considered carefully. The tendencies however should be correct. Nevertheless, the experiment has to be repeated.

The *mis15-68^{ts}* strain showed aberrant segregation phenotypes in 15.7 % of the cells analyzed (Figure 3-24 C). In the *asp1^{H397A} mis15-68^{ts}* double mutant strain the amount of aberrant segregation phenotypes was reduced to 8.6 % (Figure 3-24 C). In the *aps1Δ mis15-68^{ts}* strain aberrant segregation phenotypes were reduced to 9 % (Figure 3-24 C).

Thus increasing intracellular IP₈-levels by different means rescued the chromosome missegregation phenotype of the *mis15-68^{ts}* strain partially.

As the rescue of growth is more evident at higher temperatures the effect of increased IP₈-levels on aberrant segregation phenotypes in the *mis15-68^{ts}* strain should be analyzed at temperatures ≥ 32°C.

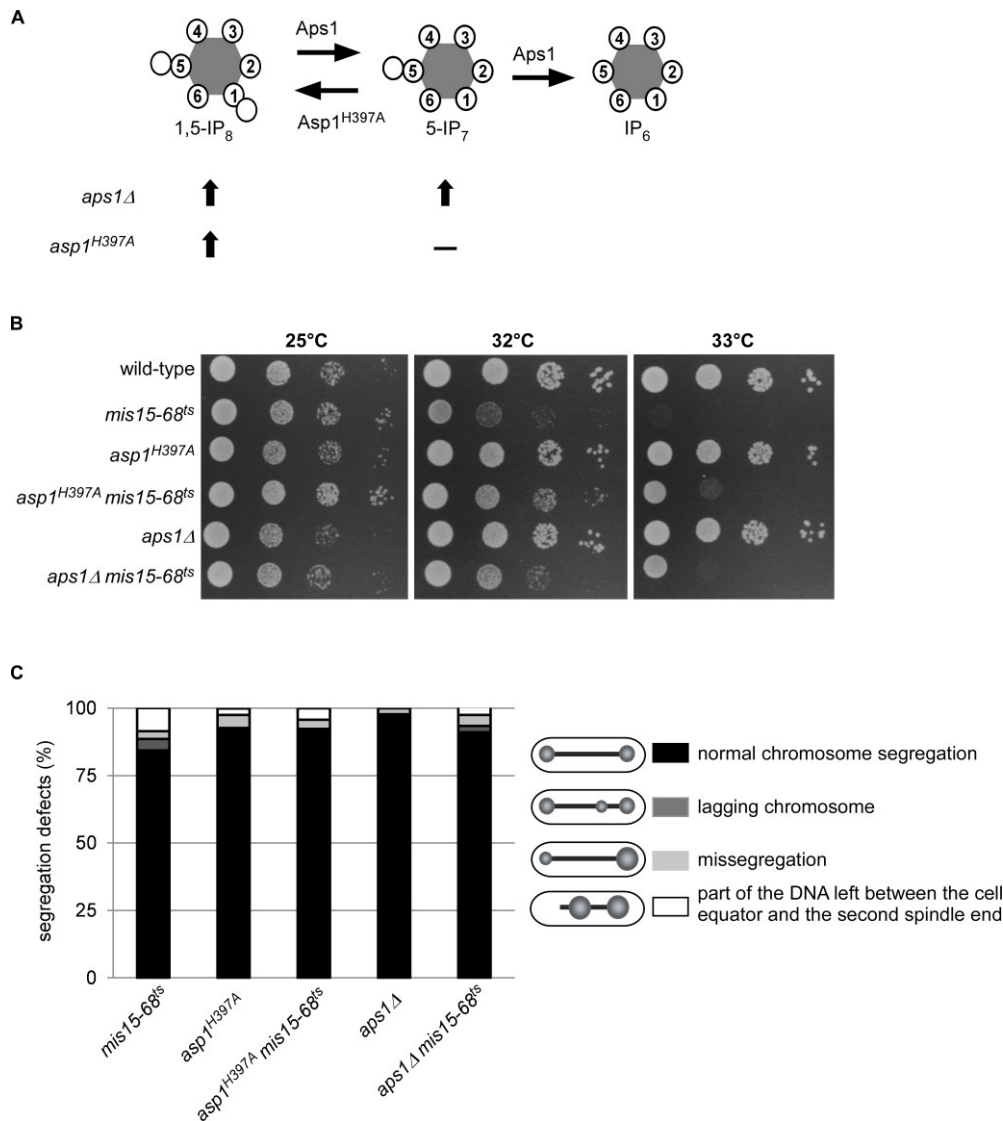


Figure 3-24 In *asp1^{H397A}* and *aps1Δ* backgrounds the aberrant segregation phenotypes of the *mis15-68^{ts}* strain are partially rescued.

A: Top: Schematic overview of the enzymatic reactions catalyzed by the Aps1 and Asp1 proteins. Grey = Inositol-ring, white = phosphate groups. Bottom: Expected accumulation of IPP species. **B:** Serial dilution patch tests (10^4 - 10^1 cells) of the indicated strains. The strains were incubated on YE5S at the indicated temperatures for 4 days. **C:** Diagram of the chromosome segregation defects of the indicated strains. Strains were grown overnight in MM with all supplements at 25°C and cells fixed with 3 % PFA. Aberrant segregation phenotypes were analyzed via immunofluorescence with an α -TAT1 antibody to visualize the mitotic spindle and DAPI staining to visualize DNA. Phenotypes observed are indicated on the right. (*mis15-68^{ts}*: 4 % lagging chromosomes, 3 % missegregation, 9 % part of the DNA left at the cell equator, n = 140; *asp1^{H397A}*: 5 % missegregation, 2 % part of the DNA left at the cell equator, n = 82; *asp1^{H397A} mis15-68^{ts}*: 1 % lagging chromosomes, 3 % missegregation, 4 % part of the DNA left at the cell equator, n = 117; *aps1Δ*: 2 % missegregation n = 88; *aps1Δ mis15-68^{ts}*: 2.5 % lagging chromosomes, 4 % missegregation, 2.5 % part of the DNA left at the cell equator n = 122).

3.4.1.10 Plasmid-borne expression of *asp1*³⁶⁵⁻⁹²⁰ reduces Mis15-68-GFP kinetochore localization

To analyze whether the phenotypes seen in the patch test experiment (Figure 3-12 E) were related to KT targeting of Mis15-68-GFP the *mis15-68^{ts}* gene was C-terminally *gfp* tagged at its native locus (Chapter 2.18 (p. 70)). The *mis15-68^{ts}-gfp* strain showed an increased temperature-sensitivity compared with the *mis15-68^{ts}* strain (Figure 3-25 A).

Next, the *mis15-68^{ts}-gfp* strain was transformed with a vector control or *asp1*¹⁻³⁶⁴ or *asp1*³⁶⁵⁻⁹²⁰ expressed on plasmids and the growth analyzed. Neither low expression of *asp1*¹⁻³⁶⁴ nor *asp1*³⁶⁵⁻⁹²⁰ had an effect on the growth of the *mis15-68^{ts}-gfp* strain compared to the vector control (Figure 3-25 B, top panel). High expression of both *asp1*¹⁻³⁶⁴ and *asp1*³⁶⁵⁻⁹²⁰ slightly reduced the growth of the *mis15-68^{ts}-gfp* strain at 30 and 31°C compared to the vector control (Figure 3-25 B, bottom panel).

Hence, the rescue of growth via *asp1*¹⁻³⁶⁴ expression observed for the *mis15-68^{ts}* strain was not seen for the *mis15-68^{ts}-gfp* strain. The reason for this is unclear. Either the GFP-tag hinders interaction between Asp1/ Asp1-modulated proteins and Mis15-68, or the *mis15-68^{ts}-gfp* strain is so sick that rescue is no longer possible.

However, plasmid-borne expression of *asp1*³⁶⁵⁻⁹²⁰ on the other hand still reduced the growth of the *mis15-68^{ts}-gfp* strain.

Nevertheless, microscopic analysis of Mis15-68-GFP KT signals in cells expressing *asp1*¹⁻³⁶⁴ or *asp1*³⁶⁵⁻⁹²⁰ plasmids was performed. High expression of *asp1*³⁶⁵⁻⁹²⁰ reduced Mis15-68-GFP KT fluorescence signals from 10.4 AU (vector) to 7.7 AU (Figure 3-25 C; D). Intriguingly, high expression of *asp1*¹⁻³⁶⁴ led to dot- or line-like Mis15-68-GFP fluorescence signals throughout the cell instead of the single KT signal expected (Figure 3-25 C). In addition, it was found that the cells were longer than those transformants with the vector control or *asp1*³⁶⁵⁻⁹²⁰. *mis15-68^{ts}-gfp* cells transformed with the vector control had an average length of 11 μm those expressing *asp1*¹⁻³⁶⁴ were 13 μm (Figure 3-25 E). This indicated that *mis15-68^{ts}-gfp* cells remained longer in one cell-cycle phase.

Co-staining of one transformant with the mitochondria staining Mitotracker red showed that the aberrant GFP signals partially co-localized with mitochondria. Because of the aberrant localization the Mis15-68-GFP fluorescence signals were not quantified (Figure 3-25 F).

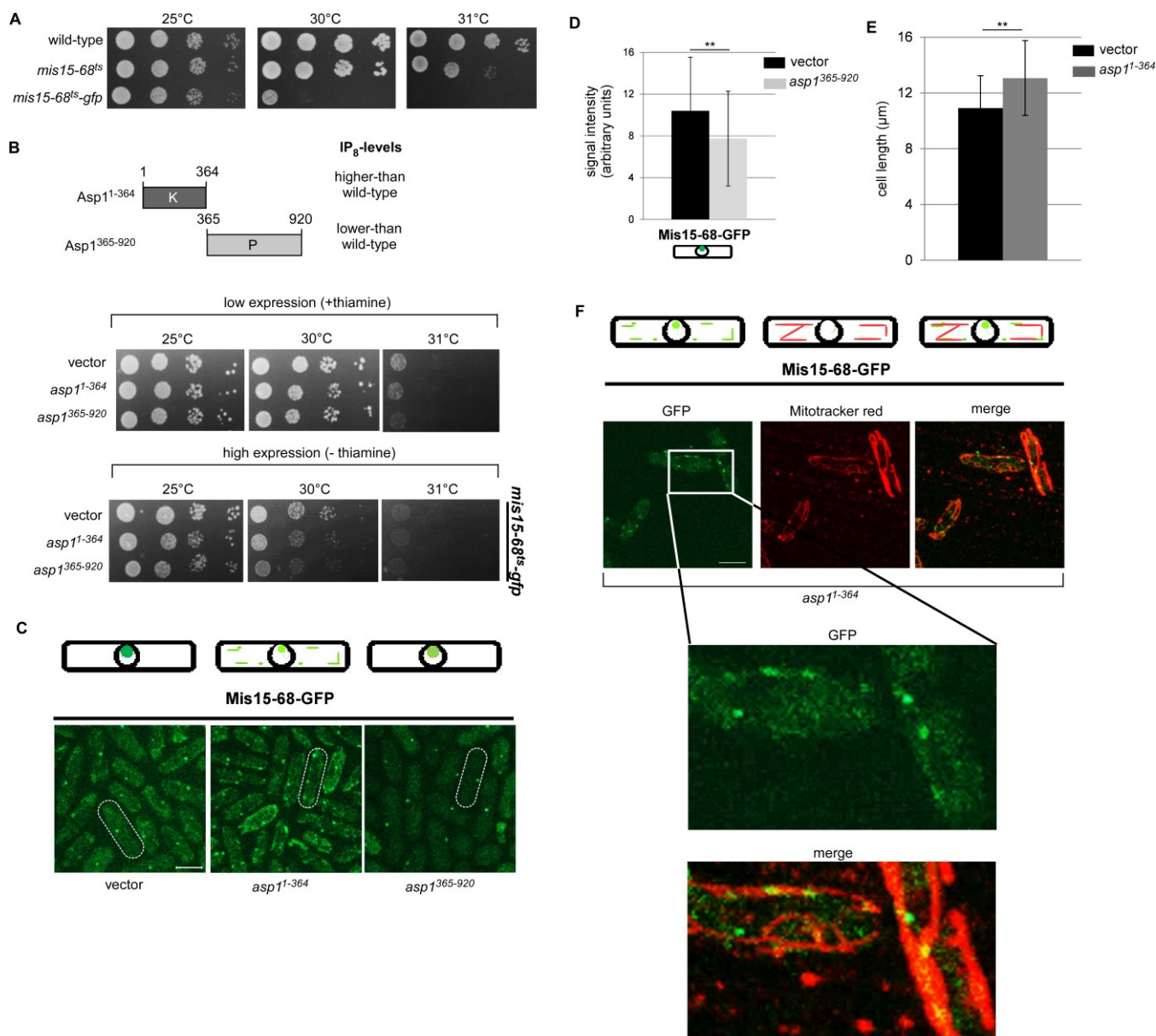


Figure 3-25 Plasmid-borne expression of *asp1*³⁶⁵⁻⁹²⁰ reduces Mis15-68-GFP KT localization.

A: Serial dilution patch tests (10^4 - 10^1 cells) of the indicated strains. Plates were incubated for 4 days at the indicated temperatures. **B:** Serial dilution patch tests (10^4 - 10^1 cells) of *mis15-68^{ts}-gfp* transformed with a vector control, *asp1*¹⁻³⁶⁴ or *asp1*³⁶⁵⁻⁹²⁰ expressed on plasmids. Transformants were grown under plasmid-selective conditions in media with or without thiamine for 6 days at the indicated temperatures. Examples of 4 transformants/ plasmid are shown. **C:** Top: Schematic overview of the Mis15-68-GFP fluorescence signal in the indicated transformants. Darker green = stronger signal. Bottom: Live fluorescence microscopy pictures of the indicated transformants expressing *mis15-68^{ts}-gfp*. Transformants were pre-incubated for 24 h at 25°C in LFM without leucine and without thiamine before they were patched on agarose pads. Pictures were taken at 25°C with 50 % laser intensity using a Zeiss Spinning Disc-Confocal microscope. Scale bar = 5 μm. **D:** Quantification of Mis15-68-GFP fluorescence signals. Pictures taken as in C for the indicated transformants: vector $10.42 \text{ AU} \pm 5.11$; *asp1*³⁶⁵⁻⁹²⁰ $7.74 \text{ AU} \pm 4.54$ ($n = 51$ / plasmid; **: $p \leq 0.01$, two-sample-t-test).

(Figure legend continued on the next page).

E: Quantification of the cell length of *mis15-68^{ts}-gfp* transformed with a vector control or *asp1¹⁻³⁶⁴* expressed on a plasmid. Pictures taken as in C for the indicated transformants: vector $10.91 \mu\text{m} \pm 2.32$; *asp1¹⁻³⁶⁴* $13.07 \mu\text{m} \pm 2.68$ ($n = 20$ / plasmid; **: $p \leq 0.01$, two-sample-t-test). **F:** Top: Schematic overview of the Mis15-68-GFP and MitoTracker signals in the indicated transformant. Bottom: Live fluorescence microscopy pictures taken as in C for a selected transformant. Cells were stained with MitoTracker red to visualize mitochondria.

3.4.1.11 *mis15-68^{ts}-gfp* interacts genetically with *asp1*

Next I analyzed Mis15-68-GFP KT localization in strains endogenously expressing *asp1⁺*, *asp1^{H397A}* or *asp1^{D333A}*.

As observed before the wild-type, *mis15-68^{ts}* and *asp1^{D333A}* strains were able to grow at temperatures of 25°C and 30°C while the *mis15-68^{ts}-gfp* strain showed an increased temperature-sensitivity compared to the non-tagged strain. This effect was increased in an *asp1^{D333A} mis15-68^{ts}-gfp* double mutant which showed a strong reduction of growth already at 25°C (Figure 3-26 A, right panel).

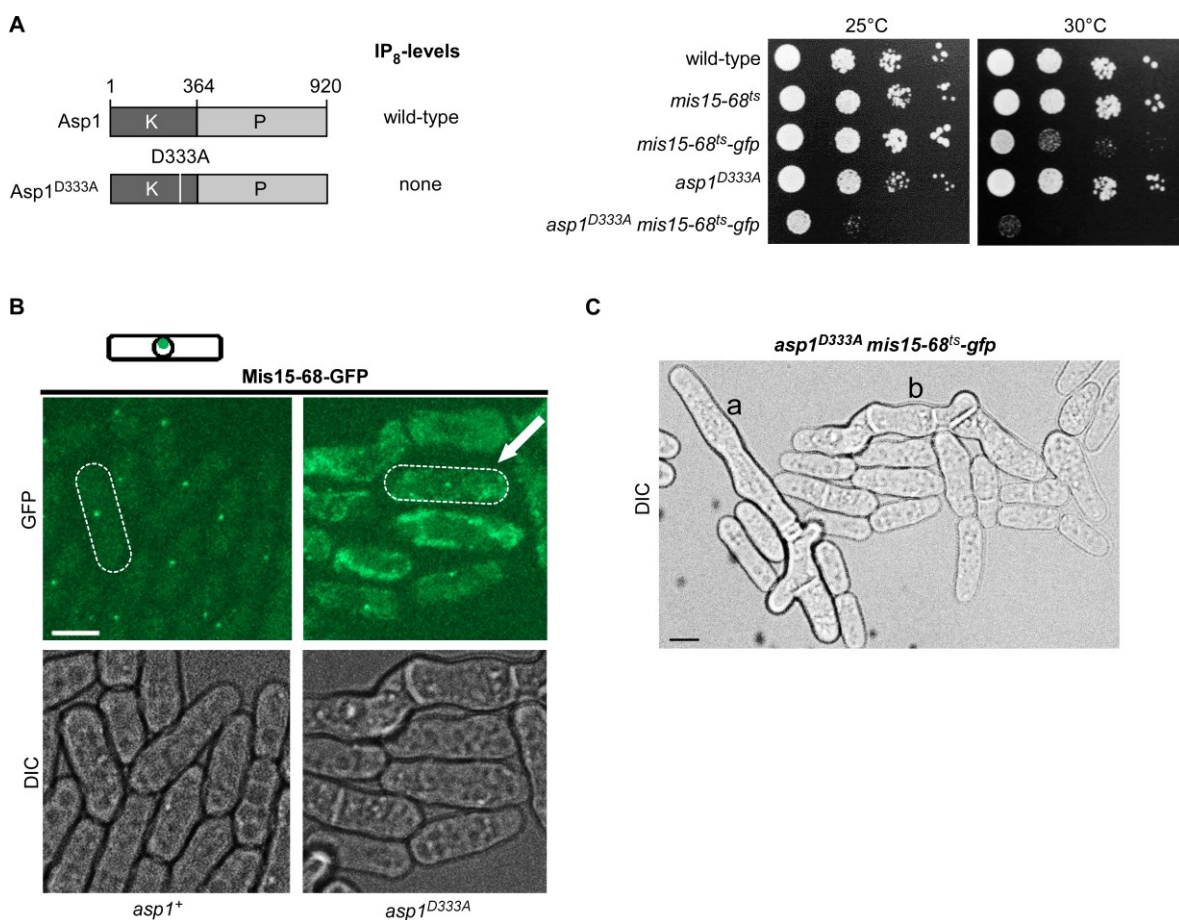


Figure 3-26 *mis15-68^{ts}-gfp* and *asp1^{D333A}* are synthetically lethal.

(Figure legend continued on the next page).

A: Serial dilution patch tests (10^4 - 10^1 cells) of the indicated strains on MM plates with all supplements. Plates were incubated for 4-6 days at the indicated temperatures. **B:** Top: Schematic overview of the Mis15-68-GFP fluorescence signal in the indicated strains. Middle: Live fluorescence microscopy pictures of the indicated strains expressing *mis15-68^{ts}-gfp*. Bottom: DIC pictures. Strains were pre-incubated for 24 h at 25°C in LFM before they were patched on agarose pads. Pictures were taken at 25°C with 60 % laser intensity using a Zeiss Spinning Disc-Confocal microscope. Scale bar = 5 μ m. **C:** Live fluorescence microscopy pictures taken as in B for *asp1^{D333A} mis15-68^{ts}-gfp*. Top: Mis15-68-GFP signal. Bottom: DIC pictures. a: long and branching cell; b: long cell with several septa.

Microscopic analysis of the *asp1^{D333A} mis15-68^{ts}-gfp* strain was performed. It was observed that only ~ 30 % of the cells showed a GFP signal at the KT (example in Figure 3-26 B (arrow)). Therefore fluorescence signals were not quantified. Moreover this strain displayed an aberrant cell shape. Examples are shown in Figure 3-26 C. Long and branching cells (a), as well as multi-septated cells (b), were seen. This indicated that the cells had cytokinesis defects. *mis15-68^{ts}-gfp asp1^{H397A}* strains were also generated. However, as the two obtained candidates showed opposite growth behavior in a patch test I was unable to analyze them further.

Hence, it was found that a combination of *mis15-68^{ts}-gfp* and *asp1^{D333A}* was synthetically lethal possibly because Mis15-68 KT localization was massively reduced.

3.4.1.12 *mis15⁺-gfp* genetically interacts with *asp1*

Next I wanted to analyze whether a similar situation might occur for the wild-type Mis15 protein. Therefore the same experimental approach was done for a *mis15⁺-gfp* strain to determine if the *gfp* tag of the protein also leads to a genetic interaction with *asp1⁺*.

asp1^{D333A} mis15⁺-gfp and *asp1^{H397A} mis15⁺-gfp* double mutants were generated and their growth was analyzed in a patch test experiment (Figure 3-27 A, bottom panel). None of the double mutant strains showed temperature-sensitivity (Figure 3-27 A, bottom panel). Mis15-GFP KT localization in these strains was investigated via fluorescence microscopy. *asp1^{H397A} mis15⁺-gfp* showed a Mis15-GFP fluorescence signal at the KT that was comparable to *asp1⁺ mis15⁺-gfp* (9.3 and 8.9 AU, respectively). In an *asp1^{D333A} mis15⁺-gfp* strain the Mis15-GFP KT was reduced to 5.9 AU (Figure 3-27 B; C). In addition apart from cells with a normal length (7-14 μ m; a in Figure 3-27 B) cells of a length of up to ~ 30 μ m were observed in an *asp1^{D333A}* background (example indicated as b in Figure 3-27 B).

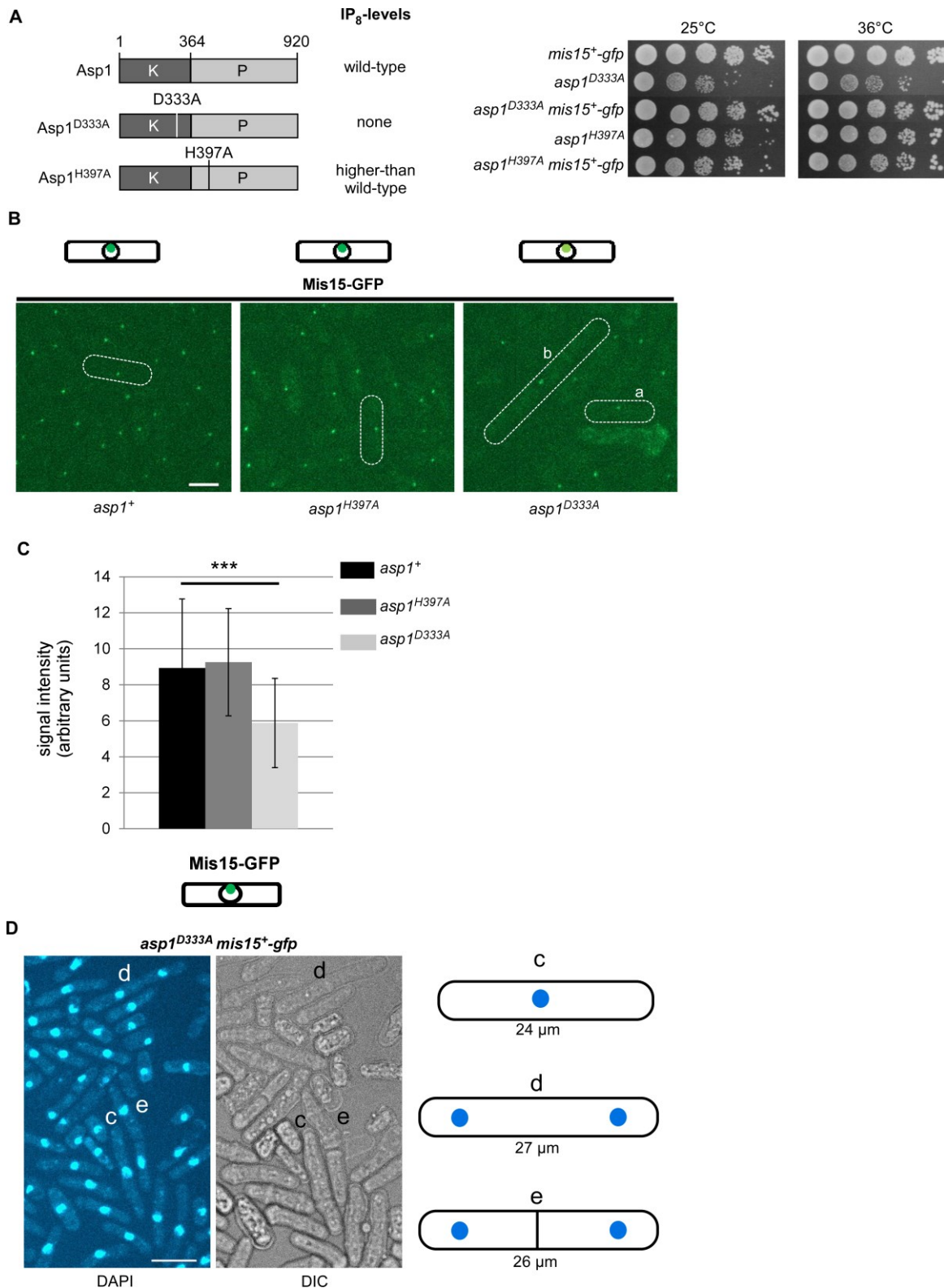


Figure 3-27 *mis15⁺-gfp* and *asp1^{D333A}* genetically interact.

A: Serial dilution patch tests (10⁴-10¹ cells) of the indicated strains on YE5S with or without TBZ. Plates were incubated for 4 days at the indicated temperatures.

(Figure legend continued on the next page).

B: Top: Schematic overview of the Mis15-GFP fluorescence signal in the indicated strains. Darker green = stronger signal. Bottom: Live fluorescence microscopy pictures of the indicated strains expressing *mis15⁺-gfp*. Strains were pre-incubated for 24 h at 25°C in LFM before they were patched on agarose pads. Pictures were taken at 25°C with 20 % laser intensity using a Zeiss Spinning Disc-Confocal microscope. Scale bar = 5 μ m. a: cell with a normal length, b: long cell (25 μ m). **C:** Quantification of Mis15-GFP fluorescence signals. Pictures taken as in B for the indicated strains: *asp1⁺* 8.93 AU \pm 3.8; *asp1^{H397A}* 9.26 AU \pm 3; *asp1^{D333A}* 5.9 AU \pm 2.5 (*asp1⁺* n= 60; *asp1^{H397A}* n= 48, *asp1^{D333A}* n= 16; ***: p \leq 0.001, two-sample-t-test). **D:** Pictures of DAPI staining of *asp1^{D333A} mis15⁺-GFP* after EtOH fixation. Left: DAPI staining. Right: DIC pictures.*: long cells. Pictures taken with a Zeiss Axiovert Microscope.

Further characterization of the aberrant phenotype of *asp1^{D333A} mis15⁺-gfp* was performed via DAPI staining to visualize DNA. Cells with a length of 24 μ m that had not started mitosis yet were found (c in Figure 3-27 D). In other cells mitosis occurred, but the cells divided with a bigger than wild-type size (examples shown as d and e in Figure 3-27 D). Thus, the cells remained longer in one cell cycle phase.

Hence, lower-than-wild-type IP₈-levels reduced Mis15-GFP and Mis15-68-GFP KT targeting, but higher-than-wild-type levels did not increase it.

A summary of the observed correlations between KT targeting of Mis15 and cellular IP₈-levels is shown in Figure 3-28.

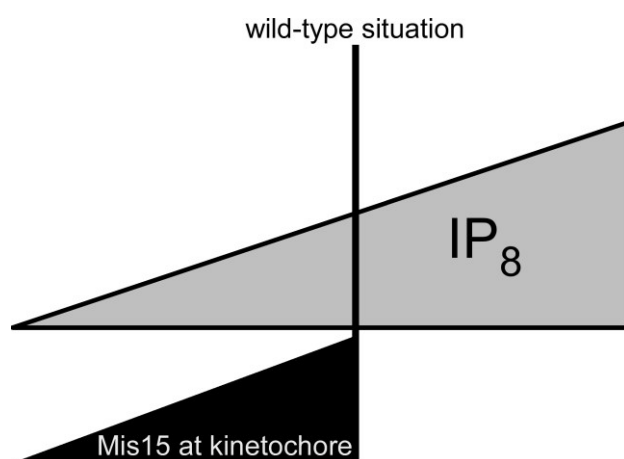


Figure 3-28 Schematic of the effect of IP₈ on Mis15 KT targeting.

3.4.1.13 Dad1-GFP KT localization is reduced in *mal2-1^{ts}* and *mis15-68^{ts}* backgrounds

Sim4-complex members bind spindle MTs indirectly via the DASH complex. Dad1, a DASH complex member, serves as a connector between the Sim4-complex and the MTs and is localized to the KTs throughout the cell cycle (Sanchez-Perez et al., 2005) (Figure 3-29 A).

One possible effect of changes in KT localization of Sim4-complex members by IP_8 could be a downstream effect on Dad1 localization and therefore DASH recruitment. Therefore I analyzed Dad1-GFP localization in *mal2-1^{ts}* and *mis15-68^{ts}* strains.

A

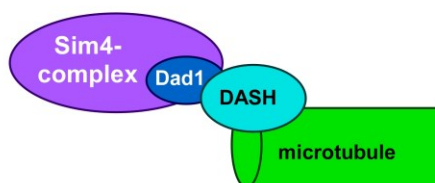
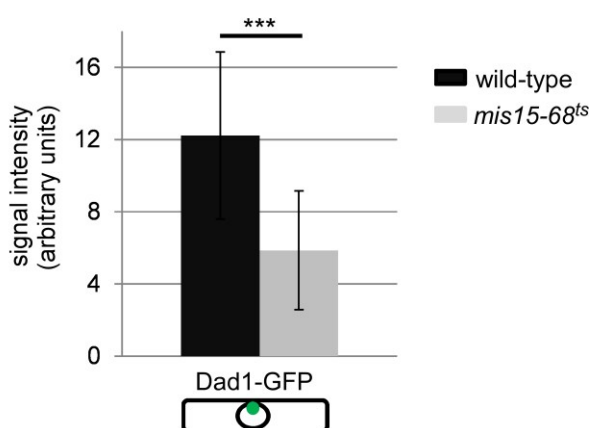


Figure 3-29 Dad1 KT targeting is reduced in *mal2-1^{ts}* and *mis15-68^{ts}* strains.

B



A: Scheme of the location of Dad1 between the Sim4- and DASH-complexes. **B:** Quantification of Dad1-GFP fluorescence signals. Strains were pre-incubated for 24 h at 25°C in LFM before they were patched on agarose pads. Pictures were taken at 25°C with 40 % laser intensity using a Zeiss Spinning Disc-Confocal microscope. Pictures taken for the indicated strains: wild-type 12.22 AU ± 4.6; *mis15-68^{ts}* 5.86 AU ± 3.3 (n= 25/ strain; ***: p ≤ 0.001, two-sample-t-test).

Thus, microscopic analysis of *dad1⁺-gfp*, *mal2-1^{ts} dad1⁺-gfp* and *mis15-68^{ts} dad1⁺-gfp* strains was performed. In a *mal2-1^{ts}* strain background the Dad1-GFP KT localization was reduced to a non-detectable level even at 25°C (data not shown). In the *mis15-68^{ts} dad1⁺-gfp* strain Dad1-GFP localized at the KT interface was detectable but strongly reduced compared to the *dad1⁺-gfp* strain. Quantification of the fluorescence signal intensity of Dad1-GFP at the KT showed that with a *mis15-68^{ts}* strain background the signal intensity was reduced massively from 12 (*dad1⁺-gfp*) to 5.9 AU (Figure 3-29 B; C).

Hence, in *mal2-1^{ts}* and *mis15-68^{ts}* strains the recruitment of Dad1-GFP to the KT interface was reduced but the reduction was stronger in the *mal2-1^{ts}* background. This indicates that Mal2 and Mis15 are important for Dad1-GFP KT recruitment. Therefore they have antagonistic tendencies but not in terms of DASH recruitment.

3.4.2 Mal2 and Mis15 act in an opposed manner

3.4.2.1 *mis15*⁺ overexpression increases missegregation in a *mal2-1^{ts}* strain

Mal2 and Mis15 showed opposite reactions to changes in cellular IP₈-levels.

Next it was analyzed if Mal2 and Mis15 also affected each other under overexpression conditions. Mal2 and Fta2 are closely correlated in terms of function and localization (Kerres et al., 2006). Therefore a plasmid with a combination of both *mal2*⁺ and *fta2*⁺ under the control of two *nmt1*⁺-promoters on one plasmid was used to ensure that the absence of an effect via overexpression of one of these proteins was not due to limited amount of interaction partner.

For this purpose *mal2*⁺, *fta2*⁺, *mis15*⁺ or (*mal2*⁺ + *fta2*⁺) expressed on plasmids were first, as a control, transformed in a wild-type strain. Overexpression of *mal2*⁺, *fta2*⁺ or *mis15*⁺ did not alter the growth of the wild-type strain. Overexpression of (*mal2*⁺ + *fta2*⁺) slightly reduced the growth of the wild-type strain (Figure 3-30 A).

Next a *mal2-1^{ts}* strain was transformed with a vector control or *mal2*⁺, *fta2*⁺, (*mal2*⁺ + *fta2*⁺) or *mis15*⁺ expressing plasmids. Under low expression conditions all transformants grew comparable at 25°C. At 28°C the *mal2-1^{ts}* strain transformed with the vector control showed reduced growth (Figure 3-30 B left panel). This reduction in growth was rescued by expression of *mal2*⁺, *fta2*⁺ or *mal2*⁺ + *fta2*⁺. The opposite was found for *mis15*⁺ expression as this reduced the growth of the *mal2-1^{ts}* strain at 28°C (Figure 3-30 B, right panel).

To analyze if the reduction in growth upon *mis15*⁺ overexpression was connected to an increase in chromosome segregation defects in the *mal2-1^{ts}* strain an immunofluorescence experiment was performed at 25°C. The *mal2-1^{ts}* strain transformed with a vector control showed 27 % of cells with segregation defects in thiamine containing medium. Low expression of extra *mal2*⁺ reduced segregation defects to 13.2 % (Figure 3-30 C, left). Low overexpression of extra *mis15*⁺ had the opposite effect and led to an increase of segregation defects to 34.6 % (Figure 3-30 C, left). In medium without thiamine the *mal2-1^{ts}* strain transformed with a vector control showed 23.7 % of cells while high expression of *mal2*⁺ reduced these segregation defects to 6.1 % (Figure 3-30 C, right).

The opposite was observed for *mis15*⁺ overexpression which led to a massive amount of segregation defects (62.7 %) (Figure 3-30 C, right).

Thus, high levels of Mis15 were negatively affecting the growth and massively increased segregation defects in the *mal2-1^{ts}* strain.

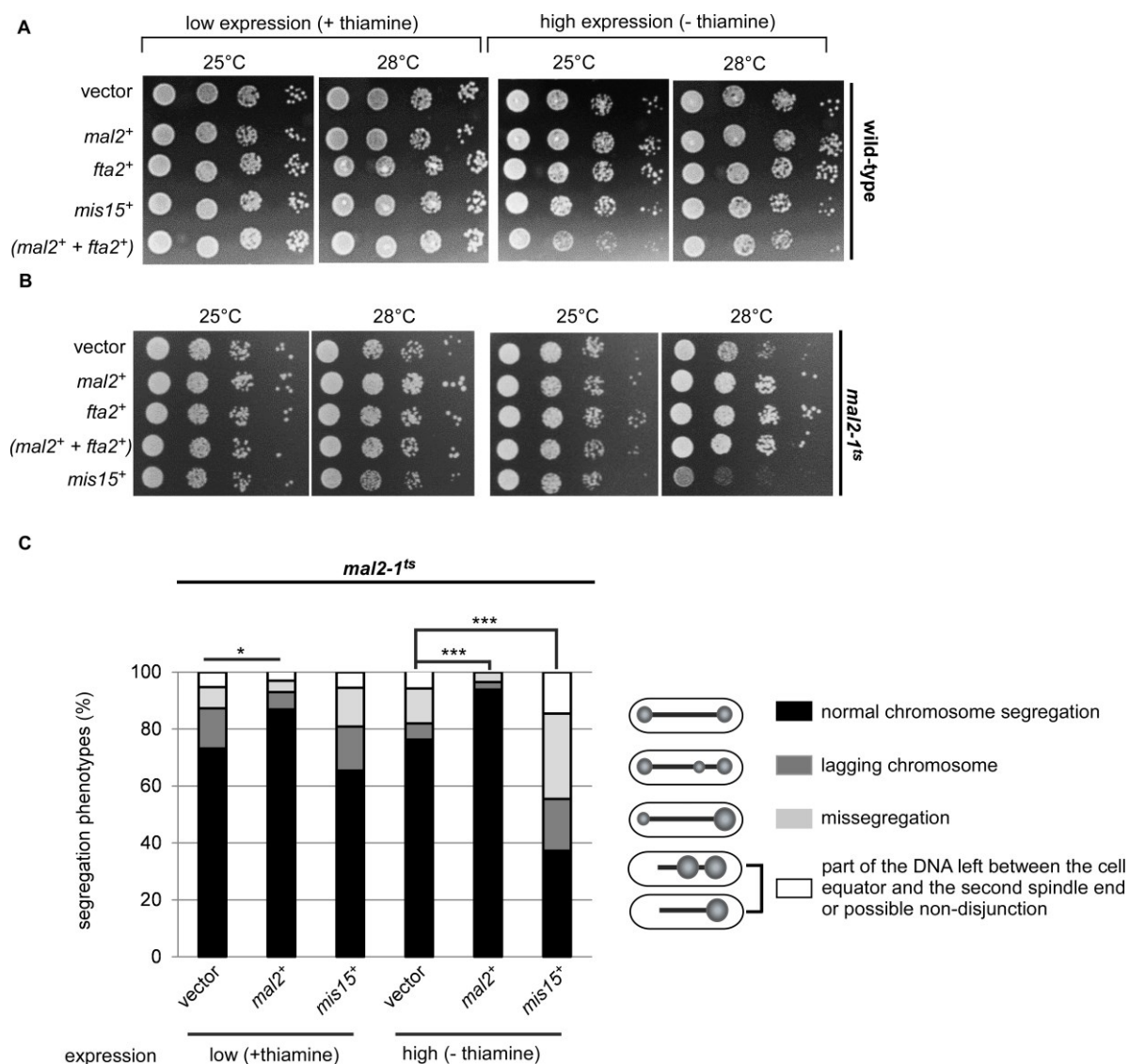


Figure 3-30 *mis15*⁺ overexpression increases missegregation events in a *mal2-1*^{ts} strain.

A: Serial dilution patch tests (10^4 - 10^1 cells) of the wild-type strain transformed with a vector control or *mal2*⁺, *fta2*⁺, *mis15*⁺ or (*mal2*⁺ + *fta2*⁺) expressed on plasmids. Transformants were grown under plasmid-selective conditions in media with or without thiamine for 4 days at the indicated temperatures. **B:** Serial dilution patch tests (10^4 - 10^1 cells) of the *mal2-1*^{ts} strain transformed with a vector control or *mal2*⁺, *fta2*⁺, (*mal2*⁺ + *fta2*⁺) or *mis15*⁺ expressed on plasmids. Transformants were grown under plasmid-selective conditions in media with or without thiamine for 6 days at the indicated temperatures. Examples of at least 4 transformants/ plasmid are shown. **C:** Immunofluorescence (α -TAT1 antibody) and DAPI staining of selected transformants of the *mal2-1*^{ts} strain as used in B. Transformants were pre-grown in plasmid-selective media overnight at 25°C. Diagram of the quantification of the phenotypes observed the indicated transformants. The phenotypes observed are depicted on the right. vector: low expression: 14 % lagging chromosomes, 7.5 % missegregation, 5 % parts of the DNA left at the cell equator (n= 134), high expression: 6 % lagging chromosomes, 12 % missegregation, 7 % parts of the DNA left at the cell equator (n= 140); *mal2*⁺: low expression: 6 % lagging chromosomes, 4 % missegregation, 3.5 % parts of the DNA left at the cell equator (n= 118), high expression: 3 % lagging chromosomes, 3.5 % missegregation (n= 115); *mis15*⁺: low expression: 15.5 % lagging chromosomes, 13.5 % missegregation, 5.5 % parts of the DNA left at the cell equator (n= 110), high expression: 18.2 % lagging chromosomes, 30 % missegregation, 14.5 % parts of the DNA left at the cell equator (n= 110). ($p \leq 0.001$, χ^2 -test; compared was the total amount of segregation defects). Patch tests performed by Eva Walla.

3.4.2.2 *mis15*⁺ overexpression reduces Mal2-GFP kinetochore targeting

To analyze whether the effects of *mis15*⁺ overexpression on the growth and segregation phenotypes of the *mal2-1^{ts}* mutant strain were connected to a change in KT localization of Mal2 the influence of *mis15*⁺ overexpression on Mal2-GFP localization was determined.

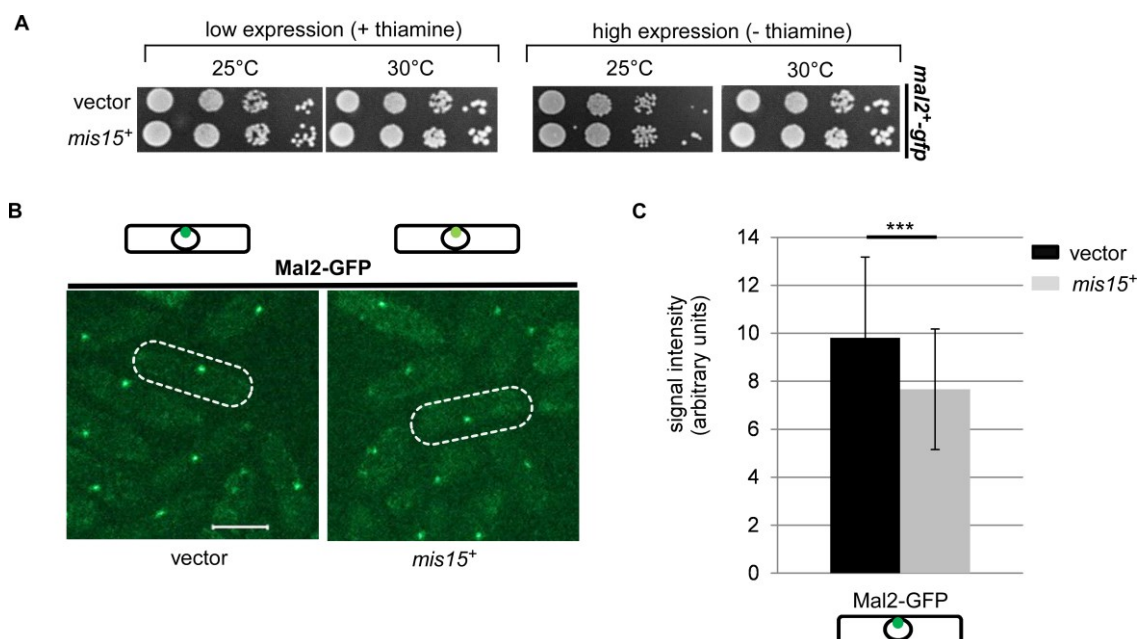


Figure 3-31 *mis15*⁺ overexpression reduces Mal2-GFP KT localization.

A: Serial dilution patch tests (10^4 - 10^1 cells) of *mal2*⁺-*gfp* transformed with a vector control or *mis15*⁺ expressed on a plasmid. Transformants were grown under plasmid-selective conditions in media with (low expression) or without (high expression) thiamine for 4 days at the indicated temperatures. **B:** Top: Schematic overview of the Mal2-GFP fluorescence signal in the indicated transformants. Darker green = stronger signal. Bottom: Live fluorescence microscopy pictures of the indicated transformants expressing *mal2*⁺-*gfp*. Transformants were pre-incubated for 24 h at 25°C in LFM without leucine and without thiamine before they were patched on agarose pads. Pictures were taken at 25°C with 40 % laser intensity using a Zeiss Spinning Disc-Confocal microscope. Scale bar = 5 μ m. **C:** Quantification of Mal2-GFP fluorescence signals. Pictures taken as in B for the indicated transformants: vector 9.8 AU \pm 3.4; *mis15*⁺ 7.7 AU \pm 2.5 (n= 50/ plasmid; 2 transformants/ plasmid ***: p \leq 0.001, two-sample-t-test).

Plasmid-borne overexpression of *mis15*⁺ had no effect on the growth of a *mal2*⁺-*gfp* strain (Figure 3-31 A). However, microscopic analysis showed that compared to the vector control the fluorescence signal of Mal2-GFP at the KT was reduced with overexpression of *mis15*⁺ from 9.8 to 7.7 AU, (Figure 3-31 B; C). Thus, overexpression of *mis15*⁺ reduced the amount of Mal2-GFP at the KT indicating that a reduced localization might be what causes an increase in chromosome segregation defects in the *mal2-1^{ts}* strain.

3.4.2.3 (*mal2*⁺ + *fta2*⁺) overexpression reduces Mis15-68-GFP kinetochore targeting

Next I analyzed if expression of *mal2*⁺, *fta2*⁺ or (*mal2*⁺ + *fta2*⁺) affected the growth of the *mis15-68*^{ts} strain.

mis15-68^{ts} strain transformants harboring the vector control grew up to 33°C on plates containing thiamine and up to 31°C on plates without thiamine. Under low expression conditions all transformants grew comparable at 25°C, 31°C and 33°C (Figure 3-32 A, left panel). Overexpression of *mis15*⁺ complemented the temperature-sensitivity of the *mis15-68*^{ts} strain (Figure 3-32 A, right panel). High overexpression of either *mal2*⁺ or *fta2*⁺ alone led only to a slight reduction of growth, while expression of (*mal2*⁺ + *fta2*⁺) abolished growth at temperatures ≥ 31°C (Figure 3-32 A, right panel). The same reduction in growth upon high (*mal2*⁺ + *fta2*⁺) expression was observed for the *mis15-68*^{ts}-*gfp* strain (Figure 3-32 B, right panel). Mis15-68-GFP KT fluorescence signals were analyzed in transformants with a vector control or with (*mal2*⁺ + *fta2*⁺) overexpression. Overexpression of (*mal2*⁺ + *fta2*⁺) decreased the fluorescence signal intensity from 12.4 (vector) to 6.5 AU (Figure 3-32 C; D).

Thus, high levels of Mal2 + Fta2 interfered with the KT targeting of Mis15-68-GFP.

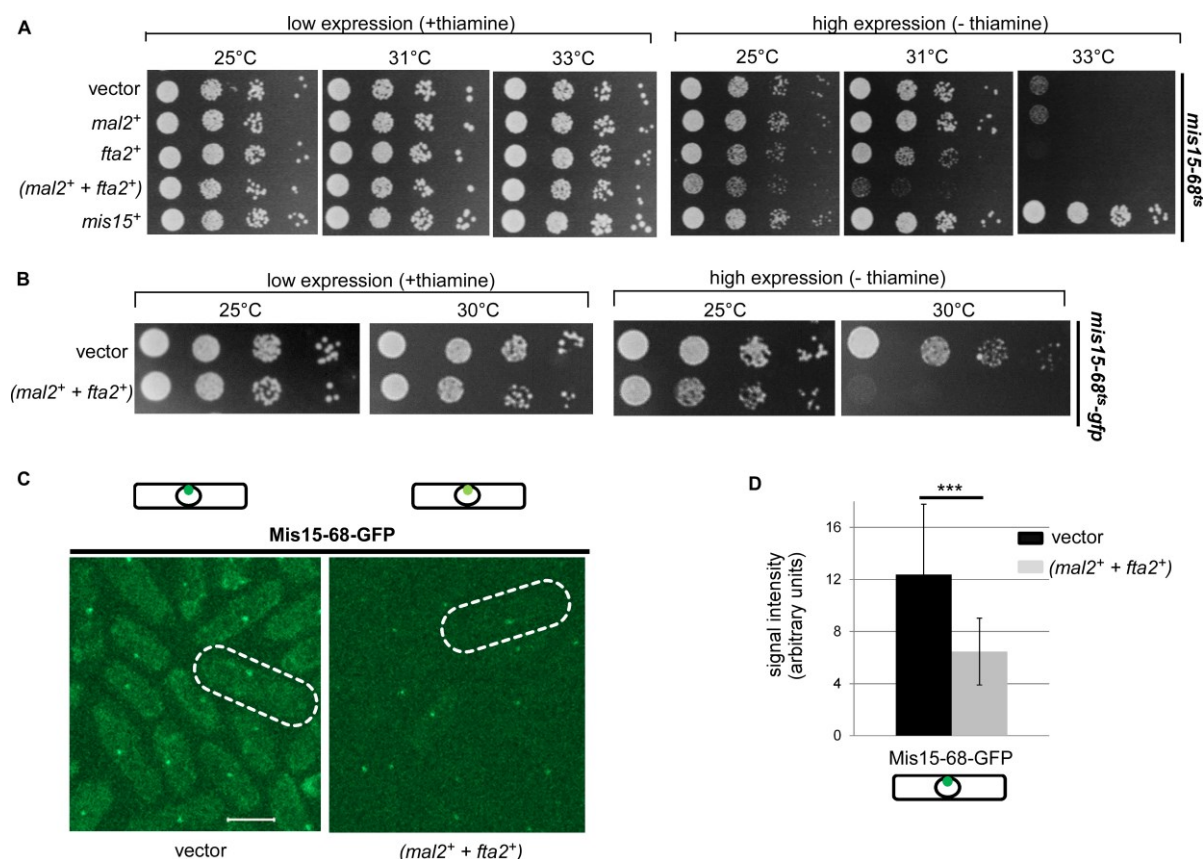


Figure 3-32 (*mal2*⁺ + *fta2*⁺) overexpression reduces Mis15-68-GFP KT localization.

(Figure legend continued on the next page).

A: Serial dilution patch tests (10^4 - 10^1 cells) of a *mis15-68^{ts}* strain transformed with a vector control or *mal2⁺*, *fta2⁺*, (*mal2⁺ + fta2⁺*) or *mis15⁺* containing plasmids. Transformants were grown under plasmid-selective conditions in media with (low expression) or without (high expression) thiamine for 5 days at the indicated temperatures. **B:** Serial dilution patch tests (10^4 - 10^1 cells) of a *mis15-68^{ts}-gfp* strain transformed with a vector control or (*mal2⁺ + fta2⁺*) expressed on a plasmid. Transformants were grown under plasmid-selective conditions in media with or without thiamine for 6 days at the indicated temperatures. **C:** Top: Schematic overview of the Mis15-68-GFP fluorescence signal in the indicated transformants. Darker green = stronger signal. Bottom: Live fluorescence microscopy pictures of the indicated transformants expressing *mis15-68^{ts}-gfp*. Transformants were pre-incubated for 24 h at 25°C in LFM without leucine and without thiamine before they were patched on agarose pads. Pictures were taken at 25°C with 60 % laser intensity using a Zeiss Spinning Disc-Confocal microscope. Scale bar = 5 μ m. **D:** Quantification of Mis15-68-GFP fluorescence signals. Pictures taken as in C for the indicated transformants: vector 12.37 AU \pm 5.4; (*mal2⁺ + fta2⁺*) 6.47 AU \pm 2.57 (vector n= 22, (*mal2⁺ + fta2⁺*) n= 23; ***: $p \leq 0.001$, two-sample-t-test).

3.4.2.4 (*mal2⁺ + fta2⁺*) overexpression leads to an aberrant phenotype in a non-tagged wild-type and a *mis15⁺-gfp* strain

Moreover, I determined the influence of (*mal2⁺ + fta2⁺*) overexpression on the *mis15⁺-gfp* strain.

To this end the *mis15⁺-gfp* strain was transformed with a vector control or (*mal2⁺ + fta2⁺*) expressed on a plasmid. The growth of the *mis15⁺-gfp* strain was unaffected if it was transformed with the vector control (Figure 3-33 A, left panel). Low overexpression of (*mal2⁺ + fta2⁺*) had no effect on the growth of the *mis15⁺-gfp* strain (Figure 3-33 A, left panel), while high overexpression of (*mal2⁺ + fta2⁺*) reduced the growth slightly (Figure 3-33 A, right panel). The effect of (*mal2⁺ + fta2⁺*) expressed on a plasmid on the growth was therefore comparable to that in the non-tagged wild-type strain (Figure 3-30 A).

High (*mal2⁺ + fta2⁺*) overexpression led to an aberrant phenotype of the *mis15⁺-gfp* strain. The transformant with the vector control showed cells with a normal length between 7-14 μ m and a clear Mis15-GFP signal at the KT. In transformants overexpressing (*mal2⁺ + fta2⁺*) the signal intensity of Mis15-GFP at the KT was reduced from 9.6 (vector) to 7.8 AU. Furthermore, 25 % of cells displayed an aberrant cell length (≥ 14 μ m; example shown as b in Figure 3-33 B) (Figure 3-33 B; C). An increase in the average cell length from 9.5 μ m (vector) to 12.4 μ m was observed if *mal2⁺ + fta2⁺* were overexpressed (Figure 3-33 D).

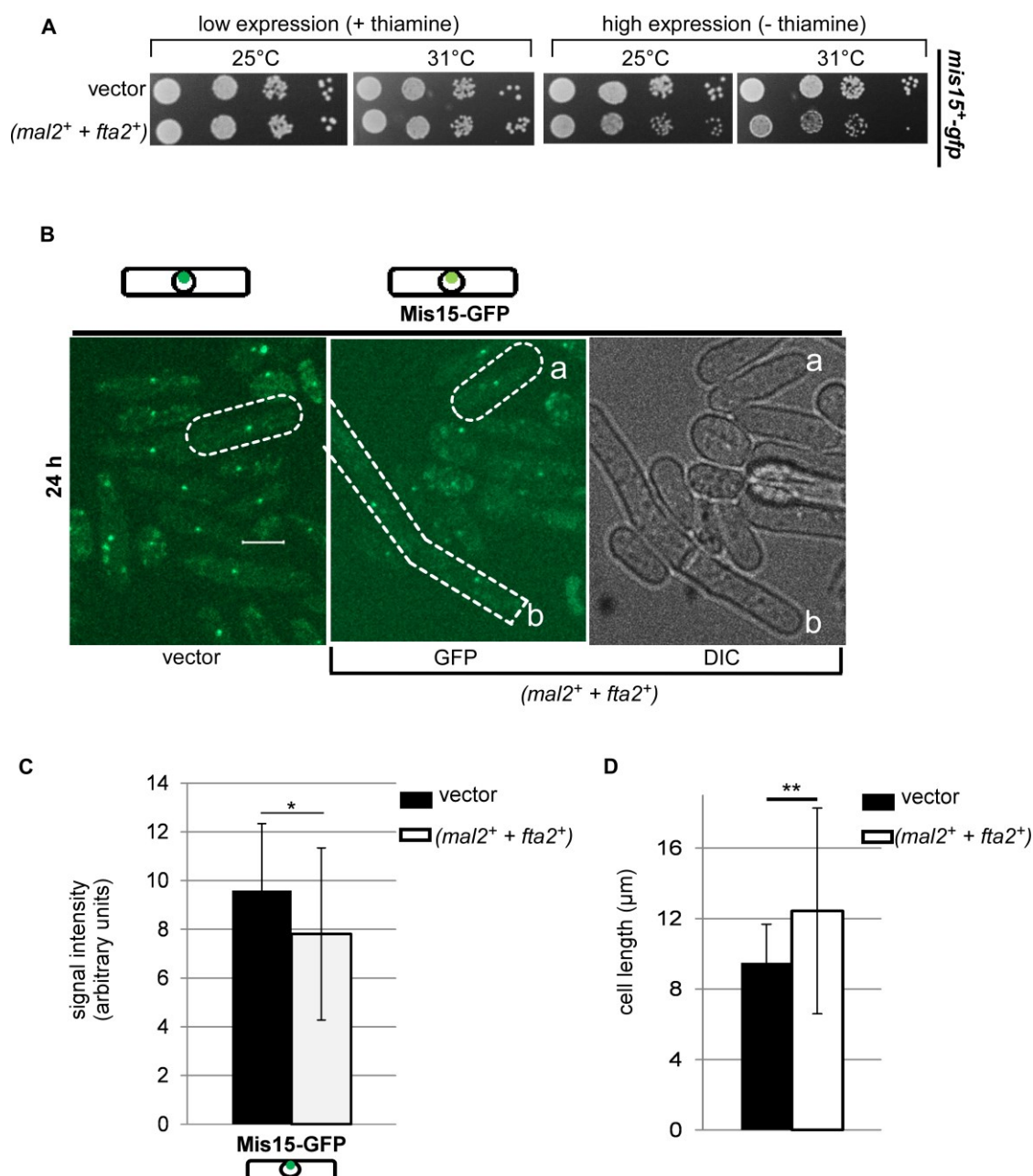


Figure 3-33 (*mal2⁺ + fta2⁺*) overexpression induces an aberrant cell shape in the *mis15⁺-gfp* strain.

A: Serial dilution patch tests (10^4 - 10^1 cells) of a *mis15⁺-gfp* strain transformed with a vector control or (*mal2⁺ + fta2⁺*) expressed on a plasmids. Transformants were grown under plasmid-selective conditions in media with (low expression) or without (high expression) thiamine for 4 days at the indicated temperatures. **B:** Live fluorescence microscopy pictures of the indicated transformants expressing *mis15⁺-gfp*. Transformants were pre-incubated for 24 h at 25°C in LFM without leucine and without thiamine before they were patched on agarose pads. Pictures were taken at 25°C with 40 % laser intensity using a Zeiss Spinning Disc-Confocal microscope. Scale bar = 5 µm. a: cell with normal length and Mis15-GFP signal; b: long cell (34.5 µm) showing two Mis15-GFP signals. **C:** Quantification of Mis15-GFP fluorescence signals. Pictures taken as in B for the indicated transformants: vector 9.6 AU ± 2.7; (*mal2⁺ + fta2⁺*) 7.8 AU ± 3.5 (n= 43/ plasmid; 2 transformants/plasmid; *: p ≤ 0.05, two-sample-t-test). **D:** Quantification of the average cell length of the indicated transformants. Pictures taken as in B. vector 9.5 µm ± 2.2; (*mal2⁺ + fta2⁺*) 12.4 µm ± 5.8 (n= 50/ plasmid; **: p ≤ 0.01, two-sample-t-test).

To test if this aberrant phenotype was also detectable in a non-tagged *mis15*⁺ strain the morphology of transformants with a vector control or (*mal2*⁺ + *fta2*⁺) expressed on a plasmid was analyzed in a wild-type strain. After 24 h of incubation without thiamine the cells transformed with the vector control or the (*mal2*⁺ + *fta2*⁺) plasmid showed a normal cell length (~ 7-14 μm; data not shown). At this point the transformants in the *mis15*⁺-*gfp* strain already showed an aberrant morphology.

However, at later time points (after 40 h of growth under high expression conditions) cells transformed with the vector control still showed a normal cell length. The transformants overexpressing (*mal2*⁺ + *fta2*⁺) on the other hand showed an aberrant phenotype. 27.5 % of cells had an increased cell length. All of these cells showed none or only one septum. Compared to the vector control (10.3 μm) the average cell length was increased to 13.2 μm (Figure 3-34 A; B).

After 72 h of incubation without thiamine the amount of aberrant long cells stayed constant with 25.8 %. However, 20 % of the aberrant long cells showed two septa (Figure 3-34 C).

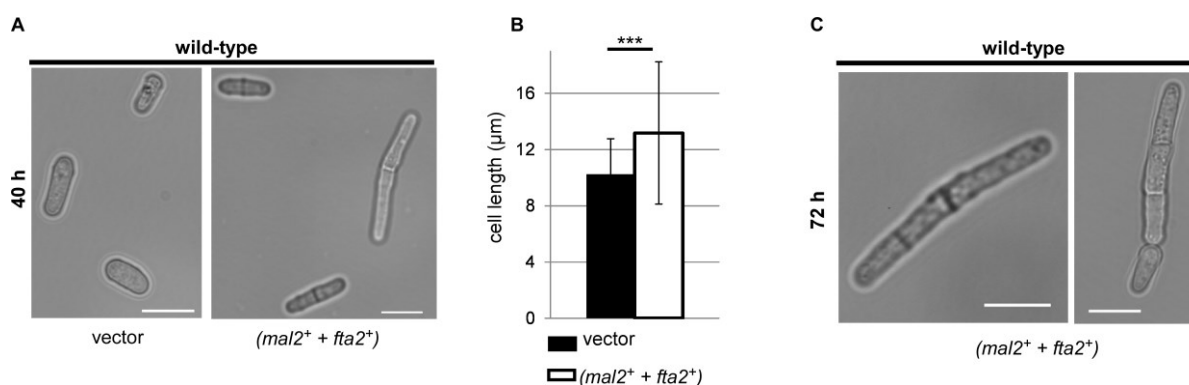


Figure 3-34 (*mal2*⁺ + *fta2*⁺) overexpression induces an aberrant cell shape in the wild-type strain.

A: DIC microscopy pictures for the indicated transformants. Transformants were pre-grown 40 h in LFM without leucine and without thiamine at 25°C before pictures were taken with a Zeiss Axiovert Microscope. Scale bar= 10 μm. **B:** Quantification of the average cell length of the indicated transformants. vector 10.25 μm ± 2.52 (n= 16); (*mal2*⁺ + *fta2*⁺) 13.17 μm ± 5.06 (n= 102) (***: p ≤ 0.001, two-sample-t-test). **C:** DIC microscopy pictures for the indicated transformant. Transformant was pre-grown 72 h in LFM without leucine and without thiamine at 25°C before pictures were taken with a Zeiss Axiovert Microscope. Scale bar = 10 μm.

To test if a longer incubation time also enhanced the phenotype of (*mal2*⁺ + *fta2*⁺) overexpression in the *mis15*⁺-*gfp* strain the morphology was analyzed after 40 h of incubation under high expression conditions. The transformant with the vector control showed wild-type length cells. The transformant overexpressing (*mal2*⁺ + *fta2*⁺) on the other hand showed even more cells with a very heterogeneous cell shape. 35.7 % were longer than 14 μm. Cells of

normal length showed a Mis15-GFP signal (a in Figure 3-35) but in aberrant long cells (up to 43 μm , branching or with several septa (depicted as b, c, d in Figure 3-35) only a very weak or no Mis15-GFP signal was observed (Figure 3-35). It is noteworthy that in transformants of the wild-type strain overexpressing (*mal2*⁺ + *fta2*⁺) no branching cells or cells with more than two septa were observed and the cells did not reach a length of ≥ 40 μm .

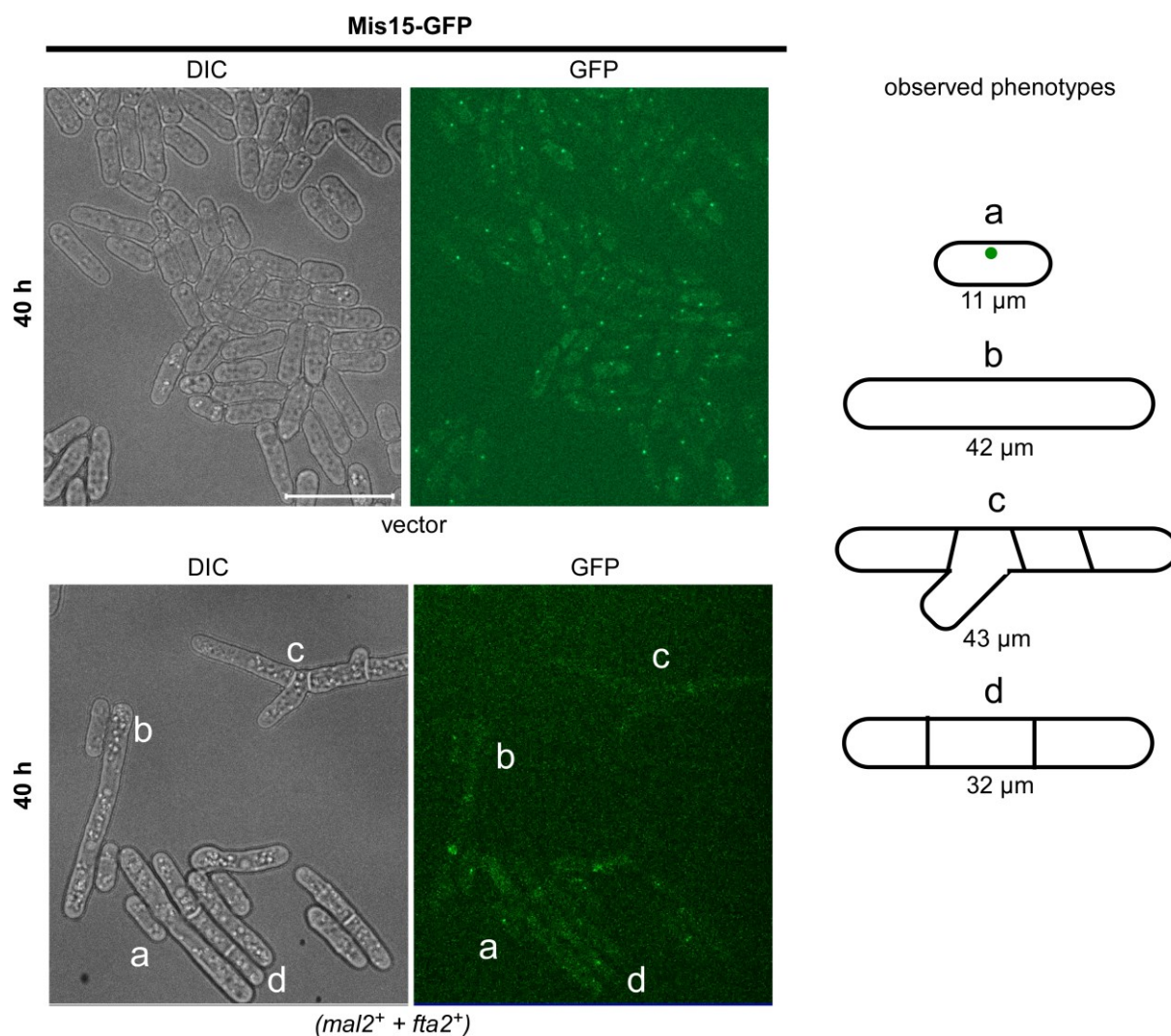


Figure 3-35 The aberrant phenotype induced by (*mal2*⁺ + *fta2*⁺) overexpression in the *mis15*⁺-*gfp* strain gets more severe over time.

Live fluorescence microscopy pictures of the indicated transformants expressing *mis15*⁺-*gfp*. Transformants were pre-incubated for 40 h at 25°C in LFM without leucine and without thiamine before they were patched on agarose pads. Pictures were taken at 25°C with 40 % laser intensity using a Zeiss Spinning Disc-Confocal microscope. Scale bar = 20 μm . Left: DIC pictures, right: GFP fluorescence pictures. a: cell with a normal length that still shows Mis15-GFP signals; b: long cell that has no septum; c: branching cell, d: cell with several septa.

The phenotypes observed indicated that the cells overexpressing (*mal2*⁺ + *fta2*⁺) remained longer, or even arrested, in one cell cycle phase and/or that they had severe cytokinesis defects.

Thus, high levels of Mal2 + Fta2 in the cell led to aberrant cell morphology in general and this effect was enhanced by the presence of Mis15-GFP.

Furthermore high levels of Mal2 + Fta2 reduced Mis15-GFP KT localization.

In summary, I found that the KT localization of Mal2 and Fta2 was increased by lower-than-wild-type IP₈-levels while that of Mis15 was decreased. Furthermore these proteins negatively influenced each others KT targeting (Figure 3-36).

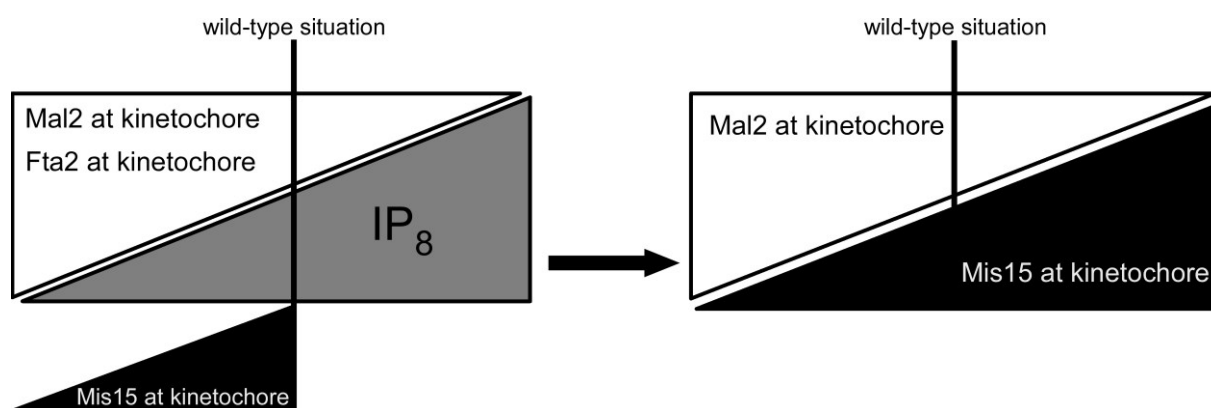


Figure 3-36 Schematic of the effect of IP₈ on Sim4-complex members and their effect on each other.

However, lowering the amount of Mal2 and Mis15 at the KT simultaneously in a *mal2-1^{ts}* *mis15-68^{ts}* double mutant strain did not balance the phenotypes observed, but had a negative synergistic effect, which led to reduced growth compared to the single mutant strains (Supplementary Figure 9 (p. 189)).

3.4.3 The effect of Asp1-generated IP₈ on the NMS-kinetochore-subcomplex

The NMS (Ndc80-MIND-Spc7)-complex is an essential KT-subcomplex that consists of 10 proteins and is further subdivided in the Ndc80-, MIND, and Spc7/Sos7-sub-complexes. Other than the Sim4-complex the NMS-complex directly connects to spindle MTs via Spc7 and Ndc80 proteins (Hsu and Toda, 2011; Jakopiec et al., 2012; Kerres et al., 2004; Tang et al., 2013).

3.4.3.1 IP₈ influences the growth of NMS-complex mutant strains

As IP₈ influenced the Sim4-KT-subcomplex composition I also analyzed the effect of IP₈ on the NMS-complex. Again ts mutant strains were used for the analysis.

First, members of the Ndc80-subcomplex were analyzed. No effect on growth of a *nuf2-3^{ts}* strain was detected with low expression of either *asp1¹⁻³⁶⁴* or *asp1³⁶⁵⁻⁹²⁰* (Figure 3-37 B, left panel). Under high expression conditions both Asp1 variants reduced the growth of the *nuf2-3^{ts}* strain compared to the vector control albeit to different degrees. At 33°C the *nuf2-3^{ts}* strain showed no growth with high expression of *asp1³⁶⁵⁻⁹²⁰* and reduced growth with *asp1¹⁻³⁶⁴* (Figure 3-37 B, right panel).

Growth of the *ndc80-21^{ts}* strain was not affected by low expression of either *asp1* variant (Figure 3-37 B, left panel). However, high expression of *asp1¹⁻³⁶⁴* led to a slight rescue of the ts phenotype at 32°C. High expression of *asp1³⁶⁵⁻⁹²⁰* had the opposite effect and led to lethality (Figure 3-37 B, right panel).

Next members of the MIND-complex were tested. No effect on growth of the *mis12-537^{ts}* strain was detected with low expression of *asp1¹⁻³⁶⁴* or *asp1³⁶⁵⁻⁹²⁰* (Figure 3-37 C, left panel). Under high expression conditions *asp1¹⁻³⁶⁴* and *asp1³⁶⁵⁻⁹²⁰* expression reduced the growth of that strain compared to the vector control. The negative effect on growth of *asp1¹⁻³⁶⁴* was stronger than that of *asp1³⁶⁵⁻⁹²⁰* expression (Figure 3-37 C, right panel).

The second tested MIND-sub-complex mutant strain *mis14-634^{ts}* showed similar growth behavior under low expression conditions. High expression of *asp1¹⁻³⁶⁴* had no effect on growth while high expression of *asp1³⁶⁵⁻⁹²⁰* led to a reduction of growth compared to the vector control (Supplementary Figure 10 A (p. 189)).

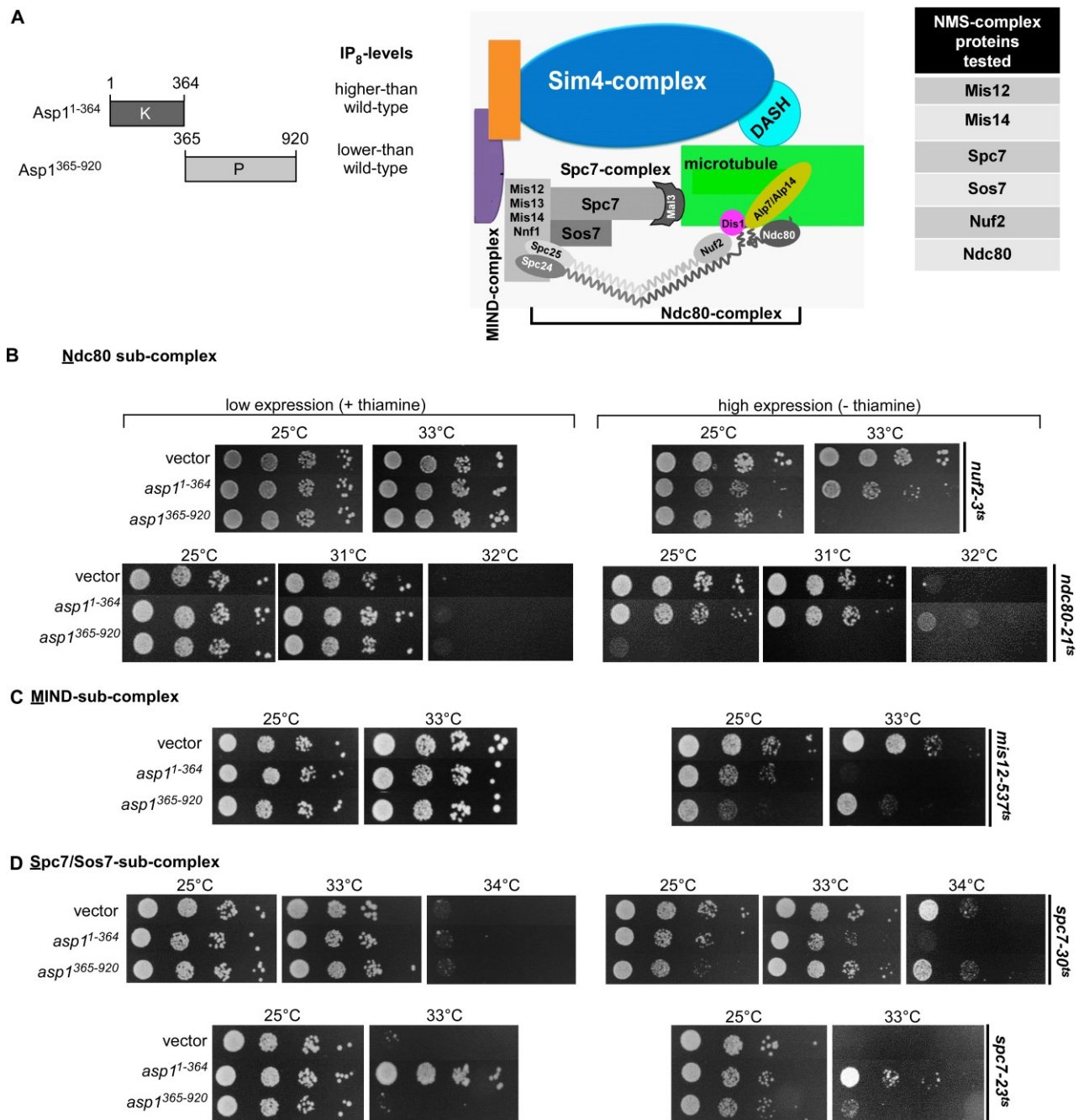


Figure 3-37 A change in cellular IP₈-levels affects the growth of NMS-complex mutant strains.

A: Left: Asp1-variants used. Right: Overview of NMS-complex components and MT-associated binding partners and which were tested in the screen. **B-E:** Serial dilution patch tests (10^4 - 10^1 cells) of the indicated strains transformed with a vector control, *asp1¹⁻³⁶⁴* or *asp1³⁶⁵⁻⁹²⁰* plasmids. Transformants were grown under plasmid-selective conditions in media with or without thiamine for 4-6 days at the indicated temperatures. The temperatures shown were selected to best demonstrate the differences in growth. Examples of at least 3 transformants/ plasmid are shown.

Finally, *ts* mutants of the Spc7/Sos7-complex were analyzed. For the three mutants *spc7-30^{ts}*, *spc7-24^{ts}* and *sos7-178^{ts}* no change in growth upon low expression of the *asp1* variants compared to the vector control was observed at the temperatures tested (Figure 3-37 D, left panel; Supplementary Figure 10 B, left panel (p. 189)). However, while high

expression of *asp1*³⁶⁵⁻⁹²⁰ did not influence growth, highly expressed *asp1*¹⁻³⁶⁴ reduced the growth of all three strains compared to the vector control (Figure 3-37 D right panel; Supplementary Figure 10 B, right panel (p. 189)).

The only Spc7/Sos7-complex mutant strain that showed a different behavior was the *spc7-23*^{ts} strain. No effect on growth was observed under low or high expression conditions with expression of *asp1*³⁶⁵⁻⁹²⁰, whereas *asp1*¹⁻³⁶⁴ expression led to a rescue of the temperature-sensitivity and the strain was able to grow at the restrictive temperature of 33°C (Figure 3-37 D, bottom panels).

A summary of all results obtained for NMS-complex mutant strains is shown in Table 3-2.

Thus, most analyzed NMS-complex mutant strains grew best with physiological levels of IP₈. Two exceptions were the *ndc80-21*^{ts} and *spc7-23*^{ts} strains whose ts phenotype was rescued by increased cellular IP₈-levels. This showed that the Ndc80 and Spc7 proteins were positively affected by Asp1-generated IP₈. Therefore the next question was if they might be influenced in terms of KT targeting.

Influence of IP ₈ on growth of NMS-complex mutants			
Category	Mutant	plasmids	
		<i>asp1</i> ¹⁻³⁶⁴	<i>asp1</i> ³⁶⁵⁻⁹²⁰
1	<i>ndc80-21</i> ^{ts}	↑	↓
2	<i>spc7-23</i> ^{ts}	↑	-
3	<i>mis12-537</i> ^{ts} <i>sos7-178</i> ^{ts}	↓	↓
4	<i>mis14-634</i> ^{ts}	-	↓
5	<i>nuf2-3</i> ^{ts}	↓	↓
6	<i>spc7-24</i> ^{ts} <i>spc7-30</i> ^{ts}	↓	-

Table 3-3 IP₈ affects the growth of NMS-complex mutant strains.

Effect of *asp1*¹⁻³⁶⁴ and *asp1*³⁶⁵⁻⁹²⁰ expression on NMS-complex mutant strains. There were four categories observed upon high level expression. ↑ growth defect partially rescued ↓ reduced growth – no effect.

3.4.3.2 Expression of *asp1*¹⁻³⁶⁴ or *asp1*³⁶⁵⁻⁹²⁰ does not affect growth of an *spc7-23*^{ts}-*GFP* strain

Previously I have shown that KT targeting of Sim4-components was modulated by IP₈. I therefore tested if this was also the case for Spc7-23 as this protein is also defective in KT targeting at the restrictive temperature (Kerres et al., 2007).

Unfortunately rescue of the non-growth phenotype via *asp1*¹⁻³⁶⁴ expression was not seen if *spc7-23*^{ts} was tagged with *gfp* (Figure 3-38, bottom panel). All transformants used showed growth with several foci at high temperatures which made an interpretation of the growth more difficult. However, it was observed that high expression of either *asp1*¹⁻³⁶⁴ or *asp1*³⁶⁵⁻⁹²⁰ did not have a positive/negative effect on the growth of the *spc7-23*^{ts}-*GFP* strain (Figure 3-38 A, bottom panel). Nevertheless selected transformants were used for microscopic analysis of the Spc7-23-GFP KT signal but no change in Spc7-23-GFP KT targeting with *asp1*¹⁻³⁶⁴ or *asp1*³⁶⁵⁻⁹²⁰ expression was detected (data not shown).

It was concluded that the effect of IP₈ on the *spc7-23*^{ts} strain might require the C-terminus of the Spc7-23 protein. Alternatively the fitness of the *spc7-23*^{ts}-*GFP* strain was reduced to a level that could not be rescued by higher-than-wild-type IP₈-levels anymore.

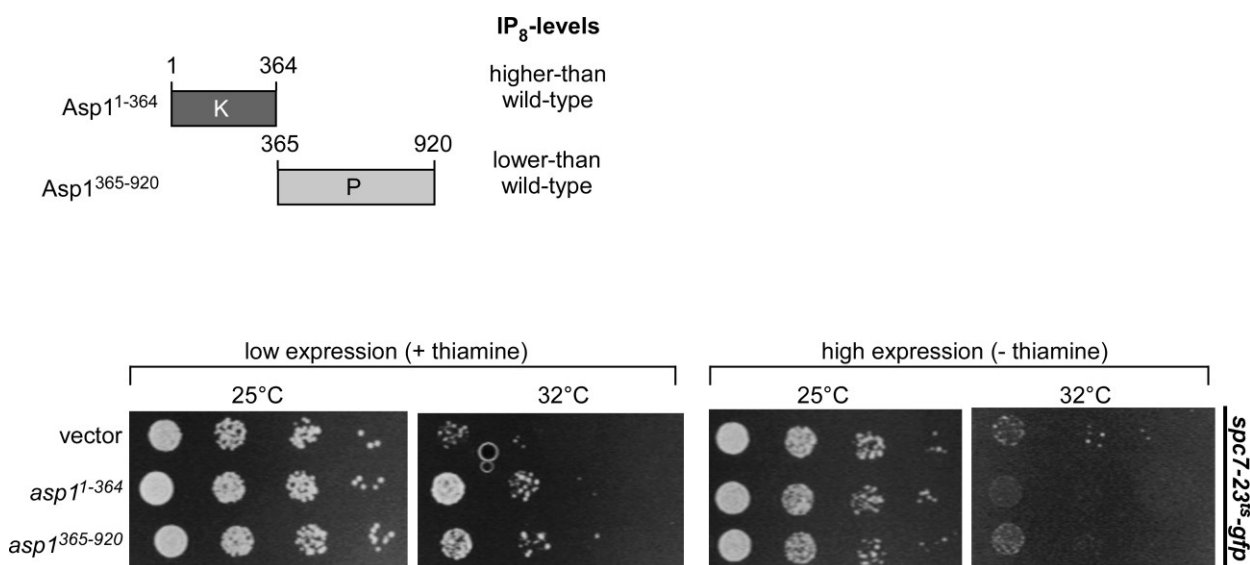


Figure 3-38 Growth of an *spc7-23*^{ts}-*gfp* strain is not influenced by variations in cellular IP₈ levels.

Top: Asp1-variants used. Bottom: Serial dilution patch tests (10^4 - 10^1 cells) of *spc7-23*^{ts}-*gfp* transformed with a vector control, *asp1*¹⁻³⁶⁴ or *asp1*³⁶⁵⁻⁹²⁰ expressed on plasmids. Transformants were grown under plasmid-selective conditions in media with or without thiamine for 5 days at the indicated temperatures.

3.4.3.3 Ndc80-GFP kinetochore targeting is reduced with non-physiological IP₈ levels

The second NMS-complex mutant strain whose growth was inversely affected by variations in cellular IP₈-levels was the *ndc80-21^{ts}* strain.

In contrast to the proteins encoded by the Sim4-complex ts mutant strains analyzed, or the Spc7-23 protein, it has been demonstrated that the Ndc80-21 protein is not defective in KT targeting at the restrictive temperature (Hsu and Toda, 2011). Nevertheless, I tested if the synthetic lethality/the rescue of the non-growth phenotype of the *ndc80-21^{ts}* strain via IP₈ (Figure 3-37 B, bottom panel) might be linked to a change in KT targeting.

Therefore, it was analyzed if variations in IP₈-levels affected the KT targeting of the Ndc80-GFP protein. For that purpose, *asp1^{D333A} ndc80⁺-gfp* and *asp1^{H397A} ndc80⁺-gfp* strains were generated. Growth analysis of the generated strains showed that the *asp1^{H397A} ndc80⁺-gfp* strain was slightly more resistant to the MT-destabilizing drug TBZ compared to the wild-type while the opposite was found for the *asp1^{D333A} ndc80⁺-gfp* strain (Figure 3-39 A, middle and bottom panel).

Microscopic analysis of Ndc80-GFP KT fluorescence signals in the generated strains was performed. Compared to *asp1⁺ ndc80⁺-gfp* the *asp1^{H397A} ndc80⁺-gfp* strain showed a slightly reduced Ndc80-GFP fluorescence signal intensity at the KT. For *asp1^{H397A} ndc80⁺-gfp* there was a reduction from 4.4 (*asp1⁺*) to 3.8 AU detectable. For *asp1^{D333A} ndc80⁺-gfp* a greater reduction of Ndc80-GFP at the KT was observed. The fluorescence signal intensity was decreased to 2.8 AU in that strain (Figure 3-39 B; C).

Hence, non-physiological levels of Asp1-generated IP₈ led to a reduced KT targeting of the Ndc80-GFP protein.

and an instable spindle with weak interpolar MTs that cause spindle collapse at high temperatures (Hsu and Toda, 2011). It was shown in our lab that high cellular IP₈-levels stabilize MTs while low levels of these molecules destabilize them (Pöhlmann et al., 2014; Topolski et al., 2016). Therefore the rescue of growth of the *ndc80-21^{ts}* strain observed at high temperatures with higher-than-wild-type IP₈-levels was possibly due to a stabilization of the spindle MTs.

Thus, the mitotic spindle in an *asp1^{H397A} ndc80-21^{ts}* strain was analyzed. To this end *ndc80-21^{ts} SV40::atb2⁺-gfp* (GFP- α -Tubulin) and *asp1^{H397A} ndc80-21^{ts} SV40::atb2⁺-gfp* strains were generated.

In a patch test experiment the *asp1⁺* strain grew on high temperatures and 8 μ g/ml TBZ. As expected, the *asp1^{H397A}* strain showed a higher resistance to TBZ. The *ndc80-21^{ts} SV40::atb2⁺-gfp* strain was ts and TBZ-sensitive (no growth at 32°C or on TBZ containing media) (Figure 3-40 A, bottom panel). The ts non-growth phenotype was partially rescued in the *asp1^{H397A} ndc80-21^{ts} SV40::atb2⁺-gfp* strain at a 32°C. Furthermore an increased TBZ-resistance compared to the *ndc80-21^{ts} SV40::atb2⁺-gfp* single mutant was observed (Figure 3-40 A, bottom panel).

Microscopic analysis of the mitotic spindle in *ndc80⁺ SV40::atb2⁺-gfp*, *ndc80-21^{ts} SV40::atb2⁺-gfp* and *asp1^{H397A} ndc80-21^{ts} SV40::atb2⁺-gfp* strains was performed. The ratio of the fluorescence signal intensity of the spindle midzone compared to one spindle end was quantified as described in Figure 3-40 B (bottom panel). Please note that a comparison of the total GFP fluorescence signal intensity along the spindle was not possible. This was due to the fact that the videos for the quantification were taken at different days to obtain enough pictures of mitotic spindles. Therefore the experimental conditions for the individual strains might have varied.

The analysis revealed that the spindle midzone staining via α -tubulin-GFP in an *ndc80-21^{ts}* mutant strain was weaker than that of the *ndc80⁺* strain. The ratio of the fluorescence signal intensity of the spindle midzone compared to one spindle end was reduced from 53 % to 40 % (Figure 3-40 C).

Interestingly in the *asp1^{H397A} ndc80-21^{ts}* double mutant the weak spindle midzone phenotype of the *ndc80-21^{ts}* strain was rescued. The ratio of the signals intensity at the spindle midzone compared to one spindle end was increased to 59 % and therefore wild-type levels (Figure 3-40 B; C).

Thus, the rescue of growth of the *ndc80-21^{ts}* strain by high IP₈-levels appears to be due to a stabilization of the spindle midzone.

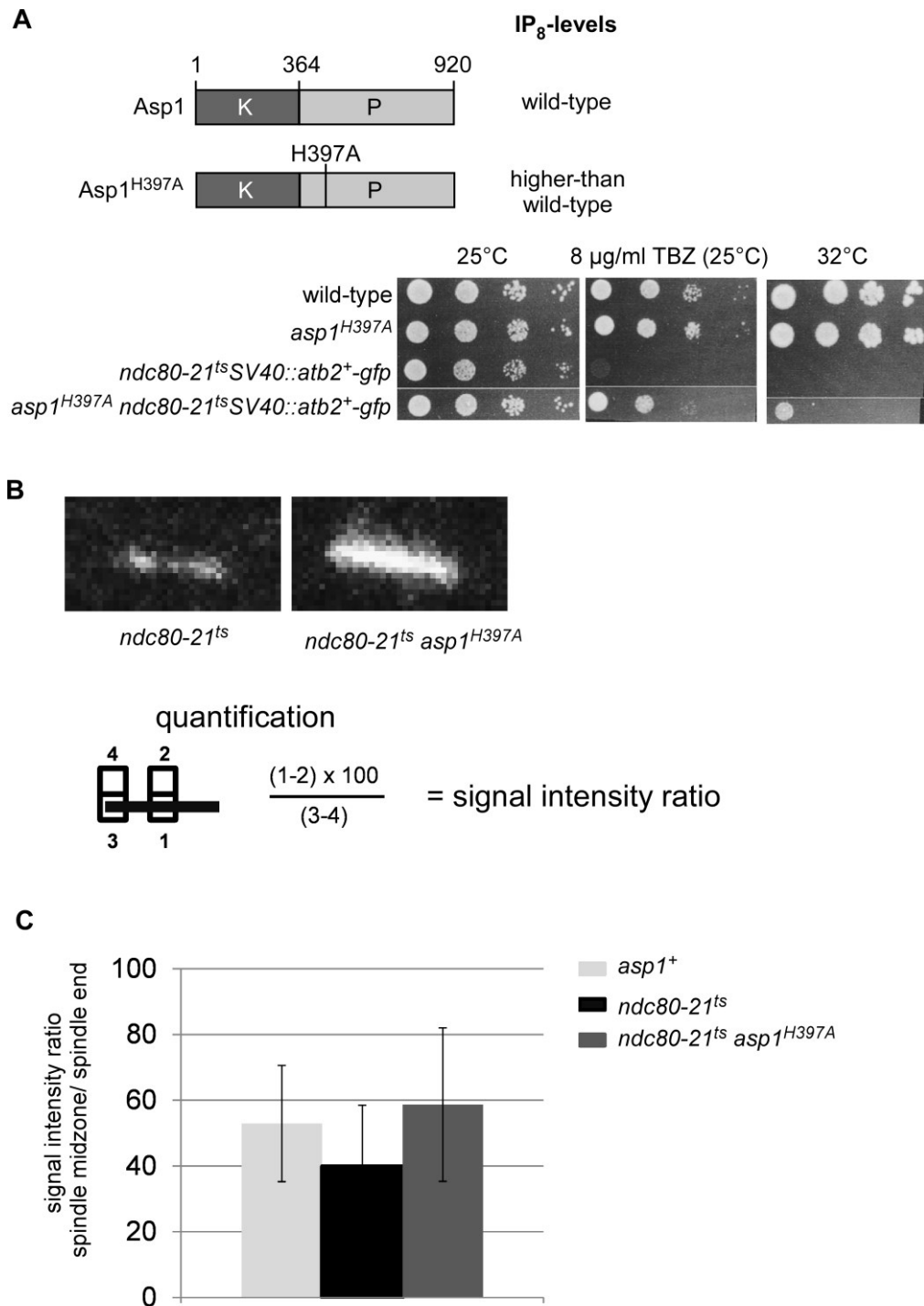


Figure 3-40 Asp1^{H397A} rescues the thin spindle midzone of the *ndc80-21^{ts}* strain.

A: Top: Asp1-variants used. Bottom: Serial dilution patch tests (10^4 - 10^1 cells) of the indicated strains on YE5S with or without TBZ. Plates were incubated for 4 days at the indicated temperatures. **B:** Photomicrographs of *ndc80-21^{ts}* and *asp1^{H397A} ndc80-21^{ts}* cells with a short spindle (3-5 µm) visualized by expressing SV40::*atb2⁺-gfp*. For relative signal intensity the fluorescence signal of the thinnest part of the spindle midzone (square 1) was measured and the background (square 2) was subtracted. This value was normalized against the signal of one spindle end (square 3 – square 4) by division. To obtain percentages the calculated values were multiplied by 100. Videos taken with a Zeiss Spinning Disc-Confocal microscope. **C:** Diagram for the relative signal intensities calculated as in B for the indicated strains: *asp1⁺* 52.95 % ± 17.66, *ndc80-21^{ts}* 39.92 % ± 18.58, *ndc80-21^{ts} asp1^{H397A}* 58.67 % ± 23.37. (n = 10/ strain).

In summary, I showed in Chapters 3.4-3.4.3 that IP_8 affected the growth of Sim4-complex and NMS-complex *ts* mutant strains. I furthermore demonstrated, that the mechanism that might be involved in the rescues observed differed among these two KT-subcomplexes.

The next question I addressed was whether there were also interactions among Sim4- and NMS-complex proteins.

3.4.4 Interdependencies among kinetochore proteins

3.4.4.1 Excess Ndc80, Mal2 and Mis15 does not influence the growth of specific KT mutant strains

Previously I have shown that intracellular IP_8 -levels influenced the growth of the *mal2-1^{ts}* and *mis15-68^{ts}* strains in opposite ways. Additionally, Mal2 and Mis15 also affected each others KT targeting. Furthermore, IP_8 affected the growth of the *ndc80-21^{ts}* strain. Thus, it was possible that Ndc80 affected the composition of the Sim4-complex and/or vice versa.

To check this possibility *ndc80⁺* was plasmid expressed under control of the *nmt1⁺*-promoter in the wild-type, *ndc80-21^{ts}*, *mal2-1^{ts}* and *mis15-68^{ts}* strains and the growth phenotype of these strains analyzed (Figure 3-41).

Expression of *ndc80⁺* had no effect on the growth of the wild-type strain (Figure 3-41 A, top panel). In an *ndc80-21^{ts}* strain the expression of *ndc80⁺* under low or high expression conditions rescued the *ts* non-growth phenotype completely (Figure 3-41 A, second panel). The *mal2-1^{ts}* strain showed no reduction in growth under high expression of *ndc80⁺* at 25°C and 28°C (Figure 3-41 A, third panel). Similar results were obtained for the *mis15-68^{ts}* strain (Figure 3-41 A, last panel).

Next it was analyzed if a vice versa effect was detected with (*mal2⁺ + fta2⁺*) or *mis15⁺* overexpression in the *ndc80-21^{ts}* strain. Low expression of (*mal2⁺ + fta2⁺*) or *mis15⁺* had no effect on the growth of the *ndc80-21^{ts}* strain (Figure 3-41 B, left panel). Under high expression conditions *mis15⁺* overexpression had no effect while (*mal2⁺ + fta2⁺*) overexpression led to a reduction of growth (Figure 3-41 B, right panel). However, this reduction was similar to that observed for the wild-type strain in previous experiments (Figure 3-30 A (p. 138)).

It was concluded, that there was no interdependency between the Ndc80 protein and the Sim4-complex members Mal2 and Mis15. This result indicated that these complexes exert

their functions independent of each other as had been proposed previously (Jakopec et al., 2012; Liu et al., 2005).

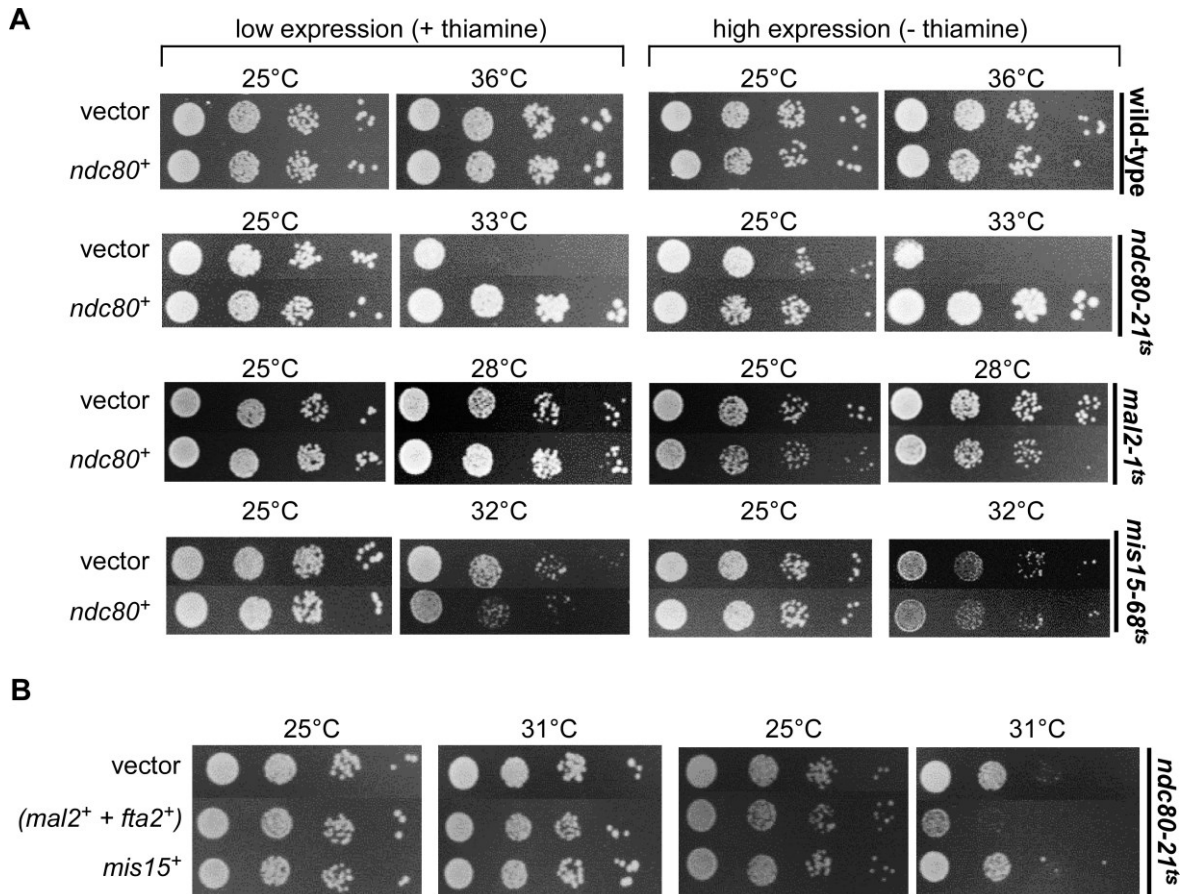


Figure 3-41 Ndc80, Mal2 and Mis15 only affect each other very slightly.

A: Serial dilution patch tests (10^4 - 10^1 cells) of the indicated strains transformed with a vector control, or *ndc80⁺* expressed on plasmids. Transformants were grown under plasmid-selective conditions in media with or without thiamine for 4-6 days at the indicated temperatures. **B:** Serial dilution patch tests (10^4 - 10^1 cells) of the *ndc80-21^{ts}* strain transformed with a vector control, (*mal2⁺ + fta2⁺*) or *mis15⁺* expressed on plasmids. Transformants were grown under plasmid-selective conditions in media with (low expression) or without (high expression) thiamine for 5 days at the indicated temperatures. Pictures shown were selected to best demonstrate differences in growth.

In summary, I found that IP₈ affected targeting of KT proteins in *S. pombe*. For the Sim4-complex the KT composition was changed by IP₈, while IP₈ affected the spindle phenotype of an NMS-complex mutant strain, namely *ndc80-21^{ts}*. The changes in KT composition and spindle phenotypes might be the foundation for a faster establishment of bipolar KT-MT attachments and therefore an influence of IP₈ on chromosome transmission fidelity.

3.5 First characterization of interaction partners of the Asp1 protein

With the above results I demonstrated that Asp1-generated IP₈ regulated different aspects of mitosis. However, the underlying mechanisms of this regulation were still unclear.

In order to identify interaction partners of Asp1 a member of our lab, Dr. Visnja Jakopec, performed a Yeast-2-Hybrid screen using an *S. pombe* cDNA library. With that method she was able to identify several putative interaction partners of the Asp1 protein.

Four of these interactors of Asp1 have been further analyzed in the course of this work (Table 3-4). All of these proteins interacted with full-length Asp1 in the Yeast-2-Hybrid screen.

Yeast-Two-Hybrid screen for Asp1		
Putative Asp1 interaction partners	Predicted function	Interaction domain within Asp1
SPCC594.01	DUF1769 family protein	kinase and pyrophosphatase domain
Hpm1	ribosome methyltransferase	kinase domain
SPBC725.03	pyridoxamine 5'-phosphate oxidase	pyrophosphatase domain
Met10	sulfite reductase NADPH flavoprotein subunit	pyrophosphatase domain

Table 3-4 Interaction partners of Asp1 identified in a Yeast-2-Hybrid screen performed by Dr. Visnja Jakopec.

Depicted are the proteins that were analyzed in the course of this work.

The proteins identified had not been studied previously and their properties and functions were largely unknown. Therefore a first characterization was performed and the results are presented in the following chapter.

3.5.1 Phenotypic analysis of *SPCC594.01*Δ, *hpm1*Δ and *SPBC725.03*Δ strains

The first protein found by Dr. Visnja Jakopec was the product of the gene *SPCC594.01* which showed an interaction with both the kinase and pyrophosphatase domains of Asp1 (data not shown). The *SPCC594.01* ORF is positioned on chromosome 3 and its 89 kDa large gene product was classified as a member of the DUF1769 protein family which is conserved in fungi. A function for this protein has not been proposed (www.pombase.org). However, it was found that this DUF1769 family protein is phosphorylated during mitosis (Koch et al., 2011).

To characterize the function of *SPCC594.01* further a deletion strain was generated via endogenous homologous recombination (Chapter 2.18 (p. 70)). Growth analysis of the obtained *SPCC594.01Δ* strain was performed. The *SPCC594.01Δ* strain was sensitive to TBZ (data not shown) indicating that the *SPCC594.01* gene product was important for MT stability. As Asp1-generated IP_8 was able to rescue TBZ-sensitivity phenotypes (Pöhlmann and Fleig, 2010) it was analyzed whether this effect was still detectable in a *SPCC594.01Δ* strain. Therefore a vector control or *asp1*¹⁻³⁶⁴ or *asp1*³⁶⁵⁻⁹²⁰ expressed on plasmids were transformed in that strain and growth analyzed (Figure 3-42).

Low expression of *asp1*¹⁻³⁶⁴ and *asp1*³⁶⁵⁻⁹²⁰ had no effect on the growth of the *SPCC594.01Δ* strain (Figure 3-42, bottom left panel). Under high expression conditions *asp1*¹⁻³⁶⁴ rescued growth while *asp1*³⁶⁵⁻⁹²⁰ slightly reduced it (Figure 3-42, bottom right). The *SPCC594.01Δ* strain therefore showed a similar growth phenotype to the wild-type strain (Figure 3-2 (p. 90)).

Further characterization of the properties of the *SPCC594.01Δ* strain has to be done in the future.

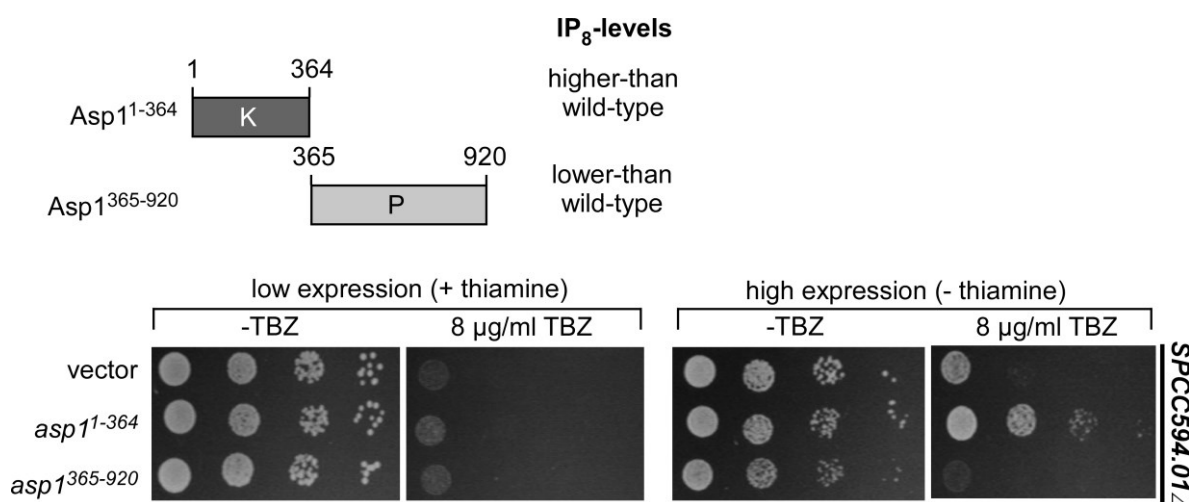


Figure 3-42 Variations in cellular IP_8 -levels affect the TBZ-sensitivity of an *SPCC594.01Δ* strain.

Top: Asp1-variants used. Bottom: Serial dilution patch tests (10^4 - 10^1 cells) of the *SPCC594.01Δ* strain transformed with a vector control, *asp1*¹⁻³⁶⁴ or *asp1*³⁶⁵⁻⁹²⁰ expressed on plasmids. Transformants were grown under plasmid-selective conditions in media with (low expression) or without (high expression) thiamine and with the indicated concentration of TBZ for 5 days at 25°C.

The second putative Asp1 interaction partner identified in the Yeast-2-Hybrid screen was Hpm1. Hpm1 interacted with the kinase domain of Asp1. The *hpm1*⁺ ORF is located on chromosome 1 and encodes for a 38 kDa protein which was designated as a predicted ribosome methyltransferase. However, the function of Hpm1 is still unknown. Ribosome methyltransferases are involved in transcriptional control (Webb et al., 2010). Hpm1 is

conserved in eukaryotes and has with HPM1 and METTL18 orthologs in *S. cerevisiae* and humans, respectively (www.pombase.org). Like SPCC594.01 also Hpm1 was found to be phosphorylated during mitosis (Koch et al., 2011). To characterize the Hpm1 protein an *hpm1* Δ strain had been generated by Marina Pascual-Ortiz.

Unlike the *SPCC594.01* Δ strain the *hpm1* Δ strain did not show sensitivity towards TBZ (Figure 3-43).

Interestingly, it was found in our lab that a deletion of *hpm1*⁺ inhibited the accumulation of Asp1-GFP in the nucleus at low temperatures (Fischbach, 2016). This result indicated that Hpm1 might be involved in the regulation of Asp1 subcellular localization.

The third protein that was further characterized was SPBC725.03 which has a predicted pyridoxamine 5'-phosphatase oxidase function. The SPBC725.03 ORF is located on chromosome 2 and the gene product has a size of 30 kDa. This protein is furthermore conserved in yeast (www.pombase.org). SPBC725.03 had not been characterized previously. To further analyze the properties of this Asp1 interaction partner we tested whether a *SPBC725.03* Δ strain was TBZ-sensitive. No TBZ-sensitivity was found for that strain (Figure 3-43).

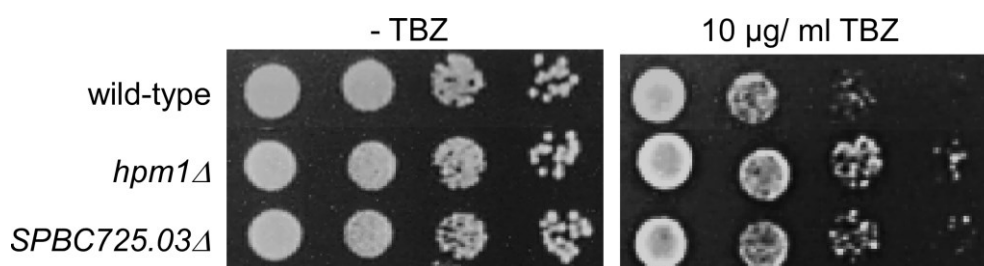


Figure 3-43 *hpm1* Δ and *SPBC725.03* Δ strains are not TBZ sensitive.

Serial dilution patch tests (10^4 - 10^1 cells) of the indicated strains. Strains were grown in media with the indicated concentration of TBZ for 6 days at 25°C. Patch test performed by Camille Marie Fortinez.

3.5.2 The effect of IP₈ on the *mis15-68*^{ts} strain is not dependent on the presence of Hpm1 or SPBC725.03

The next question that emerged was if the interaction partners found were essential for Asp1-generated IP₈ to mediate its function at the kinetochore interface.

Therefore I analyzed if Asp1-generated IP₈ still affected the growth of the Sim4-complex *mis15-68*^{ts} strain in absence of Hpm1 or SPBC725.03. For this purpose *mis15-68*^{ts} *hpm1* Δ and *mis15-68*^{ts} *SPBC725.03* Δ double mutant strains were generated. These strains were

used to test if variations in cellular IP₈-levels via plasmid-expression of *asp1*¹⁻³⁶⁴ or *asp1*³⁶⁵⁻⁹²⁰ still affected the ts non-growth phenotype observed for the *mis15-68*^{ts} single mutant strain (Figure 3-12 D (p. 108)). Low expression of *asp1*¹⁻³⁶⁴ or *asp1*³⁶⁵⁻⁹²⁰ had no effect on the growth of the double mutant strains (Figure 3-44 A; B, left panels). High expression of *asp1*¹⁻³⁶⁴ led to a rescue of the ts in the *mis15-68*^{ts} *hpm1*Δ and *mis15-68*^{ts} *SPBC725-03*Δ strains. For expression of *asp1*³⁶⁵⁻⁹²⁰ the opposite effect was observed (Figure 3-44 A; B, right panels).

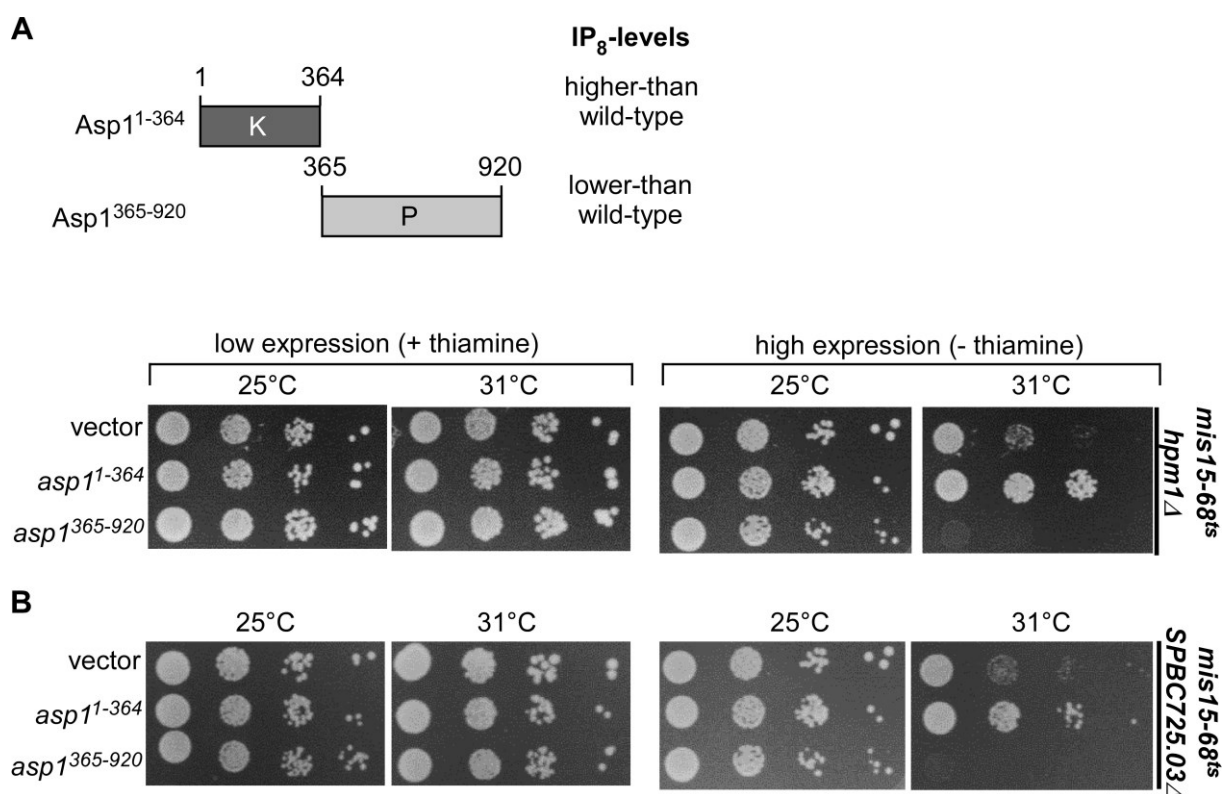


Figure 3-44 The effect of IP₈ on growth of a *mis15-68*^{ts} strain is still detectable in *hpm1*Δ and *SPBC725.03*cΔ backgrounds.

A+B: Serial dilution patch tests (10^4 - 10^1 cells) of the indicated strains transformed with a vector control, *asp1*¹⁻³⁶⁴ or *asp1*³⁶⁵⁻⁹²⁰ expressed on plasmids. Transformants were grown under plasmid-selective conditions in media with (low expression) or without (high expression) thiamine for 7 days at the indicated temperatures.

Thus, the effect of altered IP₈-levels on the ts phenotype of the *mis15-68*^{ts} strain was not dependent on Hpm1 or SPBC725.03.

3.6 Met10 and Asp1: A link between mitosis and mitochondria?

The fourth analyzed candidate identified in the Yeast-2-Hybrid screen was the Met10 protein. *met10*⁺ (ORF located on chromosome 3) encodes a 111 kDa large protein which is a predicted sulfite reductase subunit (www.pombase.org). Like for the other three candidates, the function of Met10 had not been characterized further. However, Met10 is conserved and its *S. cerevisiae* ortholog Met10 was known to have sulfite reductase function and to be involved in methionine and cysteine biosynthesis (Hansen et al., 1994).

3.6.1 Characterization of Met10 protein function

A first characterization of Met10 was performed by several members of our lab including me and the obtained results are shown in Figure 3-45 (Marina Pascual-Ortiz; (Kiffe-Delf, 2016; Schuhenn, 2016; Suessmilch, 2016)). The results in that figure will soon be published in Marina Pascual-Ortiz et al. (2017).

First the phenotype of a *met10*Δ strain was analyzed (Marina Pascual-Ortiz; unpublished data). It was found that the *met10*Δ strain was methionine and cysteine auxotroph (Figure 3-45 A) indicating that its predicted function in methionine and cysteine biosynthesis is essential for cell viability.

I next wanted to analyze the subcellular localization of the Met10 protein. For this purpose I generated a *met10*⁺-*gfp* strain where *met10*⁺ was fused to a *gfp*-cassette at its native locus (Chapter 2.18 (p. 70)). Microscopic analysis of the *met10*⁺-*gfp* strain showed that Met10-GFP localized to specific structures within the cell (Figure 3-45 B, top left panel). Co-staining with the mitochondria staining Mitotracker red revealed that Met10-GFP co-localized with mitochondria (Figure 3-45 B, top right and bottom panel).

Finally I analyzed the phenotype that was induced by overexpression of Met10. To this end I constructed a plasmid on which *met10*⁺ was expressed under control of the *nmt1*⁺-promoter (Chapter 2.17 (p. 69)). It was found that low expression of *met10*⁺ had no effect on the growth of a wild-type strain, while high expression slightly reduced the growth in presence and absence of TBZ (Figure 3-45 C).

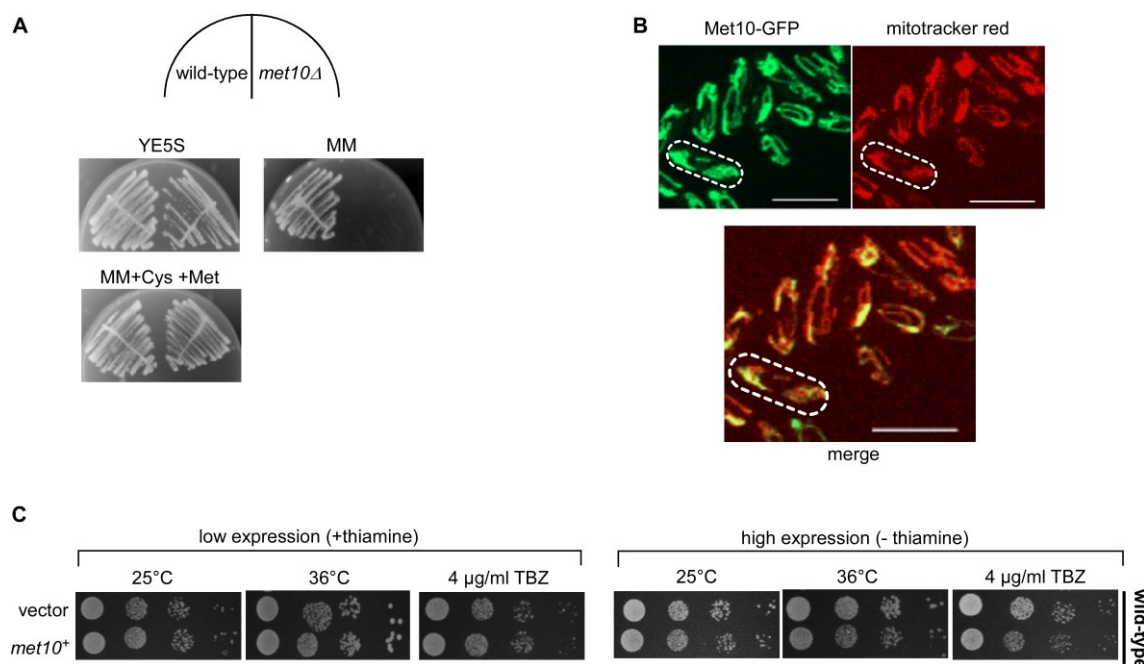


Figure 3-45 First characterization of the Met10 protein.

A: Growth analysis of a *met10*Δ strain on YE5S, MM and MM supplemented with cysteine and methionine. Experiment performed by Marina Pascual-Ortiz. **B:** Live cell microscopy pictures of a *met10*⁺-*gfp* strain stained with Mitotracker red. Pictures were taken using a Zeiss Spinning Disc-Confocal microscope at 25°C. Scale bar = 10 µm. **C:** Serial dilution patch tests (10⁴-10¹ cells) of the wild-type strain transformed with a vector control or *met10*⁺ expressed on a plasmid. Transformants were grown under plasmid-selective conditions in media with (low expression) or without (high expression) thiamine for 5 days at the indicated temperatures and TBZ-concentration.

The Met10 protein of *S. cerevisiae* interacts with the cytosolic iron-sulfur protein assembly (CIA) component MMS19 which plays a role in Fe-S protein maturation (Stehling et al., 2012). As it had been demonstrated that [2Fe-2S]²⁺-clusters regulate the pyrophosphatase function of Asp1 *in vitro* (Wang et al., 2015) it was analyzed if the Met10 protein is part of this process. Strikingly, the presence of Met10 in an *in vitro* pyrophosphatase assay inhibited the function of the Asp1 pyrophosphatase domain (data not shown; Marina Pascual-Ortiz, unpublished data). This showed that Met10 is a regulator of the enzymatic function of Asp1.

In summary, the above results demonstrated a new link between Asp1 and mitochondria over the Met10 protein.

3.6.2 Met10 in mitosis

To elucidate the localization of Met10 in mitosis I generated a *met10*⁺-*gfp* *sad1*-*mCherry* strain to visualize the Met10 protein and the SPBs in living cells. Growth analysis showed

that the generated strain showed the same growth behavior than a wild-type strain (Figure 3-46 A). As just 10 % of a cell population in a culture are currently undergoing mitosis (Gomez and Forsburg, 2004) I further arrested *met10⁺-gfp sad1-mCherry* cells in metaphase via *mph1⁺* overexpression (He et al., 1998).

Microscopic analysis of the *met10⁺-gfp sad1-mCherry* strain transformed with a vector control or *mph1⁺* overexpression was performed (Figure 3-46 B). The *met10⁺-gfp sad1-mCherry* strain transformed with a vector control showed the same localization pattern for Met10-GFP than the non-transformed strain (Figure 3-45 B; Figure 3-46 B). In case of *mph1⁺* overexpression the Met10-GFP signal was less organized in tubular structures and a localization pattern with circle-shaped aggregates at the cell ends was observed (Figure 3-46 B, bottom panel). This phenotype was typical for mitochondria during mitosis (Jajoo et al., 2016).

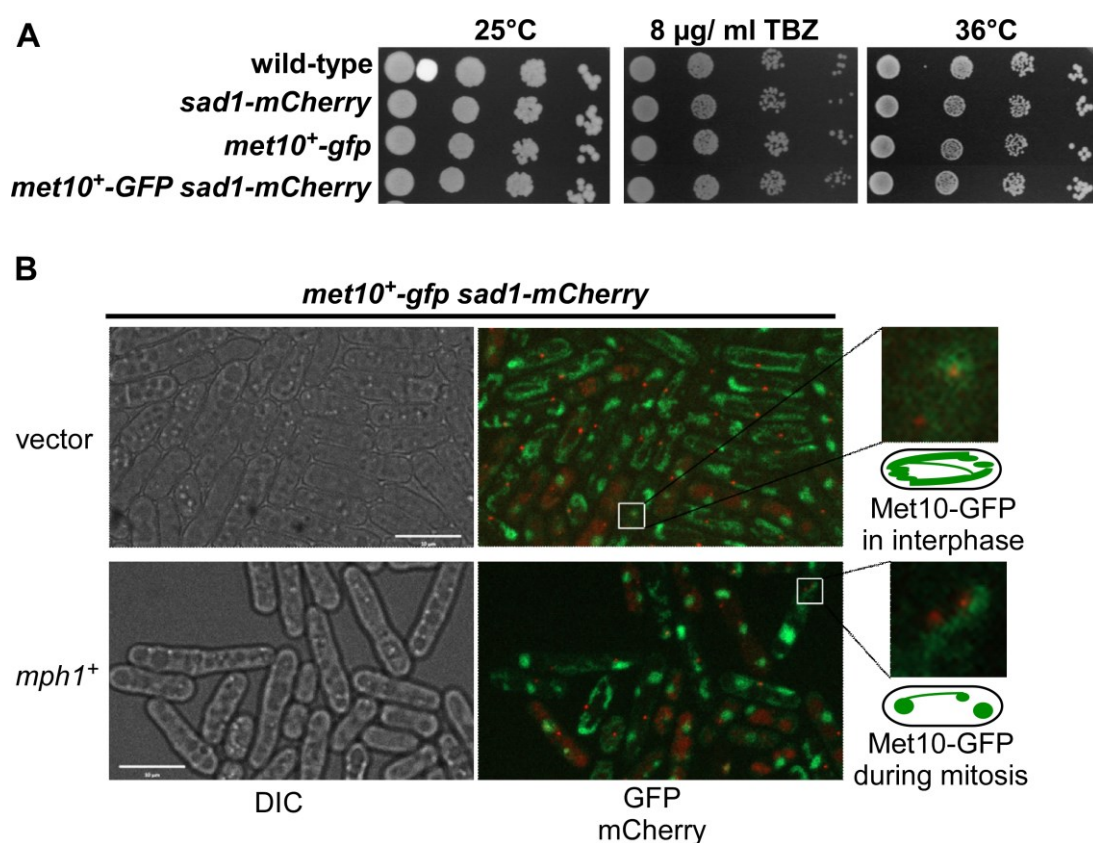


Figure 3-46 The localization pattern of Met10-GFP in interphase and mitosis.

A: Serial dilution patch tests (10^4 - 10^1 cells) of the indicated strains. Strains were grown in YE5S media with the indicated concentration of TBZ for 5 days at 25°C or 36°C. **C:** Live fluorescence microscopy pictures of the indicated transformants. A *met10⁺-gfp sad1-mCherry* strain was transformed with either a vector control or *mph1⁺* expressed on a plasmid via the *nmt1⁺*-promoter to arrest cells in metaphase. Transformants were pre-incubated for 30 h at 25 °C in plasmid selective LFM without thiamine before they were patched on agarose pads. Pictures were taken at 25°C with 15 % laser intensity for GFP and 10 % for mCherry and additional DIC pictures were taken. Scale bar = 10 µm.

3.6.3 Plasmid-borne *met10*⁺ expression reduces the growth of *mal2-1*^{ts} and *mis15-68*^{ts} strains

Interestingly, a negative genetic interaction between Met10 and the DASH-KT-subcomplex members Dad3, Ask1, Dad2 and Dam1 had been demonstrated previously in a large scale genetic interactome screen (Ryan et al., 2012). In addition, the Met10 protein had been co-purified in a TAP-Tag experiment with the NMS-KT-protein Spc7 (personal communication: Xiangwei He). Furthermore, the MMS19 protein of humans (whose *S. cerevisiae* ortholog Mms19 interacted with Met10 (Stehling et al., 2012)) was found to partially co-localize with the mitotic spindle and be crucial for proper chromosome segregation and Aurora kinase recruitment to the spindle midzone (Ito et al., 2010). All of these findings suggested that there was indeed a connection between the Met10 protein and the KT-complex and/or mitosis in general. Therefore I further analyzed the role of Met10 during mitosis in *S. pombe*.

I next addressed the question if Met10 affected Sim4-complex members. For this purpose *met10*⁺ was overexpressed on a plasmid under the control of the *nmt1*⁺-promoter in *mal2-1*^{ts} and *mis15-68*^{ts} strains and growth analyzed. It was observed that low expression of *met10*⁺ had no effect on the growth of the *mal2-1*^{ts} and *mis15-68*^{ts} strains (Figure 3-47, left panel). High expression of *met10*⁺ increased the ts phenotype of the *mal2-1*^{ts} strain and that effect was more severe than observed for the wild-type strain (Figure 3-47, right panel; Figure 3-45 C). Strikingly, high expression of *met10*⁺ in the *mis15-68*^{ts} strain even led to synthetic lethality (Figure 3-47, right panel).

Thus, I demonstrated that there was a negative genetic interaction between Met10 and Sim4-complex proteins.

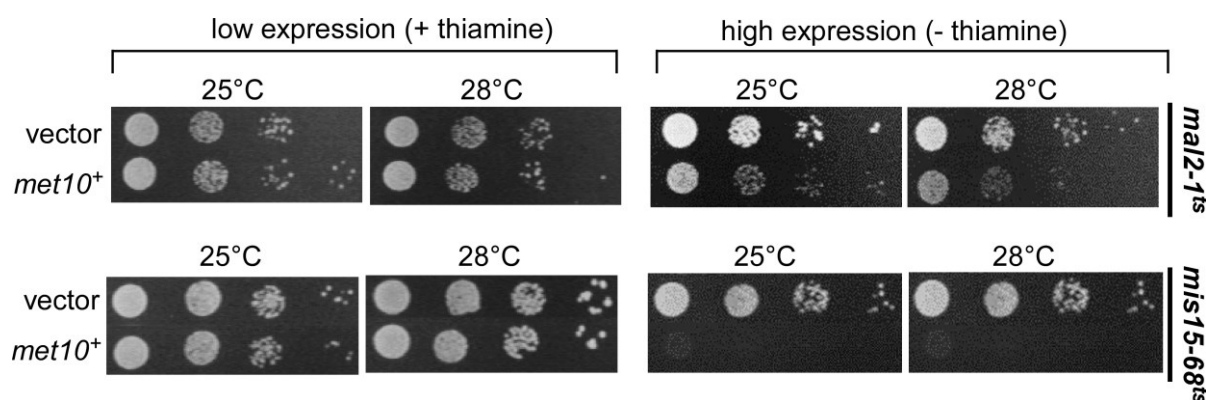


Figure 3-47 High expression of *met10*⁺ reduces the growth of *mal2-1*^{ts} and *mis15-68*^{ts} strains.

Serial dilution patch tests (10^4 - 10^1 cells) of the indicated strains transformed with a vector control or *met10*⁺ overexpressed on a plasmid. Transformants were grown under plasmid-selective conditions in media with (low expression) or without (high expression) thiamine for 5 days at the indicated temperatures.

3.6.4 Mal2-GFP partially localizes to mitochondria in an *asp1*¹⁻³⁶⁴ strain background

Normally Asp1 is localized throughout the cell and accumulates in the nucleus at low temperatures. An observation made in our lab was that certain Asp1 variants, namely the endogenous *asp1* variant *asp1*¹⁻³⁶⁴, localized to tubular structures within the cell (personal communication: Marina Pascual-Ortiz). Furthermore I had noticed that with *asp1*¹⁻³⁶⁴ plasmid-expression Mis15-68-GFP protein partially co-localized with mitochondria (Figure 3-25 D (p. 131)). These two observations taken together with the discovery of Met10 as an interaction partner of Asp1 pointed to an unexpected link between Asp1, mitochondria and the KT.

Therefore the question arose if the localization of Met10, certain Asp1 variants and KT proteins to mitochondria was connected.

To further analyze a possible network a series of strains was used for microscopic analysis. Mitochondria were visualized using *cox4-rfp*. Cox4 (cytochrome oxidase subunit IV) is a mitochondrial protein (Yaffe et al., 2003). I generated three additional strains for that analysis via tetrad analysis (Chapter 2.19.2 (p. 71)):

- 1) *mal2*⁺-*gfp cox4-rfp*: to visualize the Mal2 protein and the mitochondria in an *asp1*⁺ background
- 2) *asp1*¹⁻³⁶⁴ *mal2*⁺-*gfp*: to decipher if the presence of *asp1*¹⁻³⁶⁴ instead of wild-type *asp1*⁺ affected Mal2-GFP targeting
- 3) *asp1*¹⁻³⁶⁴ *mal2*⁺-*gfp cox4-rfp*: to elucidate whether a possible change in Mal2-GFP localization was coincident with mitochondrial structures

Growth analysis of the generated strains showed that they grew like the wild-type and the *cox4-rfp* strains (Figure 3-48 A).

Microscopic analysis of *cox4-rfp*, *mal2*⁺-*gfp cox4-rfp*, *asp1*¹⁻³⁶⁴ *mal2*⁺-*gfp* and *asp1*¹⁻³⁶⁴ *mal2*⁺-*gfp cox4-rfp* strains was performed (Figure 3-48 B). A mitochondrial localization was observed for Cox4-RFP (Figure 3-48 B, first row). In an *asp1*⁺ background (*mal2*⁺-*gfp cox4-rfp*) the typical dot-like KT signal was detected for Mal2-GFP (Figure 3-48 B, second row). Strikingly, in the strain endogenously expressing *asp1*¹⁻³⁶⁴ the localization of Mal2-GFP was changed and line-like structures were visible throughout the cell (Figure 3-48 B, third row). Further analysis of the *asp1*¹⁻³⁶⁴ *mal2*⁺-*gfp cox4-rfp* strain showed that these structures indeed co-localized with mitochondria (Figure 3-48 B, last row, magnification). Thus, endogenous expression of *asp1*¹⁻³⁶⁴ led to a partial localization of Mal2-GFP to mitochondria.

In summary, the above results demonstrated for the first time that there is a possible network between the Asp1 and Met10 proteins and the KT-complex in *S. pombe*.

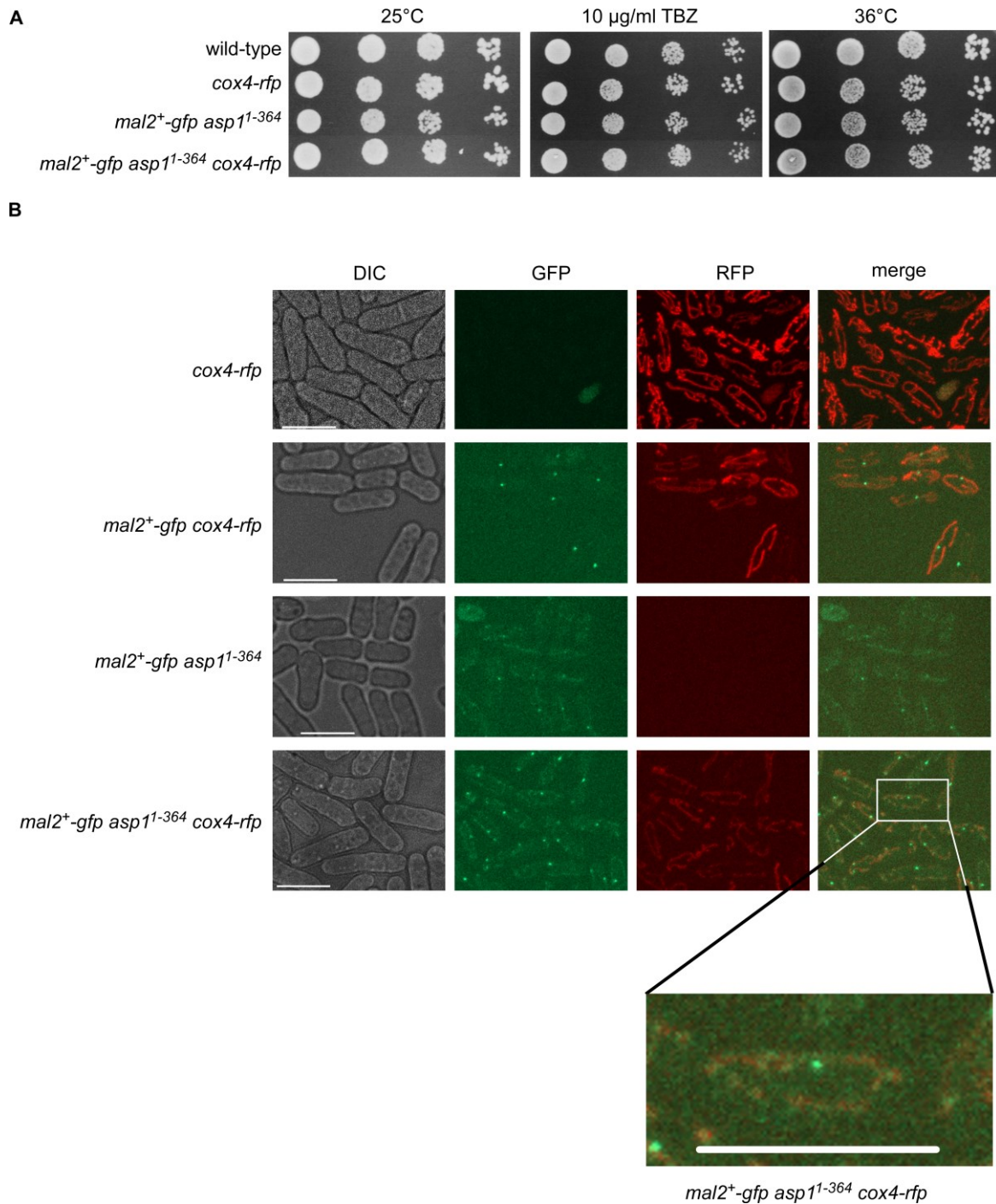


Figure 3-48 Mal2-GFP partially localizes to mitochondria in an *asp1*¹⁻³⁶⁴ strain background.

A: Serial dilution patch tests (10^4 - 10^1 cells) of the indicated strains. Strains were grown in YE5S media with the indicated concentration of TBZ for 5 days at 25°C or 36°C. **B:** Live cell fluorescence microscopy pictures for the indicated strains. Top to bottom: *cox4-rfp*, *mal2⁺-gfp cox4-rfp*, *mal2⁺-gfp asp1¹⁻³⁶⁴* and *mal2⁺-gfp asp1¹⁻³⁶⁴ cox4-rfp*. First column: DIC pictures for each strain, second column: Mal2-GFP fluorescence signal (60 % laser intensity), third column: Cox4-RFP fluorescence signal (2 % laser intensity), last column: merge for GFP and RFP signals. Strains were pre-grown overnight in LFM at 25°C before they were patched on agarose pads. Pictures were taken at 25°C. Scale bar = 10 µm.

3.7 A new approach for a minichromosome loss assay

During my PhD thesis I used a Ch16 minichromosome loss assay to analyze the effect of Asp1-generated IP₈ on the loss of Ch16. However, a disadvantage of this assay was that the Ch16 loss detected was *per se* very low and to observe differences in the loss with lower- or higher-than wild-type IP₈-levels a great amount of cells had to be analyzed (Chapter 3.2.3 (p. 99)).

Therefore we thought of an approach to analyze more cells while using less material. The idea was to generate an assay where the loss of Ch16 led to survival of the cell, while keeping Ch16 leads to lethality. An approach using a cycloheximide sensitivity for such an assay has been previously successfully introduced for *Saccharomyces cerevisiae* (Jehn et al., 1991). Therefore, I constructed a strain with a point mutation in the *rpl42*⁺ gene on chromosome 1. Rpl42 is a 60S ribosomal protein and it had been published that the *rpl42*^(P56Q) allele leads to a recessive resistance against cycloheximide (CHX) in *S. pombe* without having an influence on the growth behavior of the mutant strain (Roguev et al., 2007). CHX is a protein synthesis inhibitor that blocks the elongation step in eukaryotic translation and therefore targets ribosomes (Schneider-Poetsch et al., 2010).

First I replaced the *rpl42*⁺ ORF in a wild-type *S. pombe* strain with the *rpl42*^(P56Q) allele (Chapter 2.18 (p. 70)) and confirmed that it was resistant to CHX. In the next step I introduced Ch16 in that strain and replaced the *ade6-M216* allele on Ch16 with the *CHX*^S locus (wild-type *rpl42*⁺ gene under the control of the native promoter with flanking regions (Chapter 2.18 (p. 70)) as used in (Roguev et al., 2007). The constructed strain indeed showed CHX-sensitivity. I was therefore able to assay Ch16 loss via selection on YE5S+CHX plates (Figure 3-49).

A first test of the functionality of the system showed that plating 9x 10⁴ cells on CHX containing medium led to growth of 9 colonies. The number of colonies served as a read-out for Ch16 loss. This number was similar to the Ch16 loss events published for a wild-type *S. pombe* strain (Niwa et al., 1986).

Unfortunately, further verification of the validity of the assay and an optimization could not be performed during my thesis out of time reasons. However, the assay is a promising approach for a new Ch16 loss assay that allows a higher throughput.

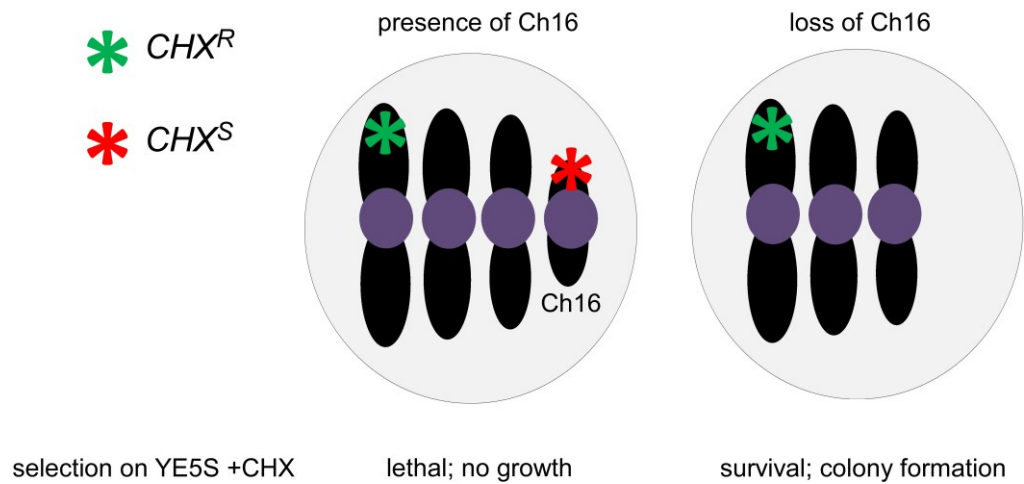


Figure 3-49 New approach for a Ch16 loss assay.

A recessive resistant allele against CHX in form of the $rpl42^{(P56Q)}$ allele was inserted at the native $rpl42^+$ locus on chromosome 1 (CHX^R). The CHX^S locus containing the $rpl42^+$ ORF and flanking regions was inserted on the Ch16 minichromosome. In the presence of Ch16 the cell is sensitive to CHX and not able to grow on YE5S +100 $\mu\text{g/ml}$ CHX plates. Loss of Ch16, and therefore a loss of the CHX^S locus, leaves the cell with the recessive CHX^R allele. The cell is then CHX-resistant and able to form colonies on plates containing CHX.

4 Discussion

4.1 Asp1-generated IP₈ modulates Sim4-complex composition

In this thesis I demonstrated that variations in Asp1-generated intracellular IP₈-levels change the composition of the Sim4-KT-subcomplex via the proteins Mal2 and Fta2 (Chapter 3.4 (p. 95)). This is a mechanism distinct from all other mechanisms of KT architecture modulation described to date.

KTs assemble on the centromere chromatin region which is marked by the specific histone H3 variant CENP-A (Cnp1 in *S. pombe*). This histone variant is deposited during the G2-phase of the cell cycle and ensures the integrity of the centromere chromatin during mitosis (Lando et al., 2012). Located at the centromeric region the KTs serve as a bridge between the spindle MTs and the chromosomes. It has been shown that in *S. pombe* most of the KT-subcomplexes are assembled throughout the cell cycle (Hayashi et al., 2006; Liu et al., 2005). These constitutive KT bound subcomplexes are the Sim4- and NMS-complexes. During mitosis the KT is expanded by the recruitment of transient KT proteins like the DASH-complex and MT-associated proteins. One member of the DASH-complex, Dad1, stays at the KT interface throughout the cell cycle (Liu et al., 2005). The DASH-complex KT-association is dependent on Sim4-complex proteins (Sanchez-Perez et al., 2005) and those are furthermore associated with chromatin over the Mis16 and Mis18 proteins (part of the Mis16-Mis20-complex). All members of the Mis16-Mis20-complex disassociate from KTs before metaphase and associate again in mid-anaphase (Hayashi et al., 2004; Subramanian et al., 2014).

Nothing is known to date about a change in the KT targeting of constitutive KT proteins of the NMS- and Sim4-complexes during the cell cycle. The only condition under which KT proteins that constitutively localize to KTs shortly delocalize has been demonstrated for cells in meiotic prophase for NMS-complex proteins, but the authors state that the physiological significance remains unclear (Hayashi et al., 2006).

The KT assembly in humans differs from the one observed in *S. pombe*. KT assembly also takes place in regions that are defined by CENP-A containing nucleosomes, which are in humans deposited in G1 phase (Foltz et al., 2009). CENP-A containing centromere chromatin serves as the basis for the recruitment of inner KT proteins that are part of the CCAN-complex (Sim4-complex in *S. pombe*). Most CCAN-complex members are localized at the KT constitutively (Musacchio and Desai, 2017). The outer kinetochore proteins, that include the human KMN network (NMS-complex in *S. pombe*) and several MT-associated proteins, are only recruited to centromeres during mitosis (Cheeseman and Desai, 2008).

The KMN network is bound to KT over inner KT proteins (Nishino et al., 2013; Screpanti et al., 2011). It has furthermore been suggested that the KT assembled on each CENP-A nucleosome contains two CCAN-complexes and several copies of KMN-complexes (Musacchio and Desai, 2017). In contrast to members of the *S. pombe* Sim4-complex the CCAN-complex proteins have already been found to form different subcomplexes that show localization dependencies that can even differ between cell cycle stages (Musacchio and Desai, 2017). Furthermore it was demonstrated that, while bound stably to mitotic KTs, different KT proteins display very different turnover dynamics in other cell cycle stages (Hemmerich et al., 2008). Extensive localization studies have been performed for CCAN-complex proteins. Binding of the CENP-O/P/U/R (Mal2/Fta2/Mis17/Fta7 in *S. pombe*)-complex to the CCAN is mediated through interactions with CENP-N/L and K (Mis15, Fta1 and Sim4 in *S. pombe*) and loading occurs in between S-phase and G2-phase (Eskat et al., 2012; McClelland et al., 2007). Furthermore KT targeting of CENP-O (Mal2) decreases during mitosis from anaphase A to anaphase B (Eskat et al., 2012; McAinsh et al., 2006; McClelland et al., 2007). The KT targeting of the human Mis15 ortholog CENP-N occurs during early S-phase and decreases during mitosis (Fang et al., 2015; McClelland et al., 2007). This indicates that a compositional change within the CCAN-KT-subcomplex is of physiological significance to prime the KT for the next cell cycle stage. It was proposed that cell cycle dependent fluctuations in CCAN-complex assembly are crucial to maintain KT function (McClelland et al., 2007).

A new mechanism for KT targeting of Sim4-complex proteins in *S. pombe*

I propose that a compositional change of the *S. pombe* Sim4-complex can be mediated by Asp1-generated IP_8 . I found that KT targeting of Mal2 and Fta2 was increased without Asp1-generated IP_8 and decreased with higher-than-wild-type IP_8 -levels (Chapter 3.4.1 (p. 107)). This regulation of KT localization of Mal2 and Fta2 was verified using different methods.

In live cell fluorescence microscopy experiments an increase in the KT targeting of Mal2 and Fta2 in cells unable to generate IP_8 was detected. As a linear relationship exists between GFP fluorescence signal intensity and the number of GFP molecules, the changes detected reliably reflect the change in KT localization of the Mal2 and Fta2 proteins (Coffman and Wu, 2012, 2014). Interestingly, the opposite was observed for a third member of the Sim4-complex, namely Mis15. The human ortholog of Mis15, CENP-N, has been proposed as a part of a CCAN-subclass that is antagonistic to CENP-O (Mal2) (McClelland et al., 2007). I found that the Mal2 and Mis15 proteins have a negative effect on each others KT targeting. However, as a *mal2-1^{ts} mis15-68^{ts}* strain did not display wild-type behavior I state that these proteins are not antagonistic but may regulate each other

(Chapter 3.4.2 (p. 137, 189). Using qChIP I found that the level of KT targeted Mal2 increased in the absence of IP₈. Similar results were obtained for non-synchronized and metaphase arrested cells, indicating that this effect is probably not cell cycle dependent.

A decrease in Mal2 and Fta2 KT localization was observed with higher-than-wild-type IP₈-levels. Again fluorescence microscopy and qChIP showed similar results. In this case the opposite effect was not observed for Mis15. However, as a C-terminal GFP-tag of Mis15 also abolished the rescue of the ts phenotype of the *mis15-68^{ts}* strain with higher-than-wild-type IP₈-levels, I suggest that the C-terminus of Mis15 is important for its function and a possible enhanced KT targeting mediated by IP₈. This assumption is strengthened by the fact that the *mis15-68^{ts}-gfp* strain had a stronger ts phenotype than the non-tagged strain. In addition it was shown that the C-terminus of human CENP-N (Mis15 in *S. pombe*) is necessary to bind other CCAN proteins and therefore for a localization of this protein to KTs (Carroll et al., 2009). To analyze if higher-than-wild-type IP₈-levels decrease Mis15 KT targeting an N-terminal GFP-Tag should be considered.

Interestingly, the effect of Asp1-generated IP₈ on the Mal2 and Fta2 proteins observed was very similar in its nature and extend. It had been demonstrated previously that the Mal2 and Fta2 proteins are closely related. They show localization dependency and overexpression of one protein can rescue the ts phenotype of the mutant strain of the other protein. This relation is strong enough that the Mal2-1 protein, which is defective in KT targeting was again KT localized if *fta2⁺* is overexpressed (Kerres et al., 2006). Moreover it was shown in double transfected human cells that the Mal2 and Fta2 orthologs CENP-O and CENP-P form a complex indicating that this interaction is conserved (Eskat et al., 2012). It would be interesting to analyze if Mal2 and Fta2 form a complex, maybe in form of a dimer, in *S. pombe* as well.

A change in the amount of Mal2 at the KT via variations in cellular IP₈-levels was not due to a change in cellular Mal2 protein levels as those were not altered in *asp1* variant strains. Therefore it can be stated that the cellular pool of Mal2 exceeds the molecules that are present at the KT indicating that it is possible to increase Mal2 deposition at KTs. How and when this mechanism is triggered and needed is presently unknown. However, it is feasible that a change of the environment or stress conditions trigger such a compositional change.

The IP₈ dependent mechanism of a compositional change within the Sim4-KT-subcomplex could also be relevant for a regulation of the architecture of the human CCAN-complex. The family of VIP1 inositol polyphosphate kinases is highly conserved and two homologs are present in humans called PPIP5K1 and PPIP5K2. Like Asp1, also these enzymes are bifunctional and able to generate 1-IP₇ and 1,5-IP₈ and hydrolyze these molecules to IP₆ and

5-IP₇ (Fridy et al., 2007; Gu et al., 2017; Shears et al., 2017). The adjustment of KT architecture, specifically concerning the human Mal2 and Fta2 orthologs CENP-O and CENP-P, via IP₈ might therefore also be a regulatory mechanism in human cells.

How is the influence of IP₈ on Sim4-complex proteins mediated?

Two modes of action have been proposed for IPPs: modification of protein function by direct binding or pyrophosphorylation (Azevedo et al., 2009; Laha et al., 2015; Lee et al., 2007).

In the first case, binding of IPPs induces a conformational change leading to altered protein function. It was shown that a binding of IP₇ to Pho81 inhibited its kinase activity which led to a nuclear localization of Pho4 (transcription factor)(Lee et al., 2008; Lee et al., 2007). The effect of the binding of IPPs can in this example not be detected at the modification site itself.

The second mode of action of IPPs is the pyrophosphorylation of a target protein. It was demonstrated that pyrophosphorylation of human AP3B1 (adaptor protein) negatively regulates its interaction with Kif3A (kinesin) and decreases the release of HIV particles (Azevedo et al., 2009) and that this kind of modification furthermore activates IRF3 (transcription factor) and therefore the interferon response of human cells (Pulloor et al., 2014). However, both studies used a backphosphorylation assay which is based on the assumption that proteins that are targets of pyrophosphorylation via IPPs *in vivo* cannot be pyrophosphorylated when they are extracted and used for an *in vitro* pyrophosphorylation assay (Azevedo et al., 2009). Therefore the optimization of the analysis of IPP-mediated functions *in vivo* is a vivid field of research (Brown et al., 2016; Saiardi, 2016).

An interactome analysis of IPPs done for *S. cerevisiae* in (Wu et al., 2016) discovered > 150 putative binding targets for IP₆ or 5-IP₇ showing the wide range of processes these molecules affect. 89 of the proteins identified were enriched 4- or 5-fold in the interactome assay.

Is the effect on KT targeting of Mal2 and Fta2 mediated by IP₈ a direct or an indirect effect?

The question was if the change in KT targeting observed for Mal2 and Fta2 is caused by a modification via IP₈ of the Mal2 or Fta2 proteins or if another protein is modified and the localization of Mal2 and Fta2 is altered as a consequence.

I found that the effect of Asp1-generated IP₈ on the KT targeting of the Mal2 and Fta2 proteins is likely due to IP₈ directly affecting the Mal2 and Fta2 proteins (Chapter 3.4.1.7 (p. 123)). GBP (GFP binding protein)-tagged versions of Asp1 were used to force these proteins to Mal2-GFP located at the KT. I found that the presence of Asp1-GBP led to less Mal2 at the KT interface and this was further reduced in presence of Asp1^{H397A}-GBP. Thus, forced IP₈ production at the KT affects Mal2 and Fta2 KT targeting. That the detected

changes in the KT localization of Mal2 and Fta2 were not more severe can be explained by the fact that the Asp1 protein *per se* localizes in the nucleus as well as in the cytoplasm (data not shown). Thus, under conditions where Asp1 is forced to the KT interface the endogenous background levels of the Asp1 protein interfere with the effect observed. Nevertheless, even with the wild-type Asp1 protein expressed in addition to the GBP protein variants the decrease in Mal2, and therefore Fta2, KT localization with higher-than-wild-type IP₈-levels was still visible. Hence, I demonstrated that IP₈ mediates its function directly in proximity to the KT structure. And I propose that this regulation is directly mediated via a modification of Fta2.

How might this direct regulation of Mal2 and Fta2 KT targeting be achieved?

A requirement for the pyrophosphorylation of a protein via IPPs is a former phosphorylation of a serine residue (Bhandari et al., 2007). It has recently been demonstrated that the Fta2 protein carries a phosphorylation site at the serine at position 16 (Kettenbach et al., 2015). As Fta2 and Asp1 could be co-immunoprecipitated I propose that Fta2 is a possible target for pyrophosphorylation by IPPs and that this modification leads to a change in KT targeting (Chapter 3.4.1.8 (p. 126)). As Mal2 and Fta2 act together this modification of Fta2 also alters the KT localization of Mal2. To analyze the possible modification in more detail in the future I already started to generate a version of Fta2 with a point mutation, namely Fta2^{S16A}, where the serine that was identified as a phosphorylation site is exchanged by alanine. It will be exciting to assay the influence of IP₈ on the chromosome segregation fidelity in an *fta2*^{S16A} strain and the KT targeting of the Fta2^{S16A} protein in future experiments.

Another possibility would be the modification of other proteins involved in mitosis. Interestingly the interactome assay for the binding of IP₆ detected the SMC1 and SMC3 gene products as interactors (Wu et al., 2016). The Smc1 and Smc3 proteins (Psm1 and Psm3 in *S. pombe*) are part of the cohesin complex (Michaelis et al., 1997; Skibbens, 2009). Interestingly, the cohesion of sister chromatids had been shown to be dependent on the phosphorylation status of cohesin complex proteins and a dissociation from chromatin required this modification (Hauf et al., 2005). Furthermore, it was previously shown that Ctf19 in *S. cerevisiae* (Fta2 in *S. pombe*) is involved in the recruitment of cohesin to pericentromeric regions (Eckert et al., 2007). Unfortunately, it is conceivable that KT proteins would not be detected in an interactome assay due to a low expression of these proteins. It can therefore be assumed that the real number of binding partners of IPPs is underrepresented in interactome assays and is much higher in the cell.

However, it is feasible that also *S. pombe* cohesins are modified by Asp1-generated IP₈ and that these molecules are therefore involved in the regulation of the coupling of sister chromatids. Another possibility is a crosstalk between the cohesion state of pericentric

chromatin regions and IP₈ modified Sim4-complex proteins. However, this is only an assumption, but the interactome assay still points to a role of IPPs in the regulation of processes that impact mitosis.

It has been shown previously that modifications in form of phosphorylations can influence the function of KT proteins. This was for example shown for the Sim4-complex protein Mis17, which is highly phosphorylated (Shiroiwa et al., 2011). It also has been proposed that the proteins Scm3, Mis16 and Mis18, which are required for Cnp1 loading at centromeres and show a cell cycle dependent localization, are disassociating before metaphase due to phosphorylation events (Pidoux et al., 2009).

Here I additionally propose a hitherto unknown modification of KT proteins by IP₈.

What is the take home message?

In summary, I demonstrated that Mal2, Fta2 and Mis15 KT targeting is affected by intracellular IP₈-levels. I propose that the Fta2 protein is pyrophosphorylated by Asp1-generated IPPs. This modification leads to a disassociation of Fta2 and its interaction partner Mal2 from KTs. It is feasible that the change in localization is caused by a conformational change of the Fta2 protein or its binding affinities to other KT proteins. Both of these mechanisms have been described as consequences of phosphorylation events (Latzer et al., 2008; Nishi et al., 2011). In case of absence of IPPs in the KT periphery the Fta2 protein is not modified which causes an accumulation of Mal2 and Fta2 and a delocalization of Mis15 from the KT interface. Hence, Asp1-generated IP₈ changes the composition of the Sim4-complex.

4.2 Variations in cellular IP₈-levels and the fidelity of chromosome segregation

Variations in cellular Asp1-generated IP₈-levels gave rise to two major phenotypes. First, it was observed that the composition of the Sim4-complex was changed. In the absence of Asp1-generated IP₈ the levels of Mal2 and Fta2 at the KT interface were increased, while those of Mis15 decreased. With higher-than-wild-type IP₈-levels a reduction of Mal2 and Fta2 KT localization was observed (Chapter 3.4 (p. 107)). It was furthermore shown that the levels of the NMS-complex protein Ndc80 decreased in cells deficient of Asp1-generated IP₈ (Chapter 3.4.3 (p. 146)). Second, the integrity of the mitotic spindle was altered. It was observed that the absence of Asp1-generated IP₈ led to abnormally thin spindle midzones, spindle collapse and accelerated spindle elongation in spindle phase I & III (Topolski et al., 2016). Higher-than-wild-type IP₈-levels had the opposite effect resulting in more stable spindle midzones (Topolski et al., 2016). Furthermore, variations in cellular IP₈-levels influenced the growth of mutant strains of MT-associated proteins. Lower-than-wild-type IP₈-levels negatively influenced the growth of all mutant strains tested, with the exception of *cut7^{ts}* strains (Chapter 3.1 (p. 86); (Topolski et al., 2016)). Cut7 is a plus-end directed motor protein that is essential for the stabilization of interdigitating MTs (Hagan and Yanagida, 1992).

The consequence of these changes upon variations in cellular IP₈-levels was an altered chromosome transmission fidelity. While cells without Asp1-generated IP₈ showed an increase in abnormal segregation phenotypes, the opposite was observed for cells with higher-than-wild-type IP₈-levels. These cells showed a decrease in aberrant segregation phenotypes and reduced loss of a non-essential minichromosome (Chapter 3.2 (p. 95); (Topolski et al., 2016)).

Thus, the effect of Asp1-generated IP₈ on chromosome segregation fidelity is likely caused by modulations on both sides of the KT-MT interface. We do not know yet how many targets Asp1 might have that are involved in mitotic processes. Therefore, I will present two possible models for the function of IP₈ at this interface, one model for each of the dominant phenotypes observed. One model involves the compositional changes of the KT. Another the effects of IP₈ on the dynamics and tension forces of the mitotic spindle.

What are the consequences of an altered KT targeting of Mal2 and Fta2?

The consequences of the loss of Mal2 and/or Fta2 from the KT interface are numerous and severe. Loss of Mal2 or Fta2 from the KT led to massive chromosome missegregation and a compromised centromere chromatin structure (Jin et al., 2002; Kerres et al., 2006). A

negative interaction between the *mal2-1^{ts}* strain and mutant strains of MT-associated proteins or APC (anaphase promoting complex)-components has also been described (Fleig et al., 1996; Jin et al., 2002). Furthermore the localization of DASH-complex members was abolished if Mal2 is absent from KTs. The DASH-complex is one of the attachment points to MTs (Sanchez-Perez et al., 2005). These consequences demonstrate that the localization of Mal2 and Fta2 to the KT does not merely affect the composition of the Sim4-complex itself, but that such a compositional change influences structures/ processes that are crucial for faithful chromosome segregation.

A small reduction of Mal2 and Fta2 KT targeting by ~ 20 %, which was observed for cells with higher-than-wild-type IP₈-levels, did not lead to the phenotypes observed for a loss of these proteins from the KT (Chapter 3.4.1.5 (p. 115)). In contrast, an optimized chromosome segregation fidelity was observed. This shows, that a rather small decrease of Mal2 and Fta2 levels at KTs is not only tolerated by the cells but might be necessary to ensure a proper course of mitotic processes. The increase in chromosome segregation fidelity of an endogenous chromosome observed for cells with higher-than-wild-type IP₈-levels was detectable, but not statistically significant, as the endogenous chromosome loss rate is very low with 0.01 % (Santaguida and Amon, 2015; Topolski et al., 2016). Nevertheless, I was able to demonstrate that the loss of a non-essential minichromosome which has a 10-fold higher loss frequency than an endogenous chromosome (Niwa et al., 1989), was significantly reduced with higher-than-wild-type IP₈-levels and therefore reduced Mal2 and Fta2 KT targeting. In order to get a better read-out of the reduction in the loss rate of a non-essential minichromosome, I have started to establish a new assay where loss of the minichromosome leads to cell survival (Chapter 3.7 (p. 166)). Unfortunately, that assay is still work in progress. Nevertheless the present findings demonstrate that the Sim4-complex structure is somewhat flexible and that some compositional changes are tolerated, and possibly needed for high chromosome transmission fidelity.

An increase of Mal2 and Fta2 KT targeting in the absence of Asp1-generated IP₈ was observed together with a decreased chromosome transmission fidelity (Topolski et al., 2016). This furthermore establishes that in terms of Mal2 and Fta2 KT localization the proposition the-more-the-better, does not apply. It rather shows that exceeding KT targeting of Sim4-complex members can be a disadvantage regarding chromosome segregation fidelity. It had been demonstrated previously that overexpression of Mal2 and Fta2 together led to a 4.5-fold increased loss rate of a minichromosome and an elevated missegregation of *S. pombe* chromosome I (Ramrath, 2010). In line with this result, we found that an overexpression of Mal2 and Fta2 together led to decreased cell viability in a wild-type strain (Chapter 3.4.2 (p. 137)). It was observed previously that higher cellular Mal2 protein amounts

via overexpression of Sui1 (translation initiation factor) were linked to an enhanced KT localization of Mal2 (Topolski, 2013). Therefore it can be proposed that overexpression of Mal2 and Fta2 also led to an increased KT targeting of these proteins.

Interestingly, we did not detect a decrease in cell viability when *mal2*⁺ or *fta2*⁺ were overexpressed separately. Higher cellular levels of only one of these proteins moreover had no effect on the transmission fidelity of a minichromosome (Ramrath, 2010). This demonstrates that Mal2 and Fta2 proteins have to be present simultaneously to mediate their function. It can be proposed that, as observed for human Mal2 and Fta2 orthologues CENP-O and -P (Eskat et al., 2012), these two proteins form a subcomplex within the Sim4-complex.

The influence of Asp1-generated IP₈ was not restricted to the Sim4-KT-subcomplex but also affected NMS-complex composition (Chapter 3.4.3 (p. 146)). The NMS-complex protein Ndc80 showed a decreased KT localization in IP₈ deficient cells by ~ 40 %. The analysis of the effects of higher-than-wild-type IP₈-levels on the *ndc80-21*^{ts} mutant strain, which shows defects in KT-MT attachments and consequently a weak mitotic spindle and chromosome congression defects (Hsu and Toda, 2011), showed that the spindle midzone was stabilized. This indicates that the nature of the effect of Asp1-generated IP₈ on different KT-complexes might differ.

Model 1: Compositional changes of the KT via Mal2 and Fta2 affect chromosome segregation

In the first model I propose a mechanism by which a higher KT targeting of Mal2 and Fta2 leads to a decreased KT localization of Ndc80 and therefore impairs the establishment of KT-MT attachments. This model relies on the finding that in absence of Asp1-generated IP₈, when the levels of Mal2 and Fta2 KT targeting increased, the KT targeting of the Ndc80 protein at the KT decreased by ~ 40 % (Chapter 3.4.3 (p. 146)).

The Ndc80 protein is part of the NMS-complex which is the major connector of KTs and MTs (Cheeseman et al., 2006; Ciferri et al., 2007; Kerres et al., 2007; McClelland et al., 2003). Ndc80 belongs to the NMS-subcomplex known as the Ndc80-complex which is a tetramer of the proteins Ndc80, Nuf2, Spc24 and Spc25 (Matsuo et al., 2017; Wei et al., 2005). Ndc80 is the crucial mediator of KT-MT attachments as it directly mediates these connections via an interaction with the MT-associated proteins/complexes Dis1 and Alp7-Alp14 (Dis1 and Alp14: XMAP/TOG family MT polymerases; Alp7: TACC (transforming acidic coiled-coil) protein) (Hsu and Toda, 2011; Tang et al., 2013). It has been shown that the N-terminal loop region of Ndc80 directly bound these proteins, albeit via different regions within the loop. Dis1 was proposed to bind to Ndc80 at KTs in early mitosis, while the Alp7-Alp14 complex is

transported there via MTs. Furthermore, a loss of Dis1 and Alp7-Alp14 at KT interfaces due to mutations in the Ndc80 loop caused different phenotypes (Hsu and Toda, 2011; Tang et al., 2013). It was demonstrated that Alp7 also recruited Klp5 (as part of the Klp5-Klp6-Pp1 (Klp5-Klp6: kinesin-8 family proteins; Pp1: protein phosphatase 1) complex), to KT interfaces via its association with Ndc80 which led to a transport of the sister chromatids to the SPBs and SAC-silencing (Tang and Toda, 2015). In addition it has been shown that the *S. pombe* Ndc80-complex can track MTs *in vitro* if the +-TIP protein Mal3 is present (Matsuo et al., 2017).

The interaction of Ndc80, MTs and MT-associated proteins is therefore complex and crucial for a proper mitotic process.

In my model higher KT targeting of Mal2 and Fta2 reduces KT association of Ndc80. Therefore less or weaker KT-MT attachments are established. The decrease of Ndc80 would lead to a reduced availability of this protein for interactions with Dis1 and Alp7-Alp14. If these interactions are abolished this leads to unstable mitotic spindles, spindle collapse, mitotic delay and/ or missegregation (Hsu and Toda, 2011; Tang et al., 2013; Tang and Toda, 2015). These phenotypes were also observed in cells without Asp1-generated IP₈ (Topolski et al., 2016).

A mutant of Ndc80 that carries a point mutation in its hairpin region was not recruiting SAC components (Mph1, Bub1, Bub3, Mad1-3) and the Aurora kinase Ark1, which dissolves KT-MT attachments, to unattached KT interfaces (Chmielewska et al., 2016). This result is in line with the finding that less Ark1 was associated with KT interfaces in prometaphase in cells without Asp1-generated IP₈ (Topolski et al., 2016). It can be stated that the Ark1 localization is not entirely abolished, but reduced in absence of IP₈ as there is still a sufficient amount of Ndc80 localized at the KT interface. Therefore the observed increase in aberrant chromosome segregation phenotypes was rather mild, but clearly detectable.

Hence, I propose that in cells without Asp1-generated IP₈ chromosome transmission fidelity is decreased due to a decrease in Ndc80 KT targeting caused by increased levels of Mal2 and Fta2 at the KT. This leads to reduced establishment of KT-MT attachments and a reduction in the KT-association of MT-associated proteins. Furthermore it causes an impaired error correction mechanism as the amount of Ark1 is decreased (Figure 4-1).

It will be interesting to analyze in the future if the amount of KT targeted Ndc80 is also decreased by Mal2 and Fta2.

Interestingly, a similar situation has been shown in human HeLa cells where depletion via siRNA of the human Mal2 homolog CENP-O led to an increase of Ndc80 and Nuf2 KT

localization (McClelland et al., 2007). The authors proposed that CCAN members can modulate the levels of Ndc80-complex members at KT and that such a fine-tuning might be important for variations in KT-MT attachments. They furthermore proposed that this effect might be regulated by post-translational modifications (McClelland et al., 2007). I propose that this modification might be a pyrophosphorylation of CCAN-complex proteins via IP_8 . A decrease in Mal2 and Fta2 KT targeting with higher-than-wild-type IP_8 -levels did not increase the amount of Ndc80 at the KTs, it slightly decreased. As sufficient levels of Ndc80 are present at the KT under these conditions the establishment of bipolar KT-MT attachments and the chromosome segregation process might take place in a wild-type like manner (Figure 4-1).

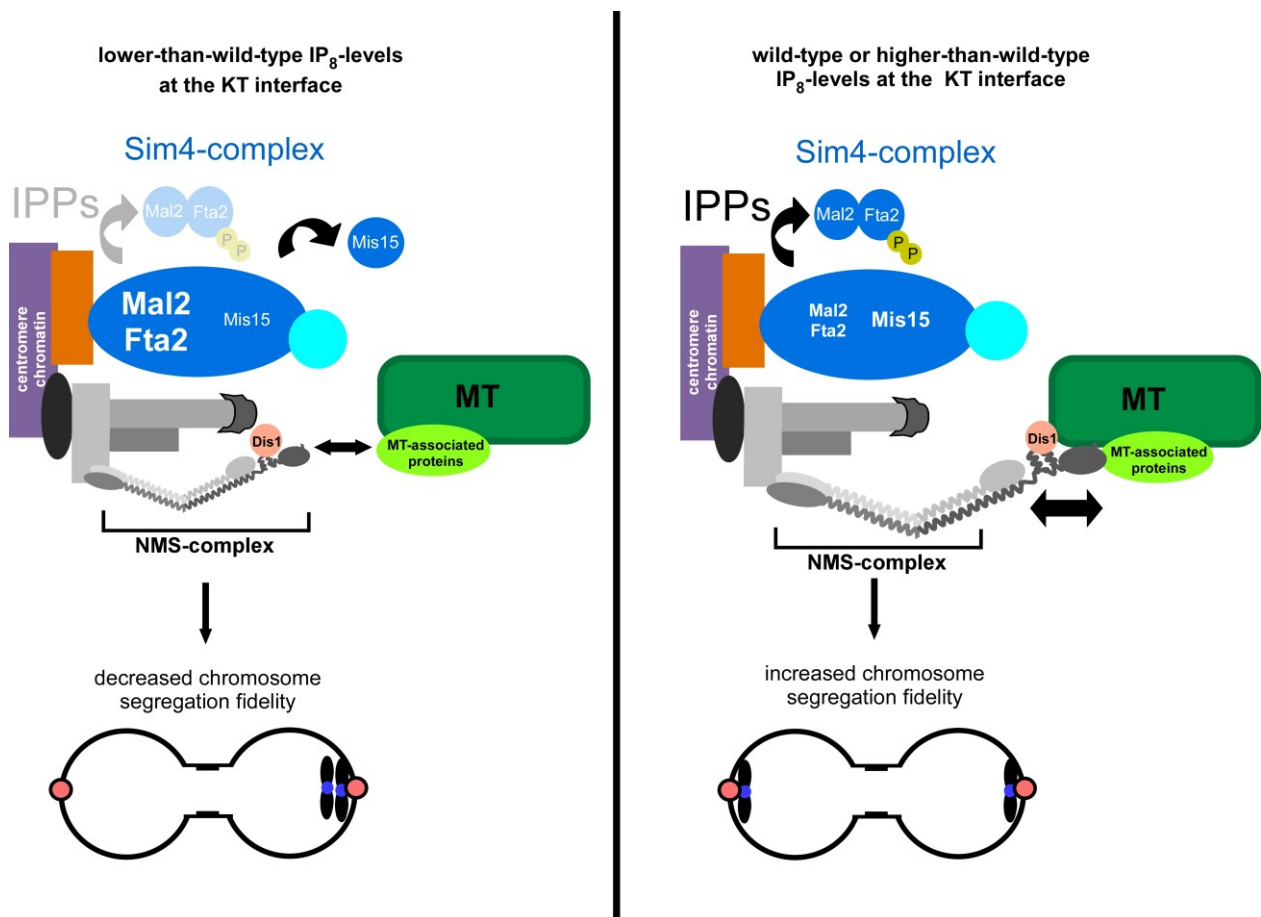


Figure 4-1 Model 1: Enhanced Mal2 and Fta2 KT targeting in the absence of Asp1-generated IP_8 reduces the level of Ndc80 at the KT.

In the absence of Asp1-generated IP_8 the level of Mal2 and Fta2 at KTs increases as Fta2 is not pyrophosphorylated and therefore delocalized. This increase in Mal2 and Fta2 at the KTs leads to highly reduced levels of Ndc80. The Ndc80 protein is as a consequence less available for the establishment of KT-MT attachments via MT-associated proteins. As a consequence the chromosome segregation fidelity decreases. With wild-type or higher-than-wild-type IP_8 -levels sufficient amounts of Ndc80 are present for the establishment of KT-MT attachments. This ensures a proper chromosome segregation process. (Parts of this model modified from (Tang and Toda, 2015)).

Model 2: Asp1-generated IP₈ affects spindle forces

The first model relies on the fact that the establishment of bipolar KT-MT attachments and spindle dynamics cannot be viewed separately.

The second model involves the impact of Asp1-generated IP₈ on the pulling and pushing forces of the mitotic spindle. I furthermore propose that a change in KT composition as described above might influence these dynamic movements by changing attachments at the KT-MT interface. Therefore both models might act combined in *S. pombe* cells.

The *ts* phenotype of the *cut7-446^{ts}* strain was rescued with lower-than-wild-type IP₈-levels ((Topolski et al., 2016); Chapter 3.1 (p. 86)). Cut7 is a kinesin-5 protein that is essential for spindle formation and elongation (Hagan and Yanagida, 1992). The Cut7 protein is involved in the regulation of metaphase spindle length, which it influences by providing outward pushing spindle forces at interpolar MTs (Syrovatkina et al., 2013). Furthermore, Cut7 function has been linked to the correction of merotelic attachments during the chromosome segregation process (Choi and McCollum, 2012; Syrovatkina et al., 2013). Therefore this protein links the effects of Asp1-generated IP₈ on spindle integrity and chromosome segregation. Interestingly, lower-than-wild-type IP₈-levels had the opposite effect on the growth of deletion strains of Klp5 and Klp6, which are major contributors to the antagonistic inward pulling forces within the mitotic spindle (Syrovatkina et al., 2013).

A deletion of *klp5⁺* or *klp6⁺* led to elongated metaphase spindles. This elongation resulted in an increased number of lagging chromosomes during mitosis, indicating that merotelic attachments are not always resolved if the inward pulling spindle forces are compromised (Garcia et al., 2002b; Syrovatkina et al., 2013; Unsworth, 2007). Moreover, a deletion of the chromodomain protein Swi6 is known to cause lagging chromosomes and an increased metaphase spindle length (Choi and McCollum, 2012; Ekwall et al., 1995). Cut7 enhanced this effect as *swi6Δ cut7-24^{ts}* double mutant cells showed a reduced metaphase spindle length compared to *swi6Δ* cells. Furthermore the interkinetochore distance was reduced in the *cut7-24^{ts}* strain which was proposed to be involved in the correction of merotelic attachments. One possibility how a lack of outward pushing forces might be correlated with a reduction in chromosomal segregation defects was proposed in (Choi and McCollum, 2012). The authors propose that the lack of outward pushing forces at interpolar MTs and the reduced interkinetochore distance might bring the KT proteins that are modulated by the Aurora kinase Ark1 into proximity of this protein which dissolves KT-MT attachments and therefore regulates the correction of merotelic attachments. Disruption of the outward

pushing forces by inhibition of the human kinesin-5 Eg5 even led to a decrease in lagging chromosomes in human tumor cells (Choi and McCollum, 2012).

As *klp6Δ* and *cut7^{ts}* mutant strains were affected in opposite ways by lower-than-wild-type IP₈-levels, a role of IP₈ in the regulation of tension within the mitotic spindle seems conceivable. It can be hypothesized that as lower-than-wild-type IP₈-levels caused an enhanced recruitment of Cut7 to short metaphase spindles the outward pushing spindle forces exceed the inward pulling forces if the other wild-type MT-associated proteins are present. And indeed, it was already shown that without Asp1-generated IP₈ a longer metaphase spindle can be observed (Topolski, 2013). A re-localization of the Cut7^{ts} protein with lower-than-wild-type IP₈-levels would then restore the force balance within the spindle and might explain the rescue of growth.

If the *klp5⁺* or *klp6⁺* ORFs were deleted the inward pulling forces were compromised which led to an increase in metaphase spindle length, fewer corrected merotelic attachments and therefore a decrease in viability (Syrovatkina et al., 2013; Unsworth, 2007). A contribution of IP₈ to the inward pulling spindle forces might explain why lower-than-wild-type IP₈-levels reduced the growth of a *klp6Δ* strain as two opposing forces to the outward pushing Cut7 were compromised. Another point that stresses the above hypothesis is that it was shown that the spindle elongation in spindle phases I and III was accelerated in cells without Asp1-generated IP₈ (Topolski et al., 2016) suggesting enhanced outward pushing spindle forces in the absence of these molecules.

Thus, I propose that IP₈ promotes inward pulling or reduces outward pushing spindle forces which brings the KTs in closer proximity to KT localized Ark1 which leads to an enhanced correction of erroneous KT-MT attachments and therefore leads to an optimized chromosome segregation fidelity (Figure 4-2).

However, the models proposed have many variables. It is also known that a great amount of proteins are modified by Asp1-generated IP₈ (Wu et al., 2016). It is therefore feasible that various proteins at the KT-MT interface, in addition to Fta2 are targets of these high-energy molecules.

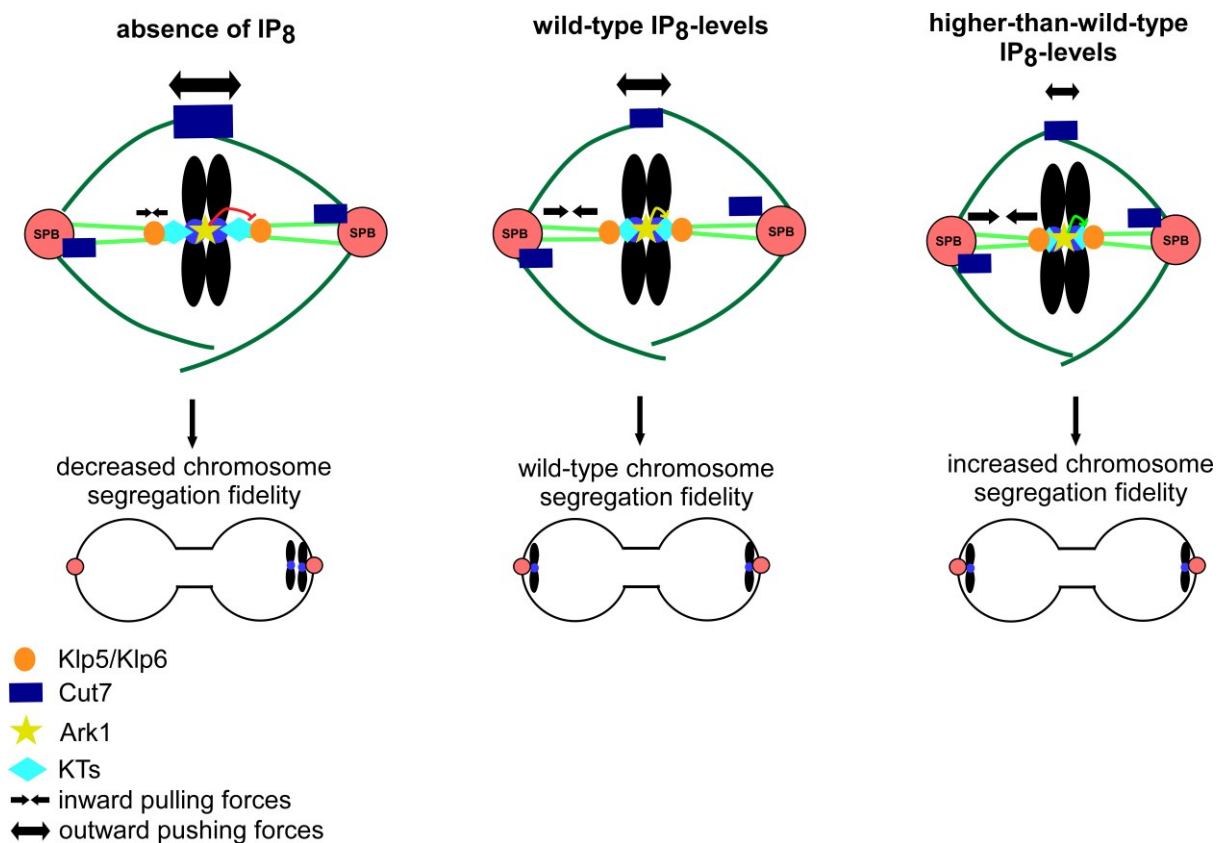


Figure 4-2 Model 2: Asp1-generated IP₈ regulates spindle forces and that affects chromosome segregation fidelity.

In the absence of Asp1-generated IP₈ the outward pushing forces within the mitotic spindle increase which pulls the KT-MT attachments out of reach of the Aurora kinase Ark1. Erroneous KT-MT attachments cannot be dissolved sufficiently. With wild-type IP₈-levels the forces are balanced. With higher-than-wild-type IP₈-levels the inward pulling exceed the outward pushing forces which brings the KT-MT attachments in closer proximity to Ark1 leading to an enhanced dissolving of KT-MT attachments. As together with the correct connections also the erroneous ones are dissolved more efficiently this leads to a decrease in merotelic attachments and therefore chromosome segregation errors. (Model in parts modified from (Choi and McCollum, 2012)).

The question remains why IP₈ modulates the KT-MT interface. This aspect will be discussed in the next and last part of the discussion.

4.3 What's the use?

It is feasible that the flexibility of the KT-MT interface discussed in the previous two chapters (Chapters 4.1 and 4.2 (p. 168 and 174)) might be of specific importance as a response to environmental changes. It has been demonstrated numerous times that IPPs are environmental sensors that affect cellular processes in response to changing environmental conditions. Extracellular conditions can lead to variations in intracellular IPP-levels and a cellular response triggered by these molecules (Lee et al., 2007; Luo et al., 2003; Pesesse et al., 2004).

For example, hyperosmotic stress induced by 0.2 M sorbitol led to a 10-25 fold increase in IP₈-levels in hamster and human cell lines, which enabled these cells to adapt to the stress conditions, while it did not affect their viability compared to non-stressed cells (Pesesse et al., 2004). Moreover, it was demonstrated that co-binding of IP₈ and jasmonate to the Ask1-COI-JAZ complex induced the transcription of VSP2 (Vegetative storage protein 2 precursor) which is involved in the defense against herbivores in *A. thaliana* (Laha et al., 2015). It has also been found that upon the switch to filamentous growth the cellular levels of UmAsp1, and therefore possibly also IPPs, decreased in *Ustilago maydis* (Pöhlmann et al., 2014).

These findings demonstrate that IPPs can modulate intracellular processes upon sensing environmental changes. Here I propose that such a sensing of specific extrinsic conditions might change intracellular IP₈-levels resulting in the compositional change of the KT-complex via Mal2 and Fta2 and a modulation of mitotic spindle forces. A first indicator of a regulation of mitotic processes via IP₈ upon changes in extracellular conditions is the finding that the non-growth phenotype of the *mal2-1^{ts}* strain was partially rescued in absence of Asp1-generated IP₈ under low glucose conditions (0.1 %) but not with higher amounts of glucose (2 %) (data not shown). It has furthermore been demonstrated that *S. pombe* cells depend on the functional DASH-complex to resist osmotic stress, but that this complex is not essential under non-stress conditions (Aoyama et al., 2000; Nakamichi et al., 2000; Sanchez-Perez et al., 2005). These results show that environmental changes can alter the significance of specific KT-complexes.

It has been shown for syncytial *Drosophila melanogaster* embryos that anoxia (extreme deprivation of O₂) led to a reduction of spindle fibers during metaphase, reduced levels of Kin-8 (kinesin-8 family protein; Klp5/6 in *S. pombe*) at the spindle midzones of metaphase spindles and a redistribution of the CENP-C (Cnp3) and Nuf2 KT proteins to spindle MTs in proximity to the centrosomes. Moreover anoxia caused a metaphase arrest consistent with the observation that more of the spindle checkpoint protein Mps1 (Mph1) was localized at KTs. Cells with a checkpoint deficiency displayed chromosome congression defects and

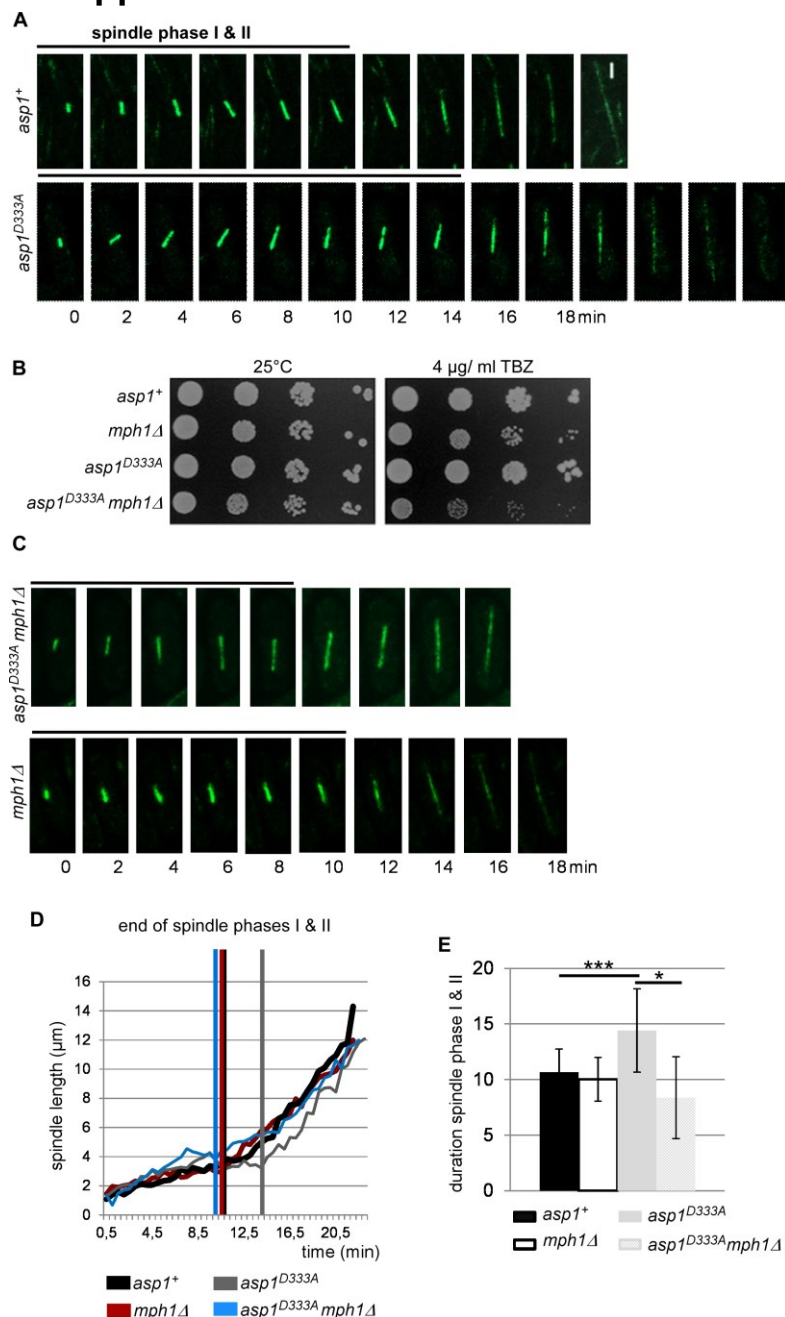
lagging chromosomes that were increased compared to normoxic conditions (Pandey et al., 2007). This shows that spindle dynamics, spindle forces and KT architecture can be altered if environmental conditions change and that this affects chromosome segregation.

These findings indicate that environmental stress conditions usually lead to a less reliable chromosome segregation process. However, it is known that organisms like the pathogenic fungus *Candida albicans* generate polyploid cells under stress conditions, for example after host defense mechanisms are activated. These polyploid cells lead to aneuploidy in the next generation. A subset of those aneuploidies can then lead to an advantage under the altered conditions which ultimately causes enhanced survivability (Berman, 2016).

The above described findings were made under extreme environmental changes. A slight variation of environmental conditions might lead to smaller changes in KT-structure that are necessary to adapt to the environment. Unfortunately, such studies have not been conducted yet.

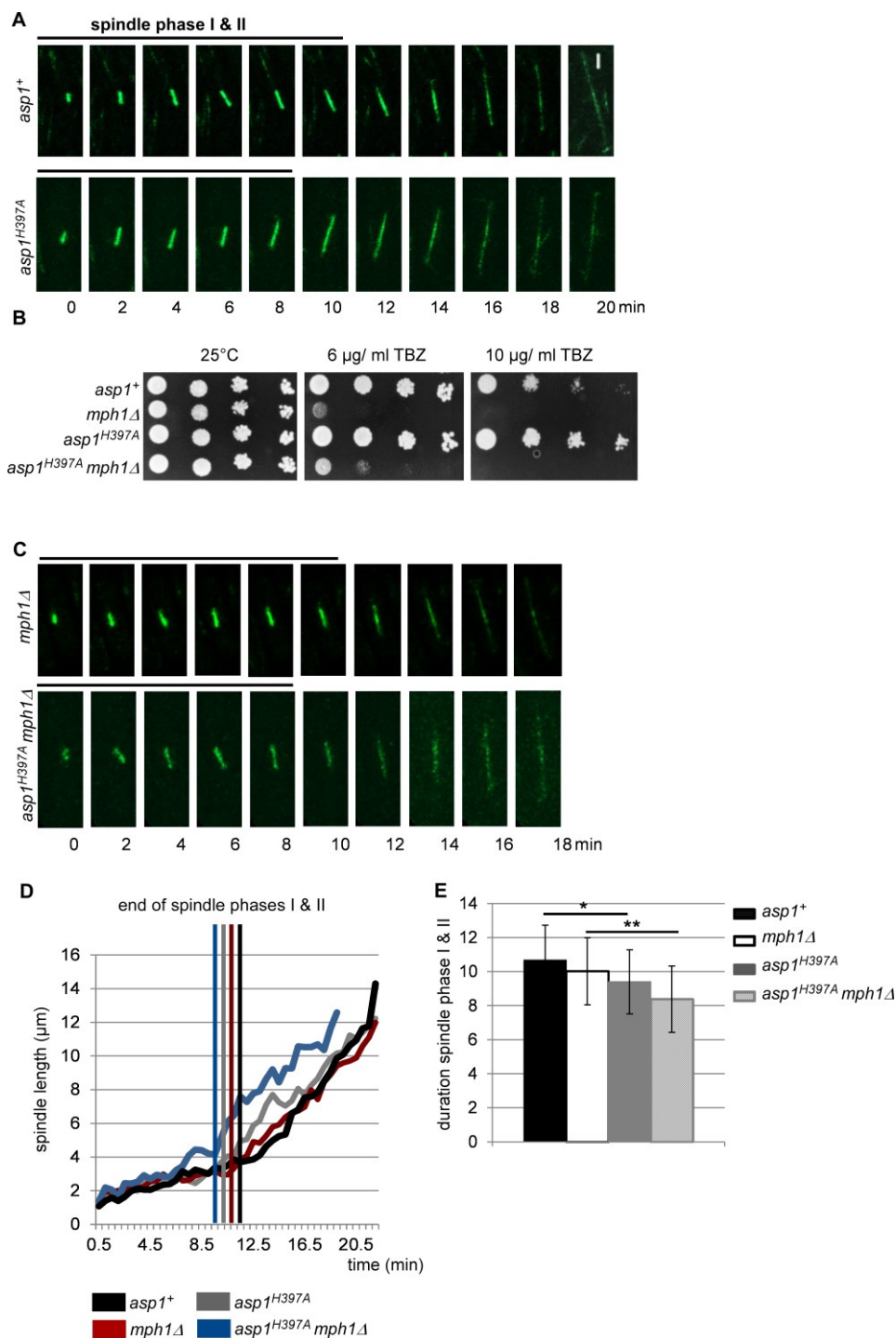
In conclusion, mechanisms where environmental changes influence mitotic processes are probably more common but have in general not been analyzed much. *S. pombe* cells might use Asp1-generated IP_8 to translate environmental signals into altered mitotic structures/processes. As the structure of the KT and mitotic regulators are conserved between organisms an alteration of these structures via IPPs might be of relevance for other organisms as well.

5 Appendix



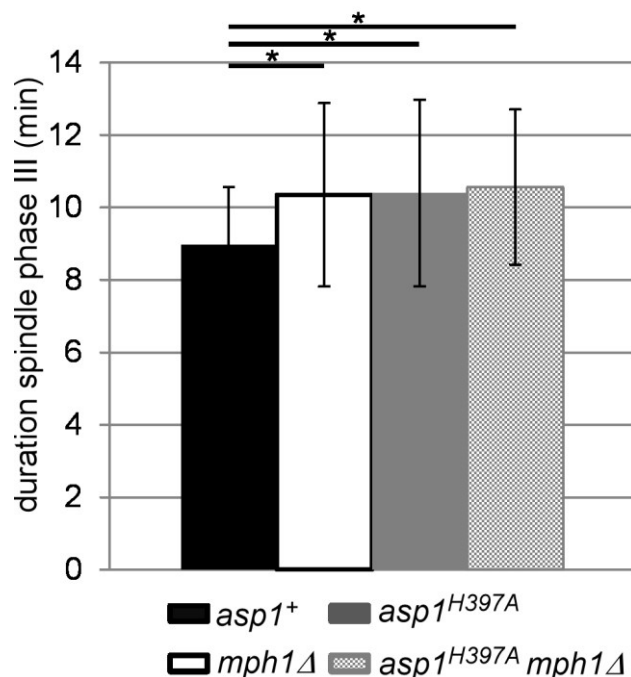
Supplementary Figure 1 Mitotic spindle phases I & II are prolonged in an *asp1*^{D333A} background.

A: Live cell microscopy photomicrographs of strains expressing SV40::*atb2*⁺-*gfp*. Cells were grown at 25°C overnight. Videos were taken at 25°C using a Zeiss Spinning Disc-Confocal microscope. Time between images: 2 min. Scale bar: 2 μm. Examples for the mitotic spindle of a wild-type and an *asp1*^{D333A} cell are shown. **B:** Serial dilution patch tests (10⁴-10¹ cells) of the indicated strains. Strains were grown on media with or without TBZ for 4 days at 25°C. **C:** Live cell microscopy photomicrographs of strains expressing SV40::*atb2*⁺-*gfp*. Cells were grown at 25°C overnight. Videos were taken at 25°C using a Zeiss Spinning Disc-Confocal microscope. Time between images: 2 min. Scale bar: 2 μm. Examples for the mitotic spindle of a *mph1Δ* and *asp1*^{D333A} *mph1Δ* cell are shown. **D:** Graph of the spindle length over time for the cells shown in A and C. **E:** Diagram showing the duration of spindle phases I & II for: wild-type 10.67 min ± 2.06 (n = 36), *mph1Δ* 10.02 min ± 1.97 (n = 30), *asp1*^{D333A} 14.4 min ± 3.74 (n = 33), *asp1*^{D333A} *mph1Δ* 8.4 min ± 3.68 (n = 4). (*: p ≤ 0.05; ***: p ≤ 0.001; two-sample-t-test). Part B of this figure has been published: (Topolski et al., 2016).



Supplementary Figure 2 Mitotic spindle phases I & II are shorter in cells with higher-than-wild-type IPP-levels.

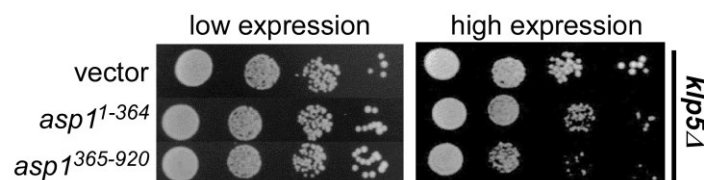
A: Live cell microscopy photomicrographs of strains expressing SV40::*atb2⁺-gfp*. Cells were grown at 25°C overnight. Videos were taken at 25°C using a Zeiss Spinning Disc-Confocal microscope. Time between images: 2 min. Scale bar: 2 μm. Examples for the mitotic spindle of a wild-type and an *asp1^{H397A}* cell are shown. **B:** Serial dilution patch tests (10^4 - 10^1 cells) of the indicated strain. Strains were grown in media with or without TBZ for 4 days at 25°C. (performed by Eva Walla) **C:** Live cell microscopy photomicrographs of strains expressing SV40::*atb2⁺-gfp*. Cells were grown at 25°C overnight. Pictures were taken at 25°C. Time between images: 2 min. Scale bar: 2 μm. Examples for the mitotic spindle of *mph1Δ* and *asp1^{H397A} mph1Δ* cells are shown. **D:** Graph of the spindle length over time for the cells shown in A. **E:** Diagram showing the duration of spindle phases I & II for: wild-type 10.67 min ± 2.06 (n = 36), *mph1Δ* 10.02 min ± 1.97 (n = 30), *asp1^{H397A}* 9.4 min ± 1.88 (n = 30), *asp1^{H397A} mph1Δ* 8.38 min ± 1.95 (n = 30). (*: p ≤ 0.05; **: p ≤ 0.01; two-sample-t-test).



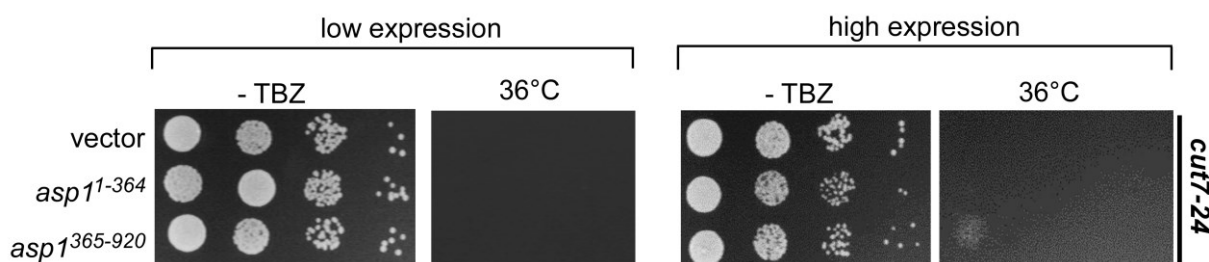
Supplementary Figure 3 *mph1*Δ and *asp1*^{H397A} cells have a longer spindle phase III.

Diagram showing the duration of spindle phases III for the strains used in Supplementary Figure 2: wild-type 8.97 min ± 1.6 (n = 36), *mph1*Δ 10.35 min ± 2.53 (n = 30), *asp1*^{H397A} 10.4 min ± 2.57 (n = 30), *asp1*^{H397A} *mph1*Δ 10.57 min ± 2.14 (n = 30). (*: p ≤ 0.05, two-sample-t-test).

A kinesin-8 family

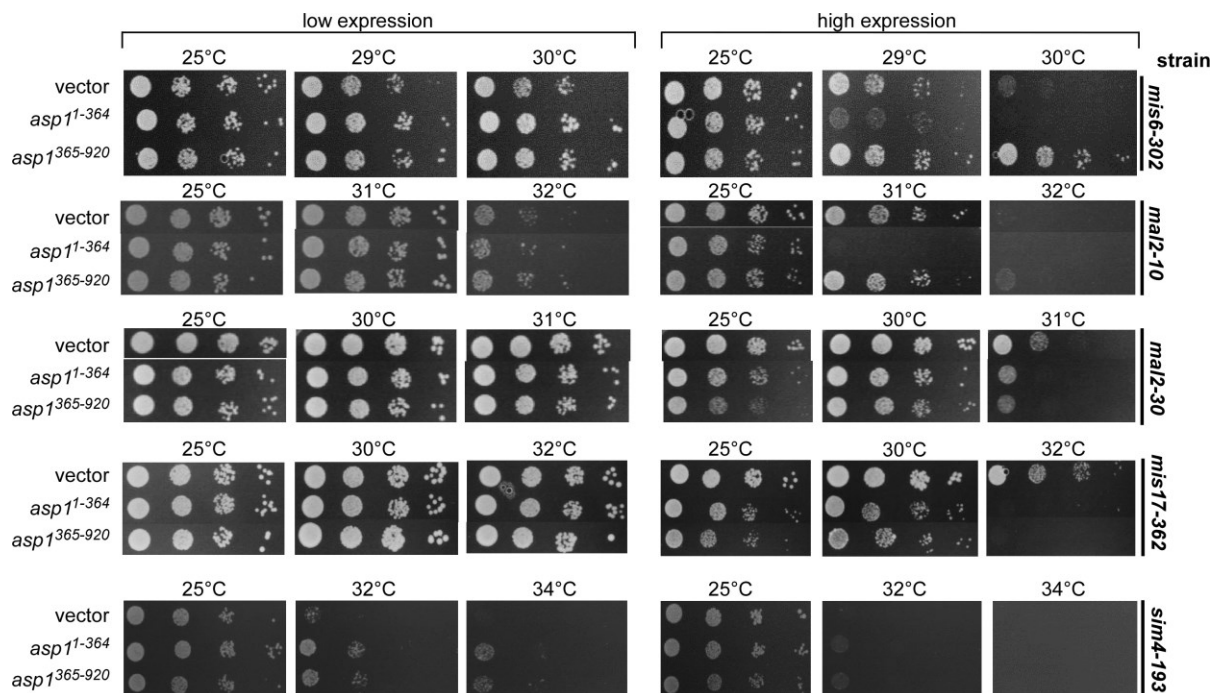


B kinesin-5



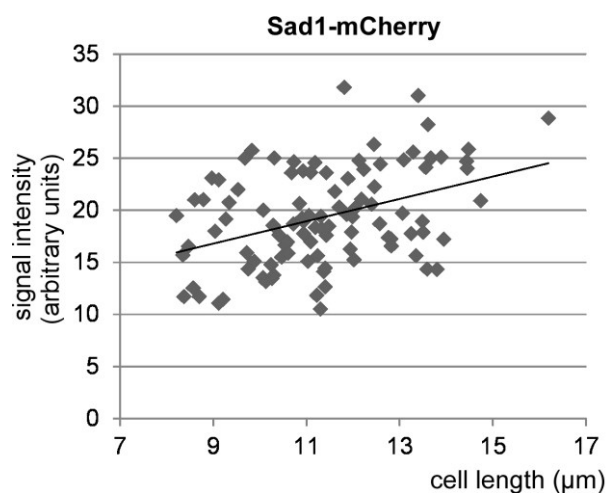
Supplementary Figure 4 Asp1-generated IP₈ influences the growth of mutant strains of MT-associated proteins.

A: Serial dilution patch tests (10^4 - 10^1 cells) of the *klp5*Δ strain transformed with a vector control, *asp1*¹⁻³⁶⁴ or *asp1*³⁶⁵⁻⁹²⁰ plasmids. Transformants were grown under plasmid-selective conditions in media with or without thiamine for 5 days at 25°C. **B:** Serial dilution patch tests (10^4 - 10^1 cells) of the *cut7-24*^{ts} strain transformed with a vector control, *asp1*¹⁻³⁶⁴ or *asp1*³⁶⁵⁻⁹²⁰ plasmids. Transformants were grown under plasmid-selective conditions in media with or without thiamine for 6 days at 25°C and 36°C. Representative examples out of at least 3 transformants/ plasmid and strain are shown.



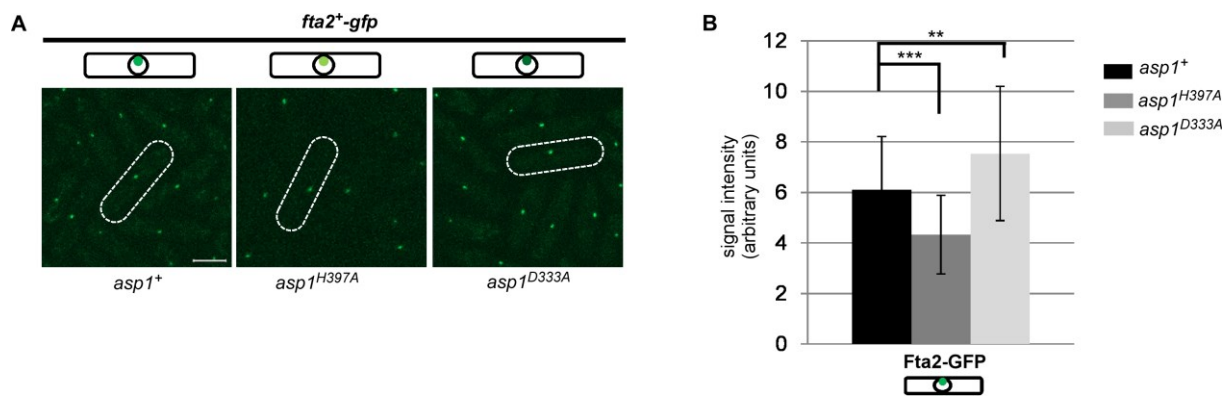
Supplementary Figure 5 *asp1*¹⁻³⁶⁴ and *asp1*³⁶⁵⁻⁹²⁰ expression influence the growth of all analyzed Sim4-complex mutant strains.

Serial dilution patch tests (10^4 - 10^1 cells) of the indicated strains transformed with a vector control, *asp1*¹⁻³⁶⁴ or *asp1*³⁶⁵⁻⁹²⁰ expressed on plasmids. Transformants were grown under plasmid-selective conditions in media with or without thiamine for 5-6 days at the indicated temperatures. The temperatures shown were selected to best demonstrate the differences in growth. Representative examples out of at least 3 transformants/ plasmid and strain are shown.



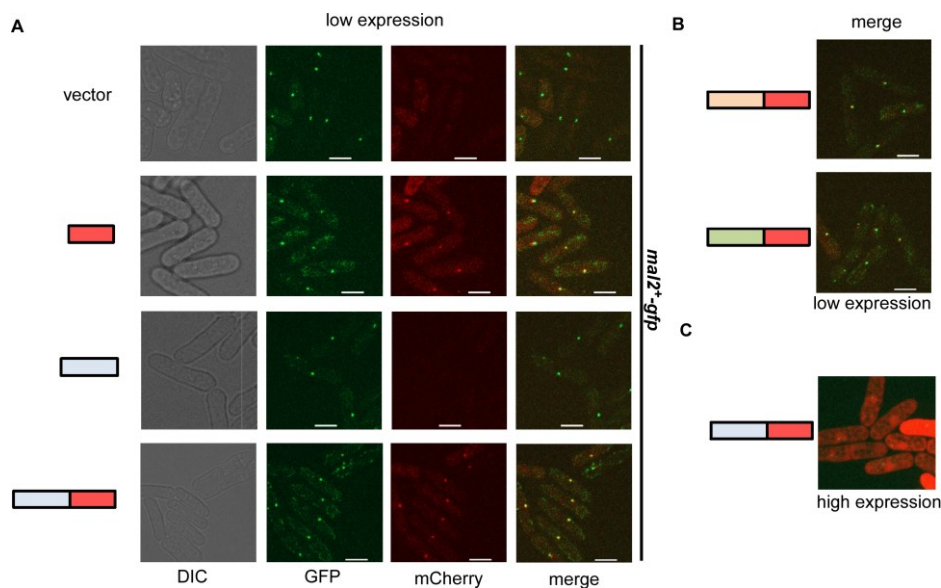
Supplementary Figure 6 Sad1-mCherry fluorescence signals get stronger with increasing cell size.

Diagram of the correlation of Sad1-mCherry signals quantified in a *sad1-mCherry cen1-gfp* strain ($n = 100$). The trendline (black) shows an upward slope.



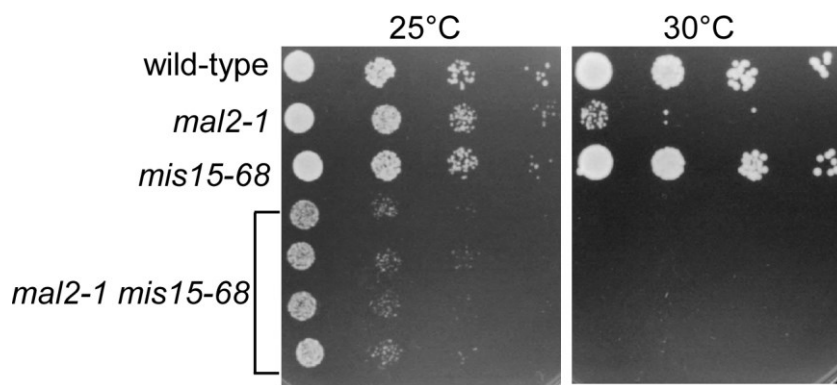
Supplementary Figure 7 Fta2-GFP KT localization is affected by changes in cellular IPP-levels.

A: Top: Schematic overview of the Fta2-GFP fluorescence signal at the KT in the indicated strains. Darker green = stronger signal. Bottom: Live fluorescence microscopy pictures of the indicated strains expressing *fta2⁺-gfp*. Strains were pre-incubated for 24 h at 25°C in LFM before they were patched on agarose pads. Pictures were taken at 20°C with 20 % laser intensity using a Zeiss Spinning Disc-Confocal microscope (pictures taken by Boris Topolski). Scale bar = 5 µm. **B:** Quantification of Fta2-GFP fluorescence signals. Pictures taken as in A for the indicated strains: *asp1⁺* 6.1 AU ± 2.1; *asp1^{D333A}* 7.5 AU ± 2.7; *asp1^{H397A}* 4.3 ± 1.6 (*asp1⁺*: n = 56; *asp1^{D333A}*: n = 43; *asp1^{H397A}*: n = 66; **: p ≤ 0.01, *** p ≤ 0.001 two-sample-t-test).



Supplementary Figure 8 All used Asp1-GBP-mCherry variants co-localize with Mal2-GFP at the KT.

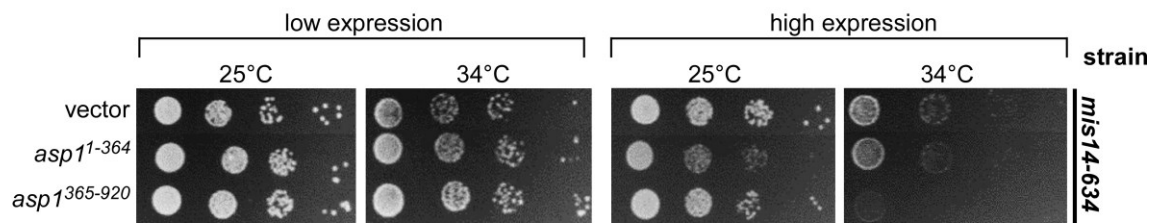
A: Live cell fluorescence microscopy pictures for the indicated transformants. Top to bottom: vector control, *GBP-mCherry*, *asp1⁺* and *asp1⁺-GBP-mCherry*. First column: DIC pictures for each transformant, second column: Mal2-GFP fluorescence signal (40 % laser intensity), third column: GBP-mCherry or Asp1-GBP-mCherry fluorescence signal (10 % laser intensity), last column: merge for GFP and mCherry signals. Transformants were pre-grown overnight in LFM without leucine and with thiamine (low expression) at 25°C before they were patched on agarose pads. Pictures were taken at 25°C using a Zeiss Spinning Disc-Confocal microscope. Scale bar = 5 µm. **B:** Merge pictures taken as in A for *asp1^{D333A}-GBP-mCherry* and *asp1^{H397A}-GBP-mCherry* plasmid expression. **C:** Merge pictures taken as in A for *asp1⁺-GBP-mCherry* plasmid expression under high expression conditions (- thiamine).



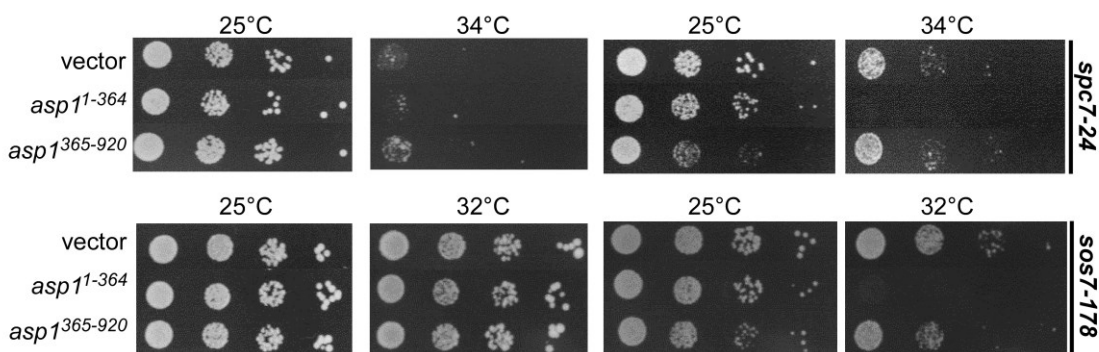
Supplementary Figure 9 *mal2-1^{ts}* and *mis15-68^{ts}* have a negative synergistic effect on growth.

Serial dilution patch tests (10^4 - 10^1 cells) of the indicated strains. Strains were grown on full media for 3 days at the indicated temperatures.

A MIND-sub-complex



B Spc7/Sos7-sub-complex



Supplementary Figure 10 Cellular IP₈-levels affect NMS-complex mutants.

A + B: Serial dilution patch tests (10^4 - 10^1 cells) of the indicated strains transformed with a vector control, *asp1¹⁻³⁶⁴* or *asp1³⁶⁵⁻⁹²⁰* plasmids. Transformants were grown under plasmid-selective conditions in media with or without thiamine for 4-6 days at the indicated temperatures. The temperatures shown were selected to best demonstrate the differences in growth.

6 Table of figures

Figure 1-1 The <i>S. pombe</i> cell cycle.....	12
Figure 1-2 Mitosis in <i>S. pombe</i>	14
Figure 1-3 Mitotic spindle phases in <i>S. pombe</i>	16
Figure 1-4 Errors in the establishment of KT-MT attachments and their consequences.....	16
Figure 1-5 The centromere of <i>S. pombe</i>	23
Figure 1-6 Overview of the <i>S. pombe</i> KT sub-complexes and their positioning.....	24
Figure 1-7 The <i>S. pombe</i> Sim4-complex members.....	26
Figure 1-8 The <i>S. pombe</i> NMS-complex.....	30
Figure 1-9 Activation of the SAC in <i>S. pombe</i> involves several proteins.....	34
Figure 1-10 Mitochondrial distribution depends on MTs.....	35
Figure 1-11 The generation of IPPs.....	38
Figure 1-12 Cellular IP ₈ -levels are altered via expression of different <i>asp1</i> -variants.....	41
Figure 1-13 Effects of Asp1-generated IP ₈ on interphase MTs and the mitotic spindle.....	42
Figure 3-1 Functions of the analyzed proteins in MT- and spindle dynamics.....	88
Figure 3-2 Asp1-generated IP ₈ affects the growth of deletion strains of MT-associated proteins.....	90
Figure 3-3 Absence of Asp1-generated IP ₈ does not induce synthetic lethality in an <i>alp14</i> Δ strain.....	92
Figure 3-4 More Cut7-GFP is recruited to the spindle midzones with lower-than-wild-type cellular IP ₈ -levels.....	94
Figure 3-5 Faithful chromosome segregation requires Asp1-generated IP ₈	96
Figure 3-6 Aberrant segregation phenotypes increase in the absence Asp1-generated IP ₈ in an <i>mph1</i> Δ strain background.....	98
Figure 3-7 Higher-than-wild-type IP ₈ -levels slightly reduce aberrant segregation phenotypes.....	99
Figure 3-8 Higher-than-wild-type IP ₈ -levels slightly reduce missegregation events in an <i>mph1</i> Δ background.....	100
Figure 3-9 Higher-than-wild-type IP ₈ -levels reduce missegregation events in SAC-less cells.....	102
Figure 3-10 Higher-than-wild-type IP ₈ -levels reduce the loss of a non-essential minichromosome.....	104
Figure 3-11 Modification of the residue S674 is not important for Asp1 function.....	106
Figure 3-12 A change in cellular IP ₈ -levels influences the growth of Sim4-complex mutant strains.....	108
Figure 3-13 Plasmid-borne expression of <i>asp1</i> ¹⁻³⁶⁴ enhances aberrant segregation events in the <i>mal2-1</i> ^{ts} mutant strain.....	111
Figure 3-14 Mal2-1-GFP KT localization is affected by <i>asp1</i> ¹⁻³⁶⁴ and <i>asp1</i> ³⁶⁵⁻⁹²⁰ expression.....	113
Figure 3-15 Mal2-GFP KT targeting is decreased in the presence of Asp1 ¹⁻³⁶⁴	114
Figure 3-16 In an <i>asp1</i> ^{D333A} strain the fluorescence signal of Mal2-GFP at the KT is increased.....	116
Figure 3-17 Mal2-GFP KT targeting is altered in <i>asp1</i> ^{D333A} and <i>asp1</i> ^{H397A} strains.....	118
Figure 3-18 Mal2-GFP KT targeting is affected by IP ₈ -levels.....	119
Figure 3-19 Schematic of the effect of Asp1-generated IP ₈ on Mal2-GFP and Fta2-GFP KT targeting.....	120
Figure 3-20 Mal2-GFP KT localization also depends on IP ₈ -levels during mitosis.....	122
Figure 3-21 Asp1 ^{H397A} present at the KT interface reduces the growth of a <i>mal2</i> ⁺ -GFP strain.....	124
Figure 3-22 Expression of <i>asp1</i> ^{H397A} -GBP-mCherry reduces Mal2-GFP fluorescence signals at the KT.....	125
Figure 3-23 Asp1 co-immunoprecipitates with Fta2-GFP.....	127

Figure 3-24 In <i>asp1</i> ^{H397A} and <i>aps1</i> Δ backgrounds the aberrant segregation phenotypes of the <i>mis15-68</i> ^{ts} strain are partially rescued.....	129
Figure 3-25 Plasmid-borne expression of <i>asp1</i> ³⁶⁵⁻⁹²⁰ reduces Mis15-68-GFP KT localization....	131
Figure 3-26 <i>mis15-68</i> ^{ts} - <i>gfp</i> and <i>asp1</i> ^{D333A} are synthetically lethal.....	132
Figure 3-27 <i>mis15</i> ⁺ - <i>gfp</i> and <i>asp1</i> ^{D333A} genetically interact.....	134
Figure 3-28 Schematic of the effect of IP ₈ on Mis15 KT targeting.....	135
Figure 3-29 Dad1 KT targeting is reduced in <i>mal2-1</i> ^{ts} and <i>mis15-68</i> ^{ts} strains.....	136
Figure 3-30 <i>mis15</i> ⁺ overexpression increases missegregation events in a <i>mal2-1</i> ^{ts} strain.....	138
Figure 3-31 <i>mis15</i> ⁺ overexpression reduces Mal2-GFP KT localization.....	139
Figure 3-32 (<i>mal2</i> ⁺ + <i>fta2</i> ⁺) overexpression reduces Mis15-68-GFP KT localization.....	140
Figure 3-33 (<i>mal2</i> ⁺ + <i>fta2</i> ⁺) overexpression induces an aberrant cell shape in the <i>mis15</i> ⁺ - <i>gfp</i> strain.....	142
Figure 3-34 (<i>mal2</i> ⁺ + <i>fta2</i> ⁺) overexpression induces an aberrant cell shape in the wild-type strain.....	143
Figure 3-35 The aberrant phenotype induced by (<i>mal2</i> ⁺ + <i>fta2</i> ⁺) overexpression in the <i>mis15</i> ⁺ - <i>gfp</i> strain gets more severe over time.....	144
Figure 3-36 Schematic of the effect of IP ₈ on Sim4-complex members and their effect on each other.....	145
Figure 3-37 A change in cellular IP ₈ -levels affects the growth of NMS-complex mutant strains.....	147
Figure 3-38 Growth of an <i>spc7-23ts</i> - <i>gfp</i> strain is not influenced by variations in cellular IP ₈ -levels.....	149
Figure 3-39 Non-physiological levels of Asp1-generated IP ₈ reduce Ndc80-GFP KT localization.....	151
Figure 3-40 Asp1 ^{H397A} rescues the thin spindle midzone of the <i>ndc80-21</i> ^{ts} strain.....	153
Figure 3-41 Ndc80, Mal2 and Mis15 only affect each other very slightly.....	155
Figure 3-42 Variations in cellular IP ₈ -levels affect the TBZ-sensitivity of an <i>SPCC594.01</i> Δ strain.....	157
Figure 3-43 <i>hpm1</i> Δ and <i>SPBC725.03</i> Δ strains are not TBZ sensitive.....	158
Figure 3-44 The effect of IP ₈ on growth of a <i>mis15-68</i> ^{ts} strain is still detectable in <i>hpm1</i> Δ and <i>SPBC725.03c</i> Δ backgrounds.....	159
Figure 3-45 First characterization of the Met10 protein.....	161
Figure 3-46 The localization pattern of Met10-GFP in interphase and mitosis.....	162
Figure 3-47 High expression of <i>met10</i> ⁺ reduces the growth of <i>mal2-1</i> ^{ts} and <i>mis15-68</i> ^{ts} strains.....	163
Figure 3-48 Mal2-GFP partially localizes to mitochondria in an <i>asp1</i> ¹⁻³⁶⁴ strain background....	165
Figure 3-49 New approach for a Ch16 loss assay.....	167
Figure 4-1 Model 1: Enhanced Mal2 and Fta2 KT targeting in the absence of Asp1-generated IP ₈ reduces the level of Ndc80 at the KT.....	178
Figure 4-2 Model 2: Asp1-generated IP ₈ regulates spindle forces and that affects chromosome segregation fidelity.....	181

7 References

- Acquaviva, C., and Pines, J. (2006). The anaphase-promoting complex/cyclosome: APC/C. *J Cell Sci* *119*, 2401-2404.
- Akera, T., Goto, Y., Sato, M., Yamamoto, M., and Watanabe, Y. (2015). Mad1 promotes chromosome congression by anchoring a kinesin motor to the kinetochore. *Nat Cell Biol* *17*, 1124-1133.
- Al-Bassam, J., and Chang, F. (2011). Regulation of microtubule dynamics by TOG-domain proteins XMAP215/Dis1 and CLASP. *Trends Cell Biol* *21*, 604-614.
- Al-Bassam, J., Kim, H., Flor-Parra, I., Lal, N., Velji, H., and Chang, F. (2012). Fission yeast Alp14 is a dose-dependent plus end-tracking microtubule polymerase. *Mol Biol Cell* *23*, 2878-2890.
- Albertson, D.G., and Thomson, J.N. (1982). The kinetochores of *Caenorhabditis elegans*. *Chromosoma* *86*, 409-428.
- Aldrup-Macdonald, M.E., and Sullivan, B.A. (2014). The past, present, and future of human centromere genomics. *Genes (Basel)* *5*, 33-50.
- Alushin, G.M., Ramey, V.H., Pasqualato, S., Ball, D.A., Grigorieff, N., Musacchio, A., and Nogales, E. (2010). The Ndc80 kinetochore complex forms oligomeric arrays along microtubules. *Nature* *467*, 805-810.
- Aoyama, K., Kawaura, R., Yamada, H., Aiba, H., and Mizuno, T. (2000). Identification and characterization of a novel gene, *hos3+*, the function of which is necessary for growth under high osmotic stress in fission yeast. *Biosci Biotechnol Biochem* *64*, 1099-1102.
- Auesukaree, C., Tochio, H., Shirakawa, M., Kaneko, Y., and Harashima, S. (2005). Plc1p, Arg82p, and Kcs1p, enzymes involved in inositol pyrophosphate synthesis, are essential for phosphate regulation and polyphosphate accumulation in *Saccharomyces cerevisiae*. *J Biol Chem* *280*, 25127-25133.
- Azevedo, C., Burton, A., Ruiz-Mateos, E., Marsh, M., and Saiardi, A. (2009). Inositol pyrophosphate mediated pyrophosphorylation of AP3B1 regulates HIV-1 Gag release. *Proc Natl Acad Sci U S A*.
- Azevedo, C., and Saiardi, A. (2017). Eukaryotic Phosphate Homeostasis: The Inositol Pyrophosphate Perspective. *Trends Biochem Sci* *42*, 219-231.
- Bahler, J., Wu, J.Q., Longtine, M.S., Shah, N.G., McKenzie, A., 3rd, Steever, A.B., Wach, A., Philippsen, P., and Pringle, J.R. (1998). Heterologous modules for efficient and versatile PCR-based gene targeting in *Schizosaccharomyces pombe* [In Process Citation]. *Yeast* *14*, 943-951.
- Baker, D.J., Dawlaty, M.M., Wijshake, T., Jeganathan, K.B., Malureanu, L., van Ree, J.H., Crespo-Diaz, R., Reyes, S., Seaburg, L., Shapiro, V., *et al.* (2013). Increased expression of BubR1 protects against aneuploidy and cancer and extends healthy lifespan. *Nat Cell Biol* *15*, 96-102.
- Baker, D.J., Jeganathan, K.B., Cameron, J.D., Thompson, M., Juneja, S., Kopecka, A., Kumar, R., Jenkins, R.B., de Groen, P.C., Roche, P., *et al.* (2004). BubR1 insufficiency causes early onset of aging-associated phenotypes and infertility in mice. *Nat Genet* *36*, 744-749.
- Beinhauer, J.D., Hagan, I.M., Hegemann, J.H., and Fleig, U. (1997). Mal3, the fission yeast homologue of the human APC-interacting protein EB-1 is required for microtubule integrity and the maintenance of cell form. *J Cell Biol* *139*, 717-728.
- Ben-Aroya, S., Pan, X., Boeke, J.D., and Hieter, P. (2010). Making temperature-sensitive mutants. *Methods Enzymol* *470*, 181-204.
- Berger, K.H., and Yaffe, M.P. (1996). Mitochondrial distribution and inheritance. *Experientia* *52*, 1111-1116.
- Berman, J. (2016). Ploidy plasticity: a rapid and reversible strategy for adaptation to stress. *FEMS Yeast Res* *16*.
- Bhandari, R., Saiardi, A., Ahmadibeni, Y., Snowman, A.M., Resnick, A.C., Kristiansen, T.Z., Molina, H., Pandey, A., Werner, J.K., Jr., Juluri, K.R., *et al.* (2007). Protein

- pyrophosphorylation by inositol pyrophosphates is a posttranslational event. *Proc Natl Acad Sci U S A* *104*, 15305-15310.
- Birnboim, H.C., and Doly, J. (1979). A rapid alkaline extraction procedure for screening recombinant plasmid DNA. *Nucleic Acids Res* *7*, 1513-1523.
- Bonatti, S., Simili, M., and Abbondandolo, A. (1972). Isolation of temperature-sensitive mutants of *Schizosaccharomyces pombe*. *J Bacteriol* *109*, 484-491.
- Bratman, S.V., and Chang, F. (2007). Stabilization of overlapping microtubules by fission yeast CLASP. *Dev Cell* *13*, 812-827.
- Britto, M., Goulet, A., Rizvi, S., von Loeffelholz, O., Moores, C.A., and Cross, R.A. (2016). *Schizosaccharomyces pombe* kinesin-5 switches direction using a steric blocking mechanism. *Proc Natl Acad Sci U S A* *113*, E7483-E7489.
- Brown, N.W., Marmelstein, A.M., and Fiedler, D. (2016). Chemical tools for interrogating inositol pyrophosphate structure and function. *Chem Soc Rev* *45*, 6311-6326.
- Buscaino, A., Allshire, R., and Pidoux, A. (2010). Building centromeres: home sweet home or a nomadic existence? *Curr Opin Genet Dev* *20*, 118-126.
- Busch, K.E., and Brunner, D. (2004). The microtubule plus end-tracking proteins mal3p and tip1p cooperate for cell-end targeting of interphase microtubules. *Curr Biol* *14*, 548-559.
- Busch, K.E., Hayles, J., Nurse, P., and Brunner, D. (2004). Tea2p kinesin is involved in spatial microtubule organization by transporting tip1p on microtubules. *Dev Cell* *6*, 831-843.
- Carbon, J., and Clarke, L. (1990). Centromere structure and function in budding and fission yeasts [published erratum appears in *New Biol* 1990 Mar;2(3):preceding 207]. *New Biol* *2*, 10-19.
- Carroll, C.W., Silva, M.C., Godek, K.M., Jansen, L.E., and Straight, A.F. (2009). Centromere assembly requires the direct recognition of CENP-A nucleosomes by CENP-N. *Nat Cell Biol* *11*, 896-902.
- Cheeseman, I.M., Chappie, J.S., Wilson-Kubalek, E.M., and Desai, A. (2006). The conserved KMN network constitutes the core microtubule-binding site of the kinetochore. *Cell* *127*, 983-997.
- Cheeseman, I.M., and Desai, A. (2008). Molecular architecture of the kinetochore-microtubule interface. *Nat Rev Mol Cell Biol* *9*, 33-46.
- Chen, Y.H., Wang, G.Y., Hao, H.C., Chao, C.J., Wang, Y., and Jin, Q.W. (2017). Facile manipulation of protein localization in fission yeast through binding of GFP-binding protein to GFP. *J Cell Sci* *130*, 1003-1015.
- Chiron, S., Bobkova, A., Zhou, H., and Yaffe, M.P. (2008). CLASP regulates mitochondrial distribution in *Schizosaccharomyces pombe*. *J Cell Biol* *182*, 41-49.
- Chmielewska, A.E., Tang, N.H., and Toda, T. (2016). The hairpin region of Ndc80 is important for the kinetochore recruitment of Mph1/MPS1 in fission yeast. *Cell Cycle* *15*, 740-747.
- Choi, E.S., Stralfors, A., Catania, S., Castillo, A.G., Svensson, J.P., Pidoux, A.L., Ekwall, K., and Allshire, R.C. (2012). Factors that promote H3 chromatin integrity during transcription prevent promiscuous deposition of CENP-A(Cnp1) in fission yeast. *PLoS Genet* *8*, e1002985.
- Choi, S.H., and McCollum, D. (2012). A role for metaphase spindle elongation forces in correction of merotelic kinetochore attachments. *Curr Biol* *22*, 225-230.
- Ciferri, C., Musacchio, A., and Petrovic, A. (2007). The Ndc80 complex: hub of kinetochore activity. *FEBS Lett* *581*, 2862-2869.
- Clarke, L., Amstutz, H., Fishel, B., and Carbon, J. (1986). Analysis of centromeric DNA in the fission yeast *Schizosaccharomyces pombe*. *Proc Natl Acad Sci U S A* *83*, 8253-8257.
- Clarke, L., and Carbon, J. (1980). Isolation of a yeast centromere and construction of functional small circular chromosomes. *Nature* *287*, 504-509.
- Clarke, L., and Carbon, J. (1985). The structure and function of yeast centromeres. *Annu Rev Genet* *19*, 29-55.
- Cleveland, D.W., Mao, Y., and Sullivan, K.F. (2003). Centromeres and kinetochores: from epigenetics to mitotic checkpoint signaling. *Cell* *112*, 407-421.
- Coffman, V.C., and Wu, J.Q. (2012). Counting protein molecules using quantitative fluorescence microscopy. *Trends Biochem Sci* *37*, 499-506.

- Coffman, V.C., and Wu, J.Q. (2014). Every laboratory with a fluorescence microscope should consider counting molecules. *Mol Biol Cell* **25**, 1545-1548.
- Coffman, V.C., Wu, P., Parthun, M.R., and Wu, J.Q. (2011). CENP-A exceeds microtubule attachment sites in centromere clusters of both budding and fission yeast. *J Cell Biol* **195**, 563-572.
- Cottarel, G., Shero, J.H., Hieter, P., and Hegemann, J.H. (1989). A 125-base-pair CEN6 DNA fragment is sufficient for complete meiotic and mitotic centromere functions in *Saccharomyces cerevisiae*. *Mol Cell Biol* **9**, 3342-3349.
- Courtheoux, T., Gay, G., Gachet, Y., and Tournier, S. (2009). Ase1/Prc1-dependent spindle elongation corrects merotelically during anaphase in fission yeast. *J Cell Biol* **187**, 399-412.
- Deluca, K.F., Lens, S.M., and Deluca, J.G. (2011). Temporal changes in Hec1 phosphorylation control kinetochore-microtubule attachment stability during mitosis. *J Cell Sci*.
- Ding, R., McDonald, K.L., and McIntosh, J.R. (1993). Three-dimensional reconstruction and analysis of mitotic spindles from the yeast, *Schizosaccharomyces pombe*. *J Cell Biol* **120**, 141-151.
- Ding, R., West, R.R., Morphew, D.M., Oakley, B.R., and McIntosh, J.R. (1997). The spindle pole body of *Schizosaccharomyces pombe* enters and leaves the nuclear envelope as the cell cycle proceeds. *Mol Biol Cell* **8**, 1461-1479.
- Dodgson, J., Chessel, A., Yamamoto, M., Vaggi, F., Cox, S., Rosten, E., Albrecht, D., Geymonat, M., Csikasz-Nagy, A., Sato, M., *et al.* (2013). Spatial segregation of polarity factors into distinct cortical clusters is required for cell polarity control. *Nat Commun* **4**, 1834.
- Dower, W.J., Miller, J.F., and Ragsdale, C.W. (1988). High efficiency transformation of *E. coli* by high voltage electroporation. *Nucleic Acids Res* **16**, 6127-6145.
- Draskovic, P., Saiardi, A., Bhandari, R., Burton, A., Ilc, G., Kovacevic, M., Snyder, S.H., and Podobnik, M. (2008). Inositol hexakisphosphate kinase products contain diphosphate and triphosphate groups. *Chem Biol* **15**, 274-286.
- Dubois, E., Scherens, B., Vierendeels, F., Ho, M.M., Messenguy, F., and Shears, S.B. (2002). In *Saccharomyces cerevisiae*, the inositol polyphosphate kinase activity of Kcs1p is required for resistance to salt stress, cell wall integrity, and vacuolar morphogenesis. *J Biol Chem* **277**, 23755-23763.
- Duesberg, P., Li, R., Fabarius, A., and Hehlmann, R. (2006). Aneuploidy and cancer: from correlation to causation. *Contrib Microbiol* **13**, 16-44.
- Durand-Dubief, M., and Ekwall, K. (2008). Heterochromatin tells CENP-A where to go. *Bioessays* **30**, 526-529.
- Eckert, C.A., Gravidahl, D.J., and Megee, P.C. (2007). The enhancement of pericentromeric cohesin association by conserved kinetochore components promotes high-fidelity chromosome segregation and is sensitive to microtubule-based tension. *Genes Dev* **21**, 278-291.
- Edamatsu, M. (2014). Bidirectional motility of the fission yeast kinesin-5, Cut7. *Biochem Biophys Res Commun* **446**, 231-234.
- Egel, R., Willer, M., Kjaerulff, S., Davey, J., and Nielsen, O. (1994). Assessment of pheromone production and response in fission yeast by a halo test of induced sporulation. *Yeast* **10**, 1347-1354.
- Ekwall, K. (2004). The roles of histone modifications and small RNA in centromere function. *Chromosome Res* **12**, 535-542.
- Ekwall, K., Javerzat, J.P., Lorentz, A., Schmidt, H., Cranston, G., and Allshire, R. (1995). The chromodomain protein Swi6: a key component at fission yeast centromeres. *Science* **269**, 1429-1431.
- Ekwall, K., and Ruusala, T. (1994). Mutations in rik1, clr2, clr3 and clr4 genes asymmetrically derepress the silent mating-type loci in fission yeast. *Genetics* **136**, 53-64.
- Eskat, A., Deng, W., Hofmeister, A., Rudolphi, S., Emmerth, S., Hellwig, D., Ulbricht, T., Doring, V., Bancroft, J.M., McAinsh, A.D., *et al.* (2012). Step-wise assembly, maturation and dynamic behavior of the human CENP-P/O/R/Q/U kinetochore sub-complex. *PLoS One* **7**, e44717.

- Fang, J., Liu, Y., Wei, Y., Deng, W., Yu, Z., Huang, L., Teng, Y., Yao, T., You, Q., Ruan, H., *et al.* (2015). Structural transitions of centromeric chromatin regulate the cell cycle-dependent recruitment of CENP-N. *Genes Dev* 29, 1058-1073.
- Fennessy, D., Grallert, A., Krapp, A., Cokoja, A., Bridge, A.J., Petersen, J., Patel, A., Tallada, V.A., Boke, E., Hodgson, B., *et al.* (2014). Extending the *Schizosaccharomyces pombe* molecular genetic toolbox. *PLoS One* 9, e97683.
- Feoktistova, A., McCollum, D., Ohi, R., and Gould, K.L. (1999). Identification and characterization of *Schizosaccharomyces pombe* *asp1(+)*, a gene that interacts with mutations in the Arp2/3 complex and actin. *Genetics* 152, 895-908.
- Fischbach, P. (2016). Modulatoren des Mikrotubulizytoskeletts in *Schizosaccharomyces pombe*. In *Eukaryotic Microbiology* (HHU Düsseldorf).
- Fleig, U., Sen-Gupta, M., and Hegemann, J.H. (1996). Fission yeast *mal2+* is required for chromosome segregation. *Mol Cell Biol* 16, 6169-6177.
- Foltz, D.R., Jansen, L.E., Bailey, A.O., Yates, J.R., 3rd, Bassett, E.A., Wood, S., Black, B.E., and Cleveland, D.W. (2009). Centromere-specific assembly of CENP-a nucleosomes is mediated by HJURP. *Cell* 137, 472-484.
- Foltz, D.R., Jansen, L.E., Black, B.E., Bailey, A.O., Yates, J.R., 3rd, and Cleveland, D.W. (2006). The human CENP-A centromeric nucleosome-associated complex. *Nat Cell Biol* 8, 458-469.
- Forsburg, S.L. (1993). Comparison of *Schizosaccharomyces pombe* expression systems. *Nucleic Acids Res* 21, 2955-2956.
- Forsburg, S.L., and Nurse, P. (1991). Cell cycle regulation in the yeasts *Saccharomyces cerevisiae* and *Schizosaccharomyces pombe*. *Annu Rev Cell Biol* 7, 227-256.
- Forsburg, S.L., and Rhind, N. (2006). Basic methods for fission yeast. *Yeast* 23, 173-183.
- Franco, A., Meadows, J.C., and Millar, J.B. (2007). The Dam1/DASH complex is required for the retrieval of unclustered kinetochores in fission yeast. *J Cell Sci* 120, 3345-3351.
- Fridy, P.C., Otto, J.C., Dollins, D.E., and York, J.D. (2007). Cloning and characterization of two human VIP1-like inositol hexakisphosphate and diphosphoinositol pentakisphosphate kinases. *J Biol Chem* 282, 30754-30762.
- Fu, C., Jain, D., Costa, J., Velve-Casquillas, G., and Tran, P.T. (2011). *mmb1p* binds mitochondria to dynamic microtubules. *Curr Biol* 21, 1431-1439.
- Fujita, Y., Hayashi, T., Kiyomitsu, T., Toyoda, Y., Kokubu, A., Obuse, C., and Yanagida, M. (2007). Priming of centromere for CENP-A recruitment by human hMis18alpha, hMis18beta, and M18BP1. *Dev Cell* 12, 17-30.
- Fukagawa, T. (2004). Centromere DNA, proteins and kinetochore assembly in vertebrate cells. *Chromosome Res* 12, 557-567.
- Furuta, K., Edamatsu, M., Maeda, Y., and Toyoshima, Y.Y. (2008). Diffusion and directed movement: in vitro motile properties of fission yeast kinesin-14 Pkl1. *J Biol Chem* 283, 36465-36473.
- Gachet, Y., Reyes, C., Courtheoux, T., Goldstone, S., Gay, G., Serrurier, C., and Tournier, S. (2008). Sister kinetochore recapture in fission yeast occurs by two distinct mechanisms, both requiring Dam1 and Klp2. *Mol Biol Cell* 19, 1646-1662.
- Galjart, N. (2010). Plus-end-tracking proteins and their interactions at microtubule ends. *Curr Biol* 20, R528-537.
- Garcia, M.A., Koonrugsa, N., and Toda, T. (2002a). Spindle-kinetochore attachment requires the combined action of Kin I-like Klp5/6 and Alp14/Dis1-MAPs in fission yeast. *Embo J* 21, 6015-6024.
- Garcia, M.A., Koonrugsa, N., and Toda, T. (2002b). Two kinesin-like Kin I family proteins in fission yeast regulate the establishment of metaphase and the onset of anaphase A. *Curr Biol* 12, 610-621.
- Garcia, M.A., Vardy, L., Koonrugsa, N., and Toda, T. (2001). Fission yeast ch-TOG/XMAP215 homologue Alp14 connects mitotic spindles with the kinetochore and is a component of the Mad2-dependent spindle checkpoint. *Embo J* 20, 3389-3401.
- Gartenberg, M. (2009). Heterochromatin and the cohesion of sister chromatids. *Chromosome Res* 17, 229-238.

- Gerasimaite, R., Pavlovic, I., Capolicchio, S., Hofer, A., Schmidt, A., Jessen, H.J., and Mayer, A. (2017). Inositol Pyrophosphate Specificity of the SPX-Dependent Polyphosphate Polymerase VTC. *ACS Chem Biol* 12, 648-653.
- Gergely, Z.R., Crapo, A., Hough, L.E., McIntosh, J.R., and Betterton, M.D. (2016). Kinesin-8 effects on mitotic microtubule dynamics contribute to spindle function in fission yeast. *Mol Biol Cell* 27, 3490-3514.
- Giam, M., and Rancati, G. (2015). Aneuploidy and chromosomal instability in cancer: a jackpot to chaos. *Cell Div* 10, 3.
- Gietz R.D., W.R.A. (2006). Yeast Transformation by the LiAc/SS Carrier DNA/PEG Method. In *Methods in Molecular Biology* 313: Yeast Protocols, 2nd edition
- W. Xiao, ed. (Totowa, New Jersey: Humana Press), pp. p. 107-120.
- Golub, E.I. (1988). 'One minute' transformation of competent E. coli by plasmid DNA. *Nucleic Acids Res* 16, 1641.
- Gomez, E.B., and Forsburg, S.L. (2004). Analysis of the fission yeast *Schizosaccharomyces pombe* cell cycle. *Methods Mol Biol* 241, 93-111.
- Gordon, D.J., Resio, B., and Pellman, D. (2012). Causes and consequences of aneuploidy in cancer. *Nat Rev Genet* 13, 189-203.
- Goshima, G., Saitoh, S., and Yanagida, M. (1999). Proper metaphase spindle length is determined by centromere proteins Mis12 and Mis6 required for faithful chromosome segregation. *Genes and Development* 13, 1664-1677.
- Gould, K.L., and Nurse, P. (1989). Tyrosine phosphorylation of the fission yeast *cdc2+* protein kinase regulates entry into mitosis [see comments]. *Nature* 342, 39-45.
- Gregan, J., Polakova, S., Zhang, L., Tolic-Norrelykke, I.M., and Cimini, D. (2011). Merotelic kinetochore attachment: causes and effects. *Trends Cell Biol* 21, 374-381.
- Gu, C., Nguyen, H.N., Hofer, A., Jessen, H.J., Dai, X., Wang, H., and Shears, S.B. (2017). The Significance of the Bifunctional Kinase/Phosphatase Activities of Diphosphoinositol Pentakisphosphate Kinases (PPIP5Ks) for Coupling Inositol Pyrophosphate Cell Signaling to Cellular Phosphate Homeostasis. *J Biol Chem* 292, 4544-4555.
- Hagan, I., and Yanagida, M. (1990). Novel potential mitotic motor protein encoded by the fission yeast *cut7+* gene. *Nature* 347, 563-566.
- Hagan, I., and Yanagida, M. (1992). Kinesin-related *cut7* protein associates with mitotic and meiotic spindles in fission yeast. *Nature* 356, 74-76.
- Hagan, I., and Yanagida, M. (1995). The product of the spindle formation gene *sad1+* associates with the fission yeast spindle pole body and is essential for viability. *J Cell Biol* 129, 1033-1047.
- Hagan, I.M., and Hyams, J.S. (1988). The use of cell division cycle mutants to investigate the control of microtubule distribution in the fission yeast *Schizosaccharomyces pombe*. *J Cell Sci* 89, 343-357.
- Hanahan, D., and Weinberg, R.A. (2011). Hallmarks of cancer: the next generation. *Cell* 144, 646-674.
- Hansen, J., Cherest, H., and Kielland-Brandt, M.C. (1994). Two divergent MET10 genes, one from *Saccharomyces cerevisiae* and one from *Saccharomyces carlsbergensis*, encode the alpha subunit of sulfite reductase and specify potential binding sites for FAD and NADPH. *J Bacteriol* 176, 6050-6058.
- Haring, M., Offermann, S., Danker, T., Horst, I., Peterhansel, C., and Stam, M. (2007). Chromatin immunoprecipitation: optimization, quantitative analysis and data normalization. *Plant Methods* 3, 11.
- Hauf, S., Roitinger, E., Koch, B., Dittrich, C.M., Mechtler, K., and Peters, J.M. (2005). Dissociation of cohesin from chromosome arms and loss of arm cohesion during early mitosis depends on phosphorylation of SA2. *PLoS Biol* 3, e69.
- Hayashi, A., Asakawa, H., Haraguchi, T., and Hiraoka, Y. (2006). Reconstruction of the kinetochore during meiosis in fission yeast *Schizosaccharomyces pombe*. *Mol Biol Cell* 17, 5173-5184.
- Hayashi, T., Ebe, M., Nagao, K., Kokubu, A., Sajiki, K., and Yanagida, M. (2014). *Schizosaccharomyces pombe* centromere protein Mis19 links Mis16 and Mis18 to recruit

- CENP-A through interacting with NMD factors and the SWI/SNF complex. *Genes Cells* 19, 541-554.
- Hayashi, T., Fujita, Y., Iwasaki, O., Adachi, Y., Takahashi, K., and Yanagida, M. (2004). Mis16 and Mis18 are required for CENP-A loading and histone deacetylation at centromeres. *Cell* 118, 715-729.
- Hayles, J., and Nurse, P. (1989). A review of mitosis in the fission yeast *Schizosaccharomyces pombe*. *Exp Cell Res* 184, 273-286.
- He, X., Jones, M.H., Winey, M., and Sazer, S. (1998). Mph1, a member of the Mps1-like family of dual specificity protein kinases, is required for the spindle checkpoint in *S. pombe*. *J Cell Sci* 111, 1635-1647.
- Heck, M.M. (1997). Condensins, cohesins, and chromosome architecture: how to make and break a mitotic chromosome. *Cell* 91, 5-8.
- Heinrich, S., Windecker, H., Hustedt, N., and Hauf, S. (2012). Mph1 kinetochore localization is crucial and upstream in the hierarchy of spindle assembly checkpoint protein recruitment to kinetochores. *J Cell Sci* 125, 4720-4727.
- Hemmerich, P., Weidtkamp-Peters, S., Hoischen, C., Schmiedeberg, L., Erliandri, I., and Diekmann, S. (2008). Dynamics of inner kinetochore assembly and maintenance in living cells. *J Cell Biol* 180, 1101-1114.
- Hoffman, C.S., Wood, V., and Fantes, P.A. (2015). An Ancient Yeast for Young Geneticists: A Primer on the *Schizosaccharomyces pombe* Model System. *Genetics* 201, 403-423.
- Hsu, K.S., and Toda, T. (2011). Ndc80 Internal Loop Interacts with Dis1/TOG to Ensure Proper Kinetochore-Spindle Attachment in Fission Yeast. *Curr Biol*.
- Ingram, S.W., Safrany, S.T., and Barnes, L.D. (2003). Disruption and overexpression of the *Schizosaccharomyces pombe* *aps1* gene, and effects on growth rate, morphology and intracellular diadenosine 5',5'''-P1,P5-pentaphosphate and diphosphoinositol polyphosphate concentrations. *Biochem J* 369, 519-528.
- Ito, S., Tan, L.J., Andoh, D., Narita, T., Seki, M., Hirano, Y., Narita, K., Kuraoka, I., Hiraoka, Y., and Tanaka, K. (2010). MMXD, a TFIIH-independent XPD-MMS19 protein complex involved in chromosome segregation. *Mol Cell* 39, 632-640.
- Jajoo, R., Jung, Y., Huh, D., Viana, M.P., Rafelski, S.M., Springer, M., and Paulsson, J. (2016). Accurate concentration control of mitochondria and nucleoids. *Science* 351, 169-172.
- Jakopec, V. (2006). Charakterisierung des Mitose-relevanten *fta2⁺* Gens in *Schizosaccharomyces pombe*
- Jakopec, V., Topolski, B., and Fleig, U. (2012). Sos7, an essential component of the conserved *S. pombe* Ndc80-MIND-Spc7 complex, identifies a new family of fungal kinetochore proteins. *Mol Cell Biol*.
- Janson, M.E., Loughlin, R., Loiodice, I., Fu, C., Brunner, D., Nedelec, F.J., and Tran, P.T. (2007). Crosslinkers and motors organize dynamic microtubules to form stable bipolar arrays in fission yeast. *Cell* 128, 357-368.
- Jehn, B., Niedenthal, R., and Hegemann, J.H. (1991). In vivo analysis of the *Saccharomyces cerevisiae* centromere CDEIII sequence: requirements for mitotic chromosome segregation. *Mol Cell Biol* 11, 5212-5221.
- Jin, Q.W., Pidoux, A.L., Decker, C., Allshire, R.C., and Fleig, U. (2002). The mal2p protein is an essential component of the fission yeast centromere. *Mol Cell Biol* 22, 7168-7183.
- Kadura, S., and Sazer, S. (2005). SAC-ing mitotic errors: how the spindle assembly checkpoint (SAC) plays defense against chromosome mis-segregation. *Cell Motil Cytoskeleton* 61, 145-160.
- Kaiser, C., Michaelis, S., and Mitchell, A. (1994). *Methods in Yeast Genetics*, 1994 edn (Cold Spring Harbor: Cold Spring Harbor Laboratory Press).
- Karig, I.E. (2004). Funktionelle Analyse mitotischer Komponenten in der Spaltheefe *Schizosaccharomyces pombe*. Dissertation HHU Düsseldorf.
- Kerres, A., Jakopec, V., Beuter, C., Karig, I., Pohlmann, J., Pidoux, A., Allshire, R., and Fleig, U. (2006). Fta2, an essential fission yeast kinetochore component, interacts closely with the conserved mal2 protein. *Mol Biol Cell* 17, 4167-4178.

- Kerres, A., Jakopec, V., and Fleig, U. (2007). The conserved Spc7 protein is required for spindle integrity and links kinetochore complexes in fission yeast. *Mol Biol Cell* **18**, 2441-2454.
- Kerres, A., Vietmeier-Decker, C., Ortiz, J., Karig, I., Beuter, C., Hegemann, J., Lechner, J., and Fleig, U. (2004). The Fission Yeast Kinetochore Component Spc7 Associates with the EB1 Family Member Mal3 and Is Required for Kinetochore-Spindle Association. *Mol Biol Cell* **15**, 5255-5267.
- Kettenbach, A.N., Deng, L., Wu, Y., Baldissard, S., Adamo, M.E., Gerber, S.A., and Moseley, J.B. (2015). Quantitative phosphoproteomics reveals pathways for coordination of cell growth and division by the conserved fission yeast kinase pom1. *Mol Cell Proteomics* **14**, 1275-1287.
- Kiffe-Delf, A.L. (2016). Funktionelle Charakterisierung des Proteins SPCC584.01c in der Spaltheife *Schizosaccharomyces pombe*. In Funktionelle Genomforschung (HHU Düsseldorf).
- Kim, D.U., Hayles, J., Kim, D., Wood, V., Park, H.O., Won, M., Yoo, H.S., Duhig, T., Nam, M., Palmer, G., et al. (2010). Analysis of a genome-wide set of gene deletions in the fission yeast *Schizosaccharomyces pombe*. *Nat Biotechnol* **28**, 617-623.
- Kim, S., and Yu, H. (2015). Multiple assembly mechanisms anchor the KMN spindle checkpoint platform at human mitotic kinetochores. *J Cell Biol* **208**, 181-196.
- Kingsbury, M.A., Yung, Y.C., Peterson, S.E., Westra, J.W., and Chun, J. (2006). Aneuploidy in the normal and diseased brain. *Cell Mol Life Sci* **63**, 2626-2641.
- Koch, A., Krug, K., Pengelley, S., Macek, B., and Hauf, S. (2011). Mitotic substrates of the kinase aurora with roles in chromatin regulation identified through quantitative phosphoproteomics of fission yeast. *Sci Signal* **4**, rs6.
- Kops, G.J., and Shah, J.V. (2012). Connecting up and clearing out: how kinetochore attachment silences the spindle assembly checkpoint. *Chromosoma* **121**, 509-525.
- Kruger, N., and Tolic-Norrelykke, I.M. (2008). Association of mitochondria with spindle poles facilitates spindle alignment. *Curr Biol* **18**, R646-R647.
- Laha, D., Johnen, P., Azevedo, C., Dynowski, M., Weiss, M., Capolicchio, S., Mao, H., Iven, T., Steenbergen, M., Freyer, M., et al. (2015). VIH2 Regulates the Synthesis of Inositol Pyrophosphate InsP8 and Jasmonate-Dependent Defenses in Arabidopsis. *Plant Cell* **27**, 1082-1097.
- Lando, D., Endesfelder, U., Berger, H., Subramanian, L., Dunne, P.D., McColl, J., Klenerman, D., Carr, A.M., Sauer, M., Allshire, R.C., et al. (2012). Quantitative single-molecule microscopy reveals that CENP-A(Cnp1) deposition occurs during G2 in fission yeast. *Open Biol* **2**, 120078.
- Latzer, J., Shen, T., and Wolynes, P.G. (2008). Conformational switching upon phosphorylation: a predictive framework based on energy landscape principles. *Biochemistry* **47**, 2110-2122.
- Lee, Y.S., Huang, K., Quioco, F.A., and O'Shea, E.K. (2008). Molecular basis of cyclin-CDK-CKI regulation by reversible binding of an inositol pyrophosphate. *Nat Chem Biol* **4**, 25-32.
- Lee, Y.S., Mulugu, S., York, J.D., and O'Shea, E.K. (2007). Regulation of a cyclin-CDK-CKI inhibitor complex by inositol pyrophosphates. *Science* **316**, 109-112.
- Legro, R.S. (2012). Turner syndrome: new insights into an old disorder. *Fertil Steril* **98**, 773-774.
- Leverson, J.D., Huang, H.K., Forsburg, S.L., and Hunter, T. (2002). The *Schizosaccharomyces pombe* aurora-related kinase Ark1 interacts with the inner centromere protein Pic1 and mediates chromosome segregation and cytokinesis. *Mol Biol Cell* **13**, 1132-1143.
- Li, T., Zheng, F., Cheung, M., Wang, F., and Fu, C. (2015). Fission yeast mitochondria are distributed by dynamic microtubules in a motor-independent manner. *Sci Rep* **5**, 11023.
- Lin, H., Fridy, P.C., Ribeiro, A.A., Choi, J.H., Barma, D.K., Vogel, G., Falck, J.R., Shears, S.B., York, J.D., and Mayr, G.W. (2009). Structural analysis and detection of biological inositol pyrophosphates reveal that the family of VIP/diphosphoinositol pentakisphosphate kinases are 1/3-kinases. *J Biol Chem* **284**, 1863-1872.

- Liu, X., McLeod, I., Anderson, S., Yates, J.R., 3rd, and He, X. (2005). Molecular analysis of kinetochore architecture in fission yeast. *Embo J* 24, 2919-2930.
- Liodice, I., Staub, J., Setty, T.G., Nguyen, N.P., Paoletti, A., and Tran, P.T. (2005). Ase1p organizes antiparallel microtubule arrays during interphase and mitosis in fission yeast. *Mol Biol Cell* 16, 1756-1768.
- Lorca, T., Labbe, J.C., Devault, A., Fesquet, D., Capony, J.P., Cavadore, J.C., Le Bouffant, F., and Doree, M. (1992). Dephosphorylation of cdc2 on threonine 161 is required for cdc2 kinase inactivation and normal anaphase. *Embo J* 11, 2381-2390.
- Luo, H.R., Huang, Y.E., Chen, J.C., Saiardi, A., Iijima, M., Ye, K., Huang, Y., Nagata, E., Devreotes, P., and Snyder, S.H. (2003). Inositol pyrophosphates mediate chemotaxis in *Dictyostelium* via pleckstrin homology domain-PtdIns(3,4,5)P₃ interactions. *Cell* 114, 559-572.
- Maiato, H., Sampaio, P., and Sunkel, C.E. (2004). Microtubule-associated proteins and their essential roles during mitosis. *Int Rev Cytol* 241, 53-153.
- Mallavarapu, A., Sawin, K., and Mitchison, T. (1999). A switch in microtubule dynamics at the onset of anaphase B in the mitotic spindle of *Schizosaccharomyces pombe*. *Curr Biol* 9, 1423-1426.
- Maniatis, T., Fritsch, E.F., and Sambrook, J. (1989). "Molecular cloning. A laboratory manual." (Cold Spring Harbor, New York: Cold Spring Harbor Laboratory Press).
- Marks, J., Hagan, I.M., and Hyams, J.S. (1986). Growth polarity and cytokinesis in fission yeast: the role of the cytoskeleton. *J Cell Sci Suppl* 5, 229-241.
- Matsuo, Y., Maurer, S.P., Surrey, T., and Toda, T. (2017). Purification and characterisation of the fission yeast Ndc80 complex. *Protein Expr Purif* 135, 61-69.
- Matsuo, Y., Maurer, S.P., Yukawa, M., Zakian, S., Singleton, M.R., Surrey, T., and Toda, T. (2016). An unconventional interaction between Dis1/TOG and Mal3/EB1 in fission yeast promotes the fidelity of chromosome segregation. *J Cell Sci* 129, 4592-4606.
- McAinsh, A.D., and Meraldi, P. (2011). The CCAN complex: linking centromere specification to control of kinetochore-microtubule dynamics. *Semin Cell Dev Biol* 22, 946-952.
- McAinsh, A.D., Meraldi, P., Draviam, V.M., Toso, A., and Sorger, P.K. (2006). The human kinetochore proteins Nnf1R and Mcm21R are required for accurate chromosome segregation. *Embo J* 25, 4033-4049.
- McAinsh, A.D., Tytell, J.D., and Sorger, P.K. (2003). Structure, function, and regulation of budding yeast kinetochores. *Annu Rev Cell Dev Biol* 19, 519-539.
- McClelland, M.L., Gardner, R.D., Kallio, M.J., Daum, J.R., Gorbisky, G.J., Burke, D.J., and Stukenberg, P.T. (2003). The highly conserved Ndc80 complex is required for kinetochore assembly, chromosome congression, and spindle checkpoint activity. *Genes Dev* 17, 101-114.
- McClelland, S.E., Borusu, S., Amaro, A.C., Winter, J.R., Belwal, M., McAinsh, A.D., and Meraldi, P. (2007). The CENP-A NAC/CAD kinetochore complex controls chromosome congression and spindle bipolarity. *Embo J* 26, 5033-5047.
- McCully, E.K., and Robinow, C.F. (1971). Mitosis in the fission yeast *Schizosaccharomyces pombe*: a comparative study with light and electron microscopy. *J Cell Sci* 9, 475-507.
- McKinley, K.L., Sekulic, N., Guo, L.Y., Tsinman, T., Black, B.E., and Cheeseman, I.M. (2015). The CENP-L-N Complex Forms a Critical Node in an Integrated Meshwork of Interactions at the Centromere-Kinetochore Interface. *Mol Cell* 60, 886-898.
- McLean, J.R., Chaix, D., Ohi, M.D., and Gould, K.L. (2011). State of the APC/C: organization, function, and structure. *Crit Rev Biochem Mol Biol* 46, 118-136.
- Meadows, J.C., Shepperd, L.A., Vanoosthuyse, V., Lancaster, T.C., Sochaj, A.M., Buttrick, G.J., Hardwick, K.G., and Millar, J.B. (2011). Spindle checkpoint silencing requires association of PP1 to both Spc7 and kinesin-8 motors. *Dev Cell* 20, 739-750.
- Michaelis, C., Ciosk, R., and Nasmyth, K. (1997). Cohesins: chromosomal proteins that prevent premature separation of sister chromatids. *Cell* 91, 35-45.
- Miranda, J.J., De Wulf, P., Sorger, P.K., and Harrison, S.C. (2005). The yeast DASH complex forms closed rings on microtubules. *Nat Struct Mol Biol* 12, 138-143.
- Mitchison, T.J., and Kirschner, M.W. (1984). Dynamic instability of microtubule growth. *Nature* 312, 237-242.

- Moreno, M.B., Duran, A., and Ribas, J.C. (2000). A family of multifunctional thiamine-repressible expression vectors for fission yeast. *Yeast* *16*, 861-872.
- Moreno, S., Klar, A., and Nurse, P. (1991). Molecular genetic analysis of fission yeast *Schizosaccharomyces pombe*. *Methods Enzymol* *194*, 795-823.
- Mulugu, S., Bai, W., Fridy, P.C., Bastidas, R.J., Otto, J.C., Dollins, D.E., Haystead, T.A., Ribeiro, A.A., and York, J.D. (2007). A conserved family of enzymes that phosphorylate inositol hexakisphosphate. *Science* *316*, 106-109.
- Musacchio, A., and Desai, A. (2017). *A Molecular View of Kinetochores Assembly and Function*. Biology (Basel) *6*.
- Musacchio, A., and Salmon, E.D. (2007). The spindle-assembly checkpoint in space and time. *Nat Rev Mol Cell Biol* *8*, 379-393.
- Nabeshima, K., Kurooka, H., Takeuchi, M., Kinoshita, K., Nakaseko, Y., and Yanagida, M. (1995). p93dis1, which is required for sister chromatid separation, is a novel microtubule and spindle pole body-associating protein phosphorylated at the Cdc2 target sites. *Genes Dev* *9*, 1572-1585.
- Nabeshima, K., Nakagawa, T., Straight, A.F., Murray, A., Chikashige, Y., Yamashita, Y.M., Hiraoka, Y., and Yanagida, M. (1998). Dynamics of centromeres during metaphase-anaphase transition in fission yeast: Dis1 is implicated in force balance in metaphase bipolar spindle. *Mol Biol Cell* *9*, 3211-3225.
- Nakamichi, N., Yamamoto, E., Yamada, H., Aiba, H., and Mizuno, T. (2000). Identification and characterization of a novel gene, *hos2+*, the function of which is necessary for growth under high osmotic stress in fission yeast. *Biosci Biotechnol Biochem* *64*, 2493-2496.
- Nakaseko, Y., Goshima, G., Morishita, J., and Yanagida, M. (2001). M phase-specific kinetochores proteins in fission yeast. Microtubule- associating Dis1 and Mtc1 display rapid separation and segregation during anaphase. *Curr Biol* *11*, 537-549.
- Nakazawa, N., Nakamura, T., Kokubu, A., Ebe, M., Nagao, K., and Yanagida, M. (2008). Dissection of the essential steps for condensin accumulation at kinetochores and rDNAs during fission yeast mitosis. *J Cell Biol* *180*, 1115-1131.
- Nishi, H., Hashimoto, K., and Panchenko, A.R. (2011). Phosphorylation in protein-protein binding: effect on stability and function. *Structure* *19*, 1807-1815.
- Nishino, T., Rago, F., Hori, T., Tomii, K., Cheeseman, I.M., and Fukagawa, T. (2013). CENP-T provides a structural platform for outer kinetochores assembly. *EMBO J* *32*, 424-436.
- Niwa, O., Matsumoto, T., Chikashige, Y., and Yanagida, M. (1989). Characterization of *Schizosaccharomyces pombe* minichromosome deletion derivatives and a functional allocation of their centromere. *Embo J* *8*, 3045-3052.
- Niwa, O., Matsumoto, T., and Yanagida, M. (1986). Construction of a mini-chromosome by deletion and its mitotic and meiotic behaviour in fission yeast. *Mol Gen Genet* *203*, 397-405.
- Nurse, P. (1990). Universal control mechanism regulating onset of M-phase. *Nature* *344*, 503-508.
- Nurse, P., and Thuriaux, P. (1980). Regulatory genes controlling mitosis in the fission yeast *Schizosaccharomyces pombe*. *Genetics* *96*, 627-637.
- Nurse, P., Thuriaux, P., and Nasmyth, K. (1976). Genetic control of the cell division cycle in the fission yeast *Schizosaccharomyces pombe*. *Mol Gen Genet* *146*, 167-178.
- Obuse, C., Iwasaki, O., Kiyomitsu, T., Goshima, G., Toyoda, Y., and Yanagida, M. (2004). A conserved Mis12 centromere complex is linked to heterochromatic HP1 and outer kinetochores protein Zwint-1. *Nat Cell Biol* *6*, 1135-1141.
- Okazaki, K., Okazaki, N., Kume, K., Jinno, S., Tanaka, K., and Okayama, H. (1990). High-frequency transformation method and library transducing vectors for cloning mammalian cDNAs by trans-complementation of *Schizosaccharomyces pombe*. *Nucleic Acids Res* *18*, 6485-6489.
- Olmsted, Z.T., Colliver, A.G., Riehlman, T.D., and Paluh, J.L. (2014). Kinesin-14 and kinesin-5 antagonistically regulate microtubule nucleation by gamma-TuRC in yeast and human cells. *Nat Commun* *5*, 5339.
- Page, B.D., and Snyder, M. (1993). Chromosome segregation in yeast. *Annu Rev Microbiol* *47*, 231-261.

- Palmer, D.K., O'Day, K., Wener, M.H., Andrews, B.S., and Margolis, R.L. (1987). A 17-kD centromere protein (CENP-A) copurifies with nucleosome core particles and with histones. *J Cell Biol* 104, 805-815.
- Pandey, R., Heeger, S., and Lehner, C.F. (2007). Rapid effects of acute anoxia on spindle kinetochore interactions activate the mitotic spindle checkpoint. *J Cell Sci* 120, 2807-2818.
- Pesesse, X., Choi, K., Zhang, T., and Shears, S.B. (2004). Signaling by higher inositol polyphosphates. Synthesis of bisdiphosphoinositol tetrakisphosphate ("InsP8") is selectively activated by hyperosmotic stress. *J Biol Chem* 279, 43378-43381.
- Peters, J.M. (2006). The anaphase promoting complex/cyclosome: a machine designed to destroy. *Nat Rev Mol Cell Biol* 7, 644-656.
- Petersen, J., Paris, J., Willer, M., Philippe, M., and Hagan, I.M. (2001). The *S. pombe* aurora-related kinase Ark1 associates with mitotic structures in a stage dependent manner and is required for chromosome segregation. *J Cell Sci* 114, 4371-4384.
- Petersen, M.B., and Mikkelsen, M. (2000). Nondisjunction in trisomy 21: origin and mechanisms. *Cytogenet Cell Genet* 91, 199-203.
- Pidoux, A.L., and Allshire, R.C. (2005). The role of heterochromatin in centromere function. *Philos Trans R Soc Lond B Biol Sci* 360, 569-579.
- Pidoux, A.L., Choi, E.S., Abbott, J.K., Liu, X., Kagansky, A., Castillo, A.G., Hamilton, G.L., Richardson, W., Rappsilber, J., He, X., *et al.* (2009). Fission yeast Scm3: A CENP-A receptor required for integrity of subkinetochore chromatin. *Mol Cell* 33, 299-311.
- Pidoux, A.L., LeDizet, M., and Cande, W.Z. (1996). Fission yeast pkl1 is a kinesin-related protein involved in mitotic spindle function. *Molecular Biology of the Cell* 7, 1639-1655.
- Pidoux, A.L., Richardson, W., and Allshire, R.C. (2003). Sim4: a novel fission yeast kinetochore protein required for centromeric silencing and chromosome segregation. *J Cell Biol* 161, 295-307.
- Pluta, A.F., Mackay, A.M., Ainsztein, A.M., Goldberg, I.G., and Earnshaw, W.C. (1995). The centromere: hub of chromosomal activities. *Science* 270, 1591-1594.
- Pöhlmann, J., and Fleig, U. (2010). Asp1, a conserved 1/3 inositol polyphosphate kinase, regulates the dimorphic switch in *Schizosaccharomyces pombe*. *Mol Cell Biol* 30, 4535-4547.
- Pöhlmann, J., Risse, C., Seidel, C., Pohlmann, T., Jakopcic, V., Walla, E., Ramrath, P., Takeshita, N., Baumann, S., Feldbrugge, M., *et al.* (2014). The Vip1 inositol polyphosphate kinase family regulates polarized growth and modulates the microtubule cytoskeleton in fungi. *PLoS Genet* 10, e1004586.
- Polizzi, C., and Clarke, L. (1991). The chromatin structure of centromeres from fission yeast: differentiation of the central core that correlates with function. *J Cell Biol* 112, 191-201.
- Przewloka, M.R., and Glover, D.M. (2009). The kinetochore and the centromere: a working long distance relationship. *Annu Rev Genet* 43, 439-465.
- Pulloor, N.K., Nair, S., Kostic, A.D., Bist, P., Weaver, J.D., Riley, A.M., Tyagi, R., Uchil, P.D., York, J.D., Snyder, S.H., *et al.* (2014). Human genome-wide RNAi screen identifies an essential role for inositol pyrophosphates in Type-I interferon response. *PLoS Pathog* 10, e1003981.
- Rago, F., Gascoigne, K.E., and Cheeseman, I.M. (2015). Distinct organization and regulation of the outer kinetochore KMN network downstream of CENP-C and CENP-T. *Curr Biol* 25, 671-677.
- Ramrath, P. (2010). Charakterisierung von Phänotypen bei Mal2, Fta2 oder Cnp1 Überexpression. In Funktionelle Genomforschung (HHU Düsseldorf).
- Rea, S., Eisenhaber, F., O'Carroll, D., Strahl, B.D., Sun, Z.W., Schmid, M., Opravil, S., Mechtler, K., Ponting, C.P., Allis, C.D., *et al.* (2000). Regulation of chromatin structure by site-specific histone H3 methyltransferases. *Nature* 406, 593-599.
- Rincon, S.A., Lamson, A., Blackwell, R., Syrovatkina, V., Fraiser, V., Paoletti, A., Betterton, M.D., and Tran, P.T. (2017). Kinesin-5-independent mitotic spindle assembly requires the antiparallel microtubule crosslinker Ase1 in fission yeast. *Nat Commun* 8, 15286.
- Rischitor, P.E., May, K.M., and Hardwick, K.G. (2007). Bub1 is a fission yeast kinetochore scaffold protein, and is sufficient to recruit other spindle checkpoint proteins to ectopic sites on chromosomes. *PLoS One* 2, e1342.

- Roguev, A., Wiren, M., Weissman, J.S., and Krogan, N.J. (2007). High-throughput genetic interaction mapping in the fission yeast *Schizosaccharomyces pombe*. *Nat Methods* 4, 861-866.
- Roque, H., Ward, J.J., Murrells, L., Brunner, D., and Antony, C. (2010). The fission yeast XMAP215 homolog Dis1p is involved in microtubule bundle organization. *PLoS One* 5, e14201.
- Rothbauer, U., Zolghadr, K., Muyldermans, S., Schepers, A., Cardoso, M.C., and Leonhardt, H. (2008). A versatile nanotrap for biochemical and functional studies with fluorescent fusion proteins. *Mol Cell Proteomics* 7, 282-289.
- Rowley, R., Subramani, S., and Young, P.G. (1992). Checkpoint controls in *Schizosaccharomyces pombe*: rad1. *EMBO J* 11, 1335-1342.
- Roy, B., Varshney, N., Yadav, V., and Sanyal, K. (2013). The process of kinetochore assembly in yeasts. *FEMS Microbiol Lett* 338, 107-117.
- Rudner, A.D., and Murray, A.W. (1996). The spindle assembly checkpoint. *Curr Opin Cell Biol* 8, 773-780.
- Rutledge, S.D., and Cimini, D. (2016). Consequences of aneuploidy in sickness and in health. *Curr Opin Cell Biol* 40, 41-46.
- Ryan, C.J., Roguev, A., Patrick, K., Xu, J., Jahari, H., Tong, Z., Beltrao, P., Shales, M., Qu, H., Collins, S.R., *et al.* (2012). Hierarchical modularity and the evolution of genetic interactomes across species. *Mol Cell* 46, 691-704.
- Saiardi, A. (2016). Protein pyrophosphorylation: moving forward. *Biochem J* 473, 3765-3768.
- Saiardi, A., Bhandari, R., Resnick, A.C., Snowman, A.M., and Snyder, S.H. (2004). Phosphorylation of proteins by inositol pyrophosphates. *Science* 306, 2101-2105.
- Saiardi, A., Erdjument-Bromage, H., Snowman, A.M., Tempst, P., and Snyder, S.H. (1999). Synthesis of diphosphoinositol pentakisphosphate by a newly identified family of higher inositol polyphosphate kinases. *Curr Biol* 9, 1323-1326.
- Saiardi, A., Nagata, E., Luo, H.R., Snowman, A.M., and Snyder, S.H. (2001). Identification and characterization of a novel inositol hexakisphosphate kinase. *J Biol Chem* 276, 39179-39185.
- Saiardi, A., Resnick, A.C., Snowman, A.M., Wendland, B., and Snyder, S.H. (2005). Inositol pyrophosphates regulate cell death and telomere length through phosphoinositide 3-kinase-related protein kinases. *Proc Natl Acad Sci U S A* 102, 1911-1914.
- Saitoh, S., Ishii, K., Kobayashi, Y., and Takahashi, K. (2005). Spindle checkpoint signaling requires the mis6 kinetochore subcomplex, which interacts with mad2 and mitotic spindles. *Mol Biol Cell* 16, 3666-3677.
- Saitoh, S., Kobayashi, Y., Ogiyama, Y., and Takahashi, K. (2008). Dual regulation of Mad2 localization on kinetochores by Bub1 and Dam1/DASH that ensure proper spindle interaction. *Mol Biol Cell* 19, 3885-3897.
- Saitoh, S., Takahashi, K., and Yanagida, M. (1997). Mis6, a fission yeast inner centromere protein, acts during G1/S and forms specialized chromatin required for equal segregation. *Cell* 90, 131-143.
- Sanchez-Perez, I., Renwick, S.J., Crawley, K., Karig, I., Buck, V., Meadows, J.C., Franco-Sanchez, A., Fleig, U., Toda, T., and Millar, J.B. (2005). The DASH complex and Klp5/Klp6 kinesin coordinate bipolar chromosome attachment in fission yeast. *Embo J* 24, 2931-2943.
- Santaguida, S., and Amon, A. (2015). Short- and long-term effects of chromosome mis-segregation and aneuploidy. *Nat Rev Mol Cell Biol* 16, 473-485.
- Sato, M., Vardy, L., Angel Garcia, M., Koonrugsa, N., and Toda, T. (2004). Interdependency of fission yeast Alp14/TOG and coiled coil protein Alp7 in microtubule localization and bipolar spindle formation. *Mol Biol Cell* 15, 1609-1622.
- Schalch, T., and Steiner, F.A. (2016). Structure of centromere chromatin: from nucleosome to chromosomal architecture. *Chromosoma*.
- Schneider-Poetsch, T., Ju, J., Eyler, D.E., Dang, Y., Bhat, S., Merrick, W.C., Green, R., Shen, B., and Liu, J.O. (2010). Inhibition of eukaryotic translation elongation by cycloheximide and lactimidomycin. *Nat Chem Biol* 6, 209-217.

- Schuhenn, J. (2016). Charakterisierung des Proteins SPCC584.01c im Bezug auf Wachstum und Interaktion mit Kinetochor-assoziierten Proteinen in *Schizosaccharomyces pombe*. In Funktionelle Genomforschung (HHU Düsseldorf).
- Screpanti, E., De Antoni, A., Alushin, G.M., Petrovic, A., Melis, T., Nogales, E., and Musacchio, A. (2011). Direct binding of cenp-C to the mis12 complex joins the inner and outer kinetochore. *Curr Biol* 21, 391-398.
- Sczaniecka, M., Feoktistova, A., May, K.M., Chen, J.S., Blyth, J., Gould, K.L., and Hardwick, K.G. (2008). The spindle checkpoint functions of Mad3 and Mad2 depend on a Mad3 KEN box-mediated interaction with Cdc20-anaphase-promoting complex (APC/C). *J Biol Chem* 283, 23039-23047.
- Shears, S.B., Baughman, B.M., Gu, C., Nair, V.S., and Wang, H. (2017). The significance of the 1-kinase/1-phosphatase activities of the PPIP5K family. *Adv Biol Regul* 63, 98-106.
- Shears, S.B., Gokhale, N.A., Wang, H., and Zaremba, A. (2011). Diphosphoinositol polyphosphates: what are the mechanisms? *Adv Enzyme Regul* 51, 13-25.
- Shepperd, L.A., Meadows, J.C., Sochaj, A.M., Lancaster, T.C., Zou, J., Buttrick, G.J., Rappsilber, J., Hardwick, K.G., and Millar, J.B. (2012). Phosphodependent recruitment of Bub1 and Bub3 to Spc7/KNL1 by Mph1 kinase maintains the spindle checkpoint. *Curr Biol* 22, 891-899.
- Shiroiwa, Y., Hayashi, T., Fujita, Y., Villar-Briones, A., Ikai, N., Takeda, K., Ebe, M., and Yanagida, M. (2011). Mis17 is a regulatory module of the Mis6-Mal2-Sim4 centromere complex that is required for the recruitment of CenH3/CENP-A in fission yeast. *PLoS One* 6, e17761.
- Skibbens, R.V. (2009). Establishment of sister chromatid cohesion. *Curr Biol* 19, R1126-1132.
- Stehling, O., Vashisht, A.A., Mascarenhas, J., Jonsson, Z.O., Sharma, T., Netz, D.J., Pierik, A.J., Wohlschlegel, J.A., and Lill, R. (2012). MMS19 assembles iron-sulfur proteins required for DNA metabolism and genomic integrity. *Science* 337, 195-199.
- Steiner, F.A., and Henikoff, S. (2014). Holocentromeres are dispersed point centromeres localized at transcription factor hotspots. *Elife* 3, e02025.
- Steiner, F.A., and Henikoff, S. (2015). Diversity in the organization of centromeric chromatin. *Curr Opin Genet Dev* 31, 28-35.
- Su, S.S., Tanaka, Y., Samejima, I., Tanaka, K., and Yanagida, M. (1996). A nitrogen starvation-induced dormant G0 state in fission yeast: the establishment from uncommitted G1 state and its delay for return to proliferation. *J Cell Sci* 109 (Pt 6), 1347-1357.
- Subramanian, L., Toda, N.R., Rappsilber, J., and Allshire, R.C. (2014). Eic1 links Mis18 with the CCAN/Mis6/Ctf19 complex to promote CENP-A assembly. *Open Biol* 4, 140043.
- Suessmilch, M. (2016). Charakterisierung des Proteins SPCC584.01c unter dem Einfluss exogener Noxen und die Interaktion mit Kinetochor-assoziierten Proteinen in *Schizosaccharomyces pombe*. In Funktionelle Genomforschung (HHU Düsseldorf).
- Syrovatkina, V., Fu, C., and Tran, P.T. (2013). Antagonistic spindle motors and MAPs regulate metaphase spindle length and chromosome segregation. *Curr Biol* 23, 2423-2429.
- Syrovatkina, V., and Tran, P.T. (2015). Loss of kinesin-14 results in aneuploidy via kinesin-5-dependent microtubule protrusions leading to chromosome cut. *Nat Commun* 6, 7322.
- Takahashi K, Murakami S, Chikashige Y, Funabiki H, Niwa O, and M., Y. (1992). A low copy number central sequence with strict symmetry and unusual chromatin structure in fission yeast centromere. *Mol Biol Cell*. 3, 819-835.
- Takahashi, K., Chen, E.S., and Yanagida, M. (2000). Requirement of Mis6 centromere connector for localizing a CENP-A-like protein in fission yeast. *Science* 288, 2215-2219.
- Takahashi, K., Yamada, H., and Yanagida, M. (1994). Fission yeast minichromosome loss mutants mis cause lethal aneuploidy and replication abnormality. *Mol Biol Cell* 5, 1145-1158.
- Tanaka, K., Chang, H.L., Kagami, A., and Watanabe, Y. (2009). CENP-C functions as a scaffold for effectors with essential kinetochore functions in mitosis and meiosis. *Dev Cell* 17, 334-343.
- Tanaka, K., and Kanbe, T. (1986). Mitosis in the fission yeast *Schizosaccharomyces pombe* as revealed by freeze-substitution electron microscopy. *J Cell Sci* 80, 253-268.

- Tang, N.H., Takada, H., Hsu, K.S., and Toda, T. (2013). The internal loop of fission yeast Ndc80 binds Alp7/TACC-Alp14/TOG and ensures proper chromosome attachment. *Mol Biol Cell* 24, 1122-1133.
- Tang, N.H., and Toda, T. (2015). Alp7/TACC recruits kinesin-8-PP1 to the Ndc80 kinetochore protein for timely mitotic progression and chromosome movement. *J Cell Sci* 128, 354-363.
- Tatebe, H., Goshima, G., Takeda, K., Nakagawa, T., Kinoshita, K., and Yanagida, M. (2001). Fission yeast living mitosis visualized by GFP-tagged gene products. *Micron* 32, 67-74.
- Thompson, S.L., and Compton, D.A. (2011). Chromosomes and cancer cells. *Chromosome Res* 19, 433-444.
- Thota, S.G., and Bhandari, R. (2015). The emerging roles of inositol pyrophosphates in eukaryotic cell physiology. *J Biosci* 40, 593-605.
- Toda, T., Adachi, Y., Hiraoka, Y., and Yanagida, M. (1984). Identification of the pleiotropic cell division cycle gene NDA2 as one of two different alpha-tubulin genes in *Schizosaccharomyces pombe*. *Cell* 37, 233-242.
- Tolic-Norrelykke, I.M., Sacconi, L., Thon, G., and Pavone, F.S. (2004). Positioning and elongation of the fission yeast spindle by microtubule-based pushing. *Curr Biol* 14, 1181-1186.
- Topolski, B. (2013). Funktionelle Analyse neuer mitotischer Regulationsmechanismen in *Schizosaccharomyces pombe*. In *Funktionella Genomforschung* (HHU Düsseldorf).
- Topolski, B., Jakopec, V., Kunzel, N.A., and Fleig, U. (2016). Inositol Pyrophosphate Kinase Asp1 Modulates Chromosome Segregation Fidelity and Spindle Function in *Schizosaccharomyces pombe*. *Mol Cell Biol* 36, 3128-3140.
- Torres, E.M., Sokolsky, T., Tucker, C.M., Chan, L.Y., Boselli, M., Dunham, M.J., and Amon, A. (2007). Effects of aneuploidy on cellular physiology and cell division in haploid yeast. *Science* 317, 916-924.
- Torres, E.M., Williams, B.R., and Amon, A. (2008). Aneuploidy: cells losing their balance. *Genetics* 179, 737-746.
- Tran, P.T., Paoletti, A., and Chang, F. (2004). Imaging green fluorescent protein fusions in living fission yeast cells. *Methods* 33, 220-225.
- Troxell, C.L., Sweezy, M.A., West, R.R., Reed, K.D., Carson, B.D., Pidoux, A.L., Cande, W.Z., and McIntosh, J.R. (2001). pkl1(+) and klp2(+): Two kinesins of the Kar3 subfamily in fission yeast perform different functions in both mitosis and meiosis. *Mol Biol Cell* 12, 3476-3488.
- Turner, J.J., Ewald, J.C., and Skotheim, J.M. (2012). Cell size control in yeast. *Curr Biol* 22, R350-359.
- Unsworth, A. (2007). The mitotic role and regulation of Kinesin-8 Klp5 and Klp6 in fission yeast. In *Faculty of Life Sciences* (University of London).
- Vader, G., Medema, R.H., and Lens, S.M. (2006). The chromosomal passenger complex: guiding Aurora-B through mitosis. *J Cell Biol* 173, 833-837.
- Vanoosthuyse, V., and Hardwick, K.G. (2009). A novel protein phosphatase 1-dependent spindle checkpoint silencing mechanism. *Curr Biol* 19, 1176-1181.
- Verdaasdonk, J.S., and Bloom, K. (2011). Centromeres: unique chromatin structures that drive chromosome segregation. *Nat Rev Mol Cell Biol* 12, 320-332.
- Wang, H., Falck, J.R., Hall, T.M., and Shears, S.B. (2011). Structural basis for an inositol pyrophosphate kinase surmounting phosphate crowding. *Nat Chem Biol* 8, 111-116.
- Wang, H., Nair, V.S., Holland, A.A., Capolicchio, S., Jessen, H.J., Johnson, M.K., and Shears, S.B. (2015). Asp1 from *Schizosaccharomyces pombe* binds a [2Fe-2S](2+) cluster which inhibits inositol pyrophosphate 1-phosphatase activity. *Biochemistry* 54, 6462-6474.
- Weaver, J.D., Wang, H., and Shears, S.B. (2013). The kinetic properties of a human PPIP5K reveal that its kinase activities are protected against the consequences of a deteriorating cellular bioenergetic environment. *Biosci Rep* 33, e00022.
- Webb, K.J., Zurita-Lopez, C.I., Al-Hadid, Q., Laganowsky, A., Young, B.D., Lipson, R.S., Souda, P., Faull, K.F., Whitelegge, J.P., and Clarke, S.G. (2010). A novel 3-methylhistidine modification of yeast ribosomal protein Rpl3 is dependent upon the YIL110W methyltransferase. *J Biol Chem* 285, 37598-37606.

- Wei, R.R., Sorger, P.K., and Harrison, S.C. (2005). Molecular organization of the Ndc80 complex, an essential kinetochore component. *Proc Natl Acad Sci U S A* *102*, 5363-5367.
- West, R.R., Malmstrom, T., and McIntosh, J.R. (2002). Kinesins klp5(+) and klp6(+) are required for normal chromosome movement in mitosis. *J Cell Sci* *115*, 931-940.
- West, R.R., Malmstrom, T., Troxell, C.L., and McIntosh, J.R. (2001). Two related kinesins, klp5+ and klp6+, foster microtubule disassembly and are required for meiosis in fission yeast. *Mol Biol Cell* *12*, 3919-3932.
- Wild, R., Gerasimaite, R., Jung, J.Y., Truffault, V., Pavlovic, I., Schmidt, A., Saiardi, A., Jessen, H.J., Poirier, Y., Hothorn, M., *et al.* (2016). Control of eukaryotic phosphate homeostasis by inositol polyphosphate sensor domains. *Science* *352*, 986-990.
- Willard, H.F. (1990). Centromeres of mammalian chromosomes. *Trends Genet* *6*, 410-416.
- Williams, J.S., Hayashi, T., Yanagida, M., and Russell, P. (2009). Fission yeast Scm3 mediates stable assembly of Cnp1/CENP-A into centromeric chromatin. *Mol Cell* *33*, 287-298.
- Wilson, M.S., Livermore, T.M., and Saiardi, A. (2013). Inositol pyrophosphates: between signalling and metabolism. *Biochem J* *452*, 369-379.
- Witters, G., Van Robays, J., Willekes, C., Coumans, A., Peeters, H., Gyselaers, W., and Fryns, J.P. (2011). Trisomy 13, 18, 21, Triploidy and Turner syndrome: the 5T's. Look at the hands. *Facts Views Vis Obgyn* *3*, 15-21.
- Woods, A., Sherwin, T., Sasse, R., MacRae, T.H., Baines, A.J., and Gull, K. (1989). Definition of individual components within the cytoskeleton of *Trypanosoma brucei* by a library of monoclonal antibodies. *J Cell Sci* *93*, 491-500.
- Wu, M., Chong, L.S., Perlman, D.H., Resnick, A.C., and Fiedler, D. (2016). Inositol polyphosphates intersect with signaling and metabolic networks via two distinct mechanisms. *Proc Natl Acad Sci U S A* *113*, E6757-E6765.
- Yaffe, M.P., Harata, D., Verde, F., Eddison, M., Toda, T., and Nurse, P. (1996). Microtubules mediate mitochondrial distribution in fission yeast. *Proc Natl Acad Sci U S A* *93*, 11664-11668.
- Yaffe, M.P., Stuurman, N., and Vale, R.D. (2003). Mitochondrial positioning in fission yeast is driven by association with dynamic microtubules and mitotic spindle poles. *Proc Natl Acad Sci U S A* *100*, 11424-11428.
- Yamagishi, Y., Sakuno, T., Goto, Y., and Watanabe, Y. (2014). Kinetochore composition and its function: lessons from yeasts. *FEMS Microbiol Rev* *38*, 185-200.
- Yamagishi, Y., Yang, C.H., Tanno, Y., and Watanabe, Y. (2012). MPS1/Mph1 phosphorylates the kinetochore protein KNL1/Spc7 to recruit SAC components. *Nat Cell Biol* *14*, 746-752.
- Yamashita, A., Sato, M., Fujita, A., Yamamoto, M., and Toda, T. (2005). The roles of fission yeast *ase1* in mitotic cell division, meiotic nuclear oscillation, and cytokinesis checkpoint signaling. *Mol Biol Cell* *16*, 1378-1395.
- Yanagida, M. (2002). The model unicellular eukaryote, *Schizosaccharomyces pombe*. *Genome Biol* *3*, COMMENT2003.
- York, S.J., Armbruster, B.N., Greenwell, P., Petes, T.D., and York, J.D. (2005). Inositol diphosphate signaling regulates telomere length. *J Biol Chem* *280*, 4264-4269.
- Yukawa, M., Ikebe, C., and Toda, T. (2015). The Msd1-Wdr8-Pkl1 complex anchors microtubule minus ends to fission yeast spindle pole bodies. *J Cell Biol* *209*, 549-562.
- Zekanowski, C., and Wojda, U. (2009). Aneuploidy, chromosomal missegregation, and cell cycle reentry in Alzheimer's disease. *Acta Neurobiol Exp (Wars)* *69*, 232-253.

8 Publications

Topolski B, Jakopec V, **Künzel NA**, Fleig U. Inositol Pyrophosphate Kinase Asp1 Modulates Chromosome Segregation Fidelity and Spindle Function in *Schizosaccharomyces pombe*. *Molecular and Cellular Biology*. 2016;36(24):3128-3140. doi:10.1128/MCB.00330-16.

9 Acknowledgments

Here I want to thank all the people that accompanied me during the last 4 years and helped me to enjoy the successes and deal with the obstacles in my time as a PhD student.

First of all I want to thank Prof. Dr. Ursula Fleig for granting me the possibility to work on an exciting project that even got me a short talk at a GRC conference in the states. Thanks for the scientific discussions and the advice that helped me with the work on my project. Special thanks for patiently discussing my manuscript with me in the last few months and giving me the opportunity to develop, not only as a scientist, but also as a person.

Next I want to thank Prof. Dr. Johannes Hegemann for being my co-supervisor and for the advices I got along the way.

I furthermore want to thank the whole team of our lab: Boris, for laying the ground-stone of the project; Visnja, for numerous scientific advices and alot of help especially in the last few months of my PhD; Eva, for help with experiments, company during numerous practical courses and nice conversations among us early-birds; Anand, for being the pillar within the PhD triangle and for always giving philosophic advice. Last, but definitely not least, I want to thank Marina, mi amiga who accompanied me from the very first day. The last years would not have been the same without her. She was there when I was excited, sad and happy and she put up with alot of cray-cray in the last few months. I wish her all the best for her future and hope that we will stay friends for years to come.

I also want to thank the “Hegemänner” for nice talks in the coffee kitchen, funny barbecues and a productive work environment. My special thanks to Alison and Coco, who were not only colleagues, but became friends, and helped me to deal with every obstacle. I hope we will share some Grappas in the future!

Thanks also to “the boys” Lasse and Patrick. I really appreciate their friendship, the Wegbier and the support I got from them in the last years. May the force be with you!

The biggest imaginable thanks to my family: My brother, Benni, who knows me better than anyone else in the world, and has been the closest person to me my entire life. Dank auch an meine Mum, die sich geduldig alles anhört, was ich zu sagen habe, mir immer hilft Probleme zu lösen, und mich unzählige Male aufgeheitert hat. Dank an meinen Dad, der mir geholfen hat mein Ziel nie aus den Augen zu verlieren und meinen Weg zu machen. Und natürlich ein riesen Dank an meine Oma, Renate, ohne deren Unterstützung ich nicht dort wäre, wo ich heute bin, und die mir die Möglichkeit gegeben hat, meinen Bildungsweg zu beschreiten. Ich habe euch sehr lieb!

10 Statutory Declaration

I declare under oath that I have compiled my dissertation independently and without any undue assistance by third parties under consideration of the 'Principles for the Safeguarding of Good Scientific Practice at Heinrich Heine University Düsseldorf'.

I declare that I have not used sources or means without declaration in the text. All the passages taken from other works in the wording or in the meaning have been clearly indicated with sources. This thesis has not been used in the same or similar version to achieve an academic grading or is being published elsewhere.

Düsseldorf,

Natascha Andrea Künzel